Jagiellonian University in Krakow

Faculty of Biochemistry, Biophysics, and Biotechnology

Role of heme oxygenase-1 in the biology of melanoma initiating cells and melanogenesis

Rola oksygenazy hemowej-1 w biologii komórek inicjujących czerniaka i melanogenezie

Ph.D. thesis prepared in the Department of Medical
Biotechnology under the supervision of
prof. Alicja Józkowicz

Praca doktorska przygotowana pod opieką
prof. dr hab. Alicji Józkowicz
w Zakładzie Biotechnologii Medycznej

Anna Kusienicka

Kraków, 2020

I dedicate this work to my husband

Acknowledgements

I would like to thank my supervisor prof. Alicja Józkowicz for her invaluable support and guidance during my work in the Department of Medical Biotechnology.

I want to thank my colleagues from the Department of Medical Biotechnology for all the help during the preparation of the work, especially Agnieszka Seretny, Witold Nowak, Karolina Bukowska-Strakova, Iwona Bronisz, Mateusz Jeż, Maciej Cieśla, Jacek Stępniewski, Grażyna Adamek and Hevidar Taha. I want to express my special gratitude to my dearest friend Monika Żukowska who was always by my side, supporting me in my work and making me laugh all the time.

I want to acknowledge dr Michał Sarna from the Department of Biophysics in the Faculty of Biophysics, Biochemistry, and Biotechnology of Jagiellonian University for help in EPR analysis.

This work would not be possible if not the support of my beloved husband Tomek. He witnessed all my struggles and all my successes and was always able to lift my spirit. During the time of my Ph.D. studies, I gave birth to my daughter Hania. She taught me how to be strong.

Last but not least I want to thank my parents who are always proud of me and always believe in me.

Abstract

Melanoma is a highly aggressive skin cancer of melanocytic origin. Late-stage disease, when distant metastases develop, is practically incurable, despite the introduction of new treatments (e.g. targeted $BRAF^{V600E/V600K}$ therapies or immune checkpoint inhibitors). Resistance to therapy is largely due to exceptionally high heterogeneity of melanoma, attributed, among others, to the existence of the cancer stem cells (CSC). It is supposed that CSC can initiate tumor growth from a single cell and then re-establish tumor heterogeneity. They give rise to highly proliferating tumor cells, but at the same time remain quiescent, and resistant to conventional therapies. Melanoma initiating cells (MIC) are thought to be responsible for tumorigenicity and aggressiveness of this cancer but it is still not clear which factors can regulate their behavior.

One of the enzymes important in cancer biology is heme oxygenase-1 (HO-1), that degrades heme to carbon monoxide (CO), biliverdin, and ferrous ions (Fe^{2+}). Upon activation in response to oxidative stress (e.g. caused by chemo- and radiotherapies or UV radiation) HO-1 acts as a cytoprotective agent, affecting also angiogenesis and immune response. The final outcome of the HO-1 activation in cancer is cell type-specific. In melanoma, overexpression of HO-1 increases aggressiveness and therapy resistance in growing tumors. However, nothing is known about the possible effects of HO-1 in MIC.

We addressed this issue and investigated the role of HO-1 in regulation of MIC activity. We used the B16-F10 murine melanoma cell line and found that it contains cells expressing MIC surface markers (CD20, CD133, CD24, ABCB1, ABCB5, Sca-1) and cells with functional CSC features (high activity of ALDH and PKH26 label retention). Expression levels of HO-1 in the MIC$^+$ and bulk cells were comparable. However, HO-1 activity facilitated non-adherent growth of melanoma cells, a typical feature of CSC.

We found that it was HO-1 overexpression, not the MIC markers expression, that predominantly affected melanoma clonogenicity. Interestingly, overexpression of HO-1 led to decreased clonogenicity of single melanoma cells *in vitro* and was unfavorable for clonal growth. Consistently, *in vivo* serial transplantation of a small fraction of B16-F10 cell line (10 or 100 cells) into syngeneic C57BL/6 recipients revealed that HO-1 overexpression decreased tumorigenicity in secondary and tertiary recipients, most probably through reduced cell self-renewal.

Our data show that phenotypic or functional MIC markers in B16-F10 murine melanoma (CD20$^+$, ALDH^{high}, PKH26$^+$ slowly cycling cells) do not select CSC-like cells. We observed

similar clonogenicity *in vitro* and tumorigenicity *in vivo* between MIC$^-$ and MIC$^+$ subsets. Moreover, MIC$^-$ and MIC$^+$ cells had similar differentiation status reflected by expression of melanoma-associated antigens (MAAs; *Tyr, Gp100, Mart-1*) and similar expression of CSC-associated genes (e.g. *Notch1, Myc*). Finally, the progeny of both MIC$^-$ and MIC$^+$ cells regain heterogeneity of the bulk subpopulation.

We also demonstrated that silencing of HO-1 with shRNAs led to the de-pigmentation of B16-F10 melanoma cells despite the fact that it did not change the expression of genes involved in melanogenesis. Instead, HO-1 overexpression was associated with decreased activity of tyrosinase, a rate-limiting enzyme in melanin synthesis. To check whether HO-1 is necessary for development of pigmentation we performed experiments in the induced pluripotent stem cells (iPSC), generated from the tail-tips fibroblasts of *Hmox-1$^{-/-}$* and *Hmox-1$^{+/+}$* mice and differentiated towards pigmented melanocytes. We detected pigmentation and upregulation of melanocytic markers in both groups, meaning that HO-1 is not required for induction of melanocytic differentiation. Moreover, experiments performed in Melan A cell line showed that HO-1 is dispensable for pigmentation of melanocytes.

To sum up, our data points at the dual role of HO-1 in melanoma. Although overexpression of HO-1 promoted the progression of growing B16-F10-derived tumors, on the other hand it seems to decrease a risk of melanoma initiation. We demonstrated that overexpression of HO-1 during clonal growth induction *in vitro* and *in vivo* can play an anti-tumorigenic role. Thus, our results suggest that pharmacological inhibitors of HO-1 in melanoma treatment, might have a different effect on tumor growth than on tumor initiation.

Streszczenie

Czerniak jest wysoce agresywnym nowotworem pochodzenia melanocytarnego. Zdiagnozowany w późnym stadium, w którym tworzą się odległe przerzuty, jest wciąż praktycznie nieuleczalny, pomimo wprowadzenia do kliniki nowych, celowanych terapii (inhibitorów kinazy BRAF lub inhibitorów punktów kontrolnych odpowiedzi odpornościowej). Oporność czerniaka na terapie jest w dużej mierze związana z jego wyjątkową heterogennością, do której mogą prawdopodobnie przyczyniać się nowotworowe komórki macierzyste (ang. *cancer stem cells*, CSC). Komórki CSC mogą inicjować wzrost guza z pojedynczych komórek, a następnie odtwarzać heterogenność guza, dając początek szybko dzielącym się komórkom. Równocześnie same CSC mają charakter spoczynkowy i dzielą się rzadko, dzięki czemu są oporne na konwencjonalne terapie przeciwnowotworowe. W czerniaku komórki inicjujące wzrost nowotworu (ang. *melanoma initiating cells*, MIC) uznawane są za czynnik nasilający powstawanie i progresję nowych guzów, jednak mechanizmy które mogą regulować ich funkcjonowanie są wciąż słabo poznane.

Jednym z białek ważnych w biologii nowotworów jest oksygenaza hemowa-1 (HO-1), enzym który rozkłada hem do tlenku węgla (CO), biliwerdyny i jonów żelaza (Fe^{2+}). HO-1 jest indukowana w odpowiedzi na stres oksydacyjny (czyli np. w odpowiedzi na chemio- i radioterapie lub promieniowanie UV), działając cytoprotekcyjnie, a jednocześnie wpływając na angiogenezę i aktywność układu odpornościowego. Ostateczny wynik aktywacji HO-1 zależy od typu nowotworu. W czerniaku wysoka ekspresja HO-1 zwiększa agresywność rosnących guzów i ich oporność na terapie. Wciąż brakuje natomiast informacji o roli HO-1 w komórkach typu MIC.

Naszym celem było wypełnienie tej luki i sprawdzenie czy HO-1 wpływa na działanie MIC. Przeprowadziliśmy badania wykorzystując linię mysiego czerniaka B16-F10 i stwierdziliśmy, że zawiera ona komórki z ekspresją powierzchniowych markerów MIC (CD20, CD133, CD24, ABCB1, ABCB5, Sca-1) oraz komórki o cechach funkcjonalnych typowych dla CSC (wysoka aktywność ALDH, utrzymywanie barwnika PKH26). Poziom ekspresji HO-1 komórkach MIC$^+$ i w pozostałych komórkach był porównywalny. Okazało się jednak, że HO-1 ułatwia wzrost komórek niezależny od podłoża, czyli aktywność typową dla MIC.

Nasze doświadczenia pokazały, że nadekspresja HO-1 wpływa na klonogenność czerniaka bardziej niż sama ekspresja markerów MIC. Wysoki poziom aktywności HO-1 zmniejszał klonogenność *in vitro* pojedynczych komórek B16-F10 oraz hamował rozwój klonów. Badania *in vivo* potwierdziły tę obserwację i pokazały, że nadekspresja HO-1

zmniejsza inicjację wzrostu guzów u biorców drugo- i trzeciorzędowych po podaniu podskórnie małej frakcji komórek czerniaka (10 lub 100 komórek do syngenicznych myszy C57BL/6). Przypuszczamy, że może to wynikać z obniżenia zdolności do samoodnowy w komórkach z nadekspresją HO-1.

Wykazaliśmy także, że fenotypowe lub funkcjonalne markery MIC (CD20^{+}, ALDH^{+}, PKH26^{+}) nie identyfikują komórek typu CSC w linii B16-F10. Stwierdziliśmy porównywalną klonogenność *in vitro* i inicjację wzrostu guzów *in vivo* w subpopulacjach MIC[-] i MIC[+]. Co więcej, komórki MIC[-] i MIC[+] wykazywały podobny stopień zróżnicowania, na co wskazuje zbliżony poziom ekspresji antygenów charakterystycznych dla czerniaka (ang. *melanoma-associated antigens* MAA; *Tyr, Gp100, Mart-1*) oraz genów związanych z fenotypem komórek CSC (np. *Notch1, Myc*). Co istotne, komórki potomne obu frakcji MIC[-] i MIC[+] odtwarzały heterogenność linii początkowej.

Wykazaliśmy również, że wyciszenie HO-1 w komórkach B16-F10 z użyciem shRNA (ang. *short harpin RNA*) prowadzi do depigmentacji komórek. Nie ma to związku z poziomem ekspresji genów regulujących melanogenezę, ale raczej z obniżeniem aktywności tyrozynazy, głównego enzymu biorącego udział w syntezie melaniny. Aby sprawdzić czy HO-1 jest niezbędna w procesie pigmentacji, przeprowadziliśmy doświadczenia na indukowanych komórkach pluripotencjalnych (ang. *induced pluripotent stem cells*, iPSC), wyprowadzonych z fibroblastów izolowanych z ogonów myszy *Hmox-1^{-/-}* i *Hmox-1^{+/+}*, a następnie różnicowanych w kierunku linii melanocytarnej. Zaobserwowaliśmy indukcję pigmentacji oraz ekspresji markerów melanocytarnych w obu grupach komórek, co oznacza że obecność HO-1 nie jest konieczna do zainicjowania różnicowania melanocytarnego. Dodatkowe doświadczenia przeprowadzone na linii Melan A potwierdziły, że HO-1 nie jest niezbędna do rozwoju pigmentacji melanocytów.

Podsumowując, nasze badania sugerują, że HO-1 może mieć dwoisty wpływ na rozwój czerniaka. Mimo, że nadekspresja HO-1 promuje rozwój istniejących guzów, jednocześnie może obniżać ryzyko inicjacji nowotworzenia. Pokazaliśmy, że wysoki poziom ekspresji HO-1 zmniejsza klonogenność komórek B16-F10 zarówno *in vitro* jak i *in vivo*. Może to oznaczać, że farmakologiczne inhibitory HO-1 lub leki pośrednio aktywujące HO-1 mogą odmiennie wpływać na wzrost niż na inicjację guzów.

Table of contents

1. Introduction

1.1. Melanoma

1.1.1. Melanoma origin and etiology

Melanoma is the malignancy of melanocytes, cells of neuroectodermal origin. The physiological role of melanocytes is the production of melanin and its transport to neighboring keratinocytes. Melanin has a crucial role in the protection of cells against the mutagenic effect of UV radiation[1]. Melanoma primarily resides in the skin but can be also found in the eye (in the uvea, conjunctiva, and ciliary body), along mucosal surfaces and in the brain (in the meninges)[2].

Melanoma can be classified as *in situ* when cancer cells reside in the epidermis, but when cells invade into the dermis it became invasive[2]. Most of the tumors are pigmented, but amelanotic forms are also described in some patients[3]. Although cutaneous melanoma (CM) accounts for only 4% of all skin cancer cases it is responsible for 75% of deaths in this group of patients[1]. Incidents of melanoma raised drastically in the last 50 years. It is diagnosed the most frequently in fair-skinned Caucasians and the highest incidents are reported in people living in Australia and New Zealand (around 60 cases/100 000 inhabitants)[4]. Exposure to UV radiation is regarded as the paramount risk factor in this disease and people with darker skin, who are better protected against UV, develop CM significantly less often[5]. The other risk factor is the preexistence, number, and size of nevi, which often (in 25% cases) give rise to melanomas[6].

Cutaneous melanoma is diagnosed relatively early in life, with a median age of diagnosis at 57 years[4]. It is also one of the most commonly diagnosed cancer in adolescents and young adults[5]. Young age women are more prone to develop melanoma (probably due to the frequent usage of indoor tanning in this group), but this phenomenon is reversed in ages 55 onwards when men start to develop melanoma more frequently[6].

1.1.2. Genetic alterations of melanoma

Around 5-12% of melanomas are familial melanomas, where one or more relatives of the patient also developed this disease[7]. The most frequent germline mutations responsible for familial forms of melanoma are mutations in cyclin-dependent kinase inhibitor 2A (CDKN2A or p16) and in cyclin-dependent kinase 4 (CDK4)[6]. When it comes to somatic mutations, melanoma has the highest described mutational rate among all other solid human cancers. This phenomenon is attributed to high carcinogenic UV light exposure in this cancer[7]. Driving

mutations of melanoma are seen in signaling pathways involved in the regulation of proliferation (BRAF, NRAS, NF1), cell metabolism and growth (PTEN and KIT), cell cycle control (CDKN2A), tumor suppressor genes (TP53), cell identity genes (ARID2) and telomerase (TERT)[8].

Up to 90% of melanomas exhibit aberrant activation of mitogen-activated protein kinase (MAPK) pathway involved in signal transduction from hormones and growth factors through activation of receptors tyrosine kinases (RTK)[6]. In healthy cells, activated MAPK pathway regulates cell proliferation, survival, and differentiation[9]. In cancers, its hyperactivation leads to cell cycle deregulation and inhibition of apoptosis and is usually caused by mutations in BRAF protein, one of the transducers in MAPK pathway[9]. Around 50% of melanomas display mutation in BRAF with V600E mutation being the most prevalent (~85% of all BRAF mutations). Identification of BRAF[V600E] mutation led to the discovery of targeted therapeutics: vemurafenib and dabrafenib which are used in the treatment of unresectable and metastatic melanoma[10]. Interestingly, BRAF mutation is seen in almost 80% of benign nevi, suggesting that this mutation alone is not enough to drive the carcinogenesis of melanoma[11]. The second most frequently mutated gene in the MAPK pathway is NRAS proto-oncogene and this mutation is present in around 20% of melanoma patients[12]. Both mutations, BRAF and NRAS, are mutually exclusive and usually are independent factors in melanoma prognosis[12].

Another mutation relevant in melanoma malignancy is neurofibromin 1 (NF1) mutation. NF1 is a suppressor gene that acts through inhibition of RAS proteins[13]. The loss-of-function of NF1 leads to hyperactivation of NRAS and activates MAPK and phosphoinositide 3-kinase (PI3K) pathway[6]. In acral and mucosal melanomas there is a frequent activation of KIT gene[14]. Among other deregulated pathways in melanoma are phosphatase and tensin homolog (PTEN) and PI3K-AKT signaling pathway[15,16], NF-κB/osteopontin/matrix metalloproteinase-9 axis[17] and WNT-3/ß-catenin[18]. Recently, whole-genome sequencing of different patient-derived melanoma cell lines revealed new genetic variants of mutations in many pathways, including Hippo and Notch signaling pathways, that contribute to diverse phenotypes of melanoma cells[19]. These discoveries might contribute to finding novel therapeutic approaches in melanoma treatment.

1.1.3. Melanoma classification and diagnosis

In 1960s dermatologist Wallace Clark proposed the classification of invasive melanoma based on histological features and the depth of tumor invasion. He distinguished three main types of melanoma: superficial spreading melanoma (SSM), nodular melanoma (NM), and

lentigo maligna melanoma (LMM)[1]. Additionally, nowadays we distinguish also acral lentiginous melanoma (ALM)[2]. Since Clark proposed this classification, melanoma was no longer classified only based on the place where it arose and clinicians started to see its exceptional heterogeneity. Later, Aleksander Breslow discovered that the outcome of the disease is correlated with the thickness of the tumor and proposed a classification based on the depth of invasion measured in millimeters (called Breslow's depth)[20].

Early signs of melanoma are called 'ABCDE' of melanoma, where 'A' stands for asymmetry, 'B' for the border, 'C' for color, 'D' stands for the diameter, and E for 'evolving' (Fig. 1.1). Melanocytic lesions are often asymmetrical, have uneven borders and multiple colors, are usually large (> 6 mm diameter) and change in time (e.g. growth, color change, bleeding)[5]. These simple rules help in the early diagnosis of melanoma by patients alone. Early diagnosis of melanoma is crucial for an increase in 5-year survival rate that reaches up to 99% when the lesion is detected at the earliest stage. Unfortunately, when melanoma is diagnosed at the stage when it already metastasized to the nearest lymph nodes (regional metastases) 5-year survival rate drops down to 65%. With distant metastases (e.g. lungs, brain) prognoses are very poor and only 25% of patients survive 5 years after diagnosis[21].

Asymmetry	Border	Color	Diameter	Evolution
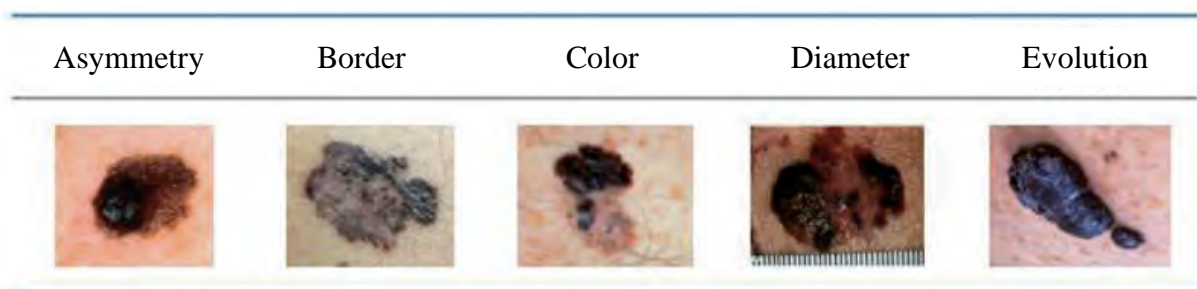
Figure 1.1. The 'ABCDE' of melanoma. From: "Clinical Presentation and Staging of Melanoma" Ward et al. 2017 in: "Cutaneous Melanoma: Etiology and Therapy".

Currently, the staging of melanoma is performed based on the tumor/node/metastasis (TNM) classification recommended by the American Joint Committee on Cancer (AJCC). It is based on the assessment of characteristics of the primary tumor (T), presence of micrometastases to lymph nodes (N), and presence and characteristics of distal metastases (M). Among many prognostic factors of melanoma are Breslow's depth of the tumor, presence of ulceration, mitotic rate of cancer cells, age, and sex[2]. Also, serum levels of lactate dehydrogenases (LDH) were shown to be a poor prognostic factor in melanoma staging[2].

1.1.4. Melanoma therapy

The primary treatment for melanoma is the surgical removal of the tumor together with surrounding healthy tissue[1]. If the thickness of lesion is greater than 0.8 mm usually biopsy of sentinel lymph nodes is performed[1]. If cancer cells metastasized there is a need for further treatment. The only chemotherapeutics used for the treatment of metastatic melanoma (MM) was dacarbazine, approved in the 1970s by the Food and Drug Administration (FDA)[22]. The effectiveness of this agent is low, only 13-20% of patients at advanced stage of the disease respond to this treatment[23]. In 1998, treatment of MM with high-dose bolus interleukin 2 (IL-2) was approved by FDA, but due to a very high risk of side effects only specialized health care centers were able to carry out this treatment[24]. Although only partially effective, treatment of advanced melanoma with IL-2 and interferon-α (IFN-α) gave the foundations for further development of immunotherapies for this malignancy[24].

It was not until 2011 when the new groundbreaking targeted therapies were approved for the treatment of advanced melanoma. As a result of intensive development of genome-wide sequencing techniques, in 2002 scientists described the high frequency of BRAF and NRAS mutations in melanoma[25]. This discovery led to the development of targeted therapeutic agents – vemurafenib, dabrafenib, and trametinib[10]. Vemurafenib and dabrafenib target BRAF protein with V600E and V600K mutations, and trametinib is an allosteric inhibitor of mitogen-activated protein kinase kinase (MEK)[10]. Treatment with vemurafenib gives response in around 50% of treated patients (that display mutated BRAF) and increases median overall survival (OS) when compared to treatment with dacarbazine (13.6 vs 9.7 months)[26,27]. Although targeted therapies are effective in many patients, long-term treatment often leads to drug resistance through many mechanisms like re-activation of MAPK signaling and other substitute pathways[28].

Development of immune checkpoint inhibitors revolutionized the treatment of many types of cancers, including melanoma. Mechanism of action of these agents is based on the blocking of cytotoxic T lymphocyte-associated antigen (CTLA-4), a negative regulator of T-cell activation[29]. CTLA-4 is expressed on activated T cells and interacts with antigen presenting cells (APCs) through binding to B7-1 and B7-2 proteins expressed on the latter[30]. Blocking CTLA-4 with anti-CTLA-4 antibodies enhances the immune response against cancer cells, both through blocking immunosuppression on activated T cells and regulatory T cells[29]. In 2011 first anti-CTLA4 antibody ipilimumab was approved by the FDA for the treatment of unresectable or metastatic melanoma[29].

Another target of immune checkpoint inhibitors is programmed cell death protein -1 (PD-1). PD-1 is expressed on activated T cells and on B cells and binds to ligands: PDL-1 and PDL-2 expressed on somatic cells. As a result, anti-self-responses are suppressed what prevents autoimmunity[31]. Cancers are using this pathway to escape anti-tumor immunity response[1]. There are two anti-PD-1 antibodies approved for melanoma treatment: nivolumab and pembrolizumab. Adverse effects of immune checkpoint inhibitors therapies can be severe and include endocrinopathies and skin toxicity[29]. Anti-PD-1 antibodies give severe adverse effects less frequently than anti-CTLA-4 antibodies and additionally display a higher overall response rate in patients (ORR; 40% for nivolumab and pembrolizumab patients vs. 15% in patients treated with ipilimumab)[24]. Thus, the first line of treatment of metastatic melanoma is nivolumab and pembrolizumab as monotherapy and they are sometimes administrated in combination with ipilimumab[24].

There are also experimental therapies based on the treatment of melanoma patients with infusions with autologous tumor-specific T cells. This approach is based on the isolation of tumor-infiltrating lymphocytes (TIL) from the patient and their expansion *ex vivo*. Then adoptive cell transfer is performed (ACT)[32]. The same procedure can also be performed after isolation of blood T lymphocytes and their *ex vivo* transduction with viral vectors harboring transgenic T-cell receptors[32]. Although promising, these therapies are very expensive and can be conducted only in specialized health centers thus they still have the status of experimental therapy[4].

1.1.5. Heterogeneity of melanoma

Treatment of advanced melanoma is very difficult, and at this stage melanoma is practically incurable. The main reason for this difficulty is the exceptionally high level of heterogeneity displayed by melanoma cells[33]. Heterogeneity is described as co-existence of cells with different molecular and phenotypic features within the same tumor (intratumor heterogeneity) or between primary lesions and metastases or different metastases within the same patient (intertumor heterogeneity)[34]. One of the example of genetic intratumor heterogeneity in melanoma is the co-existence of mutually exclusive BRAF and NRAS mutations within the same tumor[35]. Additionally, BRAF mutations can be heterogeneously expressed between primary tumor and metastases[36,37] and between different metastatic sites of the same patients[38]. This phenomenon contributes to drug resistance against targeted therapies.

Many different factors like tumor microenvironment, metabolic conditions or oxygen supply, influence melanoma heterogeneity[39,40]. As a result, scientists observe heterogeneous

expression of genes depending on what signals the tumor cells were exposed to. In melanoma, these genes were described to be involved in cell cycle[41], invasive phenotype (e.g. microphthalmia associated transcription factor MITF, metalloproteinase-1 MMP-1)[41,42], signaling pathways (e.g. Nodal, PTEN)[43,44], expression of growth factor receptors (e.g. erythropoietin receptor EPO-R)[45], genes involved in the regulation of immune response (cyclooxygenase-1 and PDL-1)[46], expression of melanoma-associated markers (e.g. tyrosine related protein-2 TRP-2)[47] and many others. Presence of so many cells with different gene profile expressions, different mutations, and different behavior, pose a big problem in melanoma diagnosis and treatment. Due to this heterogeneity a single biopsy might not be sufficient to obtain the whole picture of mutations occurring within the lesion, which can lead to problems in choosing the right therapy[34].

1.2. Clonal evolution and cancer stem cells models

The heterogeneity of tumors is explained by two different models. The older model of cancer progression is called 'stochastic model' or 'clonal evolution model'. In this model, cancer is thought to arise from somatic cells that gained several mutations making them malignant[48]. Every cell within the tumor is tumorigenic and proliferate extensively, giving rise to different clones[49] (Fig. 1.2).

The second model that aims at explaining tumor heterogeneity is the cancer stem cell (CSC)/cancer initiating cell (CIC) model. This model assumes that within the tumor there is a fraction of cells able to self-renew through asymmetrical or symmetrical divisions[50]. CSCs give rise to all lineages of more differentiated, proliferating tumor cells that maintain tumor growth. However, only CSCs are able to initiate tumor growth after transplantation to immunocompetent recipients and re-establish tumor heterogeneity (Fig. 1.2). Thus, the gold standard for the identification of human CSCs is to perform serial xenotransplantations of putative CSC subpopulations at limiting dilutions into immunocompromised mice[51]. Primary tumors need to be isolated and tumor cells are transplanted to secondary and tertiary recipients[51].
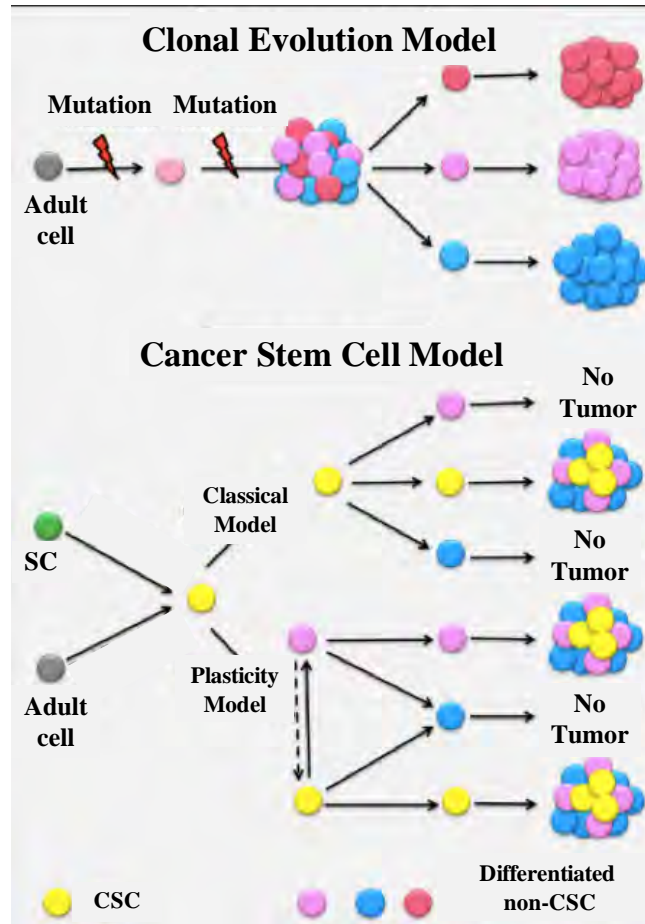
Figure 1.2. Scheme of clonal evolution and CSC model in tumor progression. From: Afify et al. *Cancers* 2019.

CSCs are thought to arise from mutations in normal stem cells but they can also be formed from transiently-amplifying progenitor cells[52]. This model is unidirectional, where the only source of heterogeneity and hierarchy is the presence of CSCs[53]. However, there is a relatively new concept in which CSC can be formed by differentiated non-CSC through de-differentiation[48]. In this new model, CSCs are a dynamic population that transiently display CSC-like phenotype depending on the signals from the environment[53]. One of the pathways involved in the de-differentiation of non-CSC is the epithelial-to-mesenchymal transition (EMT) that generates cells with stem cell properties[54]. Also, epigenetic changes characteristic for cancers can activate the expression of genes important for de-differentition[53]. Generation of induced pluripotent stem cells (iPSC) by introducing the pluripotency transcription factors (Oct-4, Klf-4, Sox-2, c-Myc) proves that the de-differentiation process of somatic cells into stem cells is possible[53]. Additionally, all four transcription factors that are used for the generation of iPSC are oncogenes that further emphasize the link between oncogenesis and reprograming[55].

CSCs were first identified in the 1990s in acute myelogenous leukemia (AML) where cell population with the $CD34^+CD38^-$ phenotype was able to recapitulate AML after transplantation to immunodeficient mice[56]. Soon after their description in AML, CSCs were characterized in many solid cancers: breast[57], melanoma[58], brain[59], gastric[60], prostate[61], lung[62], osteosarcoma[63], ovarian[64], and others. CSCs are usually described as quiescent cells, resistant to conventional chemo- and radiotherapies[49]. They are often marked by cell surface antigens (e.g. CD44[60], CD133[65]) or are characterized by more functional markers like high activity of aldehyde dehydrogenase (ALDH)[66] or the ability to efflux Hoechst dye through drug efflux pumps on the surface of cells[67].

1.3. Melanoma initiating cells (MIC)

1.3.1. CD20 antigen

In 2005, first reports describing cells with CSCs properties in melanoma were published. Fang et al. discovered that when melanoma cells are cultured as non-adherent melanospheres in the embryonic medium they are able to differentiate into melanocytic, osteogenic, adipogenic, and chondrogenic lineage[58]. Melanospheres were shown to be enriched in cells expressing hematopoietic marker CD20 and were highly tumorigenic when compared to adherent cells. Thus, researchers suggested that stem cells reside within a $CD20^+$ fraction[58]. Interestingly, experimental treatment of advanced-stage melanoma patients with anti-CD20 antibody rituximab showed a promising therapeutic value by increasing disease-free interval and causing regression of the metastasis[68,69].

1.3.2. ABCB5 transporters

In the same year as the CD20 population was described, Frank et al. identified cell population expressing ATP-binding protein ABCB5, with stem cell properties, responsible for chemoresistance in human melanoma[70]. Targeting $ABCB5^+$ inhibited the growth of human melanoma in xenotransplantation assays[71]. Cells expressing ABCB5 were shown to control their slowly cycling phenotype and chemoresistance through pro-inflammatory IL-1β/IL8/CXCR1 cytokine signaling circuit[72].

1.3.3. Side population

Side population (SP) is a functional marker of CSCs and describes subpopulation of cells capable of efflux Hoechst 33342 dye as well as anticancer drugs. These cells were identified in many cancer types and are thought to be responsible for multidrug resistance[73]. In

melanoma, SP was shown to be more tumorigenic than bulk population when transplanted into immunocompromised mice[74]. Through overexpression of ABCB1 and ABCB5 transporters and activation of other signaling pathways (e.g. NF-κB and IL-8) SP is responsible for chemoresistance in melanoma[75]. Recently, a pluripotency transcription factor SOX-2 was reported to induce ABCB1 expression in SP, leading to resistance against paclitaxel[76].

1.3.4. CD133 antigen

Another MIC subpopulation with enhanced tumorigenic potential was shown to express the CD133 antigen. It is worth noting that CD133$^+$ subpopulation isolated from the human melanoma cell line co-expressed another CSC-associated marker ABCG2. These cells were able to form spheres and differentiated into astrocytes and mesenchymal linage[77]. Downregulation of CD133 in human melanoma cells decreased their capacity to sphere formation and reduced their metastatic potential[78]. Interestingly, more recent studies showed that CD133$^+$ and CD133$^-$ subpopulation do not differ in terms of tumorigenicity but they have different characteristics – CD133$^+$ are more proliferative while CD133$^-$ more invasive[79]. A meta-analysis of 5 studies that checked CD133 expression in melanoma samples using immunohistochemistry (IHC) revealed that CD133 is highly expressed in around 48% of cancers and should be rather used together with other putative CSC marker for identification of CSCs than alone[80].

1.3.5. CD271 antigen

Cells isolated from melanoma patients that expressed the receptor for nerve growth factor (NGFR, CD271) were shown to be highly tumorigenic after transplantation to immunocompetent mice when compared to CD271$^-$ subsets[81]. The same study showed that majority of tumors formed by CD271$^+$ cells lacked typical melanoma-associated antigens tyrosinase (TYR) and melanoma antigen recognized by T cells (MART-1) what could explain the resistance of melanoma toward T cell-targeted therapies[81]. Additionally, CD271$^+$ cells were shown to be responsible for the long-term growth of human melanoma[82]. CD271 was also identified as a regulator of phenotype switch in melanoma, where low expression of CD271was associated with more proliferative state while high expression with a more invasive and migratory phenotype[83,84]. It is important to notice that there are reports describing CD271 as an imperfect MIC marker. Both CD271$^+$ and CD271$^-$ cells were shown to be capable of forming tumors in the study where several previously published protocols for cell isolation and processing were checked[85].

1.3.6. Aldehyde dehydrogenase activity

High activity of ALDH is regarded as a marker of CSC in many tumor types (e.g. breast cancer, ovarian cancer)[86], including melanoma[87]. ALDH catalyzes the oxidation of aldehyde substrates to their corresponding carboxylic acids[86]. The ALDH1A1 isoform was shown to mark cells with enhanced tumorigenicity and resistance toward therapeutic agents in human melanoma[87]. On the other hand, there are studies demonstrating that ALDH+ and ALDH- cells isolated from human melanoma have a similar tumorigenic potential when transplanted to NOD-SCID Il2rg$^{-/-}$ (NSG) mice and do not differ in sensitivity to drugs[88]. Moreover, high expression of ALDH1 in malignant melanoma cells correlates with better prognosis in patient survival[89]. These discrepancies between different studies might be caused by differences in methodologies and data interpretation[90].

1.3.7. Slowly cycling cells

One of the features attributed to normal and cancer stem cells is a slow proliferation rate[91]. It was reported that slowly cycling cells in melanoma have high expression of epigenetic enzyme – histone 3 K3 (H3K3) demethylase JARID1B[92]. Another epigenetic enzyme that was identified as an important regulator of slowly cycling cells in melanoma is Tet methylcytosine dioxygenase 2 (TET2)[93]. Recently, using label-retaining technique, researchers identified label-retaining melanoma cells (LRC) and showed that they are highly invasive and disseminate from primary tumor mass at early stage[94]. From the clinical point of view, studies on slowly cycling cell subpopulation are critical for understanding the high reoccurrence of the disease, as chemo- and radiotherapies target highly proliferative cells[91].

1.3.8. Controversies around MIC

In 2008, only three years after the identification of first MIC subpopulation, Quintana et al. published a paper in which they undermined the existence of CSCs in melanoma[95]. They proved that changes in xenotransplantation assay can increase the observed tumorigenicity of melanoma. They used highly immunocompromised NSG mice and transplanted them with different numbers of melanoma cells obtained directly from patients. Their results showed that as much as 27% of single cells, unselected for any MIC marker, are able to form tumors in NSG mice[95]. As a continuation of this study, the same group performed a broad analysis of the tumorigenic capacity of melanoma cells expressing different MIC markers[96]. They found out that melanoma cells are highly tumorigenic regardless of the MIC marker expressions. Analysis of 22 subpopulations of cells, including ABCB5$^{+/-}$, CD271$^{+/-}$ and CD44$^{+/-}$ subsets, showed that

melanoma is not hierarchically organized, what is the assumption of classical CSC model. Instead, cells were able to switch on and off the expression of markers what indicated that heterogeneity of melanoma might be caused by phenotypic plasticity of the cells[96]. However, according to Robert Weinberg, the fact that CSC and non-CSC are convertible does not mean that the CSC does not exist – these populations can be regarded as phenotypically and functionally distinct subsets in the cancer population at any given moment[97].

Another study revealed that the human melanoma contains a large fraction of tumorigenic cells independent of the expression of several MIC markers[98]. Moreover, co-injection of CSC$^-$ and CSC$^+$ melanoma cells (based on CD271 marker) into NOD/SCID mice showed that both fractions of cells contribute to tumor formation[99]. The same study uncovered that CSC$^-$ can give rise to CSC$^+$ cells when cultured from single cells[99].

The reason for such a big difference between the postulated numbers of tumorigenic cells in particular experiments lays in the differences in methodology. It is known that when human cells are transplanted into the mouse they are exposed to a foreign microenvironment, including different growth factors and host immune cells, and this influences the frequency of CSC, underestimating their number[100]. Also, the co-injection of cells with Matrigel increases the frequency of CSCs in xenotransplantation models[95]. Additionally, the level of immunocompetence of the host affects the observed tumorigenicity, with the more immunocompromised mice showing the higher frequencies of CSCs[95]. All of this does not definitely implicate whether melanoma follows or not the CSC model, but it explains that the CSC studies must be interpreted with a great caution and with regards to the animal models used for transplantation.

It is also important to mention that the niche of CSCs is crucial for the regulation of their behavior. Thus, all CSC experiments that are devoid of the niche context may not detect all physiological functions of these cells[100]. Syngeneic transplantation of AML cells showed that tumorigenic cells are not rare[101]. Using primary murine melanomas Held et al. identified the population of CD34$^+$p75$^-$ cells that were able to propagate tumors from single cells[102]. The data, where side-by-side xenotransplantations of human cells into NON/SCID mice and NSG mice were performed, show that the NK cells might be crucial for inhibiting tumor growth because melanoma injected to NSG mice lacking NK cells displayed a 100-fold increase in tumorigenic cell frequencies[95,103]. Having in mind how important an intact immune system is for MIC studies there is a need for further characterization of the biology of these cells in syngeneic systems. Moreover, as cells with CSC properties seem to play an important role in

melanoma heterogeneity and chemoresistance (regardless whether or not these cells are rare) it is very important to define the factors that regulate their behavior.

1.4. Heme oxygenase-1

Heme oxygenase-1 (HO-1), also known as heat shock protein 32 (Hsp32), is a heme degrading enzyme that plays important role in many physiological and pathophysiological settings, including cell response to oxidative stress, cell differentiation, and tumorigenesis. It catalyzes the degradation of heme to carbon monoxide (CO), ferrous ions (Fe^{2+}), and biliverdin (Fig. 1.3)[104]. HO-1 was first described in 1990 in human skin fibroblasts as a 32-kDa stress protein[105]. There are two main isoforms of heme oxygenase: inducible HO-1 and constitutively expressed HO-2. While the HO-2 is expressed mainly in the brain[106], the expression of HO-1 can be triggered by many stressors in many cell types[104]. Expression of HO-1 is induced not only by its substrate heme[107] but also by UVA radiation[105], reactive oxygen species (ROS)[108], heavy metals[109], prostaglandins[110], hypoxia[111], cytokines[112], nitric oxide (NO)[113] and lipopolysaccharide (LPS)[114] (Fig. 1.3).

HO-1 is anchored to endoplasmic reticulum (ER) where it displays catalytic activity, but can also be found in the nucleus where its role is still not fully known. Nuclear HO-1 was suggested to regulate the expression of oxidative stress enzymes[115] and to stabilize the nuclear factor erythroid 2-related factor 2 (Nrf-2), a transcription factor that regulates expression of many antioxidants proteins, including HO-1[116]. Additionally, HO-1 can localize in mitochondria[117] and in caveolae[118].

The cytoprotective outcomes of HO-1 activity are caused by removal of excess heme and production of the heme-degradation metabolites (Fig.1.3)[119]. Activated HO-1 can reduce oxidative stress, diminish immune response, decrease apoptosis, and affect angiogenesis[104]. The release of Fe^{2+} increases the expression of iron-chelating protein ferritin and activates the membrane transporter Fe-ATPase. This mechanism decreases the level of intracellular Fe^{2+} and protects cells against free radicals produced during Fenton reaction[119]. The second product of HO-1 activity, carbon monoxide, is exhaled by lungs but at the same time, it can act as a signaling molecule. CO induces soluble guanyl cyclase (sGC)[120] causing elevation of cGMP levels and subsequent vasorelaxation, induction of p38-MAPK pathway, inhibition of platelet aggregation, stimulation of blood vessels formation, and many others[104]. Through the reduction of pro-inflammatory cytokines (like TNF and IL-1ß), CO might play a role in the inhibition of inflammantion[121]. At low concentrations, CO binds reversibly to cytochrome c oxidase (COX), where it affects mitochondrial respiration and increases the production of ROS on complex

III[122]. Elevated ROS activate Nrf2 transcription factor pathway involving induction of nuclear respiratory factor 1 (NRF-1) which co-operates with nuclear respiratory factor-2α (NRF-2α) and peroxisome proliferator-activated receptor γ co-activator 1 alpha (PGC1α) what at the end leads to induction of expression of mitochondrial transcription factor A (Tfam)[123]. Tfam is a master regulator of mitochondrial biogenesis and in this way, HO-1/CO axis stimulates mitochondrial biogenesis[124]. Biliverdin, the third product of HO-1 activity, is converted to bilirubin by biliverdin reductase. Bilirubin displays anti-inflammatory and anti-apoptotic activity[125,126], protects cells from lipid peroxidation[127] and acts as a scavenger of hydroxyl radical, singlet oxygen, and superoxide anions[128].
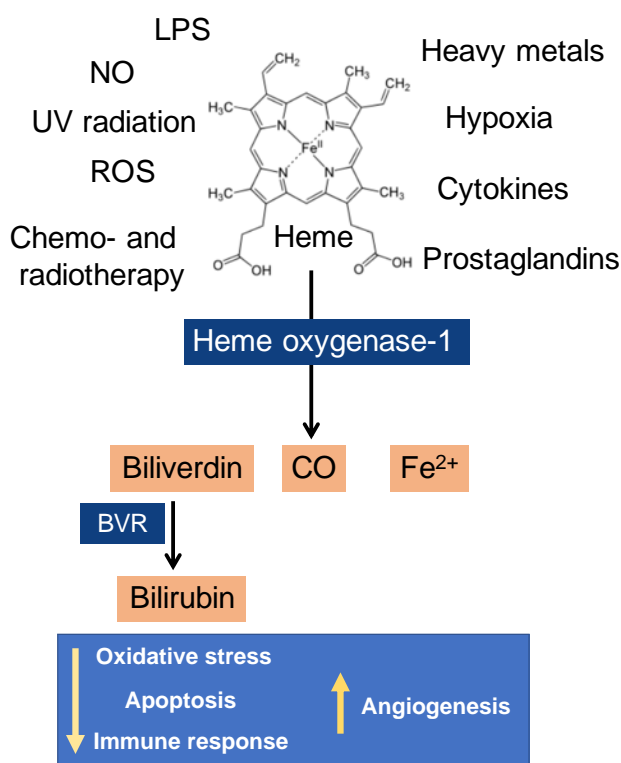
Figure. 1.3. Scheme of HO-1 induction and activity

1.4.1. HO-1 in cancer biology

All of the cytoprotective functions of HO-1 might become problematic when hijacked by tumor cells. HO-1 is often overexpressed in cancerous cells when compared to the corresponding healthy tissues[129,130] and is further induced by chemo-, radio- and photodynamic therapies[131]. Expression of HO-1 is also activated by oxidative stress in cancer tissues and by cancer stromal cells[132]. HO-1 can be also upregulated by oncogenes like oncogenic G protein-coupled receptor (vGPCR)[133], BCR/ABL[134], and fusion transcription factor Pax3/7-FoxO1[135]. Interestingly, the final outcome of HO-1 activity in tumors is cell-type dependent[136].

High HO-1 expression is correlated with poor prognosis in non-small lung carcinoma[137] and was shown to increase chemoresistance in neuroblastoma[138], breast cancer[139], laryngeal squamous cell cancer[140], lung cancer[141], urothelial cancer[142], hepatoma[143], and many others[119]. Inhibition of HO-1 was shown to be able to sensitize some cancer types to chemo- and radiotherapies[144] as well as photodynamic therapies[145] what makes this enzyme a promising target in cancer treatment. HO-1 acts on cell proliferation depending on the tumor type, for example, it can enhance proliferation in prostate cancer[146] and melanoma[147] but exerts anti-proliferative effect in lung adenocarcinoma and breast cancer[104].

It seems that the localization of HO-1 is important in the context of tumor aggressiveness. Nuclear localization of HO-1 is associated with tumor migration and invasiveness in non-small cell lung carcinoma and cervical cancer[148] and is also associated with tumor progression in prostate cancer[149] and head and neck squamous cell carcinoma[150]. The mechanisms by which HO-1 translocates to the nucleus is based on the activity of signal peptide peptidase that catalyzes the intermembrane cleavage of the HO-1[148]. Interestingly, the tumorigenic effects of nuclear HO-1 were shown to be independent of its enzymatic activity[148].

Recently, it has been demonstrated that HO-1 can act on tumors via regulation of microRNAs, the small non-coding RNA molecules that regulate the expression of genes by inhibiting the translation of complementary mRNA. Overexpression of HO-1 can slower progression of hepatocellular carcinoma through downregulation of oncogenic microRNA, including miR-30d and miR-107[151]. In lung mucoepidermoid carcinoma HO-1 inhibits tumor growth through downregulation of miR-378 and matrix metalloproteinases[152]. In another type of lung cancer, non-small cell lung carcinoma, overexpression of HO-1 leads to downregulation of miR-378, causing decreased proliferation, migration of cells and formation of smaller tumors *in vivo*[153]. Overexpression of HO-1 inhibits myoblasts differentiation through inhibition of cEBPδ-dependent transcription of myoD, and downregulating of myogenic microRNA (Myomirs)[154]. In pathological settings, HO-1 is overexpressed in the more aggressive, alveolar type of rhabdomyosarcoma (RMS) when compared to the embryonic type of this tumor[135]. Inhibition of HO-1 in RMS activates myogenic differentiation via miR-206 activation[119].

Formation of new blood vessels is crucial for the nutrition of tumors and metastasis of cancer cells. HO-1 stimulates expression and activity of vascular endothelial growth factor (VEGF), a master regulator of angiogenesis[155]. Additionally, HO-1 mediates the pro-angiogenic effects of stromal cell-derived factor 1 (SDF-1)[156]. It was shown that overexpression of HO-1 increases tumor angiogenesis *in vivo* in human pancreatic cancer transplanted to immunodeficient mice[157]. Blocking HO-1 activity with zinc protoporphyrin IX (ZnPPIX)

inhibits angiogenesis in colorectal cancer[158] and gastric cancer[159]. In mouse lung cancer cells ZnPPIX caused a reduction in VEGF concentration in tumors and decreased microvessels density[160]. Inhibition of HO-1 with ZnPPIX in urothelial carcinoma of the bladder decreased angiogenesis *in vivo* by suppressing VEGF and hypoxia-inducible factor 1-α (HIF-1α)[161]. The opposite effect of HO-1 on tumor angiogenesis was found in prostate cancer, where HO-1 overexpression led to the downregulation of many pro-angiogenic factors including VEGF, what inhibited vascularization of prostate tumors[162].

There is a growing body of evidence showing the important role of HO-1 in the suppression of immune response toward cancers. For example, high expression of HO-1 in colorectal carcinoma suppresses expression of intercellular adhesion molecule-1 (ICAM-1) and CXCL10 what inhibits antitumor immunity[163]. The reduction of HO-1 was shown to mediate CD8$^+$-dependent tumor cytotoxicity in breast cancer when fasting-mimicking diet was combined with chemotherapy[164]. In syngeneic model of neuroblastoma, targeting HO-1 with ZnPPIX prevented immune escape of the tumors[165]. Additionally, it was shown that regulatory T cells in glioma express high levels of HO-1, and inhibition of HO-1 with tin protoporphyrin (SnPP) preferentially eliminates Tregs[166]. Foxp3, the master regulator of Treg function, induces the expression of HO-1, what makes HO-1 a potential mediator of the immune suppression[167]. This highlights the importance of HO-1 in Treg biology. The main mediator of immunomodulatory functions of HO-1 is CO. Carbon monoxide produced by HO-1 was identified as critical for myeloid cell differentiation[168]. In prostate cancer, CO sensitizes cancer cells to chemotherapy and targets mitochondria causing metabolic exhaustion[169]. What is more, CO was shown to inhibit T cell proliferation and IL-2 secretion[170]. It was demonstrated that HO-1 plays a crucial role in macrophages expressing fibroblast activation protein-α (FAP). These macrophages are a major source of HO-1 in tumor stroma and inhibition of HO-1 led to the arrest of immune-suppression and inhibition of tumor growth, to the same extent as the depletion of FAP$^+$/CD45$^+$ macrophages alone[171].

1.4.2. HO-1 in melanoma

The role of HO-1 in melanoma is still not fully understood. However, the existing data show that this enzyme acts in favor of melanoma cells. The promoter of HO-1 is characterized by the presence of (GT)n dinucleotide repeat polymorphism where short repeats are associated with increased HO-1 expression and longer repeats with decreased expression[172,173]. In melanoma patients, the presence of shorter allele is more frequent than in healthy individuals what highlights the potential role of high expression of HO-1 in melanoma[173].

Data obtained previously by dr. Halina Waś from our group further confirm the importance of HO-1 in melanoma aggressiveness. Using B16-F10 murine melanoma as a model she overexpressed HO-1 in melanoma cells and observed increased proliferation rate of these cells and improved protection against H_2O_2-induced oxidative stress[147]. Media from HO-1 overexpressing cells stimulated the human umbilical vein endothelial cells (HUVEC) to increased proliferation and caused enhanced sprouting of capillaries from HUVEC spheroids embedded in collagen. *In vivo* experiments revealed that overexpression of HO-1 in tumor cells shortened the survival time of mice but the rate of tumor growth was not affected by HO-1. Tumors with overexpressed HO-1 contained a higher amount of capillaries than their WT counterparts what was connected with increased VEGF production[147]. Intravenous injection of B16-F10 WT and HO-1 cells resulted in the formation of metastases in lungs with an increased number of nodules in HO-1 group[147]. Altogether, these data proved that increased HO-1 in melanoma cells affects their biology.

There are many reports showing the important role of HO-1 activity in melanoma resistance against therapies. Treatment of melanoma cells with an inhibitor of heat shock protein Hsp90 was thought to be a promising therapeutic approach in melanoma but it appeared that it causes overexpression of HO-1 what serves as a chemoresistance mechanism[174]. Having this in mind Bargbagallo and colleagues combined inhibition of Hsp90 with the treatment of melanoma cells with HO-1 inhibitor (tin mesoporphyrin, SnMP)[174]. As a result, they observed augmented ER stress, apoptosis, decreased cell viability, and increased ROS production in melanoma cells. They concluded that inhibition of HO-1 potentiates the effects of Hsp90 inhibition what can serve as a potential therapeutic approach[174]. Another example of therapy where HO-1 activity was identified as an important resistance mechanism is photodynamic therapy (PDT). PDT is based on the administration of photosensitizers and their activation by light in the presence of oxygen. Photosensitizers preferentially enter tumor cells and after activation induce cell death by elevation of ROS and oxidative stress[175]. One of the agents used in PDT is a porphyrin precursor 5-aminolevulinic acid (ALA), that is metabolized via heme cycle and transformed to active protoporphyrin IX (PPIX)[145]. The activity of HO-1 was described as a protective mechanism against the cytotoxicity of PDT in tumor cells[176]. In melanoma cells, the treatment of cells with ALA strongly induces expression of HO-1 what in turn causes degradation of active PPIX. Inhibition of HO-1 was shown to sensitize melanoma cells to ALA-PDT therapy[175]. Another characterization of the role of HO-1 in melanoma resistance to therapies was conducted by Ivanov and Hei[177]. They discovered that the treatment of melanoma cells with low concentrations of sodium arsenite, the drug used in therapy of acute

promyelocytic leukemia and multiple myeloma, can induce apoptosis in melanoma cells[178]. However, the treatment of melanoma cells with arsenite-induced HO-1 expression what caused resistance of cells to apoptosis. Silencing of HO-1 using ZnPP increased apoptosis in arsenite-treated melanoma cells[177].

Recently it was demonstrated that HO-1 plays an important role in the resistance of BRAF[V600E] mutated melanoma cells against vemurafenib treatment and in melanoma immune escape[179]. Treatment of patient-derived melanoma cells with Vemurafenib induced apoptosis only in a fraction of cells and induced HO-1 expression in these that did not die. Inhibition of HO-1 with SnPP or silencing of the HO-1 gene enabled further sensitivity of melanoma to Vemurafenib. Additionally, the silencing of HO-1 restores the ability of NK cells to kill melanoma cells via the upregulation of NK activating ligands (NKp30L and NKG2DL) on the surface of the latter[179].

HO-1 was identified to be co-expressed with BRAF[V600E] in thyroid cancer[180], but until recently no data was available regarding its connection with BRAF in melanoma. Recent results obtained by Liu et al. identified the interaction of HO-1 with BRAF protein in melanoma[181]. BRAF and HO-1 were shown to be co-expressed in melanoma cytoplasm and co-immunoprecipitation assay revealed their direct protein-protein interaction. Overexpression of HO-1 increased *in vitro* and *in vivo* proliferation of melanoma cells through modulation of cell cycle proteins, while silencing of HO-1 reduced proliferation rate. It was shown that HO-1 induced BRAF/ERK signaling pathway what led to the activation of CDK2/cyclin E and induced melanoma cell proliferation[181].

Altogether, available literature highlights the importance of HO-1 in melanoma aggressiveness and resistance to treatments. Having in mind that melanoma initiating cells are crucial for the maintenance of melanoma we asked what is the role of HO-1 in MIC subpopulations.

1.4.3. HO-1 in stem cells

The role of HO-1 in CSCs is still not fully understood but it was evaluated in some types of cancers. In breast cancer, expression of HO-1 was increased in CSC subpopulation defined by CD24^{low}CD44^{high} phenotype when compared to control CD24^{high}CD44^{low} cells[182]. Additionally, HO-1 and cleaved Notch-1 are overexpressed in mammospheres when compared to adherent cells. The silencing of HO-1 results in decreased formation of mammospheres and this effect is reversed when cells are treated with HO-1 activators – CoPP and hemin. The HO-1 silencing caused a decline in expression of Notch-1, Jagged-1, and Hes1 and this was reversed

by overexpression of HO-1. Additionally, experiment with the treatment of cells with CO-releasing molecule (CORM-2) identified CO as a mediator of HO-1 action on mammosphere formation and Notch-1 induction[182]. This study unraveled the involvement of Notch-1 signaling in HO-1 mediated enhancement of CSC-properties in breast cancer cells.

The study under the role of HO-1 in AML discovered that HO-1 is overexpressed in stem cell-enriched $CD34^+/CD38^+$ and $CD34^+/CD38^-$ fractions. Moreover, the treatment of AML cells with two different HO-1 inhibitors caused the decreased cytokine-dependent proliferation of CSC fractions and decreased leukemia initiation in NSG mice[183]. This suggests that HO-1 can serve as an important mediator in AML CSC aggressiveness. Interestingly, glioma CSCs (defined as side-population) was shown to exhibit less 5-ALA-derived PPIX fluorescence than non-CSCs after treatment with ALA in photodynamic therapy[184]. It was demonstrated that the iron chelator was able to restore the fluorescence in glioma CSCs. Moreover, low PPIX fluorescence was associated with increased expression of HO-1 that accelerated the metabolism of PPIX heme. Thus, HO-1 plays an important role in ALA metabolism in glioma CSCs and using iron chelator and targeting HO-1 as additional therapy might sensitize glioma CSCs to PDT[184].

One of the important regulators of the CSC phenotype is redox state. CSCs have low levels of ROS due to their quiescent phenotype[185]. These low levels are caused not only by the low production of ROS but also can be linked to efficient scavenging systems. ROS play an important role as mediators of many signaling pathways in CSC, including PTEN/PI3K/AKT/mTOR, Notch, or Wnt pathways[185]. As HO-1 is a cytoprotective enzyme induced in tumor cells during oxidative stress it can also be an important regulator of redox state in CSCs[186]. However, its exact role in ROS signaling in CSCs is still unknown.

There are more data characterizing the action of HO-1 in normal stem cells. The role of HO-1 in hematopoiesis and differentiation of HSC is well characterized. Its activity is crucial to the response of hematopoietic stem and progenitor cells (HSPCs) to oxidative stress and regulates the balance between self-renewal and differentiation[187]. Furthermore, HO-1 is thought to be important regulator of erythropoiesis[188]. Through regulation of heme levels HO-1 takes part in B-cell maturation[189]. Recently, our group identified HO-1 as an important factor in the bone marrow niche of hematopoietic stem cells (HSC). We showed that deficiency of HO-1 in the niche causes premature exhaustion of long-term HSC[190]. In another study, we discovered that HO-1 is not critical for the function of mesenchymal stromal cells (MSC) and HO-1$^{-/-}$ MSC displayed similar phenotype, differentiation capacities and cytokines production as their wild-type counterparts. Moreover, HO-1 deficient MSC were able to efficiently react to oxidative

stress[191]. Interestingly, overexpression of HO-1 in MSC was shown to be a promising tool for enhancing their proliferation and differentiation in acute kidney injury[192]. Additionally, enhanced activity of HO-1 pushes MSC into osteogenic differentiation rather than adipogenic lineage[193]. The absence of HO-1 in induced pluripotent stem cells (iPSC) results in impaired cardiac differentiation[194].

Altogether these data highlight the important role of HO-1 in stem cell biology, both in physiological and pathological settings. Thus, we assume that this enzyme can play an important role in melanoma initiating cells.

1.5. Melanogenesis

One of the features that seems to be affected the most in stem cells by HO-1 is differentiation potential. In melanoma, melanogenesis can be regarded as an indicator of differentiation status although it is not such a straight forward connection.

Melanogenesis is the process of production of a pigmented biopolymer called melanin[195]. It is performed by melanocytes in melanosomes, the lysosome-like organelles, in a strictly regulated way[196]. The main function of melanin is photoprotection as it acts as a UV absorbent and is able to scavenge free radicals[196]. Melanocytes are functionally connected via cell-cell interaction with keratinocytes (~40 overlaying keratinocytes in the epidermis) and melanin is transported to keratinocytes in melanosomes through melanocytic dendrites. Additionally, they are also in contact with underlying dermal fibroblasts[195]. Melanosomes require the presence of many enzymatic and structural proteins, in order to mature and synthesize melanin. Critical enzymes for melanogenesis include, among others, tyrosinase and dopachrome tautomerase (also known as tyrosine-related protein 2, TRP2). Their activity affects quantity and quality of melanin production. Structural proteins in melanosomes include Pmel17 (also known as glycoprotein-100, gp100) and MART-1[196]. Also, proteins involved in sorting and trafficking of melanosomes (melanocyte-specific transporter protein OCA2, adaptor proteins AP-1, AP-2 and AP-3, and biogenesis of lysosome-related organelles complex-1 BLOC-1) play an important role in efficient melanin production[197].

In response to external signals like UV radiation and intrinsic factors secreted by keratinocytes and fibroblasts, melanocytes are stimulated to melanogenesis[198]. There are two types of melanin: eumelanin, the insoluble brown-black polymer which is mostly associated with dark skin and dark hair, and pheomelanin – the soluble red-yellow pigment that is found in red hair and freckled skin phenotype[198]. The substrate for melanin synthesis is L-tyrosine which is hydroxylated to L-DOPA (L-3,4-dihydroxyphenylalanine) by tyrosinase what serves as a rate-limiting step in melanogenesis (Fig. 1.4)[195]. L-DOPA is rapidly converted to DOPA-quinone also by tyrosinase. If cysteine is available, DOPA-quinone forms cysteinyl-DOPA which then oxidizes and polymerases to pheomelanin (Fig. 1.4). When cysteine is depleted in melanosomes, then DOPA-quinone can spontaneously cyclize and form DOPAchrome. DOPAchrome loses its carboxylic acid group and form DHI (5,6-dihydroxyindol) that oxidizes, polymerizes and forms dark eumelanin also called DHI-melanin. However, in the presence of TRP-2, the DOPAchrome does not lose its carboxylic acid and tautomerize to DHICA (DHI-2-carboxylicacid), that after oxidation and polymerization give rise to lighter brown eumelanin called DHICA-melanin (Fig. 1.4)[195].
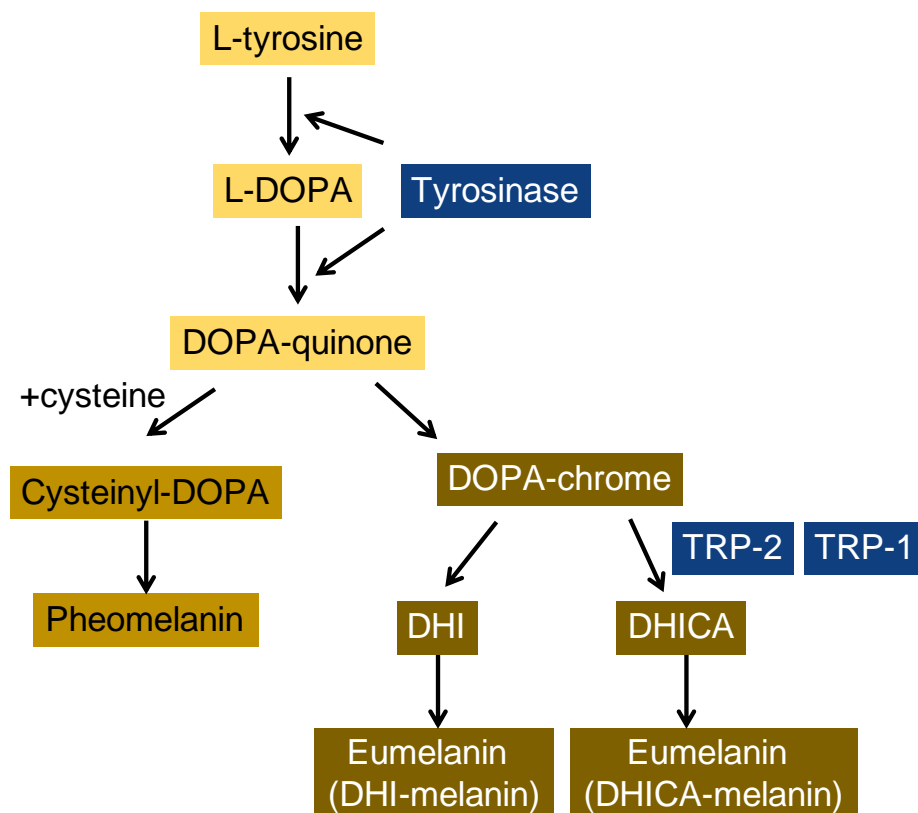
Figure 1.4. Simplified scheme of melanin synthesis.

1.5.1. Signaling pathways in melanogenesis

Melanogenesis is regulated by many signaling pathways. Melanocortin receptor 1 (MCR-1) is a membrane G-protein coupled receptor that stimulates eumelanin production when α-melanocyte-stimulating hormone (α-MSH) and adrenocorticotropic hormone (ACTH) are acting on the receptor[199]. As a response to UV radiation, keratinocytes and melanocytes upregulate proopiomelanocortin (POMC), a precursor of α-MSH and ACTH[195]. Thus, POMC serves as an important paracrine and/or autocrine stimulator of melanogenesis. Activation of MCR-1 leads to elevated cAMP levels that in turn activate expression of many genes including microphthalmia-associated transcription factor (MITF)[200].

MITF is a master regulator of melanocyte function, survival, proliferation, and differentiation[201]. It is a crucial regulator not only in melanocytes but also in melanoma cells where it is often amplificated and connected with metastatic melanoma[202]. There are several isoforms of MITF, with MITF-M restricted to melanocytic lineage[200]. Expression and action of MITF are regulated not only by activation of MCR-1 but also by many other signaling pathways including MAPK-ERK, c-KIT, WNT pathways, and the activity of SOX10, ZEB2 and PAX3 transcription factors[200,201]. Post-translational modifications of MITF protein are also important in the regulation of its activity[196]. Through binding to E-box in promoters, MITF regulates expression of main melanogenesis genes: TYR, TRP-1, TRP-2 and MART-1 thus it is regarded as a master regulator of melanogenesis[196]. Additionally, it increases expression of genes involved in cell cycle progression and proliferation (e.g. CDK2, p21)[203,204], cell survival (e.g. BCL2 and HIF1α)[205,206] or motility (c-MET)[207].

1.5.2. Melanogenesis in melanoma and its implications in differentiation status

It is important to notice that the differentiation process in the context of cancer is most probably not strictly connected to the terminal endpoint of cell fate, as it is often a case in the context of embryonic development[208]. In cancers, differentiation process should be rather regarded as a state that determines the behavior of cells. It is not always connected with lower tumorigenicity or increased sensitivity to therapies mostly due to its dynamic nature in cancers and the existence of many other factors that influence the behavior of cells, like signals from the stroma or immune response[208]. Nevertheless, studies on the differentiation are important to understand the biology and aggressiveness of the tumor cells.

High melanin content in melanoma is regarded as a poor prognostic factor in patients with metastatic disease. Melanocytic tumors are associated with shorter overall survival and

disease-free survival when compared to patients with amelanotic lesions[209]. Melanin is photo-protective in melanocytes and keratinocytes but unfortunately, it acts also as a protective agent during melanoma treatments, especially photodynamic therapy and radiotherapy[210]. Consequently, inhibition of melanogenesis was proposed as a method of increasing sensitivity to radiotherapy of malignant melanoma[210]. Interestingly, there are studies showing that mRNA expression levels of melanoma-associated antigens (MAA), TYR, TRP-2, and MART-1, were associated with favorable disease outcome in advanced-stage melanoma[211]. Moreover, decreased expression of differentiation markers is at least partially responsible for the immune escape of the melanoma, as MAA are recognized by T cells[212].

Expression of MITF, a major regulator of melanogenesis, is a driver of phenotype switch in melanoma between two distinct subpopulations with 'proliferative' and 'invasive' phenotypes[40]. These two populations have distinct profiles of gene expression, with the MITF and protein kinase receptor AXL being major phenotypic mediators. Proliferating cells are marked by MITF^{high}AXL^{low} and invasive cells by MITF^{low}AXL^{high} phenotype [41]. Proliferative cells are also marked by expression of SOX10, while invasive cells express TGF-ß and WNT5A[213,214]. Both phenotypes can be switched on and off within the same cell through intermediate transition state[215]. Pigmentation of melanoma is prone to phenotype switch[216,217]. Pinner et al. found a highly invasive subpopulation of melanoma cells characterized by no or low pigmentation accompanied by high levels of Brn2, a repressor of MITF. These cells were described as highly motile and less differentiated, resembled melanoblasts, and were able to re-differentiate in secondary tumor sites[217].

Methotrexate (MTX), a differentiating agent and competitive inhibitor of dihydrofolate reductase (DHFR), is able to induce differentiation of melanoma cells by induction of MITF[218]. Increased MITF activity leads to the upregulation of tyrosinase what is the basis for the treatment of cells with the second agent – 3-O-(3,4,5-trimethoxybenzoyl)-(-)-epicatechin (TMECG). Tyrosinase metabolizes TMECG to quinone methide TMECG (TMECG-QM) what further inhibits DHFR. As a result of this combined treatment (MTX + TMECG) melanoma cells die through E2F1-mediated apoptosis both *in vitro* and *in vivo*[218]. This is an example of using directed phenotype switching and differentiation in melanoma treatment.

Altogether, available data suggest that the differentiation associated with melanogenesis affects melanoma behavior. It is connected with phenotype switch between a more pigmented, proliferating, more differentiated cells and de-differentiated invasive cells[41,217]. It is interesting that the presence of melanin in melanoma cells, although connected with more differentiated and less invasive phenotype, can be problematic in the context of radio- and photodynamic

therapy[210]. Thus there is still a need for understanding factors that contribute to melanogenesis both in pathological and physiological settings, and we believe that HO-1 is one of the candidates.

1.5.3. HO-1 in melanogenesis

Vast majority of literature regarding HO-1 activity in melanogenesis and melanocytes focus on the role of Nrf-2/HO-1 axis in response to oxidative stress. It was demonstrated that UVA radiation induces expression of HO-1 in melanocytes what serves as a cytoprotective mechanism[219,220]. Moreover, induction of Nrf-2/HO-1 pathway protects melanocytes against H_2O_2-induced oxidative stress[221]. Activity of HO-1 in melanogenesis was ascribed to p53 signaling pathway, where inhibition of HO-1 led to decreased expression of p53 and increased expression of tyrosinase and melanin production[222].

Recently, the activity of the Keap-1/Nrf-2/HO-1 axis was identified as a regulator of melanogenesis in human and murine melanocytes[223]. In non-stress conditions, the activity of Nrf-2 is regulated by Kelch-like ECH-associated protein (Keap1)[224]. Keap1 binds to Nrf-2 outside of the nucleus, causing its ubiquitination and preventing Nrf-2 from binding to antioxidant response elements (ARE) in promoters of oxidative stress genes. Upon oxidative stress and the induction of ROS, the interaction between Keap1 and Nrf-2 is inactivated and Nrf-2 escapes from the Keap1-mediated repression[224]. Silencing of Keap1 in human and murine melanocytes results in induction of HO-1 expression (via Nrf-2 activation), protection against H_2O_2-induced stress and induction of MITF (followed by induction of melanogenesis genes) through HO-1-associated β-catenin activation[223].

Treatment of melanocytes with glycyrrhizin, herbal medicine with antiviral and antiallergy properties, protects them from H_2O_2-induced oxidative stress via Nrf-2/HO-1 pathway[225]. Another herbal medicine, a polysaccharide from *Cistanche deserticola*, induces pigmentation in human melanocytes and simultaneously reduces oxidative stress by induction of Nrf-2 and HO-1[226]. HO-1 is also involved in oxidative stress response triggered in melanocytes by PM2.5 (particular matter 2.5)[227].

To sum up, HO-1 is described as an important enzyme in oxidative stress response in melanocytes, but there are no data on its role in melanoma melanogenesis, as well as in differentiation and melanogenesis of MIC. Moreover, it seems very interesting if HO-1 affects melanocyte differentiation from normal stem cells. Thus, we decided to study these issues.

2. Aims of the work

The main goal of this study was to evaluate how HO-1 affects the biology of melanoma initiating cells. Additionally, we investigated the influence of HO-1 on the differentiation and melanogenesis of melanoma cells and melanocytes.

To achieve the aims we decided to:

1. Assess the frequency of MIC, identified on the basis of surface and functional markers, in the B16-F10 murine melanoma cell line.

2. Analyze the influence of HO-1 on function and clonogenic potential of B16-F10 MIC cultured *in vitro*.

3. Evaluate how HO-1 affects the *in vivo* tumorigenic potential of B16-F10 MIC using serial transplantations into syngeneic immunocompetent donors.

4. Investigate the influence of HO-1 on differentiation and pigmentation of MIC, the bulk population of B16-F10 melanoma cells, melanocytes and induced pluripotent stem cells (iPSC) differentiated toward melanocytes.

3. Materials and methods

3.1. Cell cultures

3.1.1. B16-F10

B16-F10 murine melanoma cell line (ATCC) was routinely cultured in RPMI 1640 medium supplemented with 2 mM L-glutamine (Lonza), 10% inactivated fetal bovine serum (FBS; Eurx), 10 000 units/ml of penicillin and 10 mg/ml streptomycin (PEST; Sigma-Aldrich). Cells were cultured in standard conditions (5% CO_2, 37°C, 95% humidity) and passaged (1:7 – 1:10) every 2-3 days. For induction of pigmentation cells were cultured in DMEM High Glucose (Lonza) supplemented with 10% FBS and PEST. For clonogenic assays and melanosphere formation, cells were cultured in melanoma initiating cells (MIC) medium described by Stecca and colleagues[228], containing DMEM/F12 (Lonza), PEST, 0.6% glucose (Sigma-Aldrich), 1x supplement N2 (Life Technogies), 20 µg/ml human recombinant insulin (Sigma-Aldrich), 10 ng/ml basic fibroblast growth factor (bFGF; PeproTech) and 10 ng/ml epidermal growth factor (EGF; PeproTech).

The hypoxia chamber (0.5% O_2; NuAire) was used for hypoxic cultures of B16-F10 cells.

3.1.2. Melan A

Melan A murine melanocytes were ordered from St George's University of London, and cultured in RPMI 1640 (Lonza) supplemented with 10% FBS, PEST and 200 nM 12-O-Tetradecanoylphorbol 13-acetate (TPA; Sigma-Aldrich) in standard conditions (5% CO_2, 37°C, 95% humidity). For induction of melanogenesis, medium was changed to DMEM HG with 10% FBS and PEST.

3.1.3. HEK293

Human embryonic kidney cells 293 were kindly gifted by Maciej Wiznerowicz (Greater Poland Cancer Center, Poznan, Poland). HEK293 were cultured in DMEM HG supplemented with 10% FBS and PEST in standard conditions (5% CO_2, 37°C, 95% humidity). Cells were passaged when they reached around 70% confluency to prevent decrease in viral vector production.

3.1.4. Phoenix Ampho and Phoenix-Eco

Phoenix Ampho cells (ATCC) and Phoenix Eco (kindly provided by dr. Christine Brostjan, Medical University of Vienna) were used as a packaging cell line for retroviral

production. Both cell lines were cultured routinely in DMEM HG supplemented with 10% FBS and PEST in standard conditions (5% CO_2, 37°C, 95% humidity) and were passaged before reaching full confluency to avoid decrease in viral vector production.

3.1.5. HMEC-1

Human microvascular endothelial cells (HMEC-1) were obtained from Dr. Francisco Candal (Centers for Disease Control and Prevention, Atlanta). HMEC-1 were cultured in MCDB 131 medium (Gibco) containing 10% FBS, PEST, 2 mM L-glutamine, 10 ng/ml EGF and 1 µg/ml hydrocortisone (Sigma-Aldrich). Cells were cultured in standard conditions (5% CO_2, 37°C, 95% humidity).

3.1.6. Mesenchymal stromal cells (MSC)

MSC were isolated from femurs and tibia of C57Bl6×FVB $Hmox1^{+/+}$ and $Hmox^{-/-}$ mice and cultured in αMEM medium (Lonza) supplemented with 10% FBS and PEST in standard conditions (5% CO_2, 37°C, 95% humidity).

3.1.7. Tail-tips fibroblasts (TTF)

Tail-tips fibroblasts were isolated from tails of C57Bl6×FVB $Hmox1^{+/+}$ and $Hmox^{-/-}$ mice and cultured on 0.1% gelatin-coated plates (Sigma-Aldrich) in DMEM HG supplemented with 20% FBS and PEST. Cells were cultured in standard conditions (5% CO_2, 37°C, 95% humidity).

3.1.8. Induced pluripotent stem cells (iPSC)

iPSC were cultured in DMEM HG medium, 20% FBS, PEST, 1% non-essential amino acids (Gibco), 0.1 mM β-mercaptoethanol (Gibco) and 1000 U/ml murine leukemia inhibitory factor (mLIF, StemCell Technologies). Cells were cultured in standard conditions (5% CO_2, 37°C, 95% humidity).

3.2. Animals

In vivo studies under the tumorigenicity of MIC were performed on C57BL/6-Tg(UBC-GFP)30Scha/J mice (obtained from The Jackson Laboratory). *In vitro* experiments with the usage of MSC (HO-1 WT and KO) and TTF (HO-1 WT and KO) cells were performed on isolated tissues from C57Bl6×FVB $Hmox1^{+/+}$ and $Hmox^{-/-}$ mice or C57Bl6×FVB $Hmox1^{+/+}$ and $Hmox^{-/-}$ constitutively expressing GFP (kindly gifted by Dr. Anupam Agarwal, University of

Alabama). Mice were bred in SPF (Specific Patogen Free) animal facility at the Faculty of Biochemistry, Biophysics and Biotechnology of Jagiellonian University. Mice were kept in individually ventilated cages (IVC) and were regularly monitored according to Federation of European Laboratory Animal Science Association (FELASA) recommendations. All procedures were approved by the Local Institutional Animal Care and Use Committee (approval number 139/2015).

3.3. Generation of stable cell lines

3.3.1. Generation of B16-F10 cell line stably expressing firefly luciferase transgene

Stable expression of the firefly luciferase gene (Luc) was obtained by the lentiviral transduction of B16-F10 cells. For this purpose we used pLenti PGK V5-Luc Neo vector, containing the gene of resistance toward the neomycin and firefly luciferase transgene (Fig. 3.1 A; Addgene) Lentiviruses (LVs) were produced in human embryonic kidney cells HEK293 (seeded at a density of 2.7 million per 6 cm culture dish, in DMEM CM). Next day after seeding, the cells were transfected with two solutions (Fig. 3.1 B). For proper viral particles assembly we used packaging plasmids: pMD2.G coding envelope proteins of the lentiviral vector (Addgene; Fig. 3.1 C) and psPAX2 (coding core proteins and reverse transcriptase; Addgene; Fig. 3.1. D). Solution B was added to solution A, mixed, and incubated 15 minutes in room temperature (Fig. 3.1 B). Mixture was added dropwise on HEK293 cells and medium with lentiviruses was collected after 48 h culture. The medium was filtered (0.45 μm PVDF filter unit, Merck), added to fresh RPMI medium (in 1:1 ratio) and used for infection of B16-F10 cells. B16-F10 were transduced on 24-well plates, 2 ml medium of with LVs was added per well and cells were incubated 48h with LVs in standard conditions (5% CO_2, 37°C, 95% humidity). After this time we removed medium with LVs and started selection of successfully infected cells with RPMI CM supplemented with 0.8 mg/ml G418 (CytoGen GmbH). Control cells started to die 5 days after the selection agent was introduced. In order to obtain a stable cell line, single transduced cells were sorted on 96-well plates for clonogenic growth using MoFlo sorter (Beckman Coulter). Clones were checked for luciferase activity using In Vivo Imaging System (IVIS) Lumina (PerkinElmer) and positive clones were pooled and regarded as stable cell line (WT Luc) for further experiments.

A.

B.

Solution A	
150 mM NaCl	208 ul
pLenti PGK V5-LUC Neo (Addgene)	4 µg
packaging plasmid psPAX2	5.7 µg
envelope expressing plasmid pMD2.G	2.3 µg
Solution B	
150 mM NaCl	208 µl
Polyethyleneimine (MW 25000, Polysciences Inc.)	12 µl

C.

D.

Figure 3.1. Generation of B16-F10 WT Luc cell line **A.** Map of the pLenti PGK V5-Luc Neo plasmid (Addgene). **B.** Composition of transfection mix for production of LVs. **C.** Map of the pMD2.G packaging plasmid (Addgene). **D.** Map of the psPAX2 packaging plasmid (Addgene).

3.3.2. Generation of B16-F10 cell line stably overexpressing HO-1

B16-F10 WT Luc cells were transduced with retroviral vectors (RVs) harboring HO-1 transgene under the CMV promoter. The pBABE-Puro-HO-1 plasmid was previously prepared by dr. Agata Szade and dr. Jacek Stępniewski for the purpose of other experiments, by cloning HO-1 transgene into the pBABE-Puro plasmid (Fig. 3.2 A; Addgene). RVs were produced in Phoenix-Ampho cells (ATCC). Transfection of packaging cells and RVs production was performed as described in chapter 3.3.1 for lentiviral vectors, but there were different plasmids used (Table 3.1). Newly transduced B16-F10 HO-1 Luc cells were selected using 2 µg/ml puromycin (Sigma-Aldrich). After 6 days there were no viable cells in control. The overexpression of HO-1 was confirmed at mRNA and protein levels and with HO-1 activity assay (Fig. 3.2 B-D).
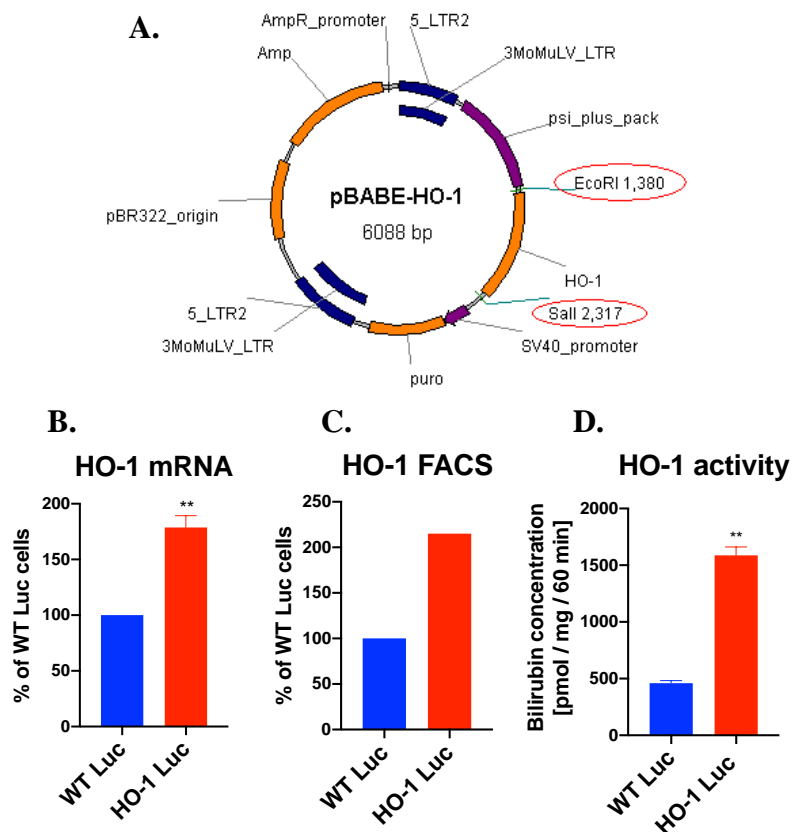
Figure 3.2. Generation of B16-F10 HO-1 Luc cell line. **A.** Map of pBABE-HO-1 plasmid **B.** Detection of HO-1 mRNA (qRT-PCR). **C.** Detection of HO-1 protein (representative FACS analysis). **D.** Measurement of HO-1 activity (bilirubin production assay). Data presented as mean±SD; ** $p < 0.01$. Results obtained with help of Agnieszka Seretny and Rościsław Krutyhołowa).

Solution A	
150 mM NaCl	208 ul
pBABE-PURO-HO-1	4 µg
packaging plasmid pM13	1 µg
Solution B	
150 mM NaCl	208 µl
Poliethyleneimine (MW 25000, Polysciences Inc.)	5 µl

Table 3.1 Transfection mix for RVs production.

3.3.3. Generation of B16-F10 HO-1 GFP Luc cell line

In some experiments we used B16-F10 HO-1 GFP Luc cell line. This cell line was established by dr. Halina Waś in the course of her research. Briefly, B16-F10 cell were transduced using RVs harbouring GFP-Luc transgene (pBMN-luc-GFP plasmid). In the next step, B16-F10 GFP Luc cells were introduced with HO-1 transgene (pLNCX-HO-1), also with RVs.

3.3.4. Generation of B16-F10 with silenced HO-1 with RVs

B16-F10 cells with silenced HO-1 (B16-F10 shHO-1) were established by Rościsław Krutyhołowa. Cells were generated in the same way as Melan A cell line with silenced HO-1 described below in the 3.3.5 chapter.

3.3.5. Generation of murine melanocytes Melan A with silenced HO-1 with RVs

For the silencing of HO-1 in Melan A cells, we used *Hmox-1* mouse shRNA (OriGENE, TF500966) (Fig. 3.3 and Table 3.2). Phoenix-Eco packaging were transfected independently with five different plasmids (four variants of shHO-1 and one scrambled control). Transfection was performed as described above using the mix from Table 3.1. but with shHO-1 and scrambled control plasmids. After 24 hours, the transfection medium was changed for DMEM CM supplemented with 25 mM HEPES. The next day, medium with RVs was collected and filtered (0.45 µm PVDF filter unit, Merck). Media with RVs were mixed in the 1:1 ratio with fresh culture medium with addition of polybrene (8 µg/ml final concentration, Sigma-Aldrich). Melan A cells were transduced on 24-well plates (2 ml of medium with RVs was added per well, cells were incubated 48h with RVs in standard conditions). For the selection of transduced

cells, 1 µg/ml puromycin was used. After 5 days of puromycin selection, all control Melan A cells died.
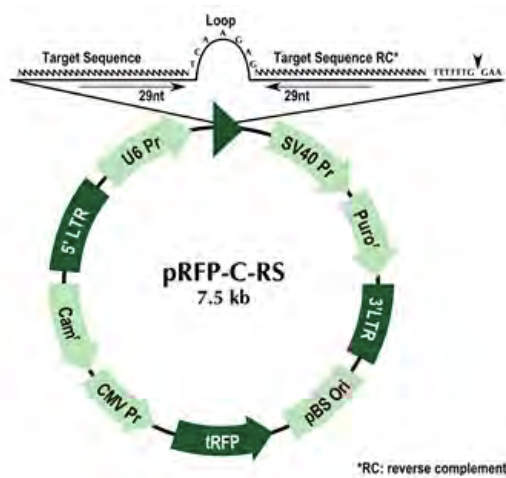
Figure 3.3. Map of plasmid used for production of RVs.

Name of plasmid	Sequence
shHO-1 A	TACACATCCAAGCCGAGAATGCTGAGTTC
shHO-1 B	ACACAGCACTATGTAAAGCGTCTCCACGA
shHO-1 C	TCTATCGTGCTCGAATGAACACTCTGGAG
shHO-1 D	TCACTCTCAGCTTCCTGTTGGCAACAGTG
scrambled	Non-targeting

Table 3.2. *Hmox-1* silencing sequences in plasmids.

3.4. Proliferation and viability test of Melan A cell lines

Melan A cells were seeded at the density of 50,000 cells/well, in 12-well plates (in duplicates for every timepoint: 24 h, 48 h, and 72 h). Cells were cultured in the RPMI CM with 200 nm TPA or in the DMEM CM. After 24 h incubation, cells were trypsinized and stained (5 minutes, room temperature, in the dark) with the Cell Count And Viability Test (Millipore) and counted using the Muse Cell Analyzer (Millipore).

3.5. Seahorse XF Cell Mito Stress Test

The Seahorse XF Cell Mito Stress Test (Agilent Technologies) was performed according to the vendor's protocol (overview Figure 3.4). Briefly, one day prior the assay, cells were seeded on the Seahorse XF Cell Culture Microplate (Agilent Technologies) at the density of 10,000 cells/well for B16-F10 and 20,000 cells/well for Melan A cells. Cells were seeded in pentaplicates in the proper culture media. Assay was performed in DMEM medium supplemented with 1 mM pyruvate, 2 mM glutamine, and 10 mM glucose (all from Sigma-Aldrich). This medium was devoid of buffering agents and was calibrated for pH=7.4. Additionally, media were supplemented with the following concentrations of inhibitors: 1 µg/ml oligomycin, 750 nM carbonyl cyanide-4-(trifluoromethoxy)-phenyl-hydrazone (FCCP) or 500 nM antymicin (all from Sigma-Aldrich). The Seahorse instrument was prepared according to the vendor's protocol. The test was run using the Agilent Seahorse analyzer and data were analyzed with the Wave Software.
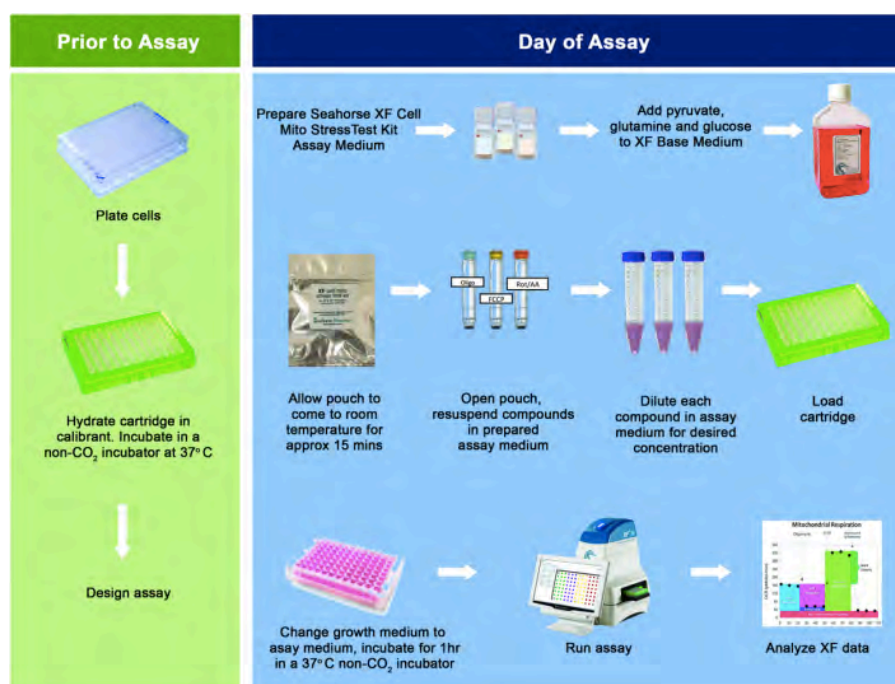
Figure 3.4. Overview of Seahorse XF Cell Mito Stress Test (From: Agilent Technology User Guide).

3.6. Detection of cell surface markers using flow cytometry

In order to recognize co-expression of MIC markers, B16-F10 cells were stained for several antigens simultaneously, while fluorescence minus one (FMO) samples were used as controls. After 48 h of culture in normoxia (21% O_2) or hypoxia (0.5% O_2) cells were detached using Accutase (Sigma-Aldrich) and counted using Bürker chamber. For each staining, 1×10^6 cells were centrifuged in a FACS tube (250 g, 5 minutes, 4°C) and pellets were re-suspended

in 100 µl of staining buffer: phosphate buffer saline (PBS) without Ca^{2+} and Mg^{2+} (Lonza) supplemented with 2% FBS and 0.2 µg/ml 4',6-diamidino-2-phenylindole (DAPI; Sigma-Aldrich). Stainings were performed with antibodies listed in Table 3.3. Additionally, cells were stained for vasculogenic mimicry (VE) markers accordingly to the same staining protocol. The analysis was performed using BD LSR II (BD Bioscience) flow cytometer.

For the detection of ABCB1 and ABCB5 we performed staining with primary and secondary antibodies. One million of cells were first stained (20 minutes, 4°C) with primary antibodies (Table 3.3), washed with PBS and centrifuged (250 *g*, 5 minutes, 4°C). Pellets were re-suspended in 100 µl of staining buffer and stained with secondary antibodies (diluted 1:100): goat anti-rabbit IgG Alexa Fluor 488 (A-11008, Invitrogen) for the detection of ABCB5 and goat anti-mouse IgG Alexa Fluor 488 (A28175, Invitrogen) for the detection of ABCB1. The analysis was performed using BD LSR II (BD Bioscience) flow cytometer.

Name of antibody	Fluorochrome, clone, company	Dilution
ABCB1	Mouse monoconal [JSB-1] to p-glycoprotein, Abcam	1:100
ABCB5	Rabbit polyclonal, Bioss	1:100
Sca-1	PE/Cy7 Anti-mouse Ly6A/E, clone E13-161.7 BioLegend	1:100
CD20	PE anti-mouse CD20, clone SA275A11, BioLegend	1:100
CD133	APC anti-mouse CD133, clone 315-2C11, BioLegend	1:100
CD24	PerCP-Cy™5.5 Rat Anti-Mouse CD24, clone M1/69, BD Pharminogen	1:100
CD44	PE-CF594, rat anti-mouse, clone IM7, BD Biosciences	1:100
VE-cadherin	PE, clone 11D4.1, BD Biosciences	1:100
Tie-2	APC, clone TEK4, BioLegend	1:100

Table 3.3. Antibodies used for FACS analysis of MIC and VE markers in B16-F10 cells.

3.7. ALDH activity assay

ALDH activity was measured using the ALDEFLUOR™ kit (StemCell Technologies) according to the vendor's protocol. Briefly, cells (0.5-1.0×10^6) were suspended in 1 ml of ALDEFLUOR™ assay buffer in the FACS tube. In the second FACS tube, 5 µl of DEAB reagent (ALDH inhibitor) was placed. Then, 5 µl of ALDEFLUOR™ reagent was mixed with the cells, stirred, and 0.5 ml of the resulting cell suspension was immediately added to the tube with DEAB to stop the reaction. Samples were incubated for 30 minutes at 37°C, centrifuged

(250 g, 5 minutes, room temperature) and suspended in 100 µl of PBS supplemented with 2% FBS. ALDH activity was analyzed using BD LSR II (BD Bioscience) flow cytometer. Cells were additionally immunostained for detection of MIC markers and/or stained with DAPI for viability assessment (see: 3.6).

3.8. PKH26 staining

For the detection of dye retaining cells, B16-F10 cells were stained with PKH26 dye (Sigma-Aldrich). Briefly, cells (2 x 10^6) were suspended in 0.5 ml of diluent C (provided by the manufacturer) in the test tube. In the second tube, 2 µl of 1 mM PKH26 dye was added to 0.5 ml of diluent C. Solutions from both tubes were mixed and samples were incubated for 5 minutes in room temperature. Staining was stopped using 10 ml of RPMI medium supplemented with 10% FBS. Cells were centrifuged and washed twice with 10 ml of PBS without Ca^{2+} and Mg^{2+} ions. Stained cells were detected by flow cytometer LSR Fortessa (BD Bioscience) or sorted with MoFlo XDP sorter (Beckman Coulter) and used for further experiments.

3.9. Cell cycle analysis

Cell cycle analysis of MIC clonal cell lines was performed after fixation of cells with 70% ice-cold ethyl alcohol (EtOH, POCh) for at least 3h in -20°C. After this, cells were centrifuged (4200 g, 10 minutes) and stained with 250 ul of PBS containing propidium iodide (PI, Sigma-Aldrich, 1:100) and RNAse A (1:1000, Merck) for 30 minutes in the room temperature, in the dark. After this time samples were harvested using BD LSR II (BD Bioscience) flow cytometer and analyzed with ModFit software.

To identify cells in the G0 phase within the PKH26-retaining and PKH26-negative subpopulations, we first applied BD IntraSure™ Kit (BD Biosciences), according to vendor's protocol. Cells were fixed using Reagent A (provided by the manufacturer), and lysed with 1x BD FACS lysing solution. Next, cells were stained (15 minutes in room temperature, in the dark) with 1 µl of anty-Ki67 antibody (clone 16A8, BioLegend, 1:100 dilution). After washing with PBS, cells were stained (10 minutes in room temperature in the dark) with 100 µg/ml Hoechst 33342 (Sigma-Aldrich). Samples were analyzed using BD LSR II (BD Bioscience) flow cytometer.

3.10. Culture with tin protoporphyrin IX (SnPP)

B16-F10 WT cells were cultured for 7 days in RPMI CM or MIC medium supplemented with 10 μM SnPP, inhibitor of heme oxygenase activity (Frontier Scientific). Empty culture media and media supplemented with dimethyl sulfoxide (DMSO; solvent of SnPP; Sigma-Aldrich) were used as controls. Cells were passaged when confluency was reached. RT-qPCR and FACS analyses were performed at the end of the experiments.

3.11. RNA isolation

Cells were lysed using Fenozol (A&A Biotechnology). Extraction was performed by the addition of the chloroform (Sigma-Aldrich). Samples were vortexed for 1 minute and incubated on ice for 20 minutes. After centrifugation (10,000 g, 20 minutes, 4°C), the upper phase was transferred to the new tube. RNA was precipitated in 100% isopropanol overnight. Next day samples were centrifuged (10,000 g, 30 minutes, 4°C), pellets were washed with 70% EtOH twice, and dissolved in RNAse-free water. The quality and concentration of isolated RNA were measured with the Nanodrop ND-1000 spectrophotometer.

3.12. Reverse transcription (RT)

Synthesis of cDNA from total RNA was performed using the RevertAid First Strand cDNA Synthesis Kit (Thermo Scientific). The reaction was performed according to vendor's protocol and is summarized in Table 3.4. In the end, cDNA was diluted in H_2O to obtain the concentration of 10 ng/μl.

Step 1	
RNA	200- 1000 ng
Oligo dT primers	1 μl (0.5 μg/μl)
H_2O	up to 6 μl
Incubation: 65°C, 5 minutes	
Step 2	
5x Reaction Buffer	2 μl
10 nM dNTPs	1 μl
RevertAid M-MuLV RT (200 U/μl)	0.5 μl
H_2O	0.5 μl
Incubation: 42°C, 60 minutes	
Termination: 70°C, 5 minutes	

Table 3.4. Scheme of RT-PCR.

3.13. Quantitative RT polymerase chain reaction (qRT-PCR)

Quantitative analysis of gene expression was performed using the SYBR® Green JumpStart™ Taq ReadyMix™ (Sigma-Aldrich) and is summarized in Table 3.5. Samples were pipetted on MicroAmp® Optical 96-Well Reaction Plates (Applied Biosystems) and PCR was performed in StepOnePlus™ thermocycler (Applied Biosystems). Sequences and melting temperatures of primers used in the study are included in Table 3.6.

Reaction mix/sample	
cDNA	10 ng
SYBR Green	5 µl
Forward primer 10 µM	0.4 µl
Reverse primer 10 µM	0.4 µl
H_2O	3.2 µl
PCR conditions	
95 °C, 10 minutes	1x
95 °C, 30 seconds	
55/60/65°C, 1 minute	40x
72°C, 45 seconds	
72°C, 10 minutes	1x
+ Melt curve analysis	

Table 3.5. Scheme of qRT-PCR.

Primer	Sequence	Length of product	Tm [°C]
Ef2 For *Ef2* Rev	5' GACATCACCAAGGGTGTGCAG 3' 5' TCAGCACACTGGCATAGAGGC 3'	214 bp	60°C
Tyrosinase For *Tyrosinase* Rev	5' GCCCAGCATCCTTCTTCTCC 3' 5' TAGTGGTCCCTCAGGTGTTC 3'	101 bp	55°C
Mitf For *Mitf* Rev	5' AGAGCAGGGCAGAGAGTGAGT 3' 5' CAGGAGTTGCTGATGGTAAGG 3'	238 bp	65°C
Gp100 For *Gp100* Rev	5' ACCACTATGGGTGTCCAGAGA 3' 5' GACACCAAGCCAGTCCTGAT 3'	108 bp	60°C

Trp2 For	5' CCCAACGCTGATTAGTCGGAAC 3'	207 bp	65°C
Trp2 Rev	5' GGAGGGCTGTCAAACTTCTGGA 3'		
Jarid1B For	5' AGTGGCTTTCCTGTTCGAGA 3'	173 bp	60°C
Jarid1B Rev	5' AAGCACATGCCCACATACAA 3'		
Hmox1 For	5' GTGGAGACGCTTTACATAGTGC 3'	250 bp	60°C
Hmox1 Rev	5' CTTTCAGAAGGGTCAGGTGTCC 3'		
Mcam For	5' GCCCCAGAGGAACCAACTAT 3'	200 bp	60°C
Mcam Rev	5' AAGCCACTGGACTCGACAAT 3'		
Mart-1 For	5' CAGTACCAGCAGCCGATAAGCA 3'	166 bp	55°C
Mart-1 Rev	5' GGGAAGGTGTCCTGTGCTGAGT 3'		
Trp1 For	5' CTGCACTGCTGGTCTCCCTACA 3'	212 bp	55°C
Trp1 Rev	5' AAAACGTCTGCGATGTCTGCAC 3'		
Sparc For	5' ATGTACATCTTCCCTGTCCAC 3'	134 bp	60°C
Sparc Rev	5' AAGAAACGTGTGGTGCAATG 3'		
Nanog For	5' CGTTCCCAGAATTCGATGCTT 3'	102 bp	60°C
Nanog Rev	5' TTTTCAGAAATCCCTTCCCTC 3'		
Rex1 For	5' AGATGGCTTCCCTGACGGAT 3'	104 bp	60°C
Rex1 Rev	5' CCTCCAAGCTTTCGAAGGATT 3'		
SallV For	5' CAGGAATTGGTGGCGGAGAG 3'	211 bp	60°C
SallV Rev	5' CAGTTCCCAGGGGAGTTCAC 3'		
ß-actin For	5' TCCTTCGTTGCCGGTCCACA 3'	93 bp	60°C
ß-actin Rev	5' GCTTTGCACATGCCGGAGCC 3'		

Table 3.6. Sequences of primers used in the study.

3.14. AmpliGrid – pre-amplification system for gene expression analysis from limited number of cells

Cells were sorted (50 cells/reaction site) on the basis of their MIC phenotype on AmpliGrid plates (Fig. 3.5 A). After the evaluation of sorted cells under the microscope (Fig. 3.5 B) slides were kept in 4°C overnight to dry. The RT was performed using the NCode Vilo mRNA cDNA Synthesis Kit (Invitrogen). The SuperScript III Reverse Transcriptase included in the kit ensures high yields of cDNA synthesis from a small amount of starting material. RT was performed according to the vendor's protocol in Stratagene Mx3005P cycler but was scaled down to 1 µl of reaction mix/reaction site. 5 µl of the cover oil was pipetted to each reaction site to prevent the evaporation of samples during PCR. After RT, 4 µl of H_2O was carefully

pipetted through the oil to dilute the cDNA sample, and samples were collected to separate tubes, and used for qRT-PCR as described above (see: 3.13).
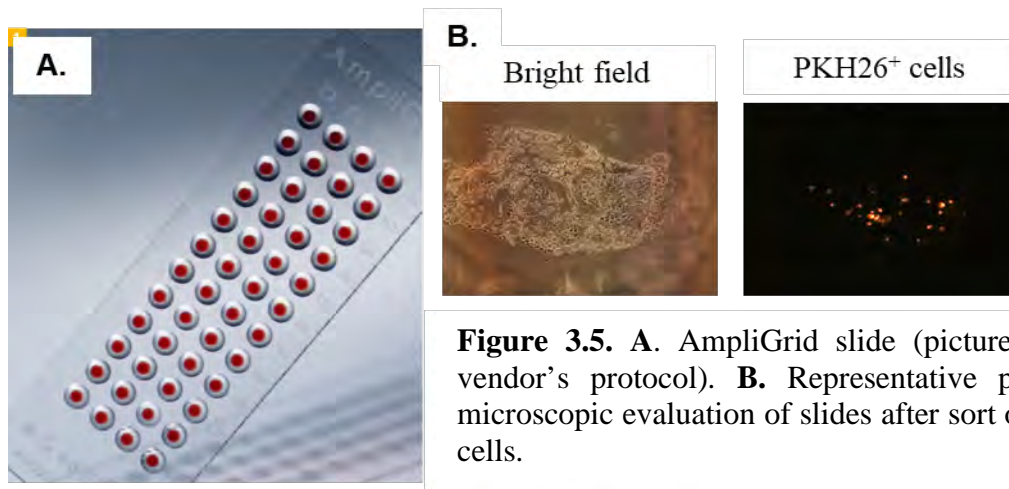
Figure 3.5. A. AmpliGrid slide (picture from the vendor's protocol). **B.** Representative pictures of microscopic evaluation of slides after sort of PKH26$^+$ cells.

3.15. RT² Profiler™ PCR Array

For the RT² Profiler™ PCR Array analysis, we sorted 2,000-10,000 of potential MIC (MIC$^+$) and bulk (MIC$^-$) B16-F10 subpopulations to 100 µl of Buffer RL (Norgen). Next, RNA was isolated using the Single Cell RNA Purification Kit (Norgen) with the On-Column DNA Removal (Norgen) step according to the vendor's protocol. RNA was eluted using 10 µl of DNase RNase-free H$_2$O. The final elution step was performed 4 times to increase the yield of material. Isolated RNA was entirely used for the RT-PCR using NCode Vilo (Invitrogen). Obtained cDNA was diluted 6 times. The RT² Profiler™ PCR Array (Qiagen) detecting murine CSC-related genes was performed according to the vendor's protocol using the Applied Biosystems StepOne Plus device.

3.16. MTT assay

Cells were seeded on the 96-well plates (1500 cells/well, in triplicates) in RPMI CM. After 24 h, the medium was changed for RPMI CM supplemented with different concentrations of doxorubicin (Sigma-Aldrich). After next 24 h, the medium was changed for RPMI supplemented with 1 mg/ml thiazolyl blue tetrazolium bromide (MTT, Sigma-Aldrich). Cells were incubated for 20 minutes in 37°C and, after removal of the medium, were lysed with the lysis buffer (containing 10 g of sodium dodecyl sulfate (SDS), 0.6 ml of 100% acetic acid in 100 ml of DMSO). Absorbance was read at 562 nm using the Tecan Infinite M200 Pro Reader.

3.17. Clonogenicity test and obtaining cell lines from single clones

MIC$^-$ and MIC$^+$ cells were sorted for the clonogenic growth using the MoFlo XDP (Becton Dickinson) cell sorter. Before sort, cells were stained with a proper antibody (in dye retaining experiment, cells were stained with PKH26 12 days before sort). Single-cell sort was performed on the 96-well plates and cells were cultured in the MIC medium. Pictures of clones were taken every second day, starting from day 5. After two weeks, wells with clones were regarded as positive events. Cell lines derived from single clones were further cultured in the MIC medium.

3.18. Soft agar assay

Soft agar assay was performed in the 2x RPMI (1.4 g of RPMI powder, Sigma-Aldrich; 0.2 g of sodium bicarbonate, Sigma-Aldrich; 50 ml of H$_2$O) with pH adjusted to 7.8-8.4 pH using pH meter. The medium was supplemented with 20% FBS (Eurx), 2x PEST (Sigma-Aldrich), and 2% Glutamax (ThermoFisher) and filtered using a 0.2 µm filter (Millipore). The bottom layer (0.8%) of the soft agar was prepared by adding an agar solution to the 2x RPMI CM in the 1:1 ratio. Next, 400 µl of the solution was quickly added to pre-heated 12-well culture dishes. The proper numbers of cells (final density of 2,000 cells/well) were mixed with the 2x RPMI CM and then 0.8% agar was added in the 1:1 ratio. Finally, 600 µl of agar with cells was added to each well as a middle layer. After 30 minutes, the upper layer of 0.8% agar was added as described above. Cells were cultured for 7 days and colonies were counted under the microscope (6 wells per cell line and 10 fields of view per well were counted by two independent investigators).

3.19. *In vitro* end point dilution assay (ELDA)

For the primary ELDA, PKH26$^-$ and PKH26$^+$ cells (selected for 12 days after PKH26 staining) were sorted on the 96-well plate and cultured in the MIC medium in the amount of 1, 3, 5, 7, or 10 cells (12 wells for each condition). Clones were counted after two weeks of culture. For the secondary ELDA, single PKH26$^-$ and PKH26$^+$ cells were sorted and cultured in the MIC medium. After clones formation, single clones (3 PKH26$^-$ and 3 PKH26$^+$) were sorted for ELDA in the same scheme as in the primary ELDA. Data analysis was performed using http://bioinf.wehi.edu.au/software/elda/index.html.

3.20. *In vivo* injection of cells

In vivo primary transplantation of cells (B16-F10 WT Luc or B16-F10 HO-1 GFP Luc) was performed after staining of cells with proper antibody/ALDEFluor/PKH26 (12 days before sort for the latter). Additionally, 0.2 µg/ml DAPI was used to distinguish live/dead cells. For each mouse, 30 cells were sorted to a 1.5 ml Eppendorf tube containing 150 µl of PBS. After the sort, 150 µl of Matrigel GFR™ (Corning) was added to each tube to obtain the concentration of 10 cells per 100 µl solution for injection. C57BL/6-Tg(UBC-GFP)30Scha/J mice were subcutaneously injected (2 plugs/mice) with 100 µl of cell suspension under the isoflurane (Baxter) anesthesia. The growth of tumors was monitored using the IVIS Lumina (PerkinElmer) once a week, starting on day 7. All *in vivo* experiments were approved by the Local Ethics Committee for Animal Research in Krakow (approval number 139/2015).

3.21. *In vivo* serial transplantations

When the primary tumors grew up to 1 cm in diameter, mice were euthanized with the use of CO_2. Excised tumors were chopped with a scalpel and digested for 1 h at 37°C in 2 ml of enzyme mix (containing 3 U/ml liberase, 25 µg/ml hyaluronidase, 25 µg/ml DNAse, and 3 U/ml dispase, all from Sigma-Aldrich) as described by Szade et al[229]. To stop digestion, RPMI with 10% FBS was added, and the digested tissues were thoroughly pipetted and filtered using the 100 µm strainer. After washing with PBS, cells were centrifuged (600g, 5 minutes, room temperature) and pellets were stained in 500 µl PBS with 7-amino-actinomycin D (7AAD, diluted 20x, BD Pharmingen) and Hoechst 33342 (160 µg/ml, Sigma-Aldrich) (15 minutes, room temperature, in the dark). Sort of GFP⁻7AAD⁻Hoechst⁺ cells was performed (300 cells to 150 µl PBS in 1.5 ml Eppendorf tube) and 150 µl of Matrigel was added to obtain the concentration of 100 cells per 100 µl. In case of B16-F10 HO-1 GFP Luc cell line there was a GFP⁻/dim subpopulation, additionally distinguished at SSC/FSC plot from the host cells. Each primary tumor was transplanted to 9-10 C57BL/6-Tg(UBC-GFP)30Scha/J secondary recipients. Tertiary transplantations were performed as described above but one secondary tumor was transplanted to one tertiary recipient.

3.22. *In vivo* detection of bioluminescence

To monitor growth of tumors, 20 minutes before imaging mice were injected i.p. with 150 µl of luciferin (15 mg/ml, TriMen Chemicals). Five minutes before measurement mice were anesthetized with isoflurane (Baxter) and 2 minute exposure time was used for detection of bioluminescence using IVIS Lumina (PerkinElmer).

3.23. *Post mortem* detection of metastases

On the day of ending *in vivo* experiment, when tumors reached around 1 cm in diameter, mice were injected i.p. with 150 µl of the luciferin (15 mg/ml, TriMen Chemicals). After 20 minutes, mice were euthanized, organs were excised, and luminescence signals were measured with IVIS Lumina (PerkinElmer).

3.24. Measurement of ALDH activity in tumor samples

Tumors that were excised and digested for serial transplantations were additionally sorted for the ALDH activity test. Briefly, 50,000-250,000 GFP$^-$7AAD$^-$Hoechst$^+$ tumor cells were added to ALDEFLUOR^{TM} assay buffer. Staining was performed as described above (see: 3.7), but was scaled down (1 µl of DEAB reagent and ALDEFLUOR^{TM} reagent and 200 µl of assay buffer were used). Then, cells were additionally stained with 7AAD (10 minutes in room temperature, in the dark) for the detection of dead cells.

3.25. Western Blot

3.25.1. Protein isolation

Cells were lysed using the RIPA buffer (Thermo Scientific) supplemented with the proteinase inhibitor cocktail (Roche). After 30 minutes of incubation on ice, lysates were centrifuged (10 minutes, 4°C, 10,000 *g*), and proteins in supernatants were measured using bicinchoninic acid assay.

3.25.2. Bicinchonic acid (BCA) assay

Albumin standard curve (0-1.5 mg/ml) was used as a reference. The colorimetric reaction was performed in 96-well plates by adding 100 µl of BCA:CuSO$_4$ solution (mixed in ratio 50:1, Sigma-Aldrich) to each well containing 5 µl of protein samples. The plate was incubated 30 minutes at 37°C and absorbance (562 nm) was measured using the Tecan Infinite M200 Pro Reader.

3.25.3. SDS-PAGE electrophoresis

Protein samples (10-50 µg) were prepared with the 5x loading buffer and were incubated 10 minutes at 95°C. Gels for electrophoresis were prepared as indicated in Table 3.7 and subsequently, electrophoresis was conducted (100 V for 15 minutes, followed by 160 V for 40-60 minutes).

SDS-PAGE gels		
	4% stacking gel	10% separation gel
H_2O	3.67 ml	2.9 ml
30 % acrylamide (BioShop)	0.75 ml	3.3 ml
Tris-HCl buffer, pH=8.8	-------	3.8 ml
Tris-HCl buffer, pH=6.8	0.625 ml	---------
20% SDS (BioShop)	25 µl	50 µl
10% APS (Sigma-Aldrich)	50 µl	100 µl
TEMED (Sigma-Aldrich)	5 µl	10 µl

Table 3.7. Formulations of gels used for proteins separation

3.25.4. Transfer and detection of proteins

The dry transfer was performed using the iBlot system (Invitrogen). The wet transfer was conducted at 4°C, with 100 V for 60 minutes. Proteins were transferred to 0.45 µm nitrocellulose membrane (BioRad) and blocked in TPBS buffer (0.05% Tween in PBS) with 5% skimmed milk for 1 h in room temperature. Next, membranes were incubated overnight with a proper primary antibody (listed in Table 3.8). After washing of membranes (5x 5 minutes in TPBS) a proper secondary antibody conjugated to HRP was added (1 h in room temperature, Table 3.8). Detection of proteins was performed using the Pierce™ ECL Western Blotting Substrate (ThermoFisher). Membranes were developed in dark-room or using ChemiDoc™ Imaging System (BioRad).

Primary WB antibodies	
Antibody	Clone and dilution
HO-1	Rabbit polyclonal, ADI-SPA-894-F Enzo and ADI-SPA-896-J Enzo
tubulin	Mouse monoclonal, T9026, Sigma-Aldrich
GAPDH	Mouse monoclonal, clone 6C5, Sigma-Aldrich
TYR	Rabbit polyclonal, (M-19)-R, sc-7834-R, Santa Cruz Biotechnology
Gp100 (Pmel17)	Mouse monoclonal, clone C-2, Santa Cruz Biotechnology
MITF	Rabbit polyclonal, ab20663, Abcam

Secondary WB antibodies	
Antibody	Clone and dilution
Goat anti-mouse Ig	HRP-linked, 554002, BD Biosciences
Goat anti-rabbit IgG	HRP-linked, 7074, Cell Signalling

Table 3.8. Antibodies used for western blots and immunofluorescence staining.

3.26. Heme oxygenase activity test

Heme degradation leads to the formation of biliverdin that is further metabolized by the biliverdin reductase (BVR) to bilirubin[230]. The concentration of the latter can be measured spectrophotometrically in the heme oxygenase activity test. Test was performed according to the protocol described previously by Foresti et al[230]. Briefly, the reaction mixture contained: cell lysate (obtained by freezing/thawing technique using dry ice), BVR (recombined form, described by Mucha et al.[231] or the rat's liver lysate), NADPH (0.8 mM, Sigma-Aldrich), glucose-6-phosphate (2 mM, Sigma-Aldrich), glucose-6-phosphate dehydrogenase (0.2 units, Sigma-Aldrich), PBS containing 2mM $MgCl_2$ (0.2 mM, Sigma-Aldrich) and hemin (20 μM; Sigma-Aldrich). Samples were incubated for 1 h at 37 ℃ in the dark. The reaction was stopped by the addition of 1 ml of chloroform and vigorous vortexing. Samples were centrifuged (500 *g*, 5 minutes) and a bottom organic phase containing reaction products was used for absorbance measurement at 464 nm and 530 nm using Tecan Infinite® 200 PRO spectrophotometer and quartz cuvette. The heme oxygenase activity was calculated using the formula:

$$\frac{A_{464}-A_{530}}{40\times(protein\ content)} \times 10^6 \left[\frac{pmol}{mg/60\ min}\right],$$

where protein content is the amount of proteins in 400 μl of cell lysate determined by BCA.

3.27. Intracellular HO-1 staining

Cells were stained using the Perm/Wash buffer (BD Biosciences) according to the vendor's protocol. Briefly, after fixation, cells were washed twice with the Wash Buffer, and stained (4 ℃, 40 minutes) with HO-1 primary polyclonal antibody (ADI-SPA 894 diluted 1:200; Enzo Life Sciences). Cells were centrifuged (1,500 *g*, 5 minutes, 4 ℃), washed twice with Perm/Wash buffer and stained with secondary antibody in 100 μl Perm/Wash buffer (goat anti-rabbit AlexaFluor 488, 1:400). Samples were analyzed using the Fortessa BD flow cytometer and data were proceeded in FACS Diva™ Software.

3.28. Adipogenic and osteogenic differentiation of CD20-derived cell lines

Cells were seeded in the DMEM CM (12,000/well, 6 well plates) and next day growth media were changed for differentiation media. For adipogenic differentiation DMEM CM supplemented with 1 µM dexamethasone, 0.5 µM isobutylmethylxanthine, and 10 ng/ml insulin (all from Sigma-Aldrich) was used. For osteogenic differentiation DMEM CM supplemented with 0.1 µM dexamethasone, 10 mM β-glycerol phosphate, and 50 µM ascorbate-α-phosphate (all from Sigma-Aldrich) was used[232]. Cells were differentiated for 11 days.

3.29. The tube formation by melanoma cells on Matrigel

B16-F10 WT Luc and B16 HO-1 GFP Luc cells were seeded in different concentrations (10,000 and 25,000/well) on 96-well plates coated with Matrigel GFR (50 µl of Matrigel/well; Corning). Pictures were taken 3, 6 and 20 h after seeding.

3.30. The co-culture of HMEC-1 cells and B16-F10 cells seeded on Matrigel

HMEC-1 cells (human dermal microvascular endothelium) were seeded on Matrigel GFR (10,000 cells/well, 96-well plates) in the EGM-2 medium (Lonza). Cells formed tubes during 8 h incubation (standard culture conditions, 37°C, 5% CO_2). Next, B16-F10 WT Luc cells were stained using the CellTrace™ Violet Cell Proliferation Kit (Invitrogen). Briefly, cells (1×10^6) were stained in 1 ml of PBS with 1 µl of CellTrace Violet dye (20 minutes, 37°C). Staining was stopped by the addition of medium with 10% FBS. B16-F10 HO-1 Luc cells were stained with PKH26 (see: 3.8). Stained cells were seeded on wells with tubes formed by HMEC-1 cells in three variants: 1) 5,000 cells/well B16-F10 WT Luc; 2) 5,000 cells/well B16-F10 HO-1 Luc and 3) 2,500 B16-F10 WT Luc cells + 2,500 B16-F10 HO-1 Luc cells. The co-operation of cells in tube formation was analyzed after a 16 h incubation using the fluorescent microscope (Eclipse T100, Nikon).

3.31. Isolation and purification of the mesenchymal stromal cells (MSC) from HO-1 WT and KO mice

Femurs and tibia of C57Bl6×FVB *Hmox1$^{+/+}$* and *Hmox1$^{-/-}$* mice or C57Bl6×FVB *Hmox1$^{+/+}$* and *Hmox1$^{-/-}$* constitutively expressing GFP were excised after the euthanasia of animals. Bones were cut into small pieces and digested with 1 mg/ml type II collagenase (Gibco; 120 minutes, 37°C in rotary shaker at 250 rpm). After digestion, cells were washed with PBS and resuspended in the αMEM (Lonza) supplemented with 10% FBS and PEST. Cells

were seeded into 6-well plates. The medium was changed every 24 hours (during the first 3 days) and then every 2-3 days. After the third passage, MACS sorting of CD45⁻ cells was performed. Briefly, cells were suspended in AutoMACS running buffer (Miltenyi Biotec) and stained with anti-mouse CD45 MicroBeads (25 minutes, 4°C; Miltenyi Biotec). After washing cells with PBS they were separated on the MACS MS columns in the AutoMACS running buffer (Miltenyi Biotec). CD45⁻ mesenchymal stromal cells were used for further experiments.

3.32. The co-culture of MSC and B16-F10 WT Luc cells

Melanoma cells (50 cells/well) were seeded on the confluent monolayer of MSC cultured in a 24-well plate. Luminescence of B16-F10 WT Luc cells was monitored using the IVIS Lumina up to day 6.

3.33. The fibrin bead assay

B16-F10 WT Luc cells were incubated with latex beads (Sigma-Aldrich) in ratio 400:1. The coating was performed in 1.5 ml RPMI CM in the FACS tube placed in the incubator (4 h, 37°C) with shaking every 20 minutes. Then, coated beads were transferred to the T25 flask in 5 ml medium and left overnight (Fig. 3.6). The next day, the fibrinogen solution was prepared (2 mg/ml; Sigma-Aldrich) and aprotinin (0.15 U/ml; Sigma-Aldrich) was added. Beads were transferred to the 15 ml

Figure 3.6. Latex beads coated with B16-F10 WT Luc cells.

canonical tube where they settled on the bottom and then they were resuspended in EGM-2 medium (Lonza). Beads were counted and resuspended in the fibrinogen solution (500 beads/ml). Thrombin (Sigma-Aldrich) at final concentration of 0.625 U/ml, was added to each well and then 0.5 ml of the fibrinogen with beads was poured and mixed with thrombin. The plate was left for 15 minutes in the incubator (37°C). On the top, the MSC isolated from the HO-1 WT or HO-1 KO mice were seeded (5,000/well) in 1 ml of the EGM-2 medium. Evaluation of proliferation and migration of melanoma cells was performed by microscopic assessment. Pictures were analyzed with the ImageJ software.

Isolation of cells from the beads in fibrin gel was performed after 6 days of culture. Fibrin gel was treated for 3 minutes with 10x trypsin-EDTA (Gibco) to detach the layer of MSC. Then, 1 ml of 10x trypsin-EDTA was used for releasing melanoma coated beads. Beads were washed with medium supplemented with 40% FBS and centrifuged (500 g, 5 min, room temperature).

This led to the disruption of beads. Pellets of cells were lysed with fenozol and RNA was isolated (see: 3.11).

3.34. Immunofluorescent staining of B16-F10 cells cultured on MSC

B16-F10 WT Luc cells were seeded (50 cells/well) on the monolayer of MSC derived from the WT and HO-1 KO mice. Cells were cultured for 6 days and then were fixed with 4% paraformaldehyde (PFA; Sigma-Aldrich) in room temperature. After washing with PBS (3 times), cells were treated with 0.05% Triton X-100 (BioShop; 5 minutes, room temperature). After washing with PBS (3 times), cells were incubated for 30 minutes with 0.25% glycine (BioShop). Next, blocking was performed using 3% BSA (BioShop) in PBS (1 h, room temperature). Primary antibody for MITF (1:400) and tubulin (1:1000; Table. 3.8) were diluted in PBS with 3% BSA. Cells were stained overnight. The next day, primary antibodies were washed with PBS (5x 5 minutes) and cells were incubated with secondary antibodies (1 h, room temperature, 1:1000): for the MITF staining – goat anti-rabbit Alexa Fluor 488 antibody IgG (Invitrogen) and for the tubulin staining – goat anti-mouse 546 IgG (Invitrogen). After washing step, immunofluorescent signals were detected using the Eclipse T100 microscope (Nikon).

3.35. Generation of the induced pluripotent stem cells (iPSC)

3.35.1. Isolation of the tail tips fibroblasts (TTF) from HO-1 WT and KO mice

The tails of C57Bl6×FVB $Hmox1^{+/+}$ and $Hmox1^{-/-}$ mice (2-3 animals per group) were isolated after euthanasia of animals with CO_2. Tails were washed in 70% EtOH and then twice in PBS. After removal of skin, the tails were cut into small pieces and digested with the type II collagenase (1.5 mg/ml; Gibco) for 2 h in a water bath set to 37°C (with vortexing every 20 minutes). After the digestion, cells were centrifuged (300 g, 5 minutes, room temperature) and the supernatant and smaller pieces of tissues were moved to the new falcon and once again centrifuged (300 g, 5 minutes, room temperature). The supernatant was moved to a new tube and pellets were seeded on the 0.1% gelatin-coated plates (Sigma-Aldrich) in DMEM HG supplemented with 20% FBS and PEST. The supernatant was once again centrifuged and seeded to a second well.

3.35.2. Production of lentiviral vectors harboring STEMCA transgene

Lentiviral vectors were produced in HEK293 cells. For cell transfection, two solutions were prepared (Table. 3.9). For solution A, pHAGE-STEMCCA plasmid (coding Oct4, Klf4, c-Myc, and Sox2 transgenes) was kindly provided by dr. Gustavo Mostoslavsky (Department of Medicine, Boston University School of Medicine)[233]. Solution B was added to the solution A, mixed, and incubated for 20 minutes in room temperature. Next, the obtained mixture was added dropwise to HEK293 cell cultures. After 48 h, media with lentiviruses were centrifuged and filtered with 0.45 µm PVDF filters (Millipore). Transgene from pHAGE-STEMCCA is regulated by the Tet-On system thus TTF were transduced with pHAGE-STEMCCA and with lentiviral vectors containing the reverse tetracyclin transactivator FUdeltaGW-rtTA (Figure 3.7; Addgene).

Solution A	
150 mM NaCl	450 ul
pHAGE-STEMCCA	20 µg
packaging plasmid psPAX2	15 µg
envelope expressing plasmid pMD2.G	6 µg
Solution B	
150 mM NaCl	450 µl
Polyethyleneimine (MW 25000, Polysciences Inc.)	41 µl

Table 3.9. Transfection mix for production of LVs.
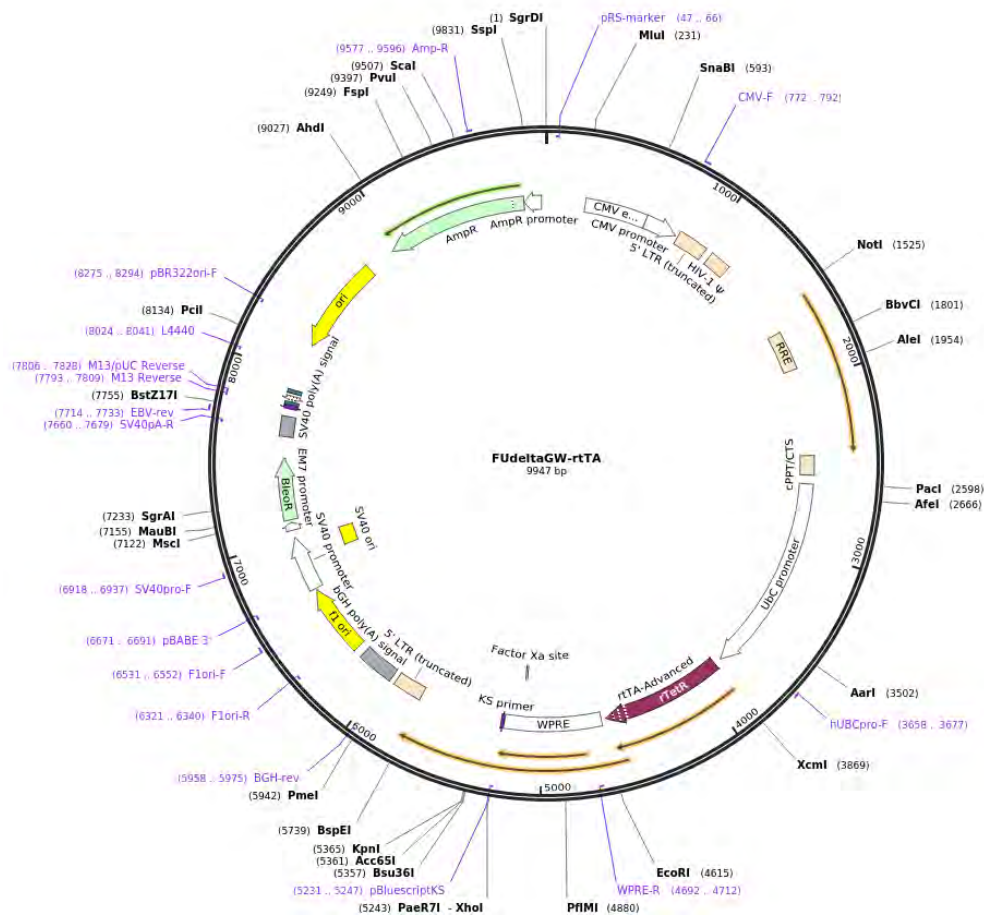
Figure 3.7. Map of FUdeltaGW-rtTA plasmid

3.35.3. Selection of transduced TTF with doxocyclin and culture of iPSC colonies

After 48 h, medium with lentiviruses was changed for iPSC medium containing: DMEM HG, 20% FBS, PEST, 1% non-essential amino acids (Gibco), 0.1 mM β-mercaptoethanol (Gibco), 1000 U/ml murine leukemia inhibitory factor (mLIF, StemCell Technologies) with the addition of 1 µg/ml doxycycline (Sigma-Aldrich) as a selection factor. At the 4th day after transduction, fibroblasts were seeded on the monolayer of inactivated murine embryonic fibroblasts (iMEF) prepared by dr. Jacek Stępniewski, as described in Stepniewski et al.[234] At day 10 after transduction, doxycycline was removed from the medium and cells were cultured for next 10 days in iPSC medium. Next, single iPSC colonies were transferred to the monolayer of iMEF to obtain stable iPSC cell lines.

3.36. Embryonic body (EB) formation and spontaneous differentiation of iPSC

For the elimination of iMEF from iPSC cultures, cells were seeded in the 6-well plates coated with 0.1% gelatin and incubated for 30 minutes at 37°C. Cells that did not attach to the gelatin were harvested, centrifuged (250 g, 5 minutes, room temperature), and seeded in non-adherent 10 cm plates. EB were forming for 5 days in iPSC medium without the addition of mLIF and then seeded into 48-well plates coated with the 0.1% gelatin. The culture of EB was continued for 12 days, until the cells started to migrate out of the EB. Immunofluorescent staining was performed to check the ability of iPSC to differentiate into three germ layers.

3.37. Alkaline phosphatase (ALP) activity test

ALP test (Sigma-Aldrich) was performed according to the vendors' protocol. Briefly, the diazonium salt solution was prepared by adding Sodium Nitrate Solution to FRV-alkaline solution (1:1, 2 minutes, room temperature). Next, the diazonium salt solution was mixed with distilled H_2O (dH_2O), and Naphthol AS-BI Alkaline Solution was added. Cells were fixed with the Citrate-Acetone-Formaldehyde Fixative solution. After the fixation, cells were stained with alkaline dye mixture (15 minutes, room temperature). Then, cells were washed with dH_2O, and staining was analyzed using an inverted microscope.

3.38. Cdy1 staining

Cdy1 is a dye that marks embryonic and pluripotent stem cells[235]. iPSC were incubated with 0.1 µg/ml Cdy1 diluted in iPSC medium (1 h, 37°C). Next, the medium was changed for fresh iPSC culture medium, and cells were incubated for 2-3 hours at 37°C. Dye retaining cells were visualized using the fluorescent microscope.

3.39. Immunofluorescent staining of iPSC

Cells were fixed with 4% PFA (10 minutes, room temperature) and after washing with PBS they were treated with 0.1% Triton in PBS (15 minutes, room temperature). After washing with PBS (3 times), samples were blocked with 4% BSA (1 h, room temperature). Primary antibodies were diluted in PBS (Table 3.10). After overnight incubation with antibodies at 4°C, cells were washed with PBS (5 times) and the secondary antibodies were added (1 h, room temperature; Table 3.10). Nuclei were stained with Hoechst 33342 (Sigma-Aldrich; 1 µg/ml) and cells were analyzed using the fluorescent microscope.

Primary antibodies		
Epitope	**Clone, host, company**	**Dilution**
Oct4	N19, sc8628, goat, Santa Cruz	1:200
Nanog	ab80892, rabbit, Abcam	1:100
SSEA-1	MSXSSEA-1 90230, mouse, Millipore	1:200
Gata-4	C-4, sc25310, mouse, Santa Cruz	1:200
AFP	C-19, sc8108, goat, Santa Cruz	1:200
Vimentin	ab11256, goat, Abcam	1:200
Nestin	ab6142, mouse, Abcam	1:200
NFH	ab8135, rabbit, Abcam	1:200
α-SMA	ab5694,rabbit, Abcam	1:200
Secondary antibodies		
Rabbit anti-goat 488	A11078, Invitrogen	1:400
Goat anti-rabbit 488	A11008, Invitrogen	1:400
Rabbit anti-mouse 488	A11059, Invitrogen	1:400
Goat anti-rabbit 546	A11035, Invitrogen	1:400
Goat anti-mouse 488	A28175, Invitrogen	1:400
Rabbit anti-goat 568	A11079, Invitrogen	1:400

Table 3.10. List of primary and secondary antibodies used for IF staining of iPSC.

3.40. Differentiation of iPSC toward melanocytes

Differentiation of murine iPSC toward melanocytes was performed according to the protocol published by Yang et al.[236] WT and HO-1 KO iPSC were seeded in the non-adherent 10 cm culture dishes in the iPSC medium without mLIF. After 2 days of culture, the retinoic acid (Sigma-Aldrich; final concentration of 1 μM) was added, and EB were cultured for the next 3 days. Then, EB were seeded on the fibronectin (Sigma-Aldrich; 10 ng/ml) coated plates and cultured in melanocyte differentiation medium (MDM, Table 3.11).

Ingredient	**Company**	**Final concentration**
DMEM High Glucose	Lonza	45%
Medium 254	Gibco	45%
FBS	EURx	10%
PEST	Sigma-Aldrich	1%

Wnt3	PeproTech	25ng/ml
Dexamethasone	Sigma-Aldrich	0.5 µM
Insulin-transferrin-selenium (100x)	Gibco	1x
Linoleic Acid-Albumin from bovine serum albumin	Sigma-Aldrich	1 mg/ml
L-ascorbic acid	Sigma-Aldrich	1 mM
SCF	PeproTech	50 ng/ml
Endothelin-3	Sigma-Aldrich	100 nM
Cholera toxin	Sigma-Aldrich	20 pM
TPA	Sigma-Aldrich	50 nM
β-FGF	PeproTech	ng/ml

Table 3.11. Composition of melanocyte differentiation medium (MDM).

3.41. Immunofluorescent staining of iPSC differentiated toward melanocytes

Staining was performed according to the protocol used for iPSC immunofluorescence staining (see: 3.39). The antibodies and dilutions are included in Table 3.12.

Primary antibodies		
Epitope	**Clone, host, company**	**Dilution**
MITF	Abcam	1:200
TYR	Santa Cruz	1:100
Secondary antibodies		
Goat anti-rabbit 488	A11008, Invitrogen	1:400

Table 3.12. Antibodies used for immunofluorescence staining of differentiated iPSC.

3.42. Statistical analysis

Data analysis was performed using GraphPad Prism 8 software or Microsoft Excel software. Results are represented as mean ± SEM and each experiment was performed at least in two independent biological repetitions unless stated otherwise. Data were analyzed with two-tailed Student t-test (two groups), one-way or two-way ANOVA with Bonferroni post-test (three or more groups) and with two-tailed Fisher exact test (for clonogenic events calculations). When comparing two groups with non-normal distribution Mann-Whitney test was used (box and whiskers plots). *In vivo* survival of mice was calculated using Mantel-Cox test. Results were considered statistically significant at p value <0.05.

4. Results

4.1. Identification of the potential MIC subsets in the B16-F10 murine melanoma cell line

4.1.1. Small fractions of B16-F10 cells express MIC markers

Several cell surface markers have been proposed to be expressed on cultured MIC, suggesting that MIC can be prospectively isolated and characterized[237]. Therefore, in the first step, we checked if the B16-F10 murine melanoma cell line contains subpopulations with MIC signatures. As melanoma cell heterogeneity can be driven by hypoxia[238] we cultured the cells for 48 h under normoxic (21% O_2) or hypoxic (0.5% O_2) conditions.
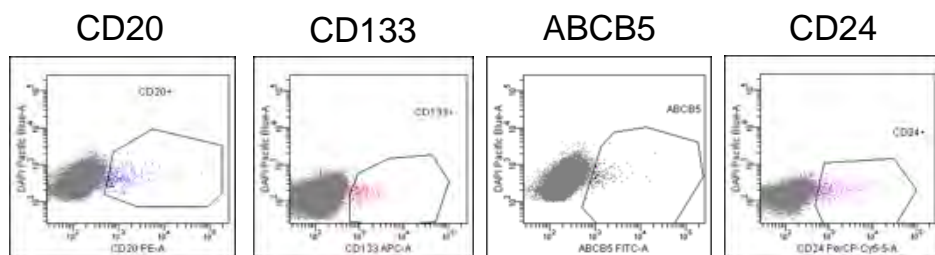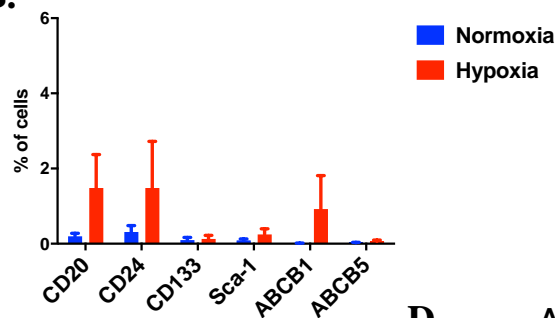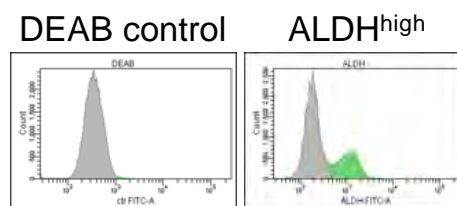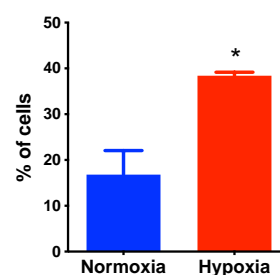
	CD20+	CD24+	CD133+	Sca-1+	ABCB1+	ABCB5+	ALDH^high
Normoxia (21% O2)							
Mean	0.196%	0.338%	0.153%	0.105%	0.015%	0.012%	16.802%
SEM	0.064	0.172	0.069	0.049	0.005	0.003	5.286
Hypoxia (0.5%O_2)							
Mean	1.484%	1.502%	0.202%	0.255%	0.917%	0.064%	38.420%
SEM	0.725	1.233	0.092	0.146	0.892	0.038	0.764

Figure 4.1. Frequency of MIC fractions in B16-F10 murine melanoma cells. **A.** Representative dot plots of surface MIC markers. **B.** MIC surface markers in the cells cultured 48 h in normoxia (21% O_2) or hypoxia (0.5% O_2); flow cytometry analysis; each bar represents mean + SEM;. **C,** Representative histograms of ALDH^{high} cells detected with ALDEFLUOR^{TM} kit. **D.** ALDH^{high} cells cultured in normoxia or hypoxia; flow cytometry analysis; each bar represents mean + SEM; * - $p<0.05$ versus normoxia. **E.** Table showing the percentages of MIC subsets in the cells cultured in normoxia and hypoxia; data represented as mean + SEM.

Flow cytometry analysis showed that small subpopulations of B16-F10 cells express the MIC surface markers: CD20, CD133, ABCB1, ABCB5, CD24, and Sca-1 (Fig. 4.1 A). Percentages of cells expressing the MIC surface markers (MIC$^+$ cells) in normoxia were very low, not exceeding 0.5% even for the most frequent, namely CD24$^+$ and CD20$^+$, fractions (Fig. 4.1 B, E). In hypoxia, the frequency of MIC$^+$ cells was slightly increased, but still remained low (Fig. 4.1 B, E). We did not observe any distinguishable subpopulations that co-expressed investigated MIC markers (data not shown), which might suggest that MIC are a heterogeneous population of cells.

Additionally, we used a functional marker – high aldehyde dehydrogenase activity (ALDH^{high}) to distinguish a potential subpopulation of MIC (Fig. 4.1 C). ALDH^{high} cells were much more frequent than cells expressing MIC cell surface markers, and their frequency increased significantly in hypoxia (Fig. 4.1 D). It should be stressed, however, that percentages of cell surface markers and ALDH^{high} cells can vary between experiments.

4.1.2. MIC$^+$ cells do not differ from bulk cells in melanoma associated antigens

In the next step, we compared the expression of known melanoma associated antigens (MAAs)[239] in the bulk (MIC$^-$) and MIC$^+$ cells. For this purpose we sorted 50 MIC$^-$ and 50 MIC$^+$ (CD20$^+$, CD24$^+$, CD133$^+$ or ALDH^{high}) cells on AmpliGrid slides, and after pre-amplification of the material, we performed qRT-PCR analysis for MAAs involved in melanogenesis: tyrosinase, *Gp100* (glycoprotein 100; Pmel-17), and *Mart-1* (melanoma antigen recognized by T cells).

The obtained results showed that expression of MAAs did not differ meaningfully between MIC$^+$ and MIC$^-$ cells (Fig. 4.2). Although we observed some increase in Gp100 in CD24$^+$ and ALDH^{high} cells (Fig. 4.2 B, D), there was no clear expression pattern of genes associated with melanogenesis in different MIC$^+$ subpopulations. For example, the level of tyrosinase, the rate-limiting enzyme for controlling the production of melanin, was unchanged in CD20$^+$ and CD24$^+$ cells (Fig. 4.2 A, B), decreased in CD133$^+$ cells (Fig. 4.2 C) and increased in ALDH^{high} (Fig. 4.2 D) cells.
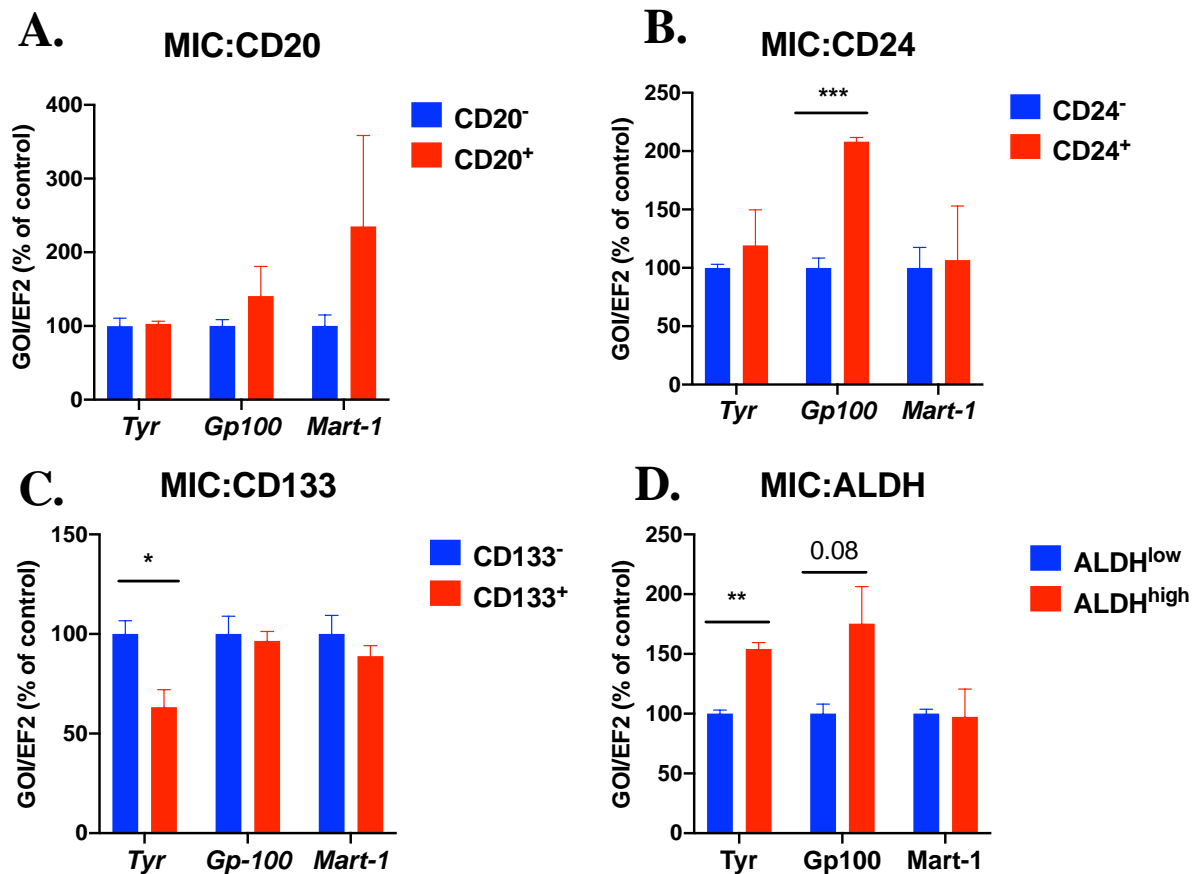
Figure 4.2. Expression of MAA genes involved in melanogenesis in MIC$^+$ cells in comparison to control, MIC$^-$ cells. **A.** CD20$^+$ cells. **B.** CD24$^+$ cells. **C.** CD133$^+$ cells. **D.** ALDH^{high} cells. qRT-PCR analysis on 50 sorted cells, after pre-amplification with the AmpliGrid system; GOI – gene of interest; EF2 was used as a reference gene; each bar represents mean + SEM; * - $p<0.05$, *** - $p<0.001$ versus MIC$^-$ cells.

4.1.3. Label-retaining cells are present in B16-F10 cell line

One of the features of CSCs is a quiescent phenotype reflected in the slow proliferation rate. Recently, a highly aggressive subpopulation of label-retaining cells (LRC) was discovered in human melanoma[94]. There is, however, no information whether such cells are also present in murine melanoma cell lines. To identify slowly cycling cells we performed staining of cells

with PKH26, the fluorescent lipophilic dye that binds to the cell membranes and dilutes with each division. During culture, only cells that divide slowly or do not divide, retain the dye.

Flow cytometry analysis showed that cells were stained uniformly and then PKH26 dye was rapidly diluted in the vast majority of them. On day 6, two fractions of LRC were observed,
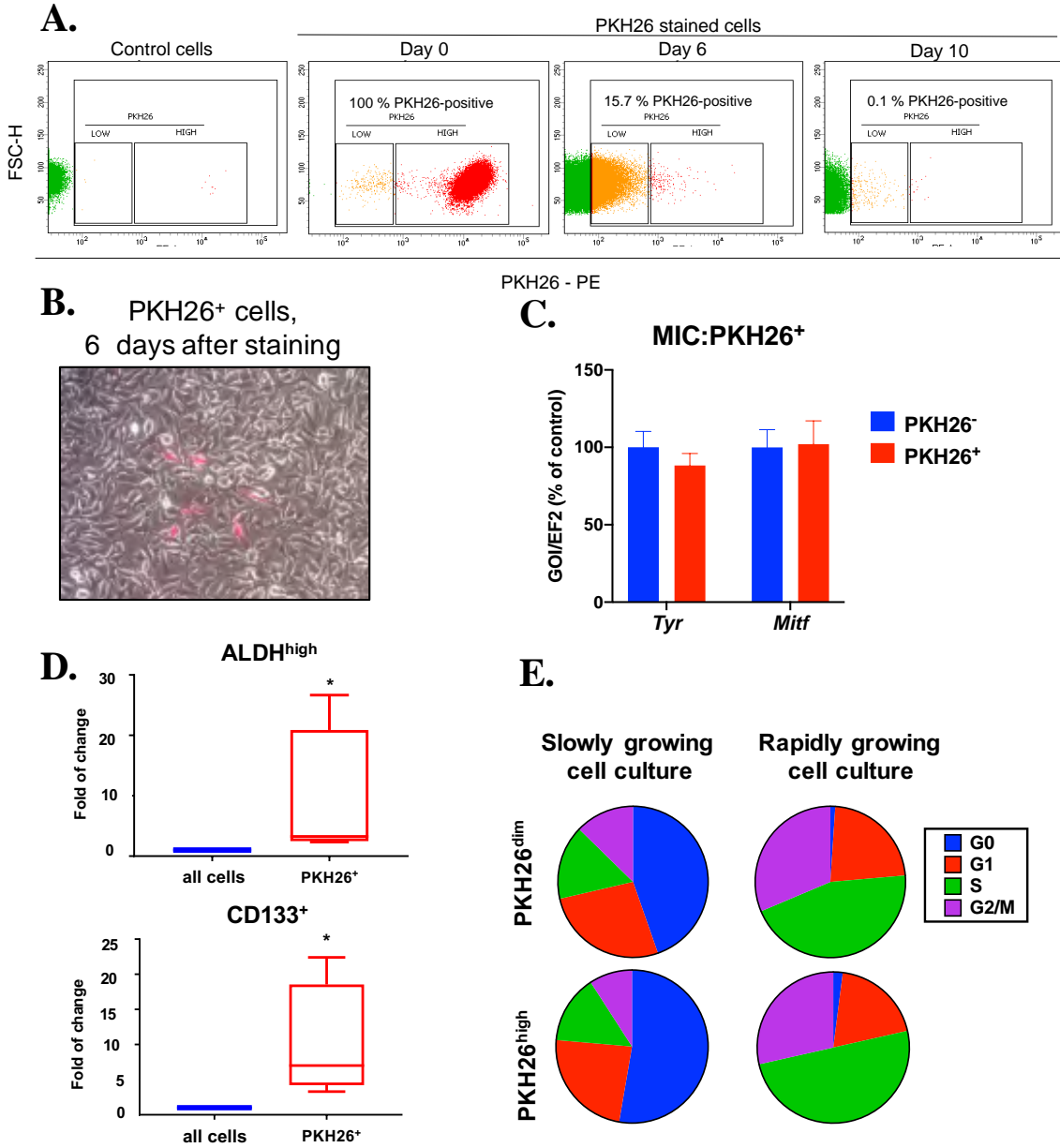
Figure 4.3. Identification of PKH26 dye retaining cells in the B16-F10 cell line. **A.** Dilution of PKH26 dye in cultured cells (representative FACS dotplots). **B.** Representative microscopic view of PKH26$^+$ cells 6 days after staining (multichannel picture). **C.** Expression of tyrosinase (Tyr), Mitf and Jarid1b genes in PKH26$^+$ cells in comparison to control, PKH26$^-$ cells. qRT-PCR analysis on 50 sorted cells, after pre-amplification with the AmpliGrid system; GOI – gene of interest; EF2 was used as a reference gene; each bar represents mean + SEM; * - p<0.05 versus PKH26$^-$ cells. **D.** CD133$^+$ cells and ALDH^{high} cells in the PKH26$^+$ fraction, 7 days after PKH26 staining. Flow cytometry analysis; box and whisker plots with median value, normalized to unsorted control; * - p<0.05 versus control. **E.** Cell cycle of PKH26$^-$ and PKH26$^+$ cells. Flow cytometry analysis; representative experiments showing a slowly growing (p=0.72, NS) and rapidly growing (p=0.86, NS) cell cultures; analysis done with help of Jan Wolnik.

with low and high PKH26-derived fluorescence, and on day 10 only around 0.1% of cells retained PKH26 dye (Fig. 4.3 A). Microscopic observations did not reveal any changes in the morphology of PKH26$^+$ fraction (Fig. 4.3 B).

Results of qRT-PCR (using the AmpliGrid technology) revealed that PKH26 retaining cells do not differ in tyrosinase and Mitf (melanocyte inducing transcription factor) expression from their rapidly dividing counterparts (Fig. 4.3 C).

We also checked whether LRC fraction is enriched in MIC$^+$ cells. Indeed, cytometric analysis performed 7 days after PKH26 staining showed that CD133$^+$ and ALDH^{high} cells were more common in the PKH26 retaining B16-F10 cell fraction in comparison to unsorted cells (Fig. 4.3 D). During culturing of B16-F10 cells we observed different patterns in their growth depending on the confluency and probably other factors like availability of nutrients in the medium. There were two types of cell cultures: slowly growing (with a big fraction of cells in G0 phase) and rapidly growing cell cultures (where most cells reside in S phase). Importantly, our analysis of cell cycle using Ki67 and Hoechst 33342 staining demonstrated that neither in slowly growing nor in rapidly growing B16-F10 cells the PKH26$^+$ fraction was enriched in cells at G0 or G1 phase, as it could be anticipated (Fig. 4.3 E). This indicates an important issue that the ability to retain PKH26 dye in cultured B16-F10 cell line is not connected with the quiescent phenotype. Instead, it possibly identifies slowly dividing cells but not a specific subpopulation blocked at the G0 cell cycle phase.

4.2. Evaluation of the role of HO-1 in the CSC properties of B16-F10 cells

4.2.1. MIC subsets do not share the HO-1 expression pattern

Development of melanoma is facilitated by a high expression level of HO-1, as has been demonstrated in B16-F10 melanoma in mice[147] and suggested by analysis of *Hmox-1* promoter polymorphism in human population[173]. Therefore, we compared the expression of HO-1 in MIC$^+$ subsets and bulk MIC$^-$ cells.

Set of qRT-PCRs showed that HO-1 is differently regulated in different MIC+ subsets (Fig. 4.4). Namely, *Hmox-1* level was significantly increased in CD24+ cells, and showed a tendency to be increased in CD20+ cells (Fig. 4.4 A). In contrast, *Hmox-1* level was slightly but significantly decreased in Sca-1+ cells, and showed a tendency to be decreased in CD133+ cells (Fig. 4.4 A). No differences were found in ABCB5+ cells (Fig. 4.4 A) and in subpopulations identified using functional markers – ALDH+ and PKH26+ cells (Fig. 4.4 B). This suggests that HO-1 up- or down-regulation is not a determinant of MIC cells. However, the question remained, whether a certain level of HO-1 activity is needed for MIC function.
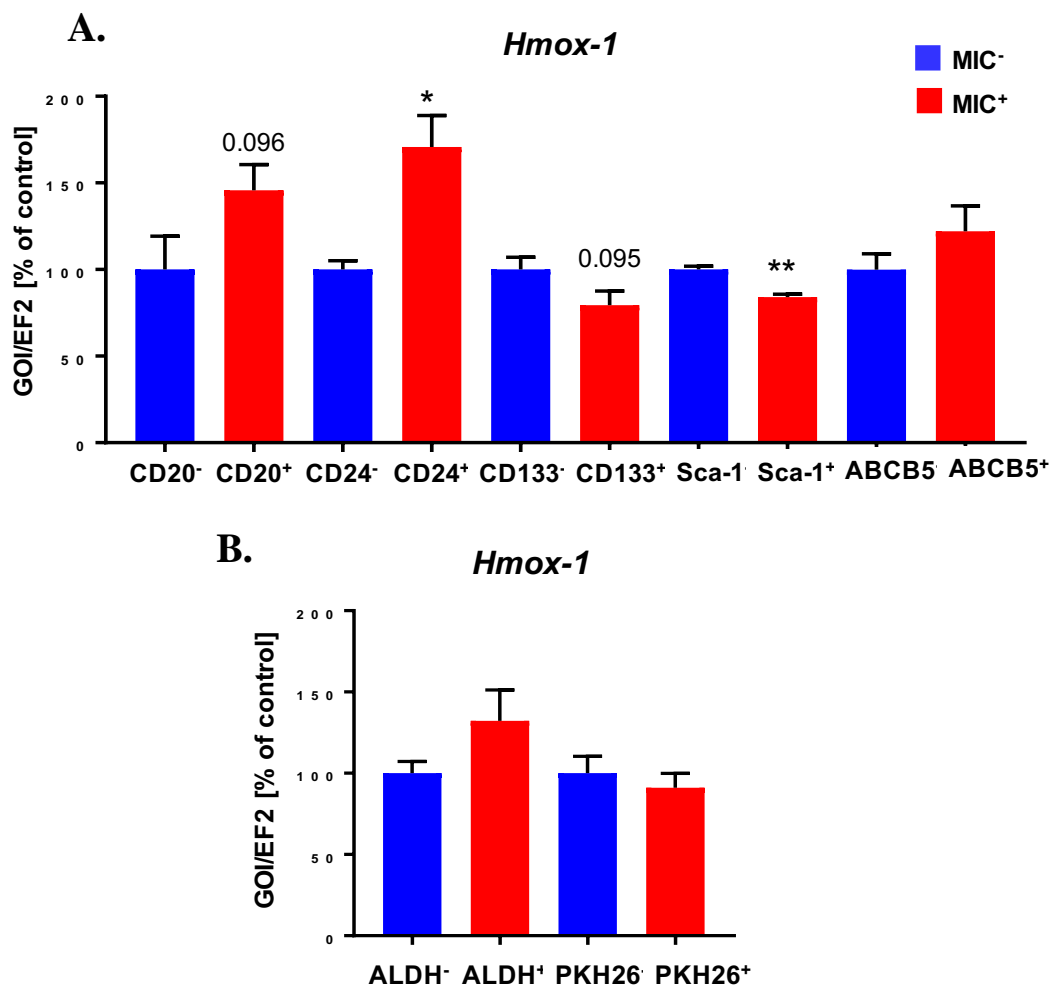
Figure 4.4. Expression of *Hmox-1* in MIC subsets. **A** – subpopulations selected on the basis of surface markers. **B** – subpopulations selected on the basis of functional markers. qRT-PCR on 50 sorted cells after pre-amplification with AmpliGrid system. GOI – gene of interest; EF2 was used as a reference gene; each bar represents mean + SEM; * - $p<0.05$, ** - $p<0.01$ versus MIC- cells.

4.2.2. HO-1 activity is necessary for non-adherent growth of B16-F10 melanoma cells cultured in MIC medium

B16-F10 cells are routinely cultured in the RPMI 1640 medium supplemented with 10% FBS. However, when CSC properties of cell lines are investigated, chemically-defined serum-free media should be used[240]. Thus, we tested B16-F10 cells in melanoma initiating cells (MIC) medium described by Stecca et al[228]. After 7 days of culture in MIC medium melanoma cells started to grow as non-adherent melanospheres (Fig. 4.5 A). Interestingly, cells treated with heme oxygenase inhibitor, tin protoporphyrin IX (SnPP), were not able to grow non-adherently

A.
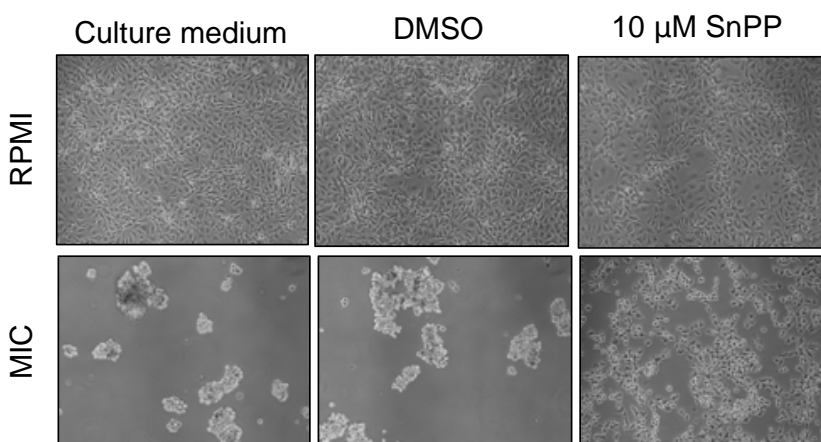
B.
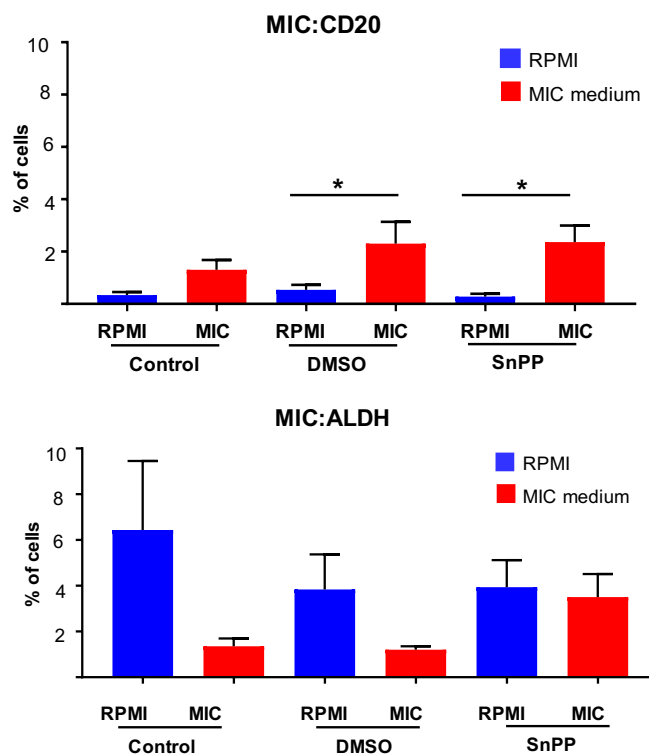
Figure 4.5. Comparison of B16-F10 cells after 7 day culture in RPMI or MIC medium, in the presence or absence of SnPP. **A.** Adherent and non-adherent growth - morphology of cells after 7 day culture (representative pictures). **B.** Flow cytometry analysis of MIC markers – CD20 expression and ALDH^{high} activity. Each bar represents mean + SEM; * - $p < 0.05$ versus MIC$^-$ cells.

(Fig. 4.5 A). This observation indicates that heme oxygenase activity plays an important role in CSC-properties of murine melanoma.

We also checked if culture of B16-F10 cells in MIC medium impacts the expression of MIC markers. It turned out that in the MIC medium the B16-F10 lines significantly increase the fraction of CD20^{+} cells (Fig. 4.5 B). In contrast, cells with a high ALDH activity tended to be less abundant in MIC medium, and SnPP abolished this trend (Fig. 4.5 B).

4.2.3. Overexpression of HO-1 decreases the clonogenic potential of melanoma cells *in vitro*

Because enzymatic activity of heme oxygenase is required for a non-adherent growth (chapter 1.1.2) and HO-1 overexpression improves progression of melanoma[147] we checked whether HO-1 overexpression can increase the clonogenic potential of B16-F10 cells. Clonogenicity is one of the features attributed to CSCs[241]. To investigate if it can be affected by overexpression of HO-1 we performed soft agar assay, that allows to study non-adherent clonogenic growth, using two lentivirally modified cell lines: with normal level of HO-1 (WT Luc) and with overexpressed HO-1 (HO-1 Luc). Unexpectedly, we found that HO-1 overexpression decreases the ability of B16-F10 cells to form spheres in the soft agar (Fig. 4.6 A, B).
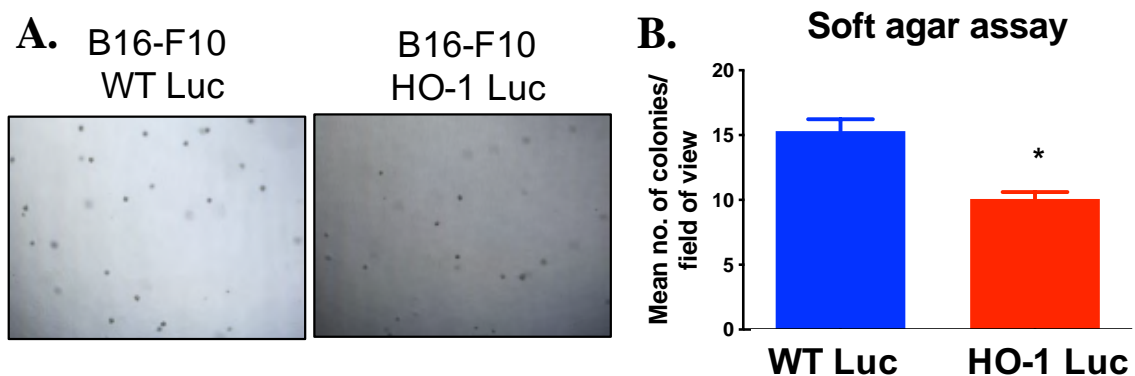
Figure 4.6. Effect of HO-1 overexpression on clonogenic potential of B16-F10 melanoma cells. Soft agar assay; WT Luc – control cells, HO-1 Luc – HO-1 overexpressing cells. **A.** Microscopic view of melanoma spheres 7 days after seeding. **B.** Number of spheres. Each bar represents mean + SEM; * - p<0.05 versus WT Luc cells.

To verify this observation we additionally analyzed formation of clones by single-cell sorted WT Luc and HO-1 Luc melanoma cells. Cells were cultured in MIC medium in normoxia (21% O$_2$) or hypoxia (0.5% O$_2$), and observed under a microscope every second day (starting at day 5 after sorting). In this experimental setting, only a minority of B16-F10 melanoma cells

(22.6%) was able to initiate clonal growth in normoxia, but this fraction was higher in hypoxia (35.2%) (Fig. 4.7 A). In accordance with the results of the soft agar assay, overexpression of HO-1 decreased the ability of single cells to form clones, both in normoxia (11.1%) and hypoxia (23.4%) (Fig. 4.7 A).

We also found that some cells started to proliferate, but eventually were not able to continue the growth and died. Clones counted after 13 days were regarded as stable, and the percentage of sorted cells that initiated clonal growth and were able to continue it, was calculated as a clonal survival rate. In standard, normoxic cell culture conditions, the survival rates of WT Luc and HO-1 Luc clones were comparable (Fig. 4.7 B). Similarly as the initiation of clone formation, also the survival rate of WT Luc clones was improved under hypoxic conditions (from 55.3% in normoxia to 85.7% in hypoxia). Such improvement was not observed, however, if cells overexpressed HO-1: the survival rate of HO-1 Luc clones was 62.3% in normoxia and 64.7% in hypoxia (Fig. 4.7 B). Thus, the reduced ability of HO-1 overexpressing cells to form the stable clones (6.9% in normoxia and 14.2% in hypoxia for HO-1 Luc versus 12.5% in normoxia and 30.1% in hypoxia for WT Luc cells) (Fig. 4.7 C) resulted from the reduced initiation of clone formation, not their subsequent survival.
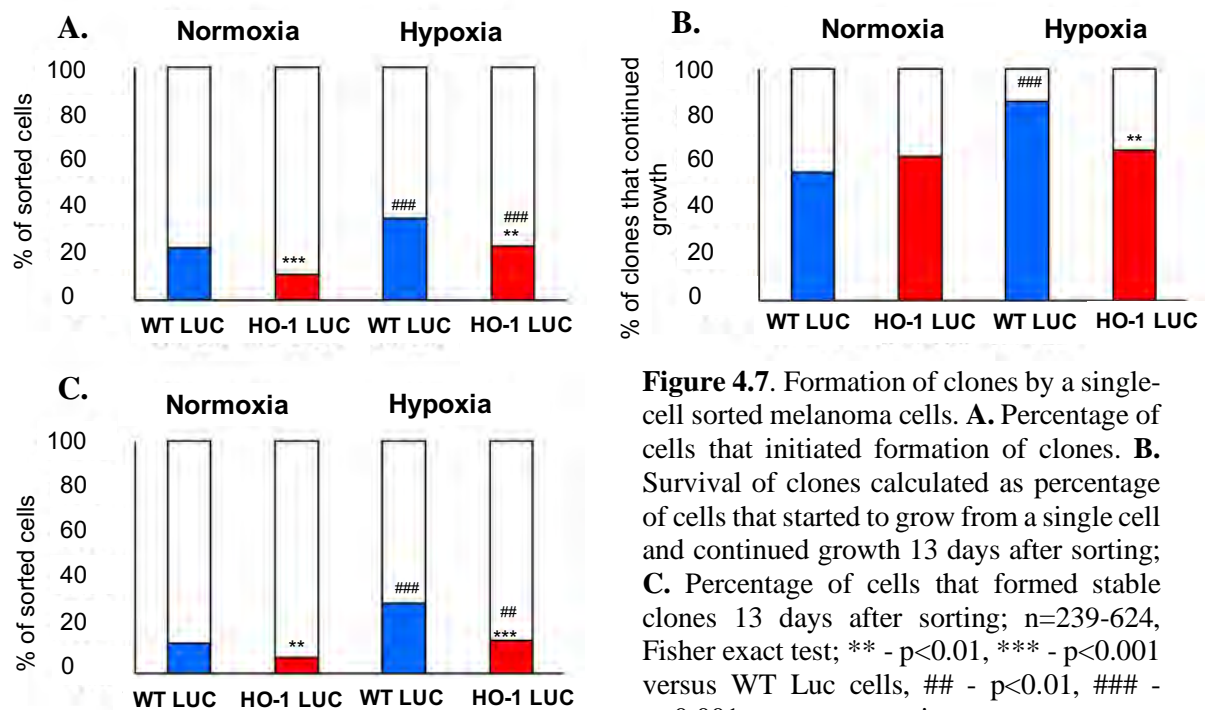
Figure 4.7. Formation of clones by a single-cell sorted melanoma cells. **A.** Percentage of cells that initiated formation of clones. **B.** Survival of clones calculated as percentage of cells that started to grow from a single cell and continued growth 13 days after sorting; **C.** Percentage of cells that formed stable clones 13 days after sorting; n=239-624, Fisher exact test; ** - p<0.01, *** - p<0.001 versus WT Luc cells, ## - p<0.01, ### - p<0.001 versus normoxia

4.2.4. Overexpression of HO-1 affects the morphology of melanoma clones

Microscopic observations revealed that B16-F10 clones differed in some morphological features. We distinguished three criteria: the size of clones (Fig. 4.8 A), presence of melanospheres (Fig. 4.8 B), and level of pigmentation (Fig. 4.8 C). Most clones formed by B16-F10 cells cultured in normoxia were classified as "small", regardless of HO-1 status. The significant differences were visible in hypoxia: 13 days after sorting approximately 60% of clones formed by control cells were "big", whereas HO-1 overexpressing cells formed almost exclusively small clones, which might reflect a lower proliferation rate (Fig. 4.8 A). Melanospheres were present in almost all clones, regardless of oxygen availability and HO-1 expression (Fig. 4.8 B). Similarly, strong pigmentation of cells (high melanin content) was characteristic for majority of control (~60%) and HO-1-overexpressing clones (~80%) in normoxia. The trend towards the development of more pigmented clones by HO-1 Luc cells was not statistically significant. In hypoxia, however, this relationship was stronger: more than
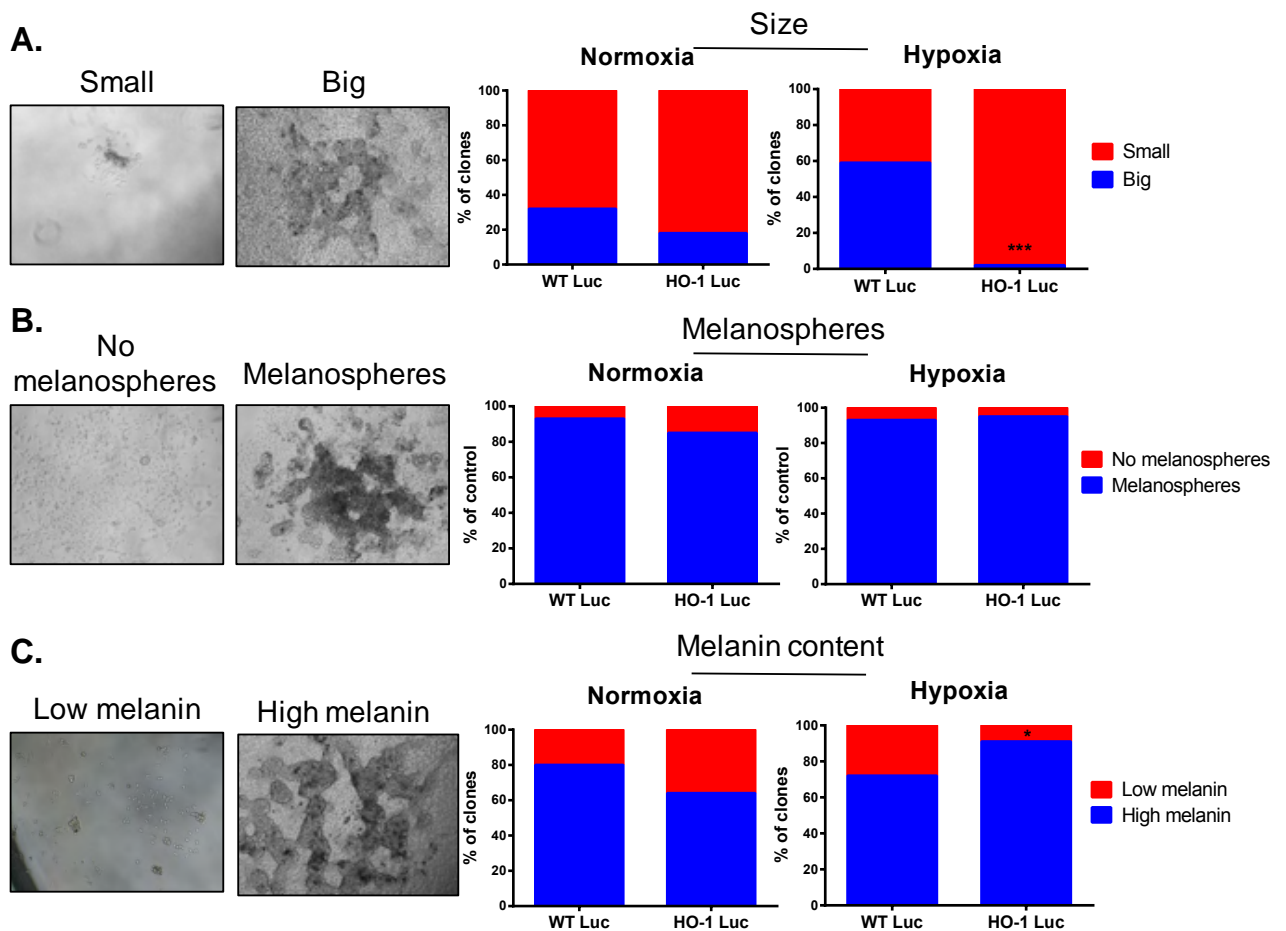
Figure 4.8. Morphology of clones formed by WT Luc and HO-1 Luc melanoma cells in normoxia and hypoxia,13 days after a single cell sorting. **A**. Size of clones **B**. Presence of melanospheres and **C.** Melanin content in clones; n=39-76, Fisher exact test; * - p<0.05, *** - p<0.001 versus WT Luc cells.

90% of clones derived from HO-1 Luc cells were highly pigmented, significantly more than in case of WT Luc clones (Fig. 4.8 C).

4.2.5. Expression of MIC markers do not influence the clonogenic potential of melanoma cells

The same clonogenic test was performed for MIC fractions. For this purpose we choose two MIC subsets: cells expressing surface antigen CD20 and cells displaying functional marker – high ALDH activity (Fig. 4.9 A). Result showed similar tendencies as observed for bulk cells, towards the increased clonogenicity in hypoxia and reduced clone formation by HO-1 overexpressing cells. Importantly, neither expression of CD20 nor ALDH activity influenced
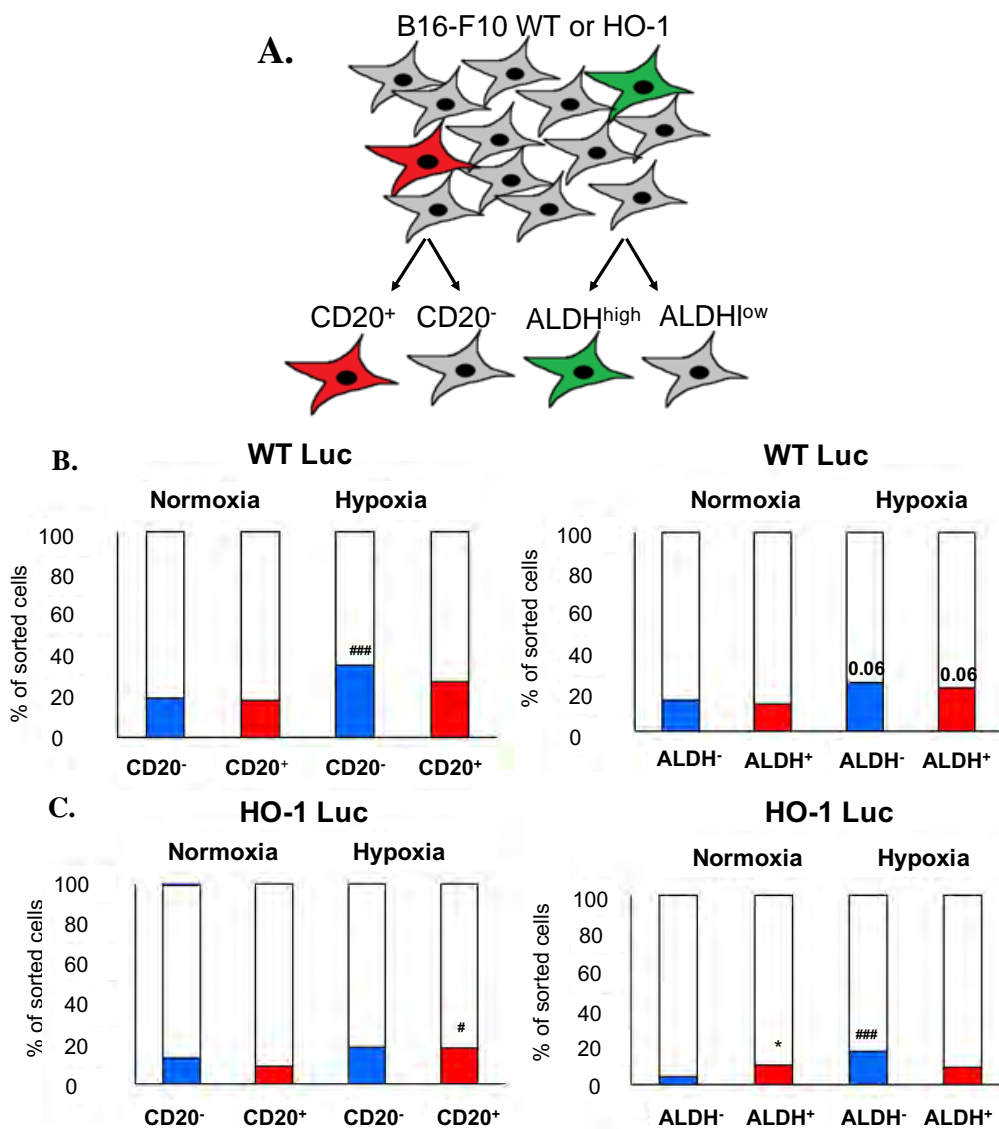
Figure 4.9. Formation of stable clones by a single-cell sorted MIC⁺ melanoma cells cultured in normoxia or hypoxia. **A.** Scheme of sorting. **B.** Comparison of MIC subsets in WT Luc cell line **C.** Comparison of MIC subsets in HO-1 Luc cell line; n=116-216; Fisher exact test, * - p<0.05 versus WT-Luc cells, # - p<0.05 versus normoxia.

the clonogenic potential of WT Luc (Fig. 4.9 B) and HO-1 Luc (Fig. 4.9 C) melanoma cell lines. Only HO-1 Luc cells with high ALDH activity increased clone formation in normoxia when compared to HO-1 Luc ALDH^{low} cells (Fig. 4.9 C), but this might be an indirect effect of a lower than normally observed clonogenicity of control cells. These results show that phenotypic or functional MIC markers in murine melanoma cell line do not identify cell fractions with increased clonogenic potential.

4.2.6. Overexpression of HO-1, but not the expression of MIC markers, alters the morphology of clones formed by MIC cells

Consistently to what was observed for bulk populations, HO-1 overexpression led to the formation of smaller clones after sorting of MIC$^-$ and MIC$^+$ cells (Fig. 4.10 A). This was once again more pronounced in hypoxia. Interestingly, cells expressing MIC markers displayed
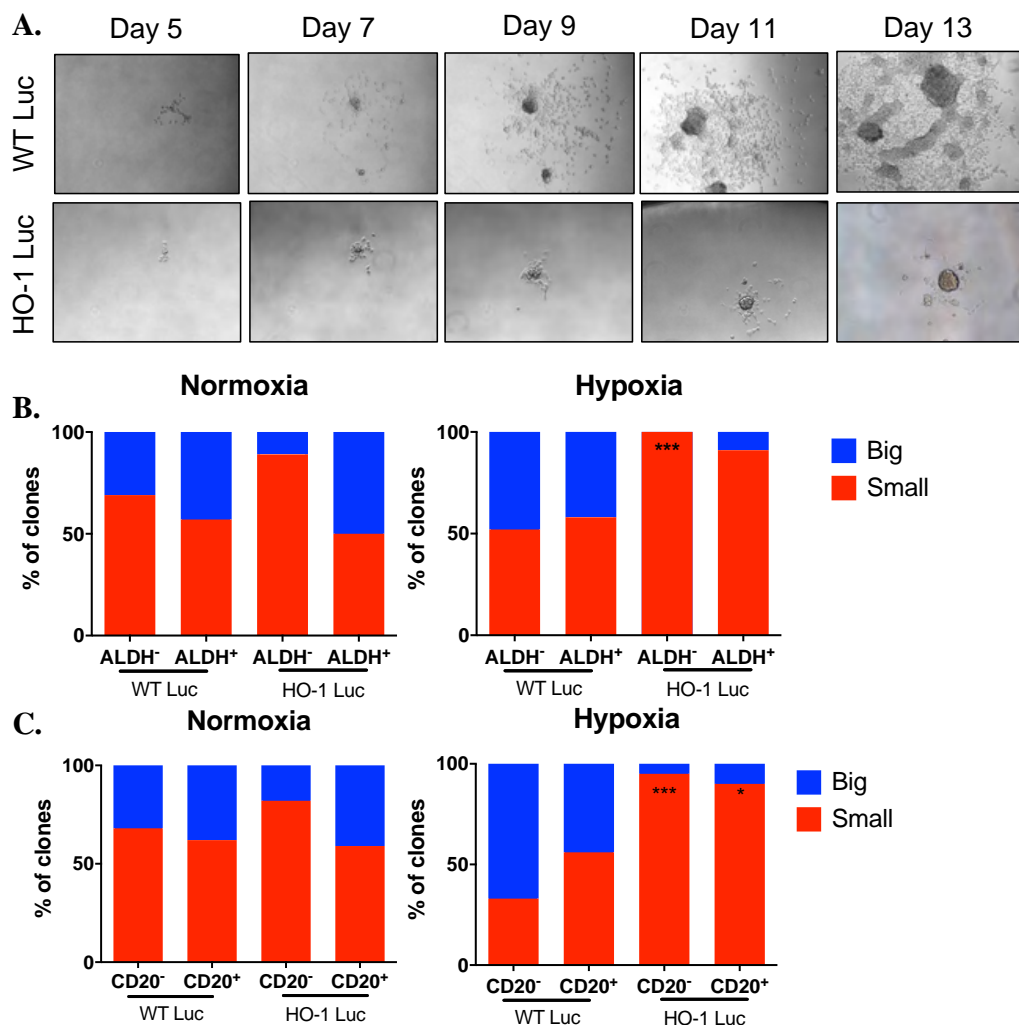
Figure 4.10. Morphology of MIC clones 13 days after sorting. **A**. Exemplary pictures of clones growing in hypoxia. **B**. Frequency of small and big ALDH^{high} and ALDH^{low} clones (n=9-32, Fisher's exact test). **C**. Frequency of small and big CD20$^-$ and CD20$^+$ clones (n=9-42, Fisher exact test; * - p<0.05, *** - p<0.001 versus WT Luc).

similar morphology as their MIC⁻ counterparts in all three measured morphological features: size (Fig. 4.10), the formation of melanospheres, and pigmentation of clones (data not shown).

4.2.7. PKH26 retaining cells are less clonogenic than PKH26- bulk cells

Next, we checked *in vitro* clonogenicity of PKH26$^+$ label retaining cells. Noteworthy, in this experiment, we observed a higher clone formation than in previous tests, and approximately 60-70% of single cells formed clones (Fig. 4.11 A). This points at an important issue, that the B16-F10 cell line is highly variable, and often the numerical values obtained using these cells may differ between experiments. Interestingly, WT Luc PKH26$^+$ cells displayed a tendency toward a lower clonogenic capacity than their PKH26⁻ counterparts (Fig. 4.11 A). Morphologically, WT-Luc PKH26$^+$ cells formed smaller and more pigmented clones (Fig. 11 B and D). Almost all clones, regardless of the PKH26$^+$ status, contained melanospheres (Fig. 4.11 C).
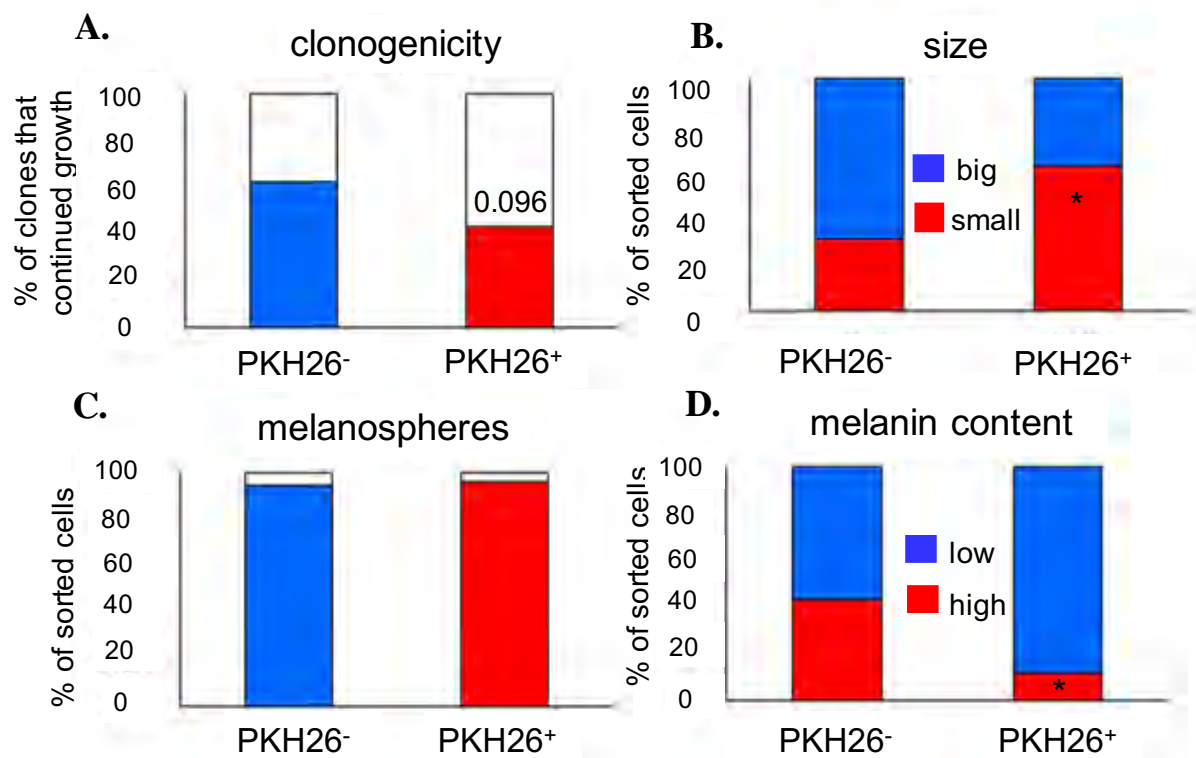
Figure 4.11. Formation of clones by single-cell sorted WT Luc PKH26⁻ and PKH26$^+$ cells: (**A**) clonogenic potential, (**B**) size of clones, (**C**) presence of melanospheres and (**D**) melanin content, analyzed 13 days after sorting (n=60 sorted cells; Fisher exact test, * - $p < 0.05$ versus PKH26⁻ cells).

In cells overexpressing HO-1, the decrease in clone formation by PKH26$^+$ cells was statistically significant (Fig. 12 A), but differences in morphology between PKH26$^-$ and PKH26$^+$ clones were less pronounced (Fig. 4.12 B-D).
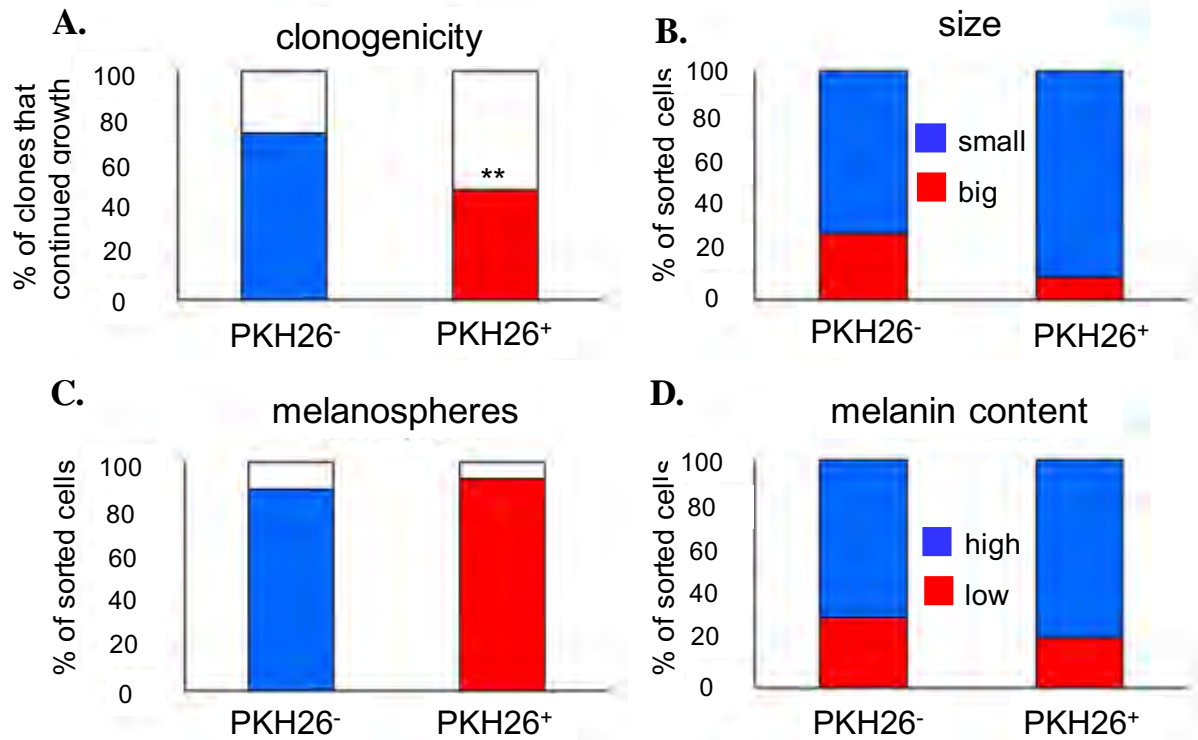
Figure 4.12. Formation of clones by single-cell sorted HO-1 Luc PKH26$^-$ and PKH26$^+$ cells: (**A**) clonogenic potential, (**B**) size of clones, (**C**) presence of melanospheres and (**D**) melanin content, analyzed 13 days after sorting (n=60 sorted cells; Fisher exact test, ** - p<0.01 versus PKH26$^-$ cells).

4.2.8. PKH26$^+$ subpopulation contains fewer clonogenic cells than PKH26$^-$ fraction and this reduction is prevented by HO-1 overexpression

Assays carried out on the individually sorted cells revealed that murine B16-F10 melanoma cell lines have a variable, but generally high ability to form clones, and that such an ability appears to be reduced in the PKH26$^+$ fraction. To validate this observation and check more exactly the active fraction of clone initiating cells (CIC) *in vitro,* we performed the extreme limiting dilution assay (ELDA). WT Luc and HO-1 Luc PKH26$^-$ and PKH26$^+$ cells were sorted in different numbers (1, 3, 5, 7, 10 per well) and cultured in the MIC medium. Positive wells were counted after two weeks of culture and frequency of clone initiating cells was calculated using ELDA software[242].

Indeed, the obtained data confirmed that CIC are relatively frequent among B16-F10 cells (1 per 4.4 and 1 per 5.6 cells for WT Luc and HO-1 Luc, respectively). Moreover, there was a clear tendency (p=0.07) to reduced CIC fraction in WT Luc PKH26$^+$ cells (1 per 8.4

cells), but overexpression of HO-1 in PKH26^{+} cells prevented this reduction (Fig. 4.13). Thus, the results of ELDA supported our earlier assumptions driven from the clonogenic assay (chapter 4.2.3). However, the goodness-of-fit test of primary ELDA data suggests that the observed effects reflect rather heterogeneity of cell population and indicate the cooperating effects between tumor cells, what limits the precision of actual determination of CSC frequency. Therefore, we performed also a secondary ELDA for a more rigorous detection of self-renewing cancer initiating cells.

Confidence intervals for 1/(clone initiating cell frequency)			
Group	Lower	Estimate	Upper
WT PKH26^{-}	6.08	4.43	3.27
WT PKH26^{+}	12.27	8.44	5.86
HO-1 PKH26^{-}	7.82	5.61	4.07
HO-1 PKH26^{+}	7.45	5.36	3.91
p value	p=0.0696		
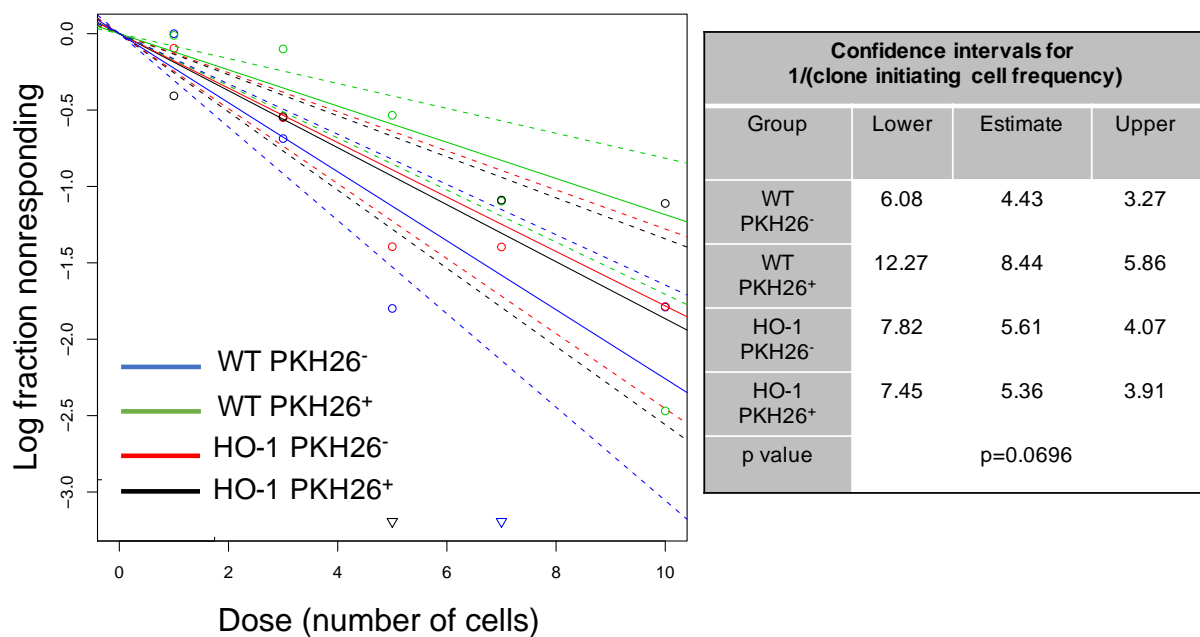
Figure 4.13. Extreme limiting dilution assay (ELDA) performed *in vitro* on sorted WT Luc and HO-1 Luc PKH26^{-} and PKH26^{+} cells. Primary ELDA was performed on primary sorted cells. Trend lines represent the estimated frequency of active cells that are able to form clones, and dotted lines represent 95% confidence intervals.

To check the CIC frequency in secondary clones, single PKH26^{-} and PKH26^{+} cells were sorted for primary clone formation. Then, the formed clones were dissociated into single cells, and sorted for secondary ELDA assay. We observed a smaller number of positive wells in secondary ELDA but the tendency that WT Luc PKH26^{+} cells have a smaller fraction of CIC remained unchanged (1 per 12.5 cells and 1 per 35.9 cells for PKH26^{-} and PKH26^{+}, respectively) (Fig. 4.14). Moreover, HO-1 overexpression once again caused the reversal of this effect. The goodness-of-fit test showed that in the secondary ELDA we actually observed the active CIC with self-renewal capacities.
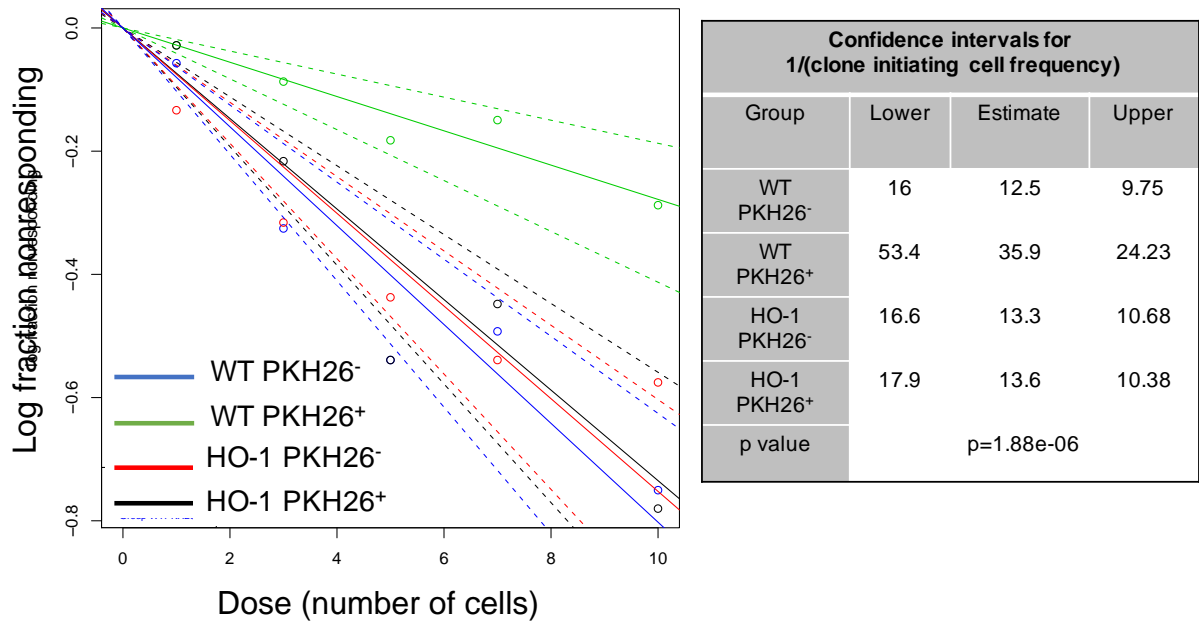
Figure 4.14. Secondary extreme limiting dilution assay (ELDA) tested *in vitro* on cells sorted after primary clones formation. Trend lines represent the estimated frequency of active cells that are able to form clones and dotted lines represent 95% confidence intervals.

4.2.9. HO-1 overexpression, not MIC markers expression, increases the expression of CSC-associated genes

Previous tests revealed that CD20^{+} or ALDH^{high} cell subpopulations have a similar clonogenic potential as the bulk, MIC^{-} B16-F10 melanoma cells (chapter 4.2.5). Here, we checked whether these subpopulations may differ from the bulk cells in the expression of genes associated with CSC function, and how such a gene expression profile is modified by overexpression of HO-1. We used the RT^{2}Profiler Array, the system that enables analysis of many genes on one plate, starting from as little as 25 ng of RNA. We analyzed 84 CSC-associated genes and used 5 housekeeping genes as controls to ensure that no particular reference gene influences the final results.

The obtained data showed that the differences in CSC-gene expression profile between WT Luc CD20^{-} and CD20^{+} B16-F10 melanoma cells are marginal. In CD20^{+} cells we only noted a decreased level of *Alcam* (coding for cell adhesion molecule that shapes the interaction of cancer cells with microenvironment), *Nfkb1* (coding for NFκB subunit, involved in regulation of cell survival and proliferation), and *Sirt1* (coding for protein deacetylase responsible for epigenetic gene silencing, that plays a role in metabolic regulation and maintaining of self-renewal) (Fig. 4.15).

Signalling pathway	CD20⁺ vs CD20⁻ WT Luc	
NF-kB signalling pathway	Nfkb1	
Cell adhesion molecule	Alcam	
Epigenetic modifiers	Sirt1	

p value	Downregulated
*	
**	
***	
****	

Figure 4.15. RT^{2}Profiler PCR array detecting genes connected with the CSC phenotype. Analysis was performed on CD20⁻ and CD20⁺ B16-F10 subpopulations sorted from B16-F10 WT Luc cell line.

Interestingly, at the same time, HO-1 overexpression was associated with upregulation of many genes, both in CD20⁻ and CD20⁺ subsets (Fig. 4.16). Generally, HO-1 overexpressing cells have an elevated expression of epigenetic modifiers (*Sirt1*), NFκB-associated genes (*Nfkb1*, *Ikbkb*), oncogenes (*Myc, Bmi1*), regulators of metabolism (*Etfa*, *Gsk3b*), as well as several mediators from the Notch (*Notch1*, *Notch2*), Hippo (*Sav1, Lats1*), and *Wnt* (Fzd7) signaling pathways (Fig. 4.16).

Signalling pathway	Gene	HO-1 vs WT	
		CD20⁻	CD20⁺
Epigenetic modifiers	Sirt1		
NF-kB signalling pathway	Nfkb1		
	Ikbkb		
Oncogenes	Bmi1		
	Erbb2		
	Myc		
Notch signalling pathway	Notch1		
	Notch2		
	Maml1		
	Jag1		
Hippo signalling pathway	Sav1		
	Lats1		
Hedgehog signalling pathway	Smo		
CSC markers	Cd44		
Integrins	Itga4		
	Itgb1		
Metabolic enzymes	Etfa		
	Gsk3b		
Pluripotency TFs	Klf4		
	Foxp1		
Wnt signalling pathway	Fzd7		
TGF-B signalling pathway	Eng		
Collagen signalling pathway	Ddr1		

p value	Upregulated
*	
**	
***	
****	

Figure 4.16. RT^{2}Profiler PCR array detecting genes connected with the CSC phenotype. Analysis was performed on CD20⁻ and CD20⁺ B16-F10 subpopulations sorted from WT Luc and HO-1 Luc cell lines.

The CSC array performed on PKH26⁻ and PKH26⁺ cells revealed that, as in the case of CD20 subsets, it is rather an overexpression of HO-1 that influences gene expression than the ability to retain dye. The only genes differently expressed in WT Luc PKH26⁺ and PKH26⁻ cells were: *Id1* (coding for transcriptional repressor that controls, among others self-renewal – downregulated in PKH26⁺ cells), *Nos2* (coding for inducible nitric oxide synthase that was suggested to promote Notch1 signaling – downregulated in PKH26⁺ cells), and *Snai2* (coding for transcription factor involved in epithelial-to-mesenchymal transition – upregulated in PKH26⁺ cells) (Fig. 4.17).

Signalling pathway	Gene	PKH26- vs. PKH26+
		WT-Luc
Epithelial-mesenchymal transition	*Snai2*	
Oxidative stress enzymes	*Nos2*	
Transcription repressor	*Id1*	

Figure 4.17. RT²Profiler PCR array detecting genes connected with the CSC phenotype. Analysis performed on PKH26⁻ and PKH26⁺ subpopulations sorted from B16-F10 WT Luc.

Both in PKH26⁻ and PKH26⁺ fractions, overexpression of HO-1 was associated with upregulation of epigenetic modifier *Dnmt1* (DNA methyltransferase that regulates self-renewal), *Abcg2* transporter (that supports chemoresistance), *Cd38* (ADP-rybosyl cyclase involved in calcium signaling, that may play a role in tumor cell escape from immune control), and *Notch1* (important for cell-renewal and epithelial-to-mesenchymal transition) (Fig. 4.18).

Signalling pathway	Gene	HO-1 vs WT			p value	Upregulated
		PKH26-	PKH26+			
CSC markers	*Abcg2*				*	
Calcium sgnalling	*Cd38*				**	
Epigenetic modifiers	*Dnmt1*				***	
Notch signalling	*Notch 1*				****	

Figure 4.18. RT²Profiler PCR array detecting genes connected with the CSC phenotype. Analysis performed on PKH26⁻ and PKH26⁺ subpopulations sorted from B16-F10 WT Luc and B16-F10 HO-1 Luc cell lines.

Unfortunately, when we attempted to sort ALDH^high cells from the B16-F10 cell line overexpressing HO-1 we were not able to detect any ALDH^high cells despite the fact that during earlier studies they were present. Therefore, the CSC array was performed only on ALDH^low and ALDH^high cells sorted from the B16-F10 WT Luc cell line. Interestingly, expression of several CSC-associated genes, like epigenetic modifier *Sirt1*, transcriptional repressor *Id1*, metabolic regulators *Etfa* and *Gsk3b*, as well as *Stat3* and its target *Foxp1* (that regulate CSC

persistence), *Scf* (Kitl, an upstream regulator of JAK/STAT, WNT, and NOTCH pathways, involved also in melanogenesis), or *Lats1* (Hippo signaling pathway) were decreased in ALDH^high cells (Fig. 4.19). This result suggests that the high activity of ALDH in B16-F10 melanoma does not mark cells with a gene expression profile typical for CSC.

Signalling pathway	ALDHhigh vs. ALDHlow WT Luc	
Epigenetic modifiers	Sirt1	
	Dnmt1	
Transcription repressor	Id1	
Metabolic enzymes	Etfa	
	Gsk3b	
Pluripotency TFs	Foxp1	
Cell survival	Stat3	
Melanogensis cytokine	Scf	
Integrins	Itga4	
Notch signalling pathway	Maml1	
CSC markers	CD44	
Plasminogen activation	Plaur	
Tumor supressor gene	Dach1	
TGF-B signalling pathway	Eng	
	Tgfbr1	
Collagen signalling pathway	Ddr1	
Epithelial-mesenchymal transition	Zeb1	

p value	Downregulated
*	
**	
***	
****	

p value	Upregulated
*	
**	
***	
****	

Figure 4.19. RT^{2}Profiler PCR array detecting genes connected with the CSC phenotype. Analysis performed on ALDH^low and ALDH^high subpopulations sorted from B16-F10 WT Luc cell line.

4.3. Characterization of MIC progeny

4.3.1. Progeny of MIC$^+$ cells reconstitute the heterogeneity of the parental cell line

Clones formed by MIC$^+$ cells continued to grow, giving rise to new clonogenic cell lines. We checked if these cell lines differ from the parental ones. For this purpose, we analyzed cell cycle, expression of MIC markers, and expression of MAAs (Fig. 4.20).

Cell cycle was investigated after staining of cells with propidium iodide and treatment with RNase A. Analysis was performed using ModFit software (Fig. 4.21 A). The obtained data revealed that the frequency of cells at different cycle phases in the MIC$^+$-derived cell lines was very similar to that of the parental cell line (Fig. 4.21 B). Moreover, HO-1 overexpression affected cell cycle neither in parental nor in the MIC$^+$-derived lines (Fig. 4.21 B).
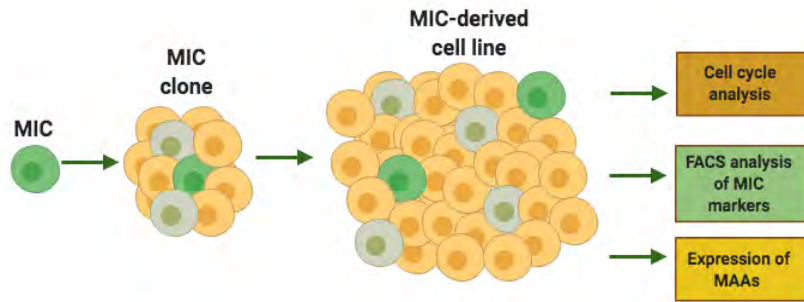
Figure 4.20. Characterization of MIC-derived clonogenic cell lines. Illustration created in BioRender.
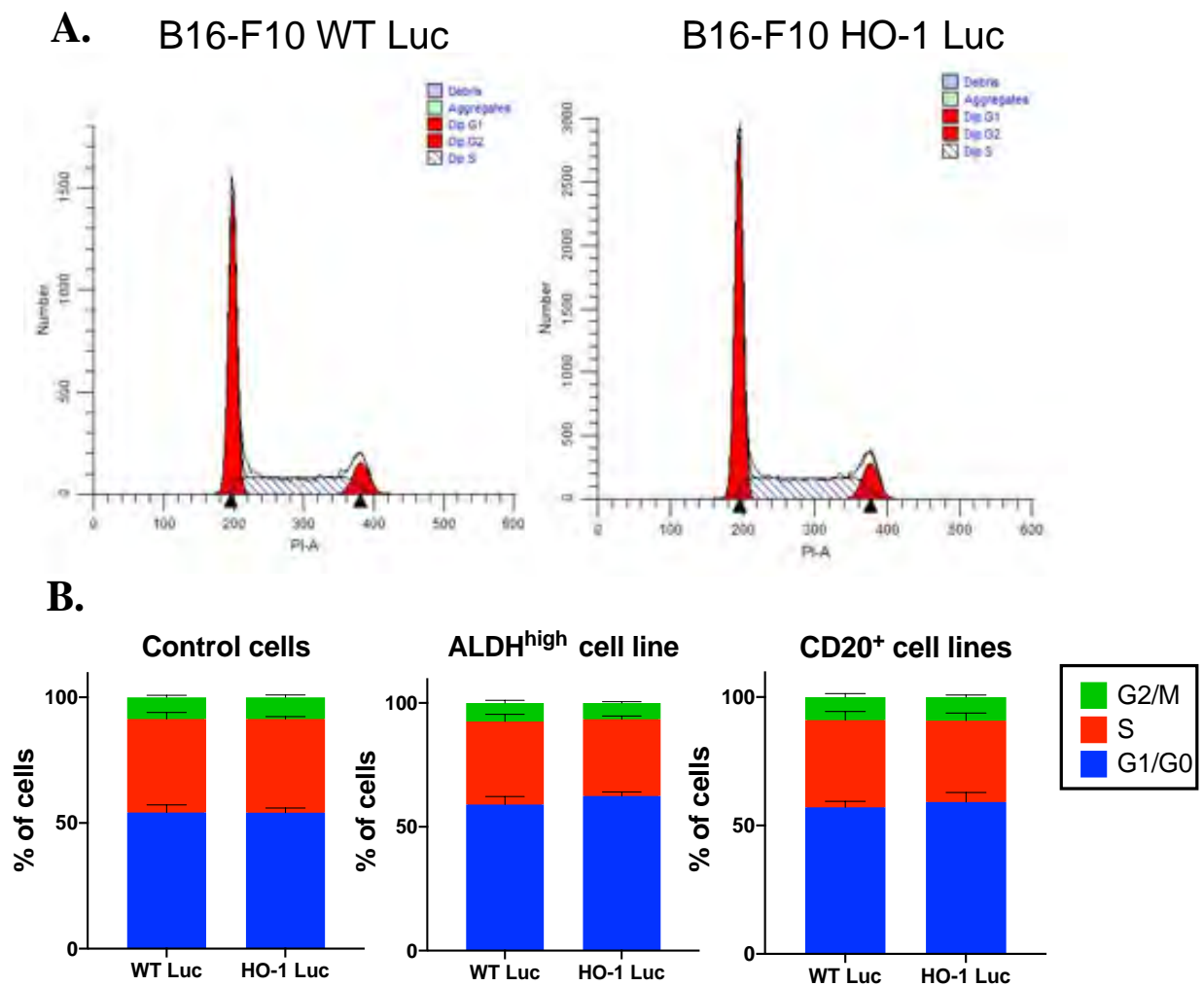
Figure 4.21. Frequency of cells at different cell cycle phases in parental (control) lines and in cell lines derived from ALDH^{high} and CD20$^+$ clones. Flow cytometry; bars represent means + SEM.

Next, we checked if MIC[+]-derived cell lines are enriched in MIC[+] subsets. Surprisingly, ALDH[high]-derived cell lines showed a tendency (p=0.052) to a lower frequency of ALDH^{high} cells than the parental B16-F10 line (Fig. 4.22 A). However, other MIC^{+} subpopulations (CD20^{+}, CD24^{+} and CD133^{+}) were not significantly changed in clonogenic cell lines, regardless of the founder cell phenotype (Fig. 4.22 A). Thus, we demonstrated that MIC[+]-derived clonogenic cell lines were not enriched in MIC-expressing cells. Also, overexpression of HO-1 did not further influence MIC composition. As shown in Fig. 4.22 B, frequency of MIC^{+} cells

A.

B.
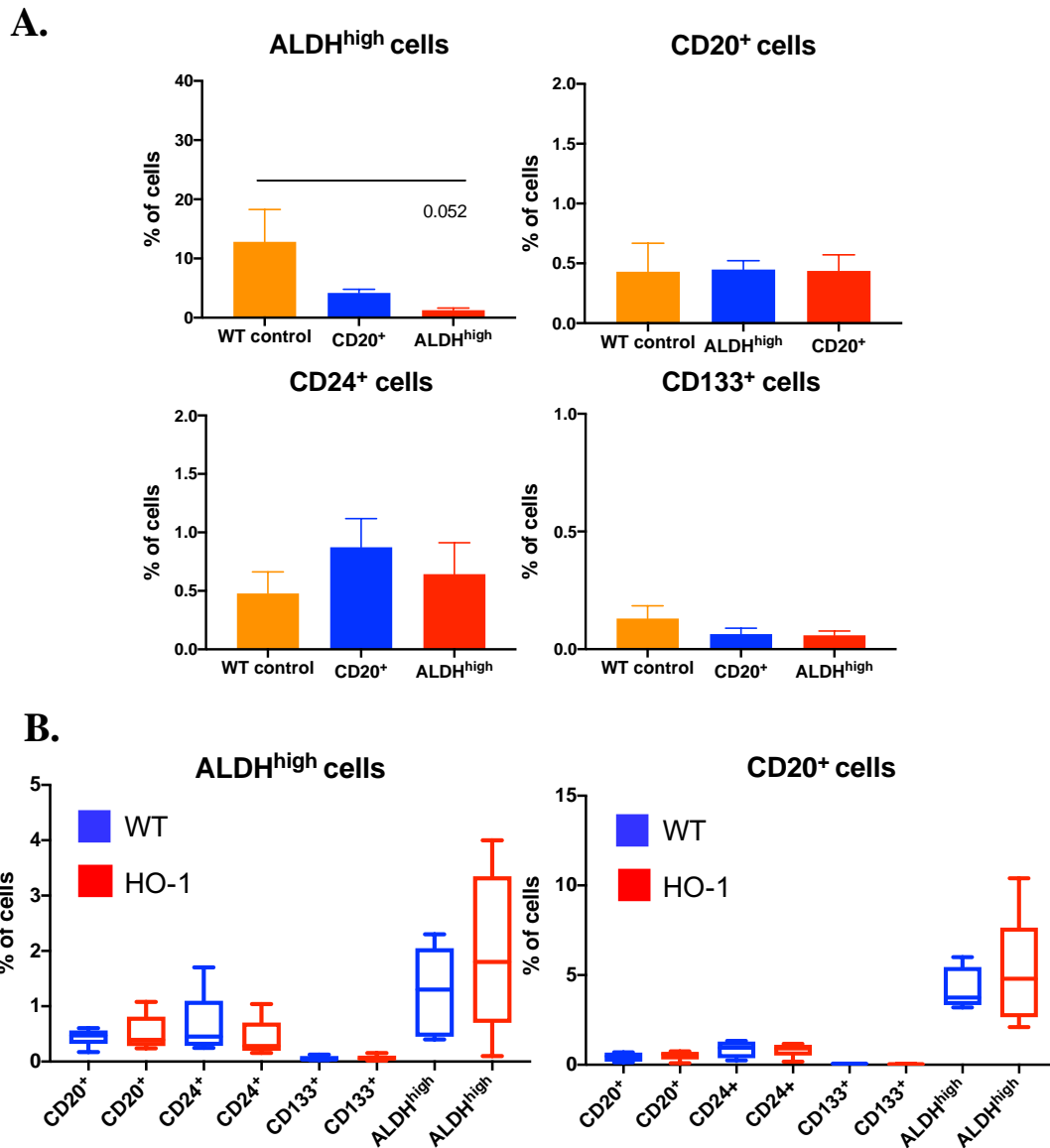
Figure 4.22. A. Frequency of MIC^{+} cells (ALDH^{high}, CD20^{+}, CD24^{+}, and CD133^{+}) in the parental cell lines (WT luc), CD20-derived clonogenic cell lines and ALDH^{high}-derived clonogenic cell lines. Flow cytometry analysis. Each bar represents mean + SEM. **B.** Frequency of MIC-expressing cells in the wild type (WT) and HO-1 overexpressing (HO-1) ALDH^{high}-derived and CD20^{+}-derived cell lines. Box and whisker plots.

(CD20$^+$, CD24$^+$, CD133$^+$, ALDH^{high}) in CD20-derived and ALDH^{high}-derived cell lines is similar in wild type cells and HO-1 overexpressing cells.

In the final step of the characterization of clonogenic cell lines, we analyzed expression of MAAs. We compared CD20$^-$ and CD20$^+$-derived (Fig. 4.23 A) as well as ALDH^{low} and ALDH^{high}-derived (Fig. 4.23 B) lines. We did not find any statistically significant differences in expression of *Tyr*, *Mitf*, *Gp100* and *Mart1*. So, we conclude that cell lines derived from a single MIC$^+$ cell can restore the heterogeneity of phenotype and gene expression profile typical for parental cell line.
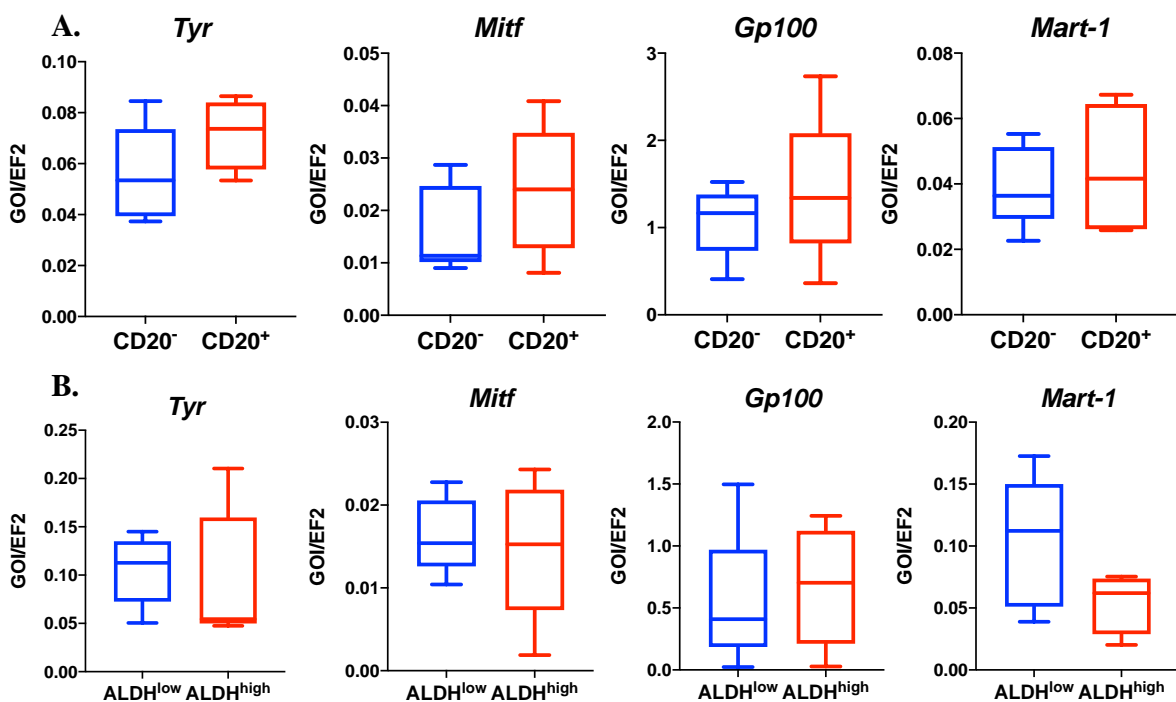
Figure 4.23. Expression of MAAs (tyrosinase, Mitf, Gp100 and Mart1) in cell lines derived from single CD20$^-$ and CD20$^+$ cells (**A**) or single ALDH^{low} and ALDH^{high} cells (**B**). qRT-PCR analysis, EF2 was used as a housekeeping control; box and whisker plots.

4.3.2. Progeny of PKH26$^+$ cells is not enriched in MIC subsets and functionally resembles the PKH26$^-$-derived cells

We analyzed also the clonogenic cell lines derived from the single, slowly dividing PKH26$^+$ cells, and compared them with clonogenic cell lines derived from the single PKH26$^-$ cells. First, we compared the frequency of PKH26$^+$ and ALDH^{high} subpopulations (Fig. 4.24). FACS analysis showed that PKH26$^+$-derived clonogenic cell lines were not enriched either in slowly dividing PKH26$^+$ cell fraction (Fig. 4.24 A) or in the cells with a high ALDH activity (Fig. 4.24 B). Next, we checked the expression of MAAs. Quantitative RT-PCR revealed that

PKH26[+] progeny has a decreased expression of *Gp100* and *Trp2* antigens, and shows a tendency to decrease also the expression of *Mitf* (Fig. 4.25).

A.

PKH26^{high} cells

B.
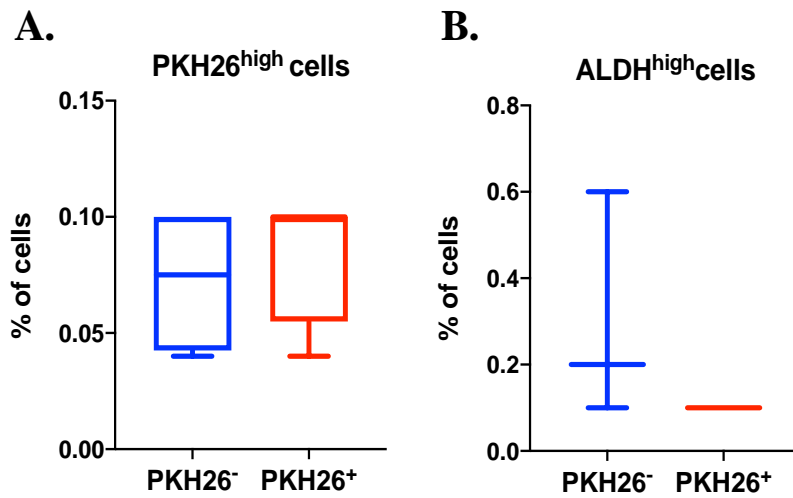
ALDH^{high} cells

Figure 4.24. Frequency of PKH26^{high} (**A**) and ALDH^{high} cells (**B**) in clonogenic cell lines derived from PKH26^{+} and PKH26^{-} cells, identified 10 days after staining with PKH26. Flow cytometry analysis; box and whisker plots.

MAAs

cell viability
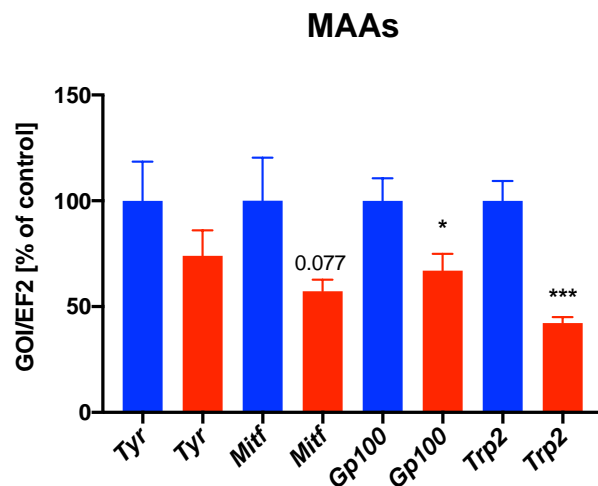
Figure 4.25. Expression of melanoma associated antigens (MAAs) in clonogenic cell lines derived from PKH26^{-} and PKH26^{+} cells. Quantitative RT-PCR analysis, EF2 was used as a housekeeping control; each bar represents mean + SEM; * - $p<0.05$, *** - $p< 0.001$ versus PKH26^{-}-derived cell lines).
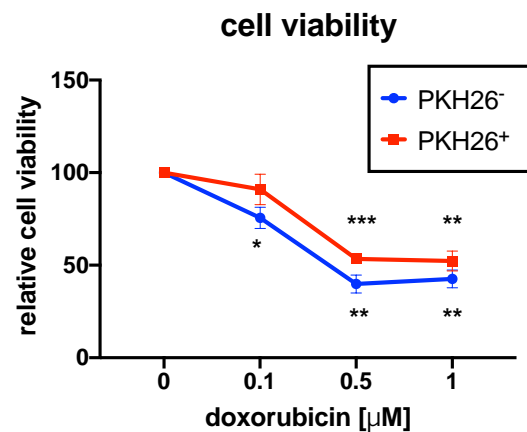
Figure 4.26. Effect of doxorubicin on viability of clonogenic cell lines derived from PKH26^{-} and PKH26^{+} cells. Cells were treated with doxorubicin for 24 h. MTT reduction assay; each point represents mean ± SEM; * - $p<0.05$, ** - $p< 0.01$, *** - $p< 0.001$ versus untreated cells).

As a slow cycling is regarded to be one of the factors contributing to chemoresistance of cells[91] we investigated whether the progeny of PKH26^{+} cells is more resistant to different concentrations of doxorubicin. MTT reduction assay performed after a 24 h incubation period showed a dose-dependent toxicity of doxorubicin. Statistically significant decrease in cell viability was observed at the concentration of 0.1 µM for PKH26^{-}-derived cells, but not in PKH26^{+}-derived cells. At the concentration of 0.5 µM and 1.0 µM concentrations no

meaningful differences were found in response to doxorubicin between the PKH26^{-}-derived and PKH26^{+}-derived cell lines.

4.3.3. Progeny of ALDH^{high} cells does not show increased resistance to doxorubicin

High activity of ALDH was previously described to be responsible for chemoresistance of different cancer cell types[66]. Thus, we checked if the progeny of these cells are more resistant to doxorubicin. Cytotoxicity of doxorubicin was strongly pronounced in this set of experiments, but we did not observe any differences in response to the treatment between ALDH[high] clonogenic cell lines and control cells (Fig. 4.27).
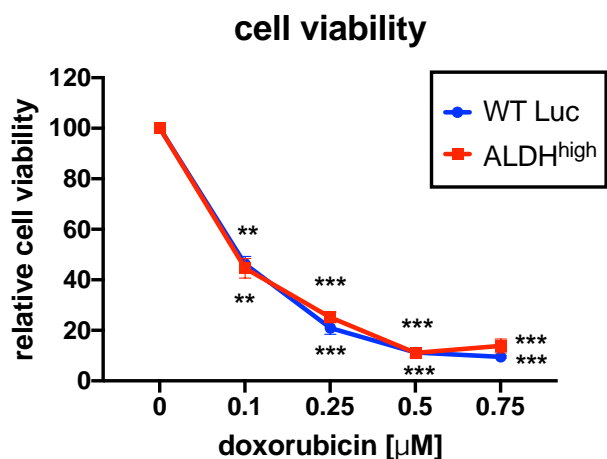
Figure 4.27. Effect of doxorubicin on viability of clonogenic cell lines derived from ALDH^{high} cells and control cell line. Cells were treated with doxorubicin for 24 h. MTT reduction assay; each point represents mean ± SEM; ** - p< 0.01, *** - p< 0.001 versus untreated cells). Experiments were performed with help of Michalina Mróz and Estera Krzak.

4.3.4. Progeny of CD20^{+} murine melanoma cells do not differentiate into osteogenic or adipogenic lineage

In human melanoma, long-established cell lines cultured as spheroids were shown to upregulate the expression of CD20 antigen[58]. On the other hand, human melanoma spheroids were reported to be capable of differentiation into mesenchymal linage, similarly to multipotent neural crest cells. Interestingly, when CD20^{+} and CD20^{-} fractions were cultured under conditions that promote mesenchymal differentiation, only CD20^{+} spheroids retained a potential for adipogenic, chondrogenic, and osteogenic commitment[58].

Therefore, we decided to check if within the progeny of CD20^{+} murine melanoma there are cells that display the potential to differentiate to mesenchymal linage, just like it was shown in human melanoma. We cultured CD20^{-} and CD20^{+} clonogenic cell lines in osteogenic and adipogenic media[232]. After 3 days of culture cells changed their morphology: they had a mesenchymal-like shape, and some of them formed syncytia and contained vacuoles (Fig. 4.28 A). We continued the cell differentiation up to day 11 and performed the Oil Red O staining

(for visualization of adipocytes) and alkaline phosphatase activity staining (ALP; to check osteogenic differentiation). Despite the changes in morphology we did not find any positive cells (data not shown). Additionally, differentiated cells did not express Fabp2 (fatty acid-binding protein 2) nor Pparg (peroxisome proliferator-activated receptor-γ), the markers of adipogenic differentiation (data not shown). We only observed the expression of osteonectin (Sparc), which was present in at similar level in CD20^{-} and CD20^{+}-derived cells cultured in DMEM, and was significantly elevated in osteogenic medium. Fold of change in of Sparc expression, induced by osteogenic medium, was comparable between CD20^{-} and CD20^{+} clonogenic cell lines (Fig. 4.28 B). Nevertheless, the expression of Sparc alone cannot be regarded as a proof of functional differentiation toward osteogenic lineage. This gene contributes also to melanoma dissociation[243] and is involved in directing melanoma cells to form metastases in the lungs[244].

Generally, experiments performed in clonogenic cell lines derived from MIC^{+} cells demonstrated that such lines restore heterogeneity of parental cells and do not differ both phenotypically and functionally from clonogenic lines derived from MIC^{-} cells.
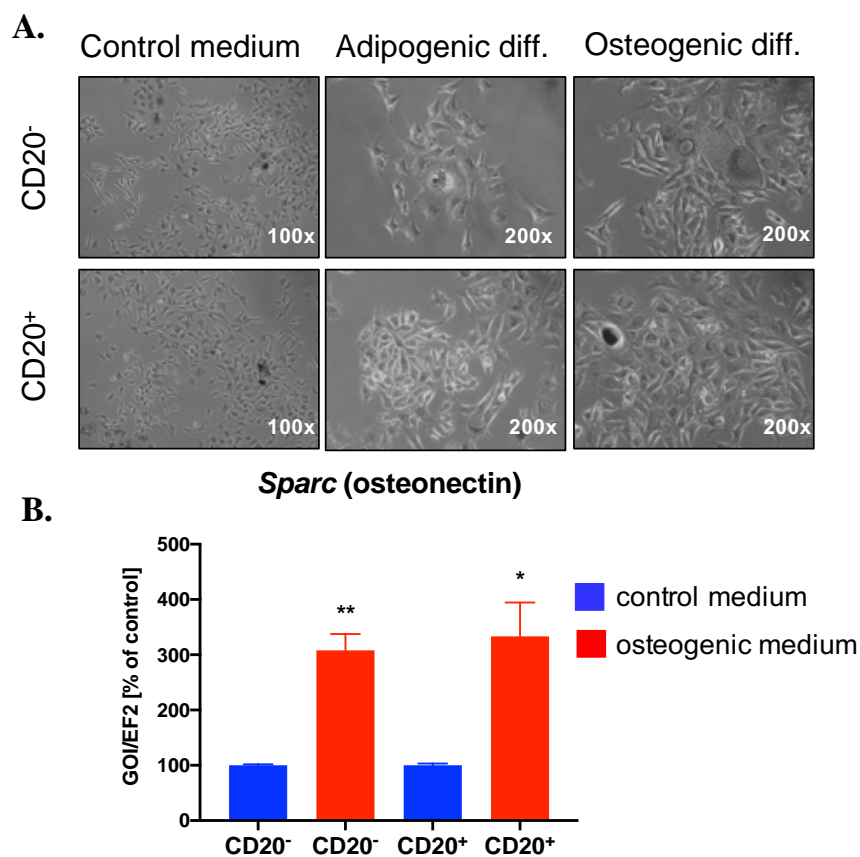
Figure 4.28. Differentiation of B16-F10 WT CD20^{-} and CD20^{+} derived cell lines in adipogenic and osteogenic medium. Cells were cultured for 11 days, DMEM medium was used as a control. **A**. Representative microscopic pictures of cells after 3 days of differentiation. **B.** Expression of *Sparc*. Quantitative RT-PCR, EF2 was used as a housekeeping control; each bar represents mean + SEM; * - p<0.05 versus control.

4.4. *In vivo* evaluation of tumorigenicity and self-renewal of MIC[+] subsets

4.4.1. Overexpression of HO-1 enhances survival of melanoma cells but decreases their self-renewal and tumorigenicity in serial transplantation assay

Our *in vitro* experiments suggested that HO-1 overexpression leads to the decreased clonogenicity of B16-F10 melanoma cells (chapter 4.2.3). To verify this inference we performed a series of *in vivo* experiments. The gold standard in research on CSC tumorigenicity is the injection of a small number of cells or even single cells *in vivo* and, after tumor formation, serial transplantations of the tumor-derived cells. Such an approach allows to check if the transplanted cells retain the tumorigenic potential and self-renew. The assumption here is that only cells with CSC properties are able to form heterogeneous tumors from single cells[245].

The presence of CSCs in human melanoma has been put in question when it appeared that changes in xenotransplantation assays seem to have a higher influence on the tumorigenic potential of melanoma cells than the expression of CSC markers[95,96]. Thus, there is a need for further evaluation of the tumorigenic potential of melanoma cells, especially in immunocompetent hosts. B16-F10 cell line is syngeneic to C57BL/6 mice which makes it a unique and interesting model for *in vivo* evaluation of MIC cells.

First, we performed *in vivo* transplantation of cells that were not selected for any MIC marker. We used B16-F10 WT Luc and HO-1 Luc cells, sorted them, and injected 10 cells per plug to the primary recipients, namely to the GFP-expressing C57BL/6 transgenic immunocompetent mice (Fig. 4.29 A). After formation of primary tumors, mice were sacrificed, tumors were digested, and 100 tumor-derived cells were injected to the secondary recipients. The same procedure was performed for the tertiary recipients (Fig. 4.29 A).

The obtained data showed that after injection of 10 B16-F10 WT-Luc melanoma cells, tumors were formed in 15% of injected Matrigel plugs, even though no purification of MIC subpopulation was performed (Fig. 4.29 B, C). Overexpression of HO-1 increased the efficacy of primary tumor formation up to 35% (Fig. 4.29 C), what might be a result of improved melanoma cell survival[147]. Interestingly, when primary tumors were transplanted to the secondary recipients, as much as 90% of transplanted plugs formed tumors in the WT group, but only 57% in the HO-1 group. A similar relationship, with a lower tumor formation rate by HO-1 overexpressing cells, was found in tertiary transplantation (Fig. 4.29 B, C).
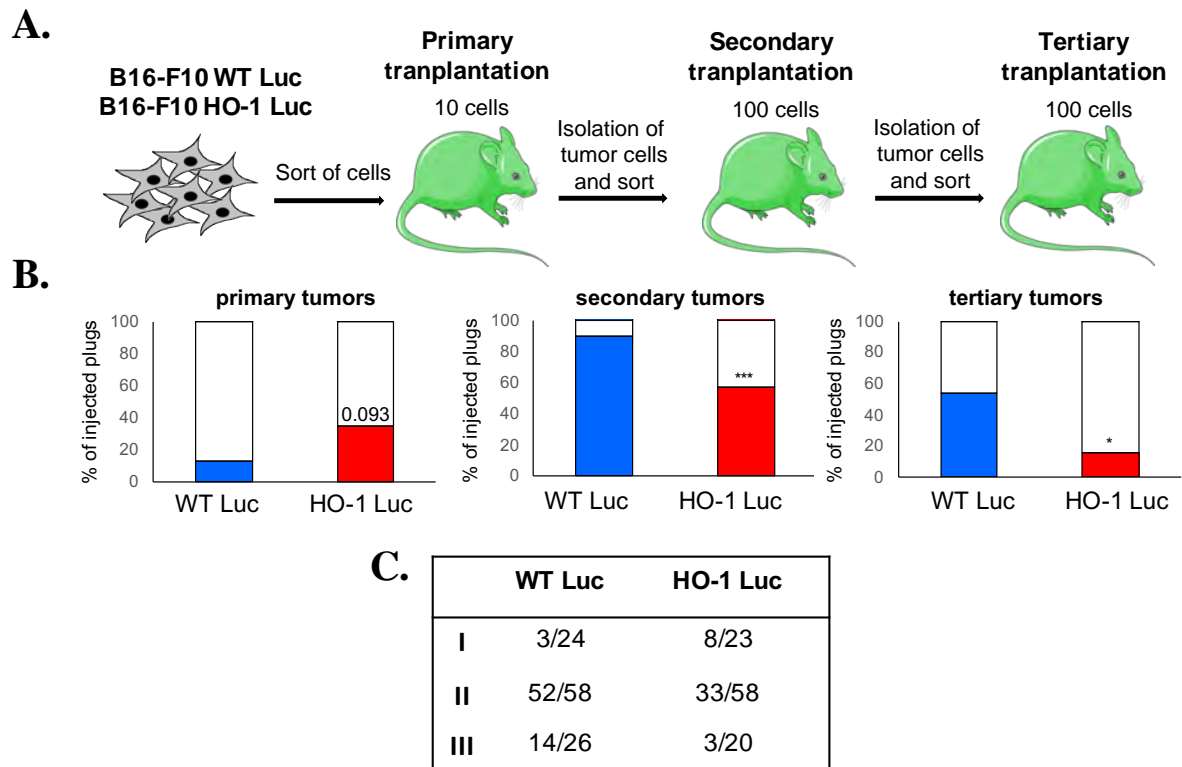
Figure 4.29. *In vivo* syngeneic transplantation of B16-F10 WT Luc and HO-1 Luc cells. **A.** Scheme of the experiment. Primary recipients (C57BL/6-Tg(UBC-GFP)30Scha/J mice) were injected with 10 sorted cells (two Matrigel plugs, each with 10 cells per mouse). After tumor formation, mice were sacrificed, tumors were excised, and GFP⁻/7AAD⁻/Hoechst⁺ cells were sorted and transplanted to the secondary recipients (100 cells per plug). The tertiary transplantations were performed in the same way. **B.** Tumor formation efficacy presented as a percentage of injected plugs that grew as tumors in each group. Fisher exact test (N=20-58); * - p<0.05, *** - p<0.001 versus WT Luc **C.** Table with number of tumors that grew in each experimental group (growth/injection).

The growth of tumors was monitored with IVIS, starting from the day 7th after transplantation (Fig. 4.30). Overexpression of HO-1 increased the growth rate of primary tumors at the beginning, as indicated by a stronger luminescence of the luciferase-expressing melanoma cells (Fig. 4.30 B), but with time the differences in the signal levels between WT-Luc and HO-1-Luc tumors were blurred (Fig. 4.30 A), and HO-1 overexpressing tumors reached later the point at which experiment had to be terminated. Mice that did not develop tumors after melanoma injection were monitored for up to 15 weeks, but no tumorigenesis was observed at later time points. Survival rate of mice injected with WT-Luc and HO-1-Luc B16-F10 cells was comparable (although slightly, not significantly reduced in the HO-1-Luc group), and mortality was observed only in animals that developed tumors (Fig. 4.27 C) .

A. B16-F10 WT Luc

Mouse ID	Plug	7 days	15 days	28 days	35 days		Total Flux [p/s]
1721D	R	(white)	10^4–10^5 (yellow)	10^7–10^9 (dark)	X		$< 10^4$ (white)
1713D	L	10^4–10^5 (yellow)	10^5–10^6 (orange)	10^5–10^6 (orange)	X		10^4–10^5 (yellow)
1715D	L	10^5–10^6 (orange)	10^6–10^7 (red)	10^7–10^9 (dark)	X		10^5–10^6 (orange)
							10^6–10^7 (red)
							10^7–10^9 (dark)

B16-F10 HO-1 Luc

Mouse ID	Plug	7 days	15 days	28 days	35 days	42 days	49 days
1790D	L	(white)	10^7–10^9 (dark)	10^7–10^9 (dark)	10^7–10^9 (dark)	10^5–10^6 (orange)	X
1790D	R	(white)	(white)	10^7–10^9 (dark)	10^6–10^7 (red)	10^5–10^6 (orange)	X
1785D	L	10^6–10^7 (red)	10^6–10^7 (red)	10^6–10^7 (red)	10^7–10^9 (dark)	X	X
1786D	L	(white)	(white)	10^6–10^7 (red)	X	X	X
1786D	R	(white)	(white)	10^7–10^9 (dark)	X	X	X
1787D	L	10^6–10^7 (red)	10^5–10^6 (orange)	10^7–10^9 (dark)	10^7–10^9 (dark)	X	X
1787D	R	10^6–10^7 (red)	10^4–10^5 (yellow)	10^7–10^9 (dark)	10^7–10^9 (dark)	X	X
1783D	R	10^4–10^5 (yellow)	10^5–10^6 (orange)	10^5–10^6 (orange)	10^7–10^9 (dark)	X	X
1785D	R	10^5–10^6 (orange)	(white)	(white)	(white)	(white)	X

B. Day 7 — Total flux [p/s] bar graph (WT Luc, HO-1 Luc)

C. Survival curve — Percent survival vs Weeks (WT Luc, HO-1 Luc)

Figure 4.30. A. Growth of tumors formed by WT Luc and HO-1 Luc melanoma cells in the primary recipients. Measurements of luminescence by IVIS. **B**. Luminescence of tumors 7 days after cell transplantation. Data represented as mean ± SEM. **C.** Survival curve of the primary recipients. Mice were sacrificed when tumors reached 10 mm in diameter. Mantel-Cox test.

When cells were transplanted to the secondary recipients (100 cells/plug) HO-1 overexpression led to the reduced initiation of tumor growth (Fig. 4.29 B) and, in a consequence, better survival of animals (Fig 4.31 A, B). Melanoma cell-derived luminescence strongly increased with time, regardless of the HO-1 status. Similar relationships were observed in the tertiary recipients (Fig. 4.29 B, Fig. 4.32 A, B), where initiation of tumor growth was reduced and survival of animals was improved if melanoma cells overexpressed HO-1. Generally, these data indicate that overexpression of HO-1 decreases the self-renewal and tumorigenicity of melanoma cells in serial *in vivo* transplantation assay. This is in line with the decreased clonogenic potential of these cells observed *in vitro* (chapter 4.2.3).

A. **B16-F10 WT Luc**

B16-F10 HO-1 Luc

Total Flux [p/s]	
	< 10^4
	10^4 - 10^5
	10^5 - 10^6
	10^6 - 10^7
	10^7 - 10^9

B.
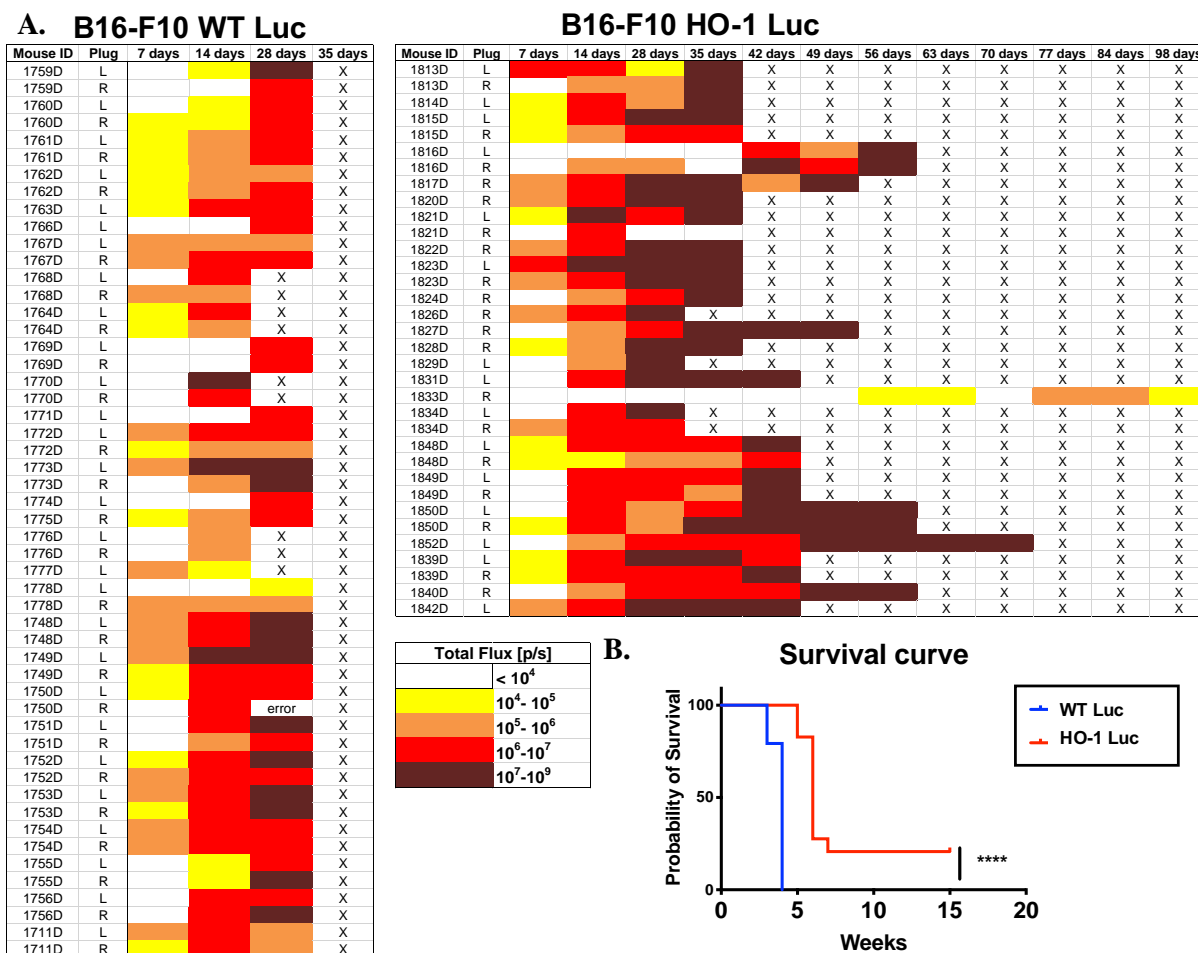
Survival curve

Figure 4.31. A. Growth of tumors formed by WT Luc and HO-1 Luc melanoma cells in the secondary recipients. Measurements of luminescence by IVIS. **B.** Survival curve of the secondary recipients. Mice were sacrificed when tumors reached 10 mm in diameter. Mantel-Cox test; *** - p<0.001.

4.4.2. HO-1 overexpression does not affect metastatic potential of melanoma cells

After the mice were killed, the organs were harvested and luminescence signals were measured to visualize tumor metastases. We found that melanoma cells metastasized preferentially to the intestine and liver, but we also observed some metastases in the spleen and lungs (Fig. 4.33 A, B). It appears that HO-1 does not influence the metastatic potential of cells in the primary recipients, as there was a similar number of animals that developed metastases (Fig. 4.33 A). Interestingly, we observed that in the secondary recipients, cells were able to form metastases also in spleen and lungs but they almost completely lost their metastatic potential in tertiary recipients (Fig. 4.33 A).

A.

B16-F10 WT Luc

Mouse ID	Plug	7 days	14 days	21 days	28 days	49 days	56 days
1798D	L					X	X
1800D	L					X	X
1800D	R					X	X
1801D	L					X	X
1801D	R					X	X
1802D	R					X	X
1794D	L				X	X	X
1794D	R				X	X	X
1795D	R				X	X	X
1796D	L						X
1797D	L					X	X
1797D	R					X	X
1806D	L				X	X	X
1810D	R						

Total Flux [p/s]:
- $< 10^4$
- $10^4 - 10^5$
- $10^5 - 10^6$
- $10^6 - 10^7$
- $10^7 - 10^9$

B16-F10 HO-1 Luc

Mouse ID	Plug	7 days	14 days	21 days	28 days	49 days	56 days	63 days
1858D	R							
1857D	R					X	X	X
1859D	R							X

Mouse ID	Plug	9 days	14 days	22 days	30 days	34 days	41 days	55 days
1835D	R							X

B.

Survival curve
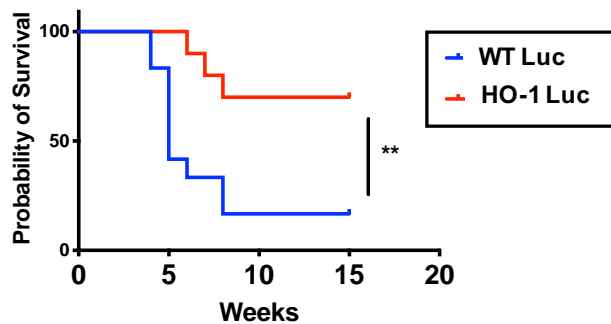
Figure 4.32. A. Growth of tumors formed by WT Luc and HO-1 Luc melanoma cells in the tertiary recipients. Measurements of luminescence by IVIS. **B.** Survival curve of the tertiary recipients. Mice were sacrificed when tumors reached 10 mm in diameter. Mantel-Cox test; ** - $p < 0.01$.

4.4.3. Tumors are not enriched in ALDH^{high} cells in serial transplantation assay

The high activity of ALDH is presumed to be associated with the increased tumorigenic potential of melanoma cells[246,247]. Therefore, we compared whether the fraction of ALDH^{high} cells increases with serial transplantation. Although in some experiments performed in B16-F10 line cultured *in vitro* we observed relatively high proportion of ALDH[high] fraction (Fig. 4.1 D), among the melanoma cells isolated from growing tumors, the ALDH[high] subset was rare,

representing less than 1% of cancer cells. In several tumors we were unable to detect any ALDH^{high} cells (Fig. 4.34). Moreover, there was no increase in frequency of ALDH^{high} subpopulation between primary, secondary and tertiary tumors in serial transplantation (Fig. 4.34 A).
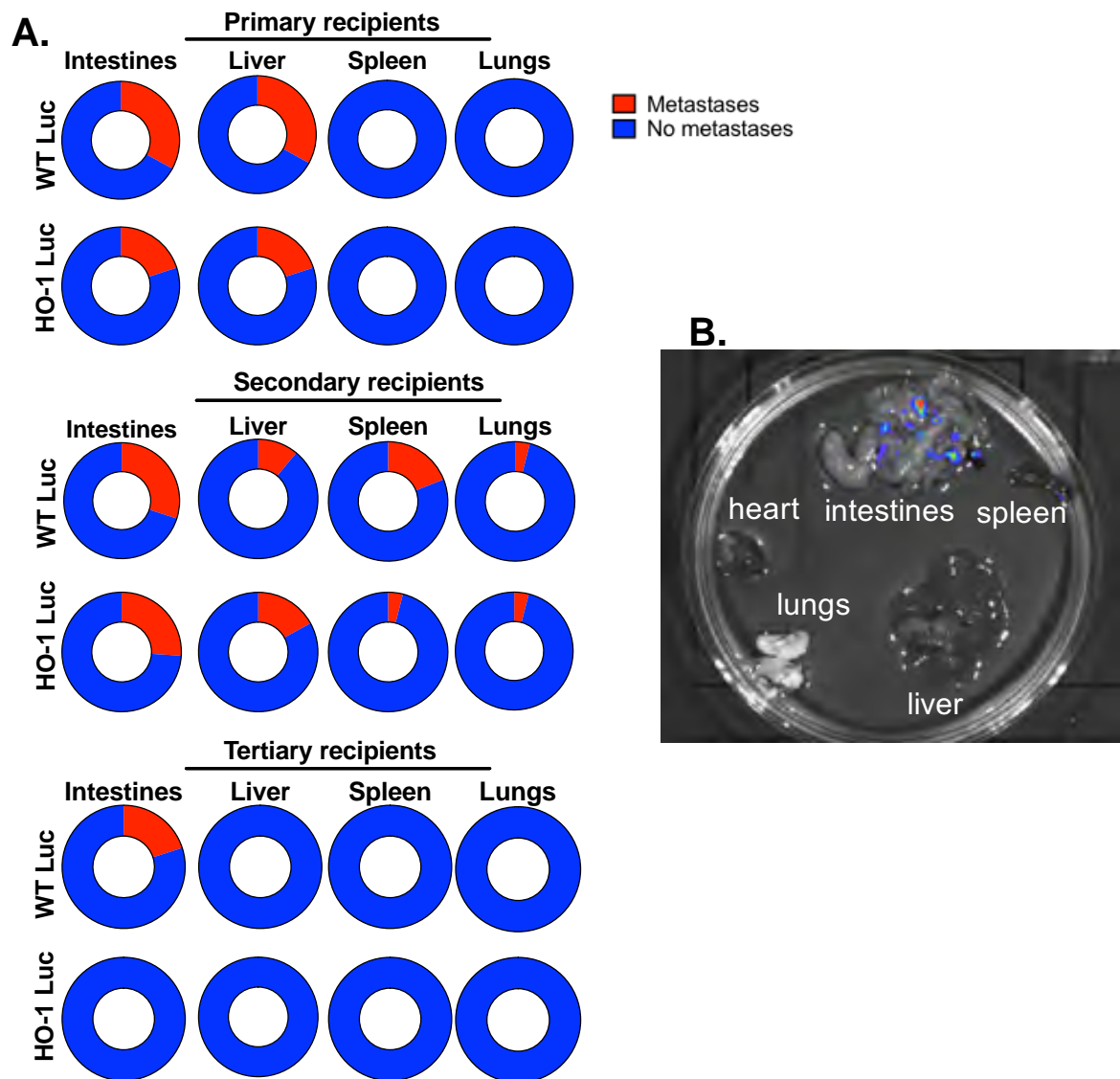
Figure 4.33. Analysis of metastases using IVIS **A.** Charts representing percentage of mice with metastases in each experimental group in the intestines, livers, spleens, and lungs**. B**. Representative picture of organs after luminescence measurement with IVIS.

Because overexpression of HO-1 was associated with reduced tumorigenicity in secondary recipients (Fig. 4.29 B), we compared the frequency of ALDH^{high} cells in WT-Luc and HO-1-Luc derived secondary tumors. There was a tendency to decrease the frequency of

ALDH^{high} cells in HO-1 overexpressing tumors (Fig. 4.34 B), but it does not reach statistical significance (p=0.103).
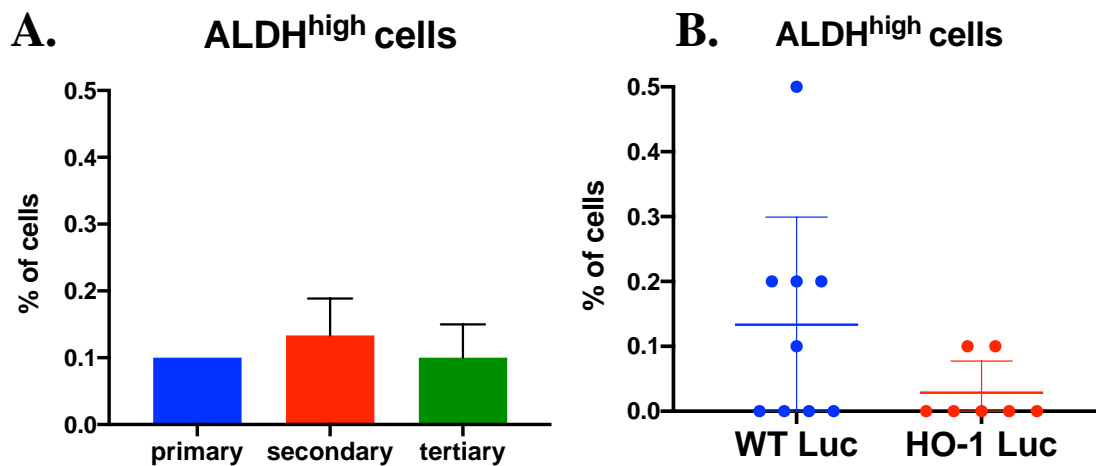
Figure 4.34. A. Frequency of ALDH^{high} subpopulation in B16-F10 WT Luc melanoma cells isolated from tumors growing in the primary, secondary and tertiary recipients. **B.** Frequency of ALDH^{high} subpopulation in B16-F10 WT Luc and HO-1 Luc melanoma cells isolated from tumors growing in secondary recipients. Flow cytometry analysis. Data are represented as mean + SEM (A) or mean ± SD with individual points (B).

4.4.4. Evaluation of tumorigenic potential of ALDH^{high} cells

We also directly compared the tumorigenicity of ALDH^{low} and ALDH^{high} cells. Our previous experiments did not show any effect of the high ALDH activity on clonogenic potential of cells cultured *in vitro* (Fig. 4.9), although we revealed that ALDH^{high} cells have a decreased expression of many CSC-associated genes (Fig. 4.19), and are less frequent if B16-F10 melanoma lines are cultured in the MIC medium (Fig. 4.5).

To evaluate cell tumorigenicity *in vivo*, we transplanted ALDH^{low} and ALDH^{high} WT Luc cells to the primary recipients (10 cells per recipient; Fig. 4. 32 A). Cells with low ALDH activity showed similar efficacy in the primary tumor initiation as that observed earlier for the bulk cells (Fig. 4.29 B). Noteworthy, cells with high ALDH activity did not induce tumor growth (Fig. 4. 35 B).

A.

ALDEFLUOR™ staining B16-F10 WT Luc

B.

Tranplantation

10 cells

Sort of ALDH^{low} and ALDH^{high} cells

	ALDH^{low}	ALDH^{high}
WT Luc	3/24	0/24
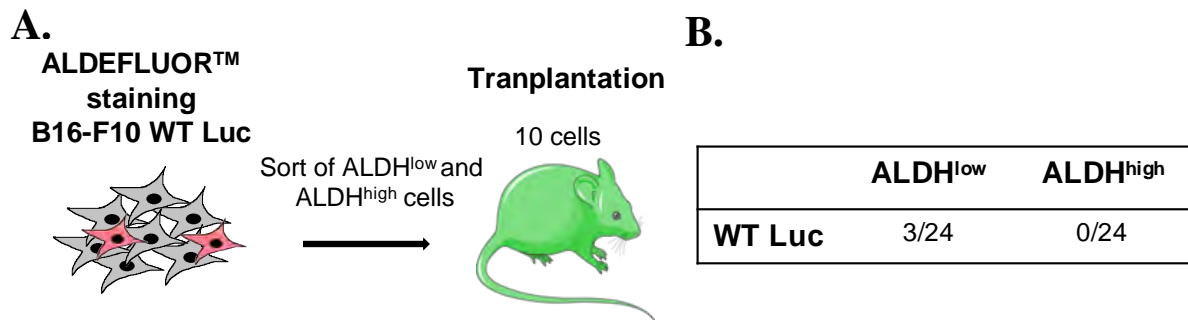
Figure 4.35. *In vivo* transplantation of ALDH^{low} and ALDH^{high} B16-F10 WT-Luc cells. **A.** Scheme of the experiment. **B.** Tumor formation efficacy (number of growing tumors/number of injected plugs).

4.4.5. Evaluation of the tumorigenic potential of CD20$^+$ cells

We also investigated the tumorigenicity of CD20$^+$ subset. Similarly as in case of ALDH^{high} cells, in earlier experiments we did not observe any differences between clonogenic potential of CD20$^-$ and CD20$^+$ melanoma cells cultured *in vitro* (Fig. 4.9). We also showed that CD20$^+$ cells have a decreased expression of some CSC-associated genes (Fig. 4.15), but are more frequent if B16-F10 melanoma lines are cultured in the MIC medium (Fig. 4.5).

To assess the tumorigenic potential of CD20$^+$ fraction we sorted CD20$^-$ and CD20$^+$ cells and injected them (10 cells/plug) to syngeneic mice (Fig. 4.36 A). In this experiment both fractions showed a higher tumorigenic efficacy than that observed in other tests, nevertheless there was no difference in formation of primary tumors between CD20$^-$ and CD20$^+$ fractions (Fig. 4.36 B). In accordance, we observed a similar growth rate of primary tumors, especially at a later time point (Fig. 4.37 A) and similar survival of the primary recipients (Fig. 4.37 B).
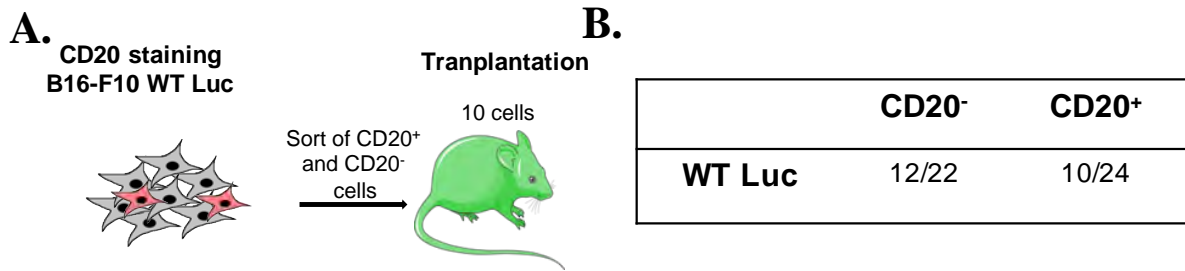
Figure 4.36. *In vivo* transplantation of CD20⁻and CD20⁺ B16-F10 cells. **A.** Scheme of the experiment. **B.** Tumor formation efficacy (number of growing tumors/number of injected plugs).

Tumor formation efficacy of CD20⁺ cells was not modified by HO-1 overexpression (data not shown).

Additionally, using IVIS to detect luminescence in isolated organs, we compared the formation of metastasis by CD20⁺ and CD20⁻ melanoma cells. Signal was detectable in the intestines, livers, spleens and lungs of the primary tumor recipients. There were no statistically significant differences between CD20⁺ and CD20⁻ derived tumors in frequency of metastatic growth (Fig. 4.38).
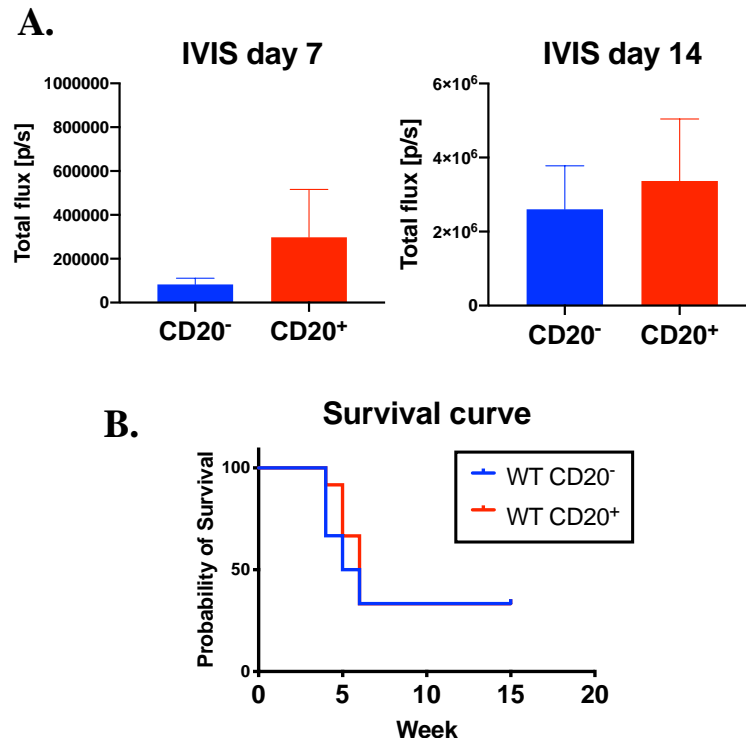
Figure 4.37. Tumor development in the primary recipients after grafting of CD20⁻ or CD20⁺ melanoma cells. **A.** Growth of tumor cells on 7th and 14th day after transplant. Detection of luciferase activity in growing tumors using IVIS luminometer. Each bar represents mean + SEM. **B.** Survival curves of recipients. Mice were sacrificed when tumors reached 10 mm in diameter.
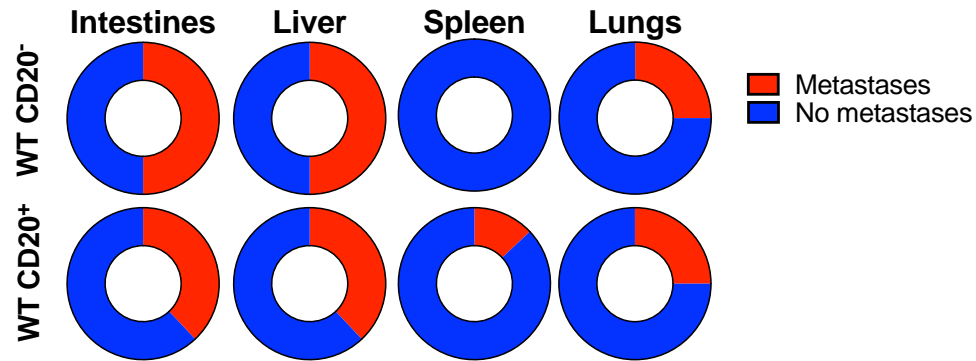
Figure 4.38. Frequency of metastases in the primary recipients, formed by CD20⁻ or CD20⁺ melanoma cells. Detection of luciferase activity in the post-mortem excised organs using IVIS luminometer.

4.4.6. Evaluation of the tumorigenic and metastatic potential of PKH26⁺ cells

In vitro experiments revealed that slowly dividing B16-F10 melanoma cells, defined as PKH26-retaining cells, despite the gene expression profile which may suggest a less differentiated state (Fig. 4.3 D, 4.17, 4.25), do not show any increase in the clonogenic potential. In fact, there was a tendency to reduced clonogenicity, clearly pronounced in the PKH26⁺ cells overexpressing HO-1 (Fig. 4.11, 4.12).

Again, to evaluate the tumorigenic potential of PKH26 retaining cells *in vivo*, we performed a serial transplantation assay (Fig. 4.39 A). Because WT Luc PKH26⁻ cells did not form the primary tumors in this particular experiment, and PKH26⁻ fraction sustains more than 99% of the bulk population, we decided to compare PKH26⁺ fraction with unfractionated WT-Luc cells. To assess the effect of HO-1 overexpression, we compared WT Luc PKH26⁺ cells with their HO-1-Luc PKH26⁺ counterparts.

The results indicate that formation of primary tumors is comparable in the bulk B16-F10 cells and PKH26⁺ fraction, regardless of the heme oxygenase-1 status of PKH26+ cells (Fig. 4.39 B). Similar efficacy of the bulk and PKH26⁺ cells was also confirmed in the secondary and tertiary recipients (Fig. 4.39 B). As in the unfractionated cell line, HO-1 overexpression reduced initiation of secondary tumors also in the PKH26⁺ subset. Formation of tertiary tumors was less effective than secondary ones, and this decrease was the same in the bulk and PKH26⁺ cells. Overexpression of HO-1 did not affect the initiation of tertiary tumors (Fig. 4.39 B).

Efficacy of tumor initiation was reflected by survival of the recipients (Fig. 4.39 C). Generally survival of mice transplanted with PKH26⁺ cells was comparable to that of mice

transplanted with bulk melanoma. In the secondary recipients, in the group transplanted with PKH26$^+$ HO-1 overexpressing cells, a reduction in tumorigenicity was accompanied with a better survival of mice (Fig. 4.39 C).

We also analyzed the presence of metastatic melanoma in the isolated organs of the primary, secondary and tertiary recipients. Like in tumors formed by CD20$^+$ and CD20$^-$ B16-F10 cells (Fig. 4.38), either the primary tumors formed by the bulk cells and PKH26$^+$ cells preferentially metastasized to the intestines and livers (Fig. 4.40 A). Interestingly, for the PKH26$^+$-derived primary tumors we found metastases also in the spleens and lungs (Fig. 4.40 A). Metastatic potential seemed to decrease in the tertiary tumors, and this lowering was the smallest with PKH26$^+$-derived tumors (Fig. 4.40 C). Overexpression of HO-1 slightly reduced the formation of metastases in the primary, secondary and tertiary recipients (Fig. 4.40 A-C), but this trend was not statistically significant.
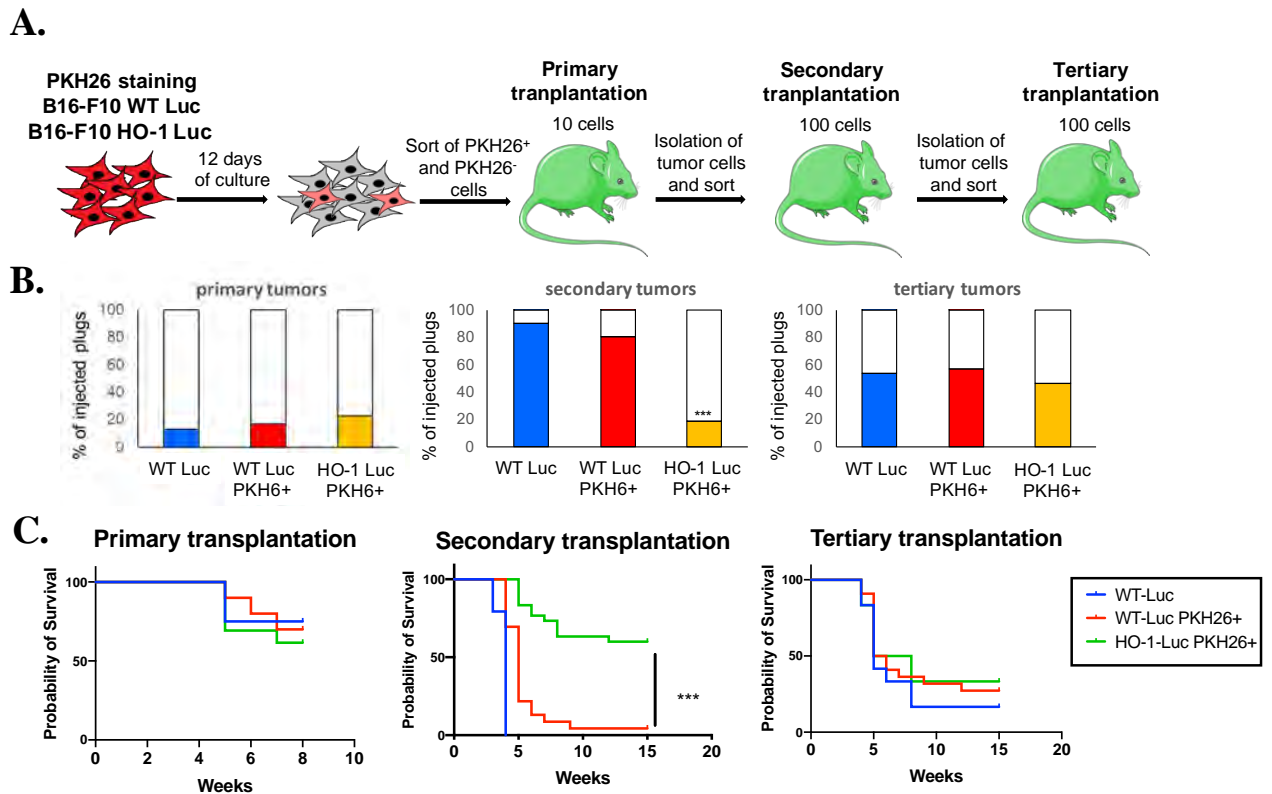
Figure 4.39. Tumor development in the primary, secondary and tertiary recipients after grafting of WT-Luc bulk and PKH26$^+$ or HO-1-Luc PKH26$^+$ melanoma cells. **A.** Scheme of the experiment. **B.** Tumor formation efficacy represented as a percentage of injected plugs that grew as tumors in each group. Fisher exact test (N=22-78); *** - p<0.001 versus WT-Luc PKH26$^+$ group. **C.** Survival curves of the recipients. Mice were sacrificed when tumors reached 10 mm in diameter. Mantel-Cox test; *** - p<0.001 versus HO-1 PKH26$^+$ group.
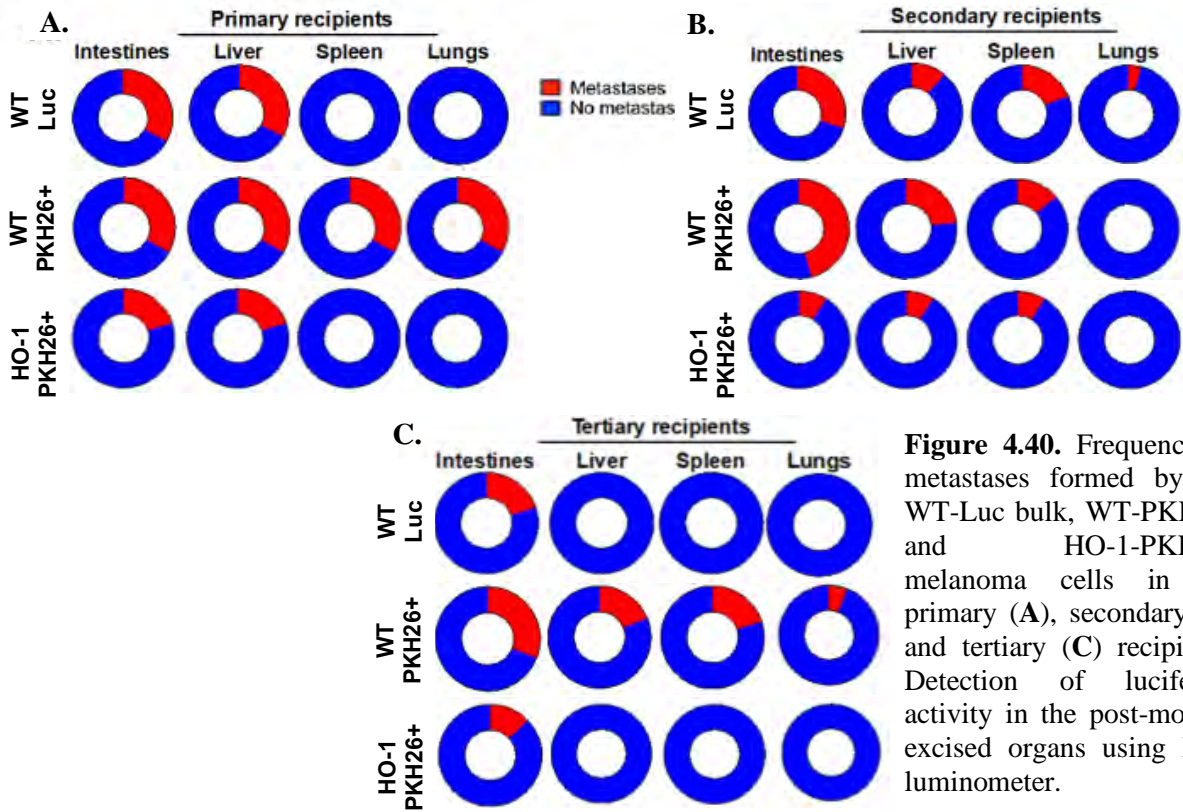
Figure 4.40. Frequency of metastases formed by the WT-Luc bulk, WT-PKH26$^+$ and HO-1-PKH26$^+$ melanoma cells in the primary (**A**), secondary (**B**) and tertiary (**C**) recipients. Detection of luciferase activity in the post-mortem excised organs using IVIS luminometer.

Finally, we checked ALDH activity in melanoma cells isolated from the growing tumors. As in the tumors derived from the bulk melanoma cells (Fig. 4.34) also in the tumors formed by PKH26$^+$ cells the ALDH^{high} fractions were rare (Fig. 4.41). We did not observe any differences between primary, secondary and tertiary tumors and no effect of HO-1
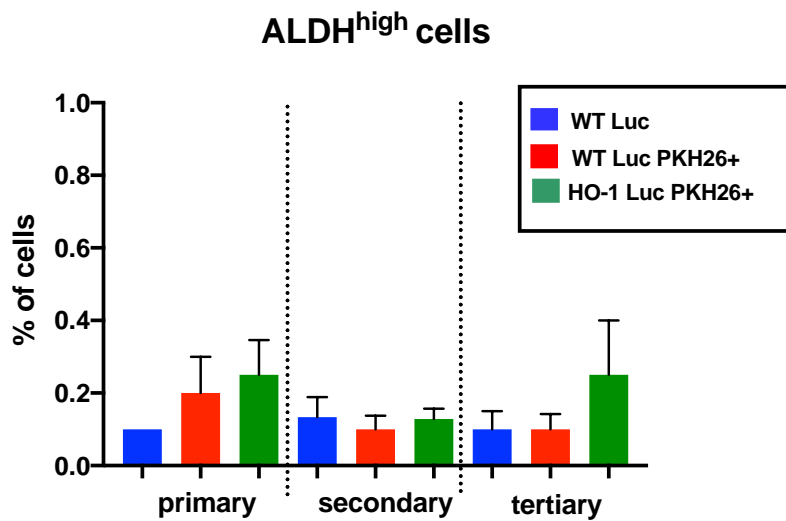
Figure 4.41. Frequency of ALDH^{high} subpopulation in B16-F10 melanoma cells isolated from tumors formed by WT Luc bulk, WT PKH26+ and HO-1 PKH26+ cells in the primary, secondary and tertiary recipients. Flow cytometry analysis. Each bar represents mean + SEM.

overexpression (Fig. 4. 41). These data suggest that ALDH^{high} cells are dispensable for the tumorigenicity and self-renewal of murine melanoma cells.

4.5. Characterization of the vasculogenic mimicry in murine melanoma

4.5.1. Murine melanoma cells have the ability to co-operate with endothelial cells in tube formation on Matrigel

One of the important features associated with the aggressiveness of melanoma is the vasculogenic mimicry (VM). It is an alternative source of microcirculation within tumors, independent of angiogenesis[248]. Some tumor cells are able to form leaky channels that provide the blood supply and form the additional route for cell trafficking. It is particularly interesting that MIC, due to their high plasticity, are supposed to contribute to the formation of vessel-like structures by melanoma cells[249]. As vasculogenic mimicry channels are not formed by CD31^{+} endothelial cells, they can be independent of VEGF and anti-angiogenic therapies are not effective in the prevention of VM[100]. One of the proangiogenic factors is HO-1, which facilitates response to VEGF but also to other mediators, such as SDF1[104,156] It was reported that overexpression of HO-1 increases angiogenesis in the growing B16-F10 melanoma tumors in mice[147]. Data on a potential effect of HO-1 on vascular mimicry are, however, lacking. Having this in mind we wanted to check if HO-1 influences VM pathway in murine melanoma.

Active VM is associated with an enhanced expression of VE-cadherin in cancer cells. Accordingly, VE-cadherin was shown to be upregulated in aggressive melanomas and its silencing abrogated the VM[250]. Thus, we checked if cultured B16-F10 cells express VE-cadherin protein. Additionally, we stained cells for Tie-2, the angiopoietin receptor, that was also shown to be expressed by tumor cells in the context of VM[251]. Using flow cytometry we found a very small (0.1-0.7%) subpopulations of VE-cad[+] or Tie-2^{+} cells in B16-F10 melanoma, and their frequency was comparable in the WT Luc and HO-1 Luc cell lines (Fig. 4.42). We also checked the presence of CD34^{+} cells and there was no such population in the B16-F10 melanoma, regardless of their HO-1 status (data not shown).

	VE-cadherin	Tie-2
WT Luc	0.35% (±0.21%)	0.15% (±0.07%)
HO-1 Luc	0.55% (±0.21%)	0.2% (±0.14%)
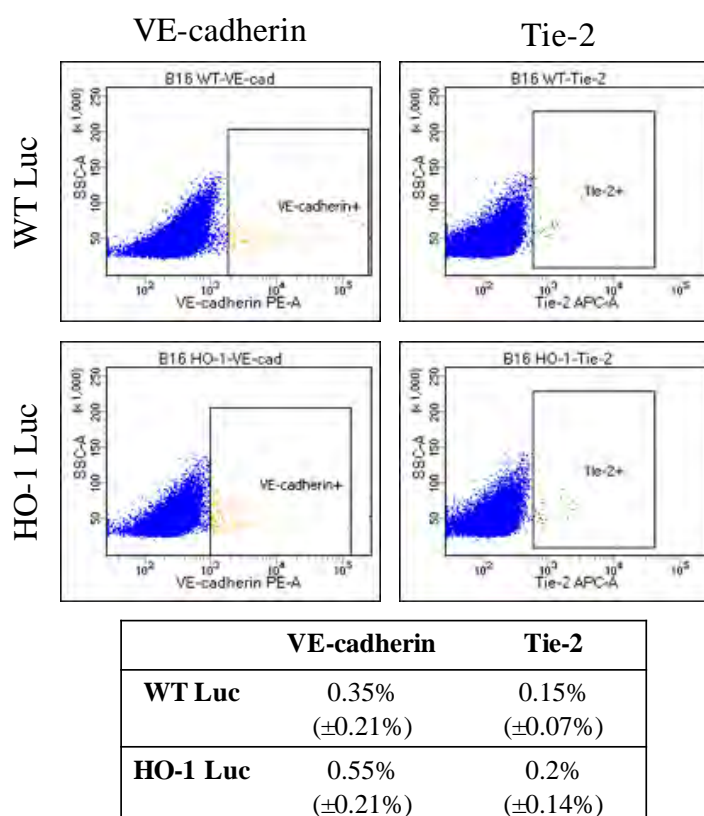
Figure 4.42. Expression of VE-cadherin and Tie-2 proteins in WT Luc and HO-1 Luc B16-F10 melanoma cell lines cultured *in vitro* under standard conditions. Flow cytometry analysis. **A.** Representative staining. **B.** Percentage of cells with expression of VE-cad and Tie-2. Data are shown as mean ± SEM. Differences are not statistically significant.

Routinely, angiogenic potential and morphogenesis of endothelial cells can be evaluated using a tube formation assay. Namely, endothelial cells are seeded on the Matrigel, where they begin to align themselves and form lumen-containing tubules within a few hours. We investigated whether melanoma cells are able to participate in formation of tubes on the

Matrigel when seeded with the endothelial cells (HMEC-1). The formation of the vessel-like structures on the Matrigel by tumor cells is regarded as a useful tool in VM studies[252].

We seeded HMEC-1 cells on the Matrigel, and after they formed tubes we seeded WT Luc (stained with Cell Violet) and HO-1 Luc (stained with PKH26) B16-F10 melanoma cells (Fig. 4.43 A). It turned out that both cell lines were able to co-operate with the endothelial cells in formation of tubes (Fig. 4.43 B). We did not notice any meaningful differences between WT Luc and HO-1 Luc cells in the ability to incorporate into pre-existing structures.
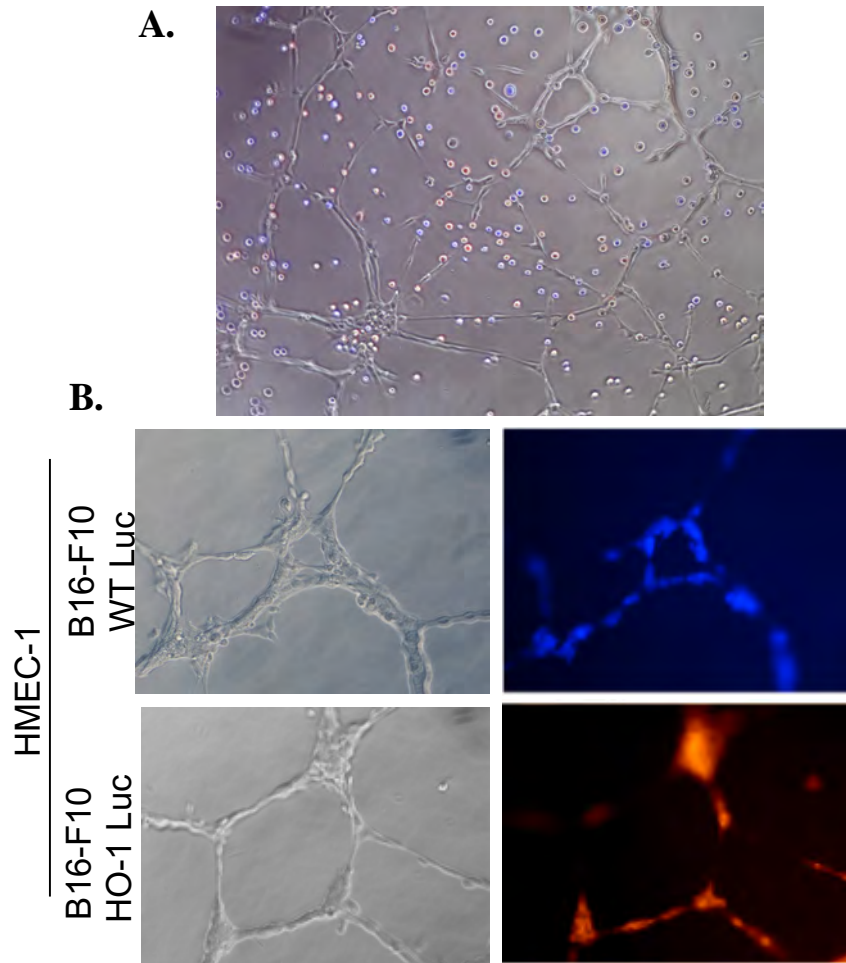
Figure 4.43. Incorporation of B16-F10 melanoma cells into endothelial tubes on the Matrigel. **A**. Tubes formed by HMEC-1 endothelial cells (unstained) with seeded B16-F10 melanoma cells (stained in blue or red). **B.** WT Luc (blue) and HO-1 Luc (red) B16-F10 melanoma cells incorporated into preexisting endothelial tubes, 16 h after seeding. Contrast phase and fluorescence microscopy; representative pictures.

4.5.2. Overexpression of HO-1 affects tube formation by melanoma cells

Next, we seeded B16-F10 cells alone, without endothelial cells, to see if they are able to form tube-like structures on the Matrigel. Pictures of the pseudo-tubes formed by B16-F10 cells were analyzed using the Angiogenesis Analyzer in the ImageJ software (Fig. 4.44). We observed that just 3 h after seeding, melanoma cells begun to form tube-like structures (Fig. 4.45 A).
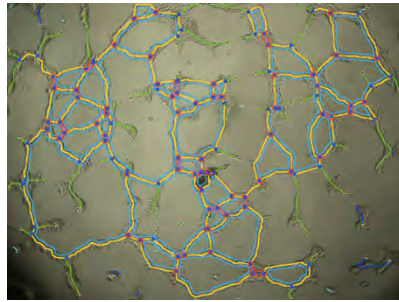
Figure 4.44. B16-F10 VM analysis using Angiogenesis Analyzer plugin in ImageJ; representative picture.
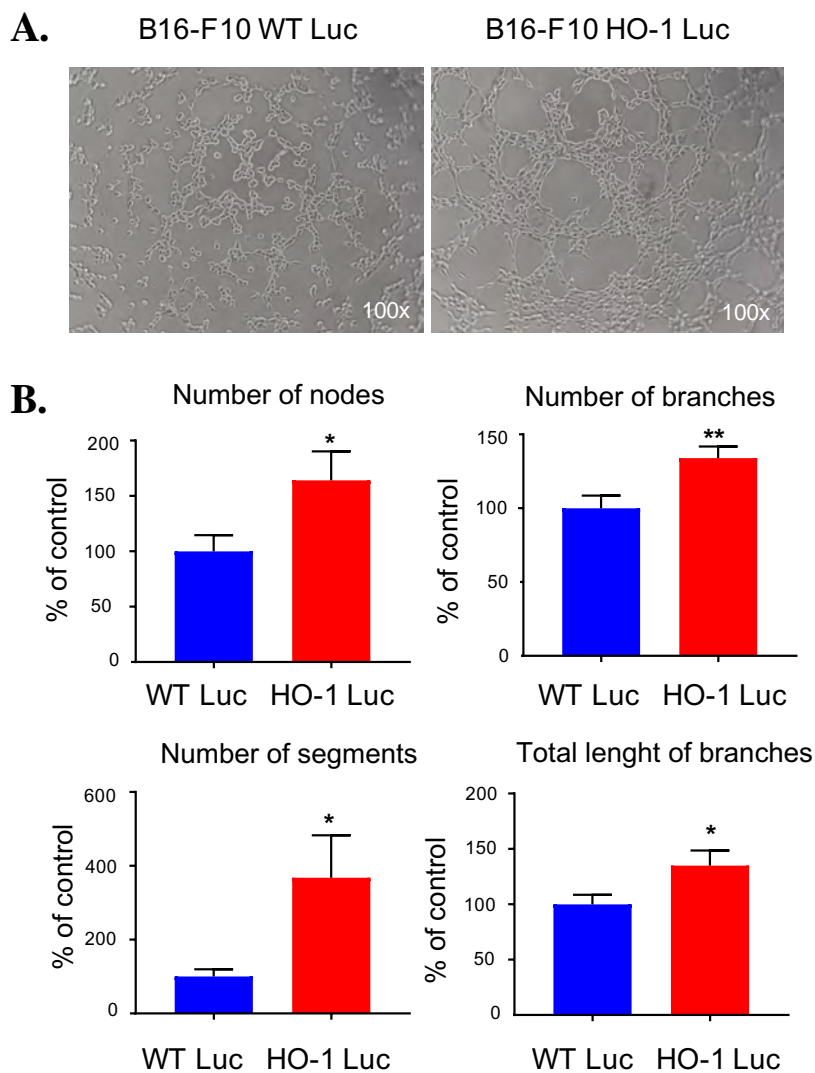
Figure 4.45. Formation of tubes on the Matrigel, 3 h after seeding of WT Luc or HO-1 Luc B16-F10 melanoma cells. Contrast phase microscopy. **A.** Representative pictures. **B.** ImageJ analysis. Data are presented as a percentage of WT control (mean + SEM); * – p<0.05, ** - p<0.01 versus WT-Luc cells.

The formation of tubes was more pronounced in HO-1 overexpressing cells, which was reflected in measurements of several characteristics of tubes (e.g. number of segments and nodes) calculated using the ImageJ software (Fig. 4.45 B). Accordingly, 20 h after seeding, the HO-1 Luc melanoma cells formed the structures resembling those generated by endothelial cells, with elongated segments (arrows, Fig. 4.46). At the same time, WT Luc melanoma cells also formed tube-like structures, however they were made of clustered cells rather than elongated cells (Fig. 4.46).

B16-F10 WT Luc   B16-F10 HO-1 Luc
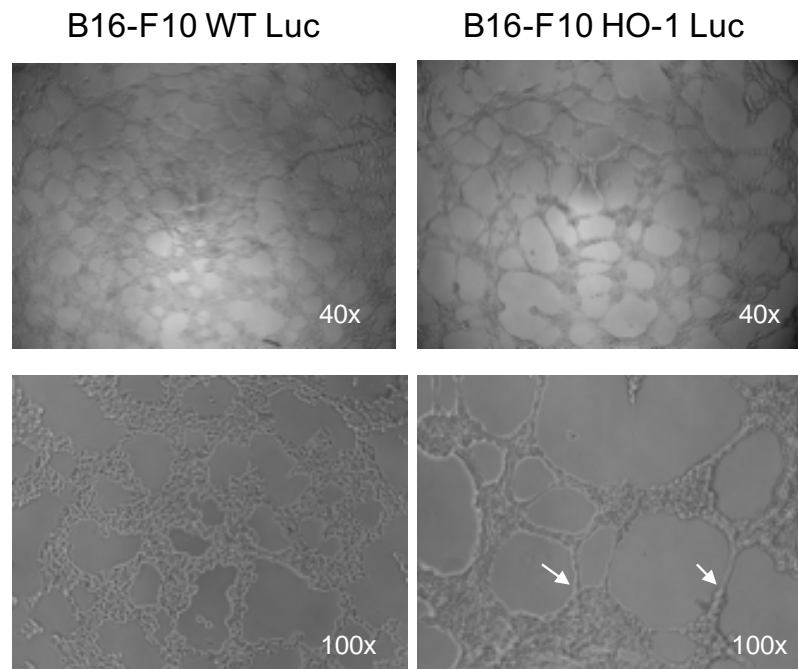
Figure 4.46. Formation of tubes on the Matrigel, 20 h after seeding of WT Luc or HO-1 Luc B16-F10 melanoma cells. Contrast phase microscopy. Representative pictures. Arrows indicate structures similar to that formed by endothelial cells.

4.5.3. Activation of HO-1 affects tube formation

In the next step, we checked if the pharmacological modulation of HO-1 enzymatic activity can affect tube formation on the Matrigel by melanoma cells. To this aim we seeded WT Luc melanoma cells on the Matrigel in the media supplemented with hemin (10 µM, HO-1 inducer) or SnPP (10 µM, HO-1 inhibitor), and analyzed tube formation after 10 h (Fig. 4.47 A, B). In accordance to the effect of HO-1 overexpression, activation of HO-1 with hemin enhanced formation of tubes by melanoma cells (Fig. 4.47 C). Inhibition of HO-1 activity did not exert any effect.

A. Untreated cells **B.** Hemin 10 μM

C.

Number of branches

Number of nodes

Number of segments

Total lenght of branches
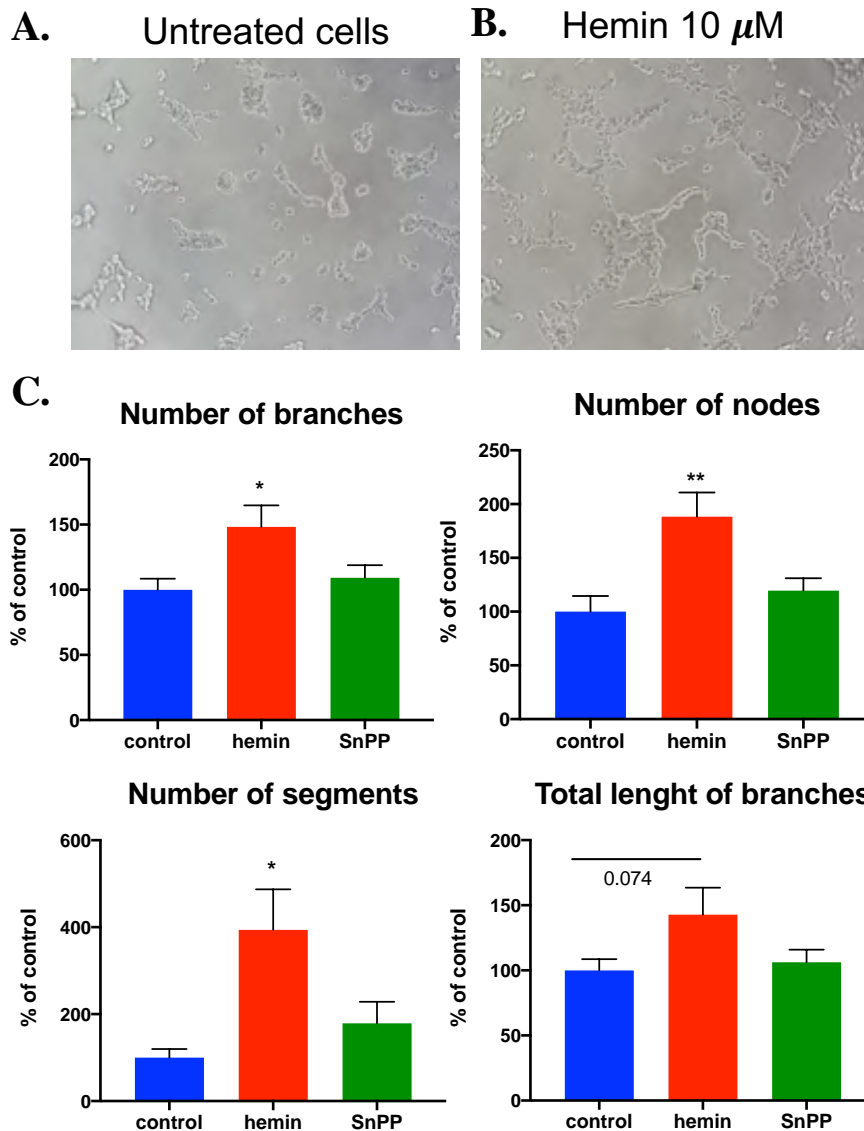
Figure 4.47. Formation of tubes on the Matrigel 10 h after seeding of WT Luc B16-F10 melanoma cells. Cells were treated with hemin (10 µM) or SnPP (10 µM). Contrast phase microscopy. **A.** Tubes formed by control, untreated cells. **B.** Tubes formed by cells stimulated with hemin. Representative pictures. **C.** ImageJ analysis. Each bar represents mean + SEM; * – $p < 0.05$, ** - $p < 0.01$ versus control cells. Experiments performed with help of Rościsław Krutychołowa.

4.6. Influence of HO-1 in the mesenchymal stromal cells (MSC) on melanoma cells

4.6.1. Conditioned media from MSC HO-1 WT and KO do not alter formation of tubules by B16-F10 cells

Vasculgenic mimicry can be promoted by tumor stromal cells, such as mesenchymal stromal cells, that produce provasculogenic mediators TGFβ and SDF1α. Mesenchymal stromal cells are recruited to tumor stroma where they modulate anticancer immunity and can favor

tumor metastasis[253]. They were also reported to regulate the vasculogenic mimicry in melanoma[254]. Therefore, we checked if expression of HO-1 in MSC can affect the formation of tubes by B16-F10 cell line.

To this purpose, we stimulated WT Luc B16-F10 melanoma cells with conditioned media, harvested from the cultured primary MSC isolated from the femurs and tibia of wild type (WT) or HO-1 deficient (HO-1 KO) mice. Before media harvesting, MSC were cultured as a confluent monolayer, and then incubated in EBM2 medium for 24 h. We did not observe any differences in melanoma tube formation between cells stimulated with WT and HO-1 KO conditioned media (Fig. 4.48)
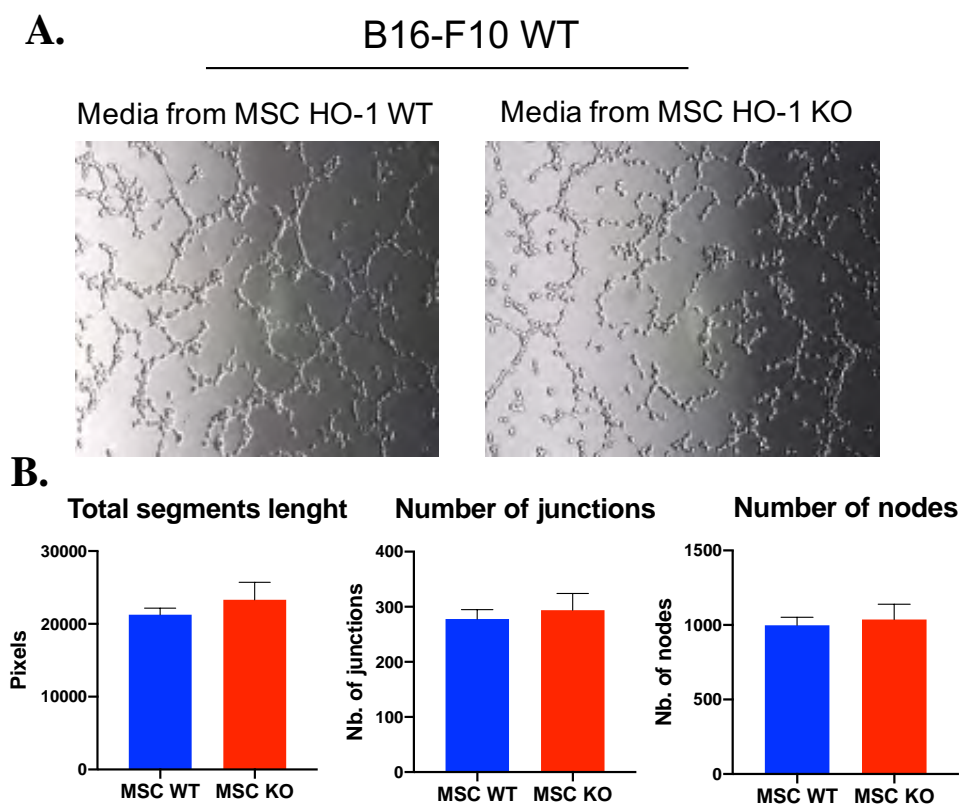
Figure 4.48. Formation of tubes on the Matrigel, 16 h after seeding of B16-F10 melanoma cells in conditioned media from WT and HO-1 KO MSC. **A.** Representative pictures; contrast phase microscopy **B.** ImageJ analysis. Data presented as mean ± SEM. Experiments were performed with help of Rościsław Krutychołowa.

4.6.2. Lack of HO-1 in MSC does not affect proliferation of co-cultured melanoma cells

In the next step we investigated whether expression of HO-1 in MSC may affect proliferation of co-cultured melanoma cells. In this experimental setting, cells directly interacted for the six-day period (Fig. 4.49 A, B). Primary MSC isolated from WT or HO-1 KO mice were co-cultured with WT-Luc B16-F10 cells in 24-well plates. Melanoma cells were seeded (50 cells/well) on the monolayer of MSC and luminescence of melanoma was measured using IVIS Lumina, starting at day 2 after seeding up to day 6. After fixing cells at day 6 and staining for MITF (a marker of melanoma cells) and tubulin (that marks both MSC and B16-F10 cells) we observed that melanoma cells grew as clustered clones on MSC monolayer (Fig. 4.49 A, B). Measurements of luminescence showed that proliferation rate was very similar, regardless the HO-1 expression status in the mesenchymal cells (Fig. 4.49 C).
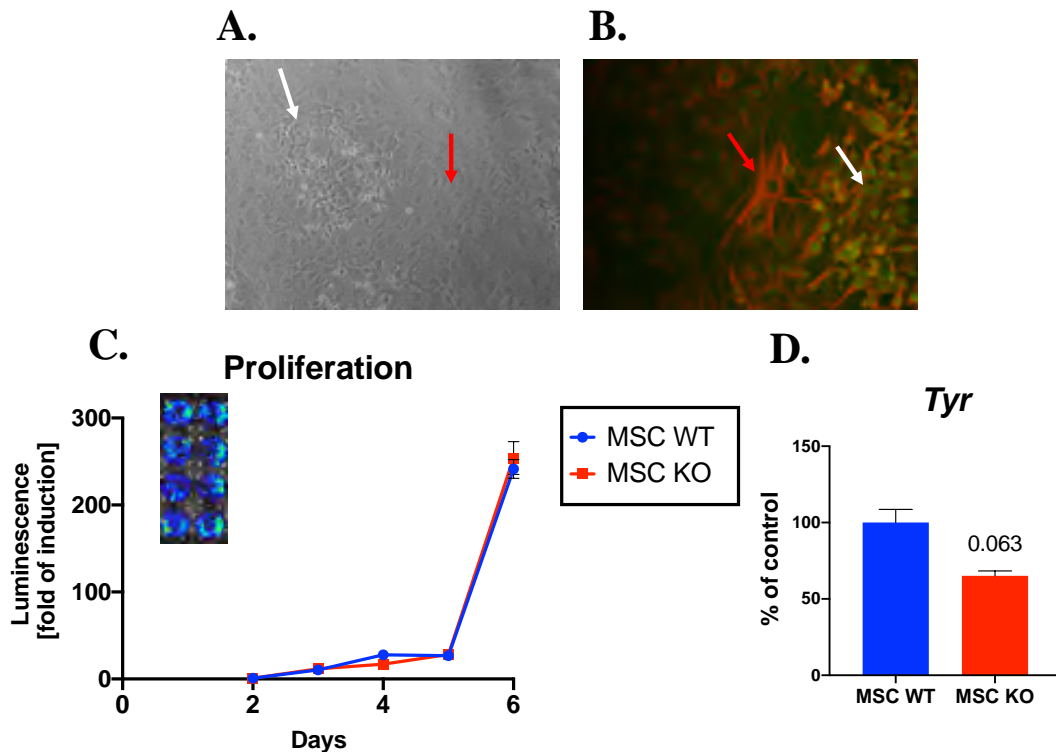
Figure 4.49. Co-culture of WT-Luc B16-F10 melanoma cells with the wild type (WT) or HO-1 deficient (HO-1 KO) MSC. **A.** Appearance of cultured cells, 6 days after seeding; melanoma cells - white arrows, MSC - red arrows. Contrast phase microscopy; representative picture. **B.** Expression tubulin (red) and MITF (green) to distinguish MSC layer from melanoma cells; melanoma cells - white arrows, MSC - red arrows. Immunocytochemistry, representative picture. **C.** Proliferation of melanoma cells. Luminometry using IVIS Lumina. Data are normalized to the first measurement (on day 2) and each point represents mean ± SEM. **D.** Expression of tyrosinase mRNA in melanoma cells. Quantitative RT-PCR; EF2 was used as a housekeeping gene. Data are presented as mean + SEM; ** - $p < 0.01$.

Additionally, we checked the expression of tyrosinase, the key enzyme in melanogenesis, in the melanoma cells seeded on WT and HO-1 KO MSC monolayer. Because we used mesenchymal cells isolated from GFP[+] animals, after a 5-day co-culture we were able to sort GFP[+] MSC and GFP^{-} melanoma cells for RNA isolation. Quantitative RT-PCR revealed that expression of tyrosinase tends to decrease in melanoma cells cultured with HO-1 deficient MSC (Fig. 4.49 D).

4.6.3. Soluble factors secreted by MSC may regulate pigmentation of melanoma cells

To checked whether the effect of MSC on the melanoma cell pigmentation results from a direct cell-cell interaction or can be mediated by some soluble factors, we adapted a fibrin gel bead assay. This test is normally used for studying sprouting of endothelial cells in fibrin gel[255]. Here, we coated latex beads with the WT Luc B16-F10 melanoma cells and suspended them in the fibrin gel. Then, on top of the gel, we seeded the wild type or HO-1 deficient mesenchymal cells (Fig. 4.50 A). We observed that melanoma cells grew as spheres in a fibrin gel and did not form any sprouts in the 3D culture. The surface area occupied by cells around a bead is a measure of the sphere growth, which results both from proliferation and migration of cells. Growth of melanoma spheres was comparable in the presence of WT and HO-1 KO MSC. Only at the last day, we observed inhibition of growth in the presence of the WT MSC (Fig. 4.50 B).

Interestingly, cells growing in the presence of HO-1 deficient mesenchymal cells were less pigmented then those cultured with the wild type MSC (Fig. 4.50 C), what was consistent with the reduced tyrosinase expression described earlier (Fig. 4.49 D). Thus, we isolated melanoma cells to analyze expression of genes involved in melanogenesis. Quantitative RT-PCR analysis showed a tendencies towards decreased mRNA levels of tyrosinase, *Gp100*, and significant decline of tyrosinase-related protein 1 (*Trp1*) in melanoma cells cultured with MSC KO (Fig. 4.51).
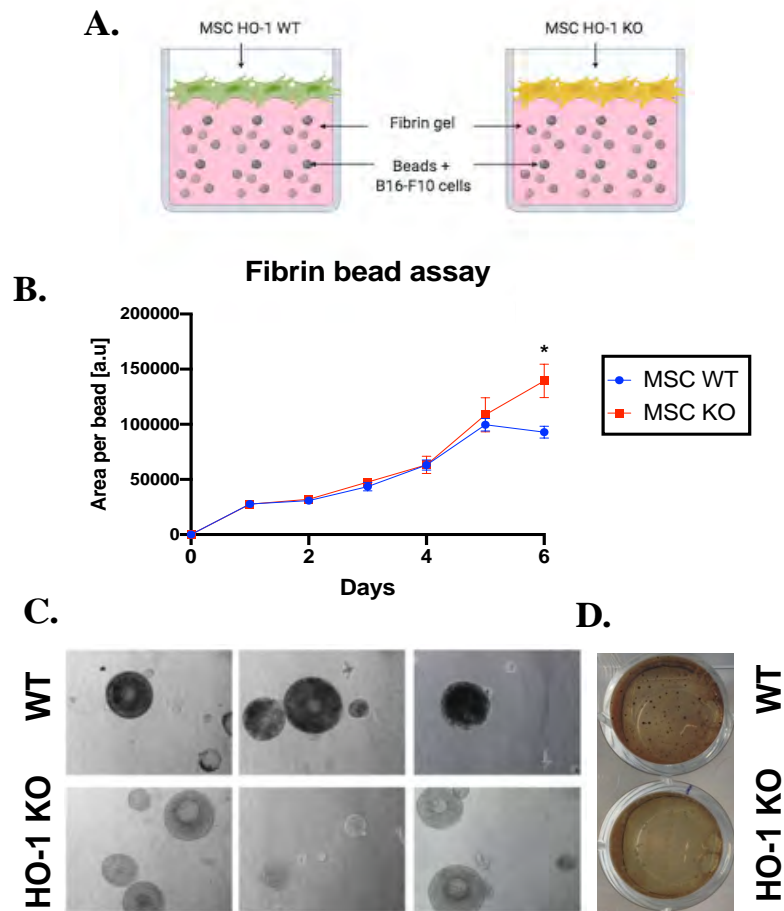
Figure 4.50. Fibrin bead assay performed using WT Luc B16-F10 melanoma cells in the presence of wild type (WT) or HO-1 deficient (HO-1 KO) MSC. **A**. Scheme of the experiment (created with the BioRender). **B**. Growth dynamic of melanoma spheres in the fibrin gel. ImageJ analysis. Each point represents mean ± SEM. Pigmentation melanoma spheres visible on microscopic (**C**) and macroscopic (**D**) representative pictures.
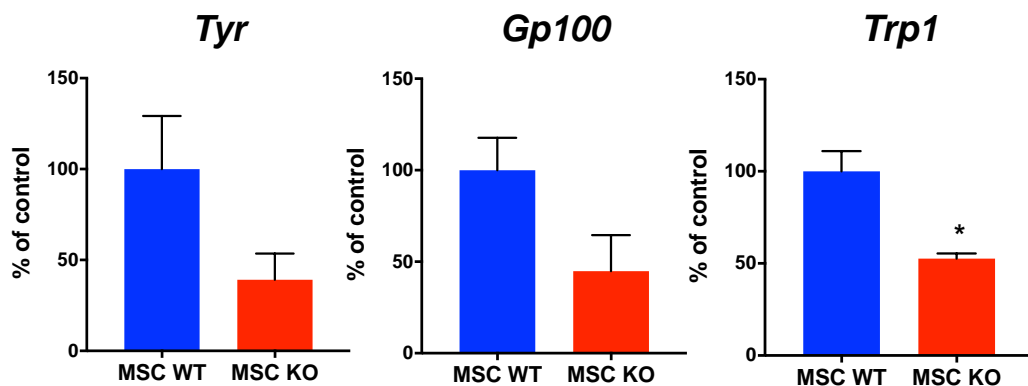
Figure 4.51. Expression of *Tyr*, *Gp100* and *Trp1* in WT-Luc B16-F10 melanoma cells co-cultured for 6 days on fibrin beads in the presence of wild type (WT) or HO-1 deficient (HO-1 KO) MSC. Quantitative RT-PCR. Data are normalized to the control (WT) values and presented as mean + SEM, * - $p < 0.05$.

We supposed that the observed influence on melanoma cell pigmentation might be mediated by changes in the release of TGFβ by mesenchymal cells, as this growth factor was reported to regulate melanogenesis[256]. The Luminex assay, however, did not show any differences in the concentration of TGF-β (TGF-β1, TGF-β2, TGF-β3) in the conditioned media harvested from the wild type and HO-1 deficient MSC (data not shown).

4.7. Effect of HO-1 on melanoma pigmentation

4.7.1. The level of HO-1 in melanoma cells is correlated with the pigmentation of cells but is independent of the expression of melanogenesis genes

Lack of HO-1 in stromal cells led to the reduced production of melanin in the co-cultured B16-F10 melanoma (Fig. 4.50 C,D). This observation prompted us to check whether expression of HO-1 in melanoma cells themselves is required for a proper melanogenesis. To this end we established the B16-F10 cell line with silenced HO-1 expression (shHO-1, with stable expression of shRNA). Indeed, at first glance we noticed that the pellets of cells with different levels of HO-1 differ in color: shHO-1 B16-F10 cells were less pigmented than HO-1 overexpressing cells (Fig. 4.52 A). Then, we checked if this effect was associated with changes in the expression of melanogenesis genes. Real-Time PCR and Western Blot analyses showed no significant differences between cell lines in the expression of tyrosinase, Mitf, Gp100 and Trp1 at either mRNA or protein levels (Fig. 4.52 B, C).

4.7.2. HO-1 levels in melanoma cells are correlated with the tyrosinase activity

Tyrosinase is an enzyme responsible for the initiation of melanin synthesis through oxidation of tyrosine to dopaquinone[257]. Its enzymatic activity does not always correspond to the level of expression and it is the level of activity that is critical for melanin synthesis[196]. Therefore we examined whether the observed differences in pigmentation of B16-F10 cell lines are connected to differences in enzymatic activity of tyrosinase. The obtained results showed that indeed, in the less pigmented shHO-1 cells, with silenced expression of HO-1, the tyrosinase enzyme is significantly less active than in the wild-type or HO-1 overexpressing melanoma cells (Fig. 4.53 A, B).
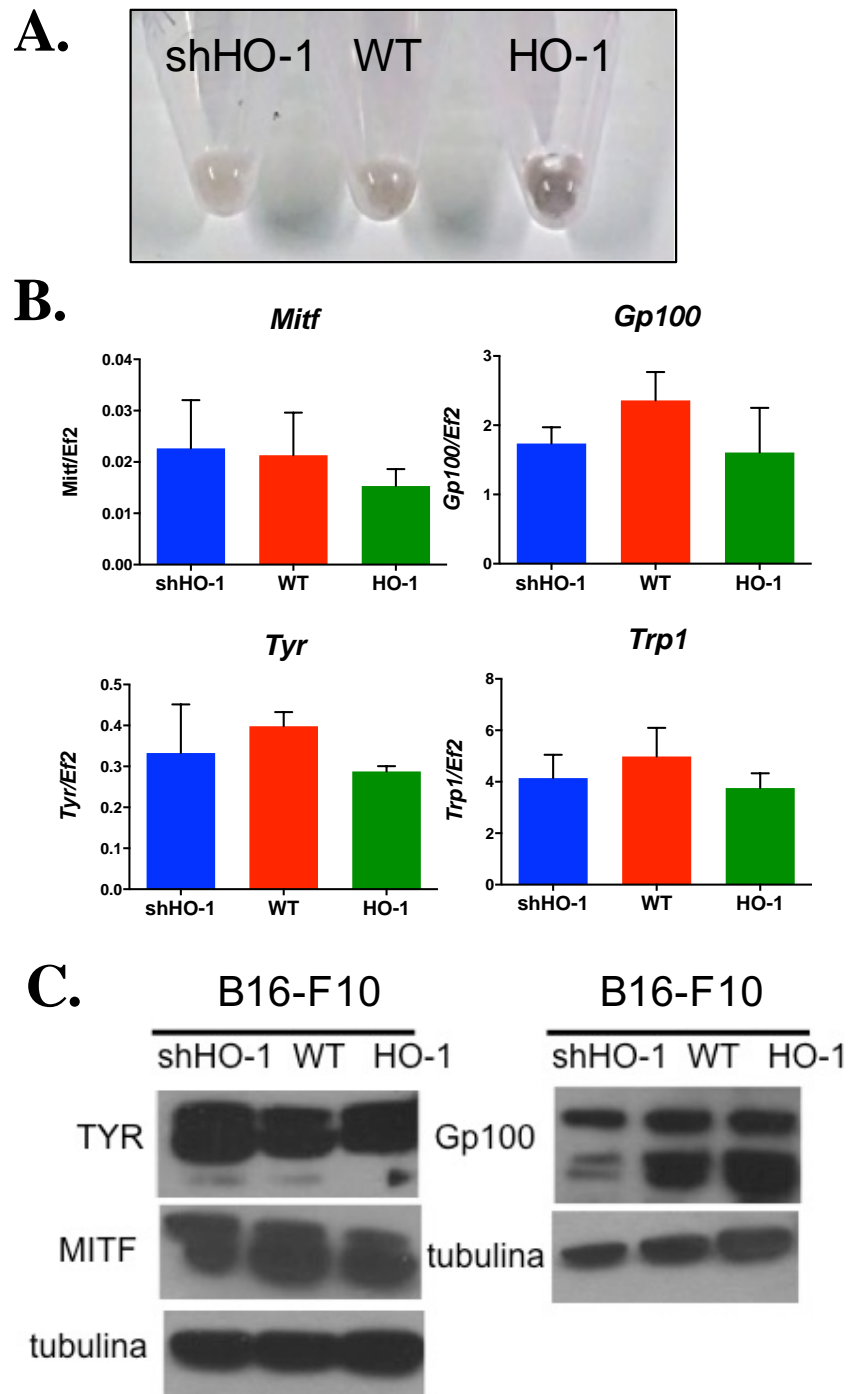
Figure 4.52. Pigmentation of melanoma cells with different levels of HO-1 expression (silenced – shHO-1, normal – WT, increased – HO-1). **A.** Representative picture of pellets of B16-F10 cell lines. **B.** Expression of genes involved in melanogenesis (*Mitf*, *Gp100*, *Tyr* and *Trp1*) at mRNA level. Quantitative RT-PCR analysis; each bar represents mean + SEM. **C.** Expression of genes involved in melanogenesis (tyrosinase, Gp100, and Mitf) at protein level. Western-blot analysis; representative blots. Experiments performed with help of Agnieszka Seretny.
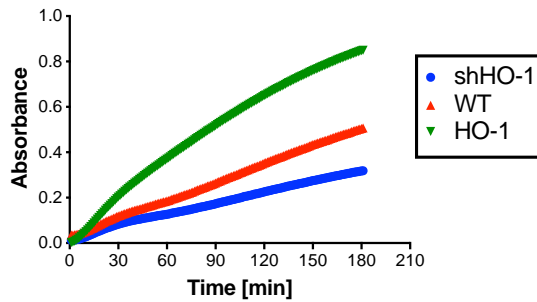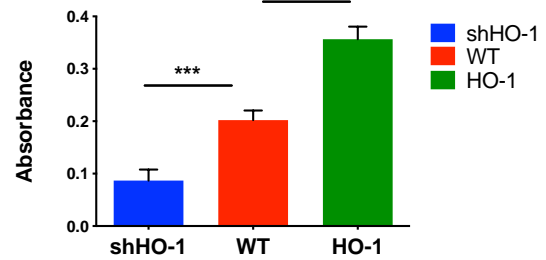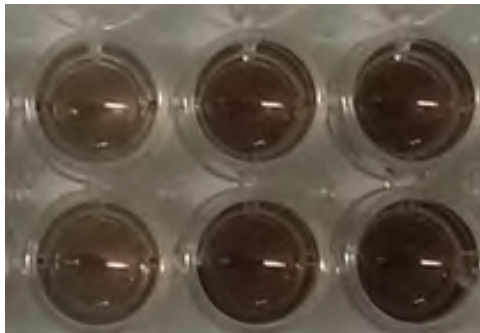
Figure 4.53. Tyrosinase activity in B16-F10 melanoma cells with different levels of HO-1 (silenced – shHO-1, normal – WT, increased – HO-1). **A**. Representative read-out (upper part) and picture of cell lysates after taking measurements (lower part). **B.** Calculations of tyrosinase activity, 60 minutes after adding the substrate L-DOPA. Colorimetric assay; each bar represents mean ± SD; *** - p<0.001. Experiments performed with help of Agnieszka Seretny.

4.7.3. Influence of HO-1 on the induction of pigmentation and excretion of melanin

Murine melanoma is routinely cultured in RPMI 1640 medium that contains a low concentration of tyrosine, the substrate for melanin synthesis. This approach allows for the long-term culture of cells without robust induction of melanogenesis that could lead to decreased proliferation and viability of cells[258]. To induce melanogenesis, we cultured B16-F10 cells in DMEM that contains almost four-fold higher concentration of tyrosine than RPMI 1640.

To check whether the level of HO-1 expression may influence the level of induction of pigmentation, we cultured sh-HO-1, WT, and HO-1 overexpressing B16-F10 melanoma cells for 4 days in DMEM (Fig. 4.54 A). It turned out that cells with silenced HO-1 have a reduced capacity to induce pigmentation, whereas melanin content in HO-1 overexpressing cells seems to be increased (Fig. 4.54 B, C). Interestingly, we noticed that media harvested from shHO-1 cells were darker than that from WT or HO-1 overexpressing cells. This suggested that HO-1 deficient cells have an enhanced capacity of melanin excretion. Indeed, we confirmed such relationship by a direct measurements of melanin concentration in the culture media (Fig. 4.54

D). Additionally, we found that cells with silenced HO-1 have possibly less melanosomes (flow cytometry analysis of cell granularity, data not shown).

A.

B.

C. Intracellular melanin

D. Extracellular melanin
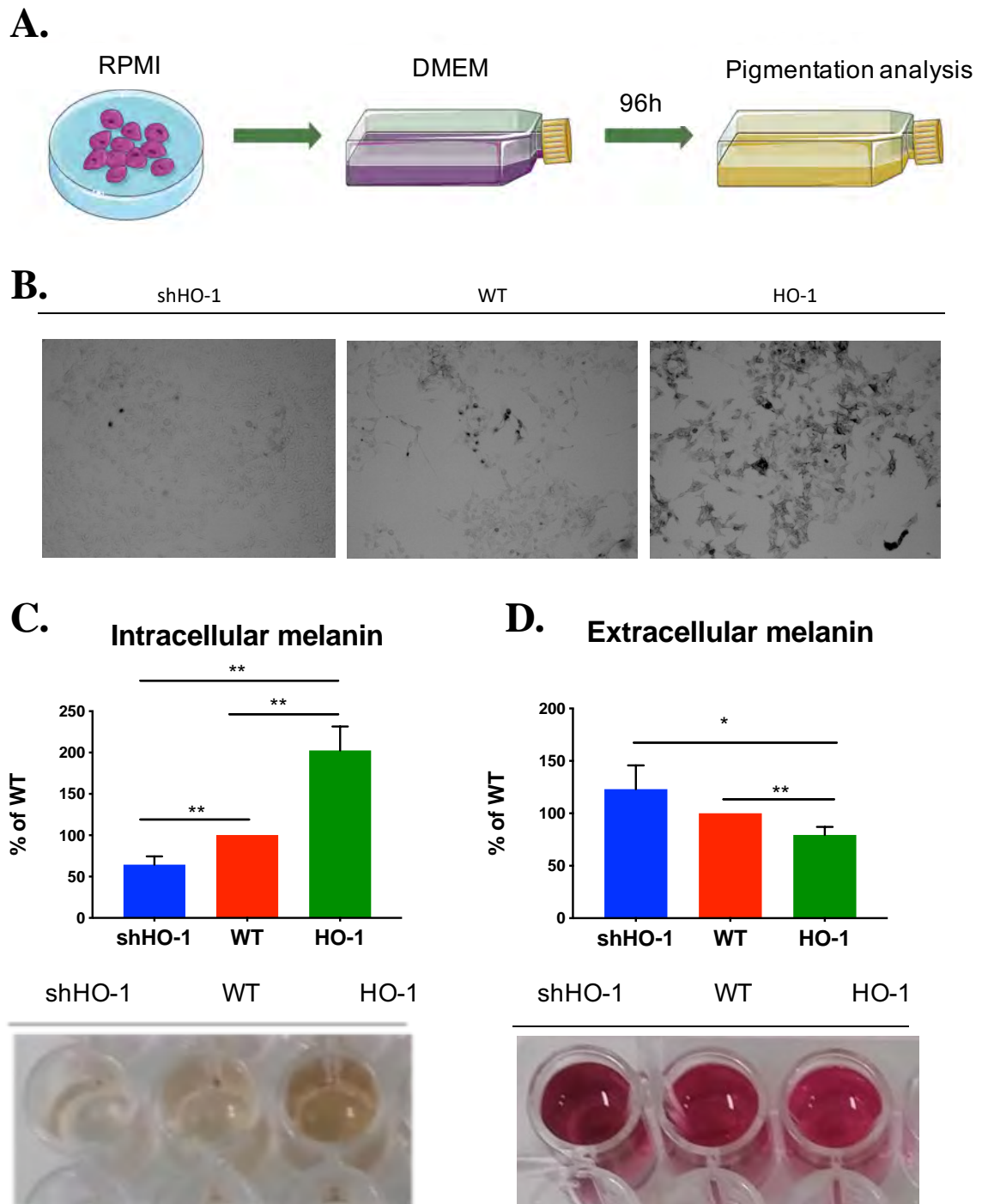
Figure 4.54. Induction of pigmentation in B16-F10 melanoma cells with different levels of HO-1 (silenced – shHO-1, normal – WT, increased – HO-1). **A.** Scheme of the experiment. **B.** Accumulation of melanin in melanoma cells after 4 days of culture in DMEM. Bright field microscopy; representative pictures. **C.** Intracellular melanin content, measured after cell lysis. **D.** Extracellular melanin content, measured in culture media harvested from the same cells. Each bar represents mean + SEM; * - $p < 0.05$, ** - $p < 0.01$, *** - $p < 0.001$. Experiments performed with help of Agnieszka Seretny.

4.7.4. Silencing of HO-1 affects the metabolism of melanoma cells

Silencing of HO-1 clearly compromised pigmentation of cells (Fig. 4.54). Interestingly, it has been demonstrated that pigmentation alters mitochondrial respiration in melanoma and melanin synthesis inhibits electron transport chain[259]. Moreover, both heme (HO-1 substrate) and carbon monoxide (HO-1 product) may directly affect the activity of respiratory chain[260,261]. Therefore, we investigated whether the decrease in melanogenesis was also reflected by changes in metabolism of HO-1-silenced cells.

We performed the Cell Mito Stress Test using the Seahorse Analyzer to measure the mitochondrial respiration (Fig. 4.55 A). The obtained data showed that HO-1 silencing is accompanied not only by attenuated melanogenesis but also by a decrease in some metabolic parameters, including ATP production and basal respiration (Fig. 4.55 B, C). Interestingly, shHO-1 cells decreased their metabolism to the level characteristic of Melan A melanocytes. In the same time we did not detect any differences between melanoma cells with normal level of HO-1 (WT Luc cells) and those with HO-1 overexpression (HO-1 Luc cells).
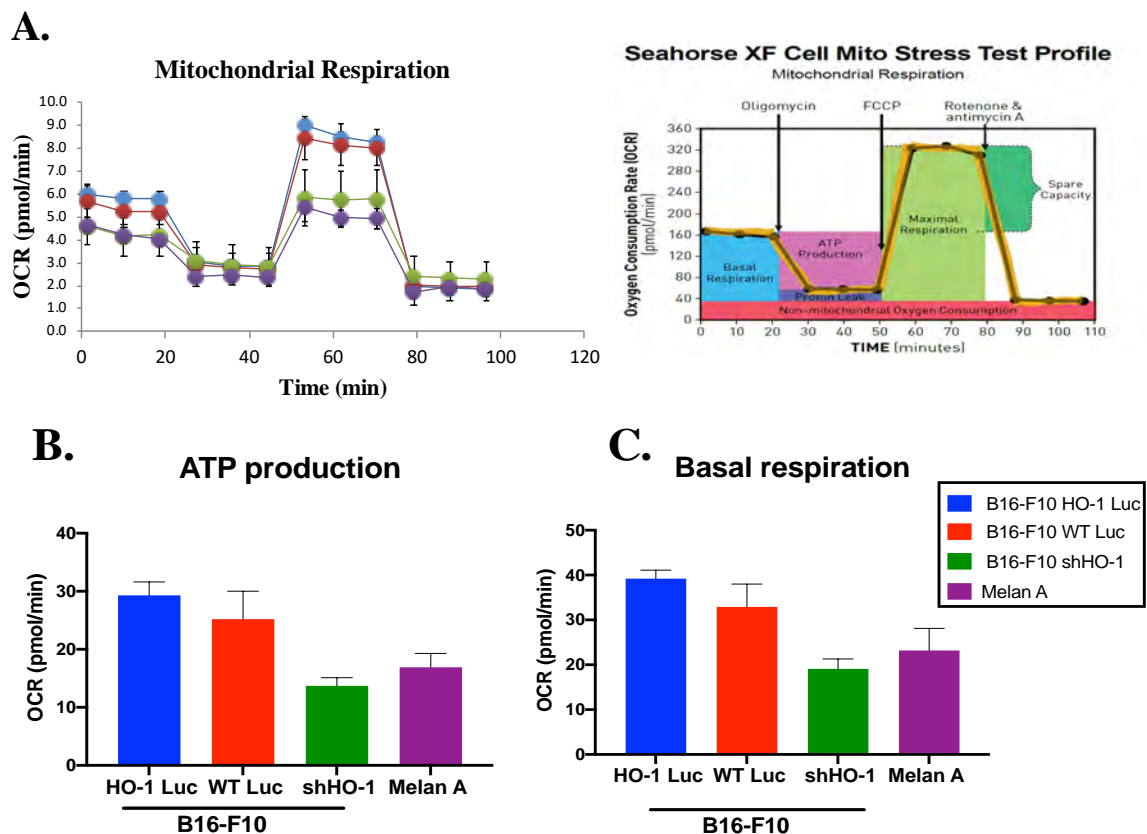
Figure 4.55. The Seahorse analysis of the mitochondrial respiration performed on B16-F10 cell lines with different HO-1 expression (silenced – shHO-1, normal – WT, increased – HO-1) and Melan A melanocytes. **A.** Oxygen consumption rate (OCR) graph and scheme of experiment. **B.** ATP production **C.** Basal respiration. Each bar represent mean + SD of representative experiment.

4.8. Effect of HO-1 on the differentiation of the induced pluripotent stem cells (iPSC) toward melanocytes

4.8.1. Generation of HO-1 WT and KO iPSC

After we observed the effect of HO-1 silencing on reduced pigmentation of melanoma cells, in the next step we wanted to see if HO-1 is important for melanocyte differentiation. Particularly, we wanted to see if HO-1 deficient cells can develop towards pigmented melanocytes.

In this set of experiments we used induced pluripotent stem cells generated from the primary tail tip fibroblasts (TTF) isolated from the wild type (WT) or HO-1 deficient (HO-1 KO) mice (C57BL/6×FVB $Hmox1^{+/+}$ and $Hmox1^{-/-}$, respectively). To generated iPSC, TTF
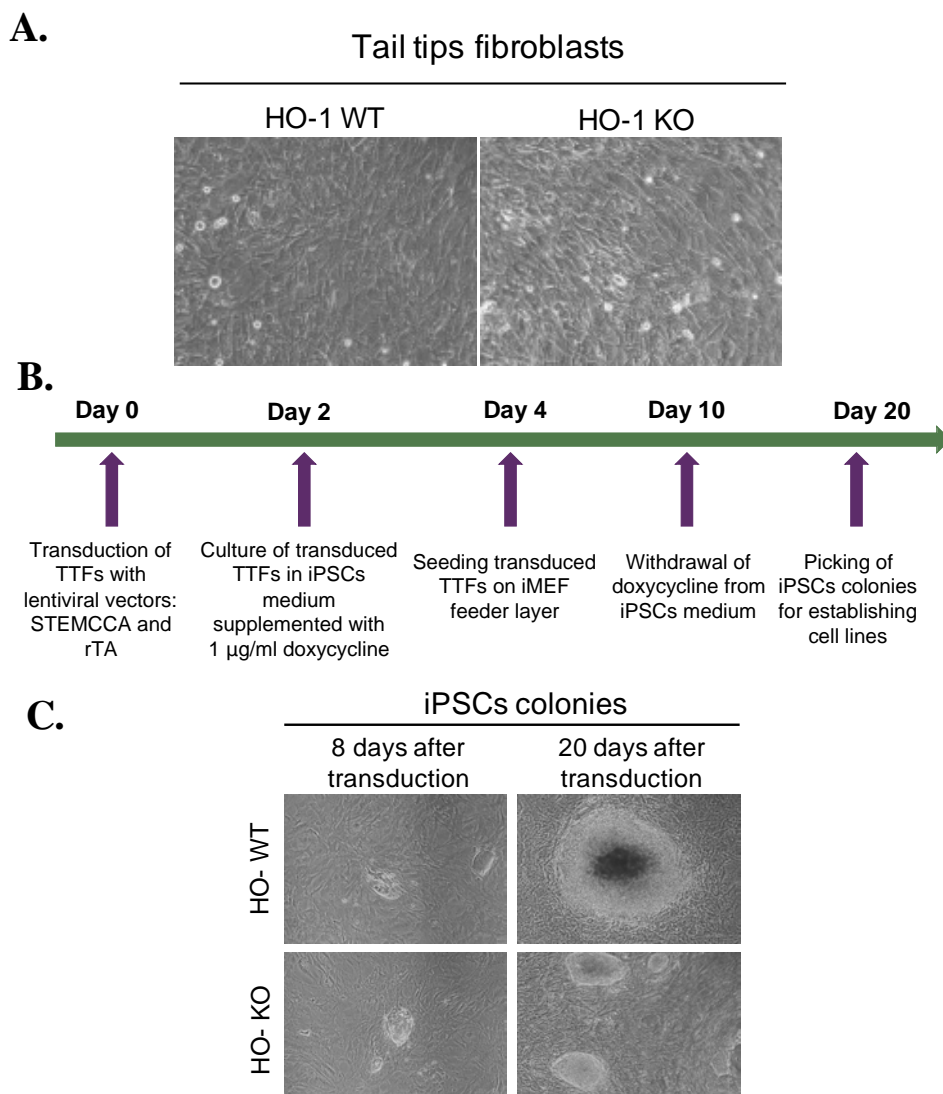
Figure 4.56. Generation of murine WT and HO-1 KO iPSC. **A.** Representative pictures of fibroblasts isolated from the tail tips of C57BL/6×FVB $Hmox1^{+/+}$ and $Hmox1^{-/-}$mice. **B.** Timeline of the iPSC generation. **C**. Pictures of the iPSC colonies 8 and 20 days after transduction of fibroblasts with the lentiviral vectors coding STEMCCA sequence.

were transduced with lentiviral vectors delivering the STEMCCA sequence (coding for Oct4, Klf4, c-Myc, and Sox2) and tetracycline transactivator (rTA) to enable the working of Tet-On system. After the transduction, cells were cultured for 8 days in the presence of doxycycline and seeded on the feeder layer of inactivated mouse embryonic fibroblasts (iMEF) (Fig. 4.56 A, B). On day 8, we observed the formation of first iPSC colonies (Fig. 4.56 C). On day 20, the colonies were picked and new iPSC lines were established.
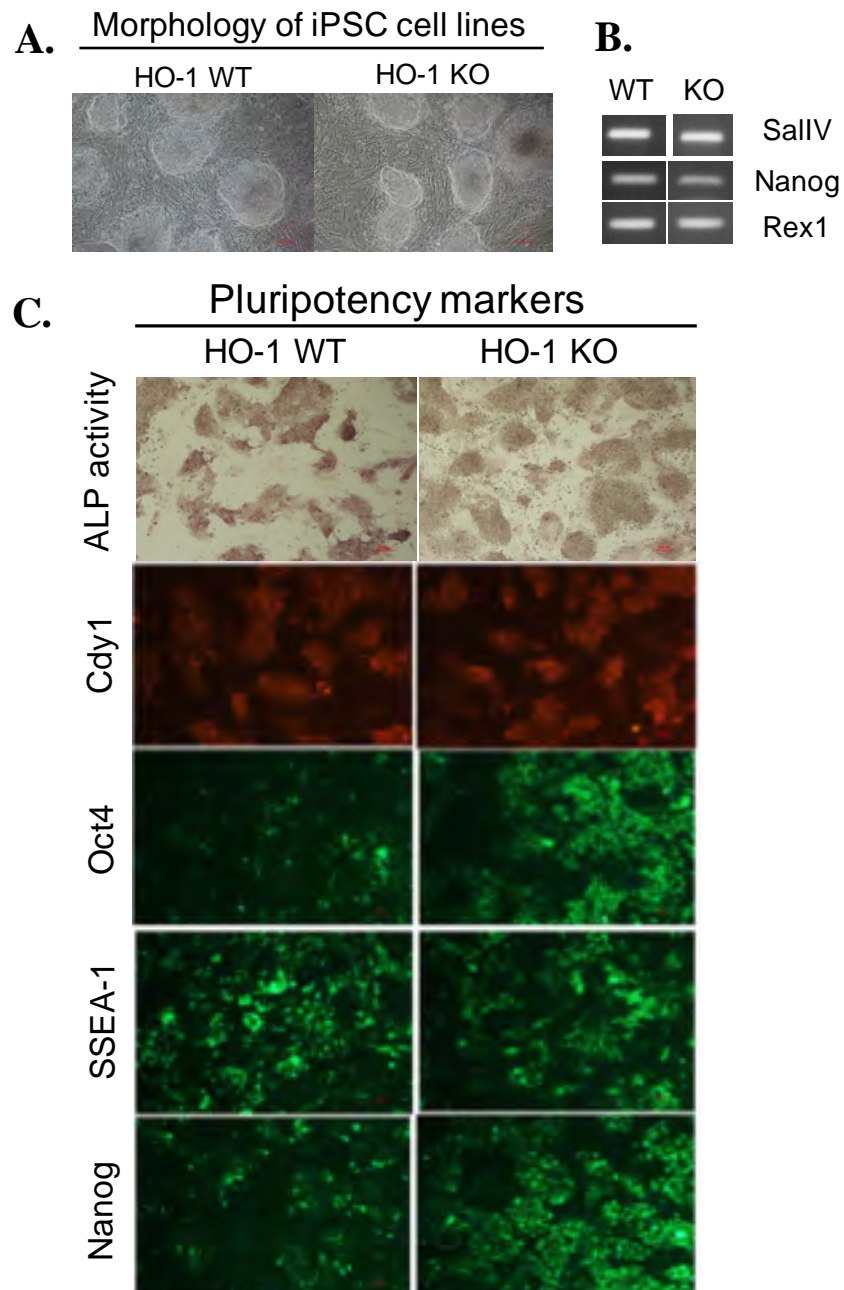
Figure 4.57. Characterization of murine WT and HO-1 KO iPSC lines. **A.** Morphological appearance of cell cultures. Contrast-phase microscopy. **B.** Expression of the pluripotency markers at the mRNA level. RT-PCR. **C.** Markers of pluripotency: alkaline phosphatase activity, Cdy1 retention, Oct4, Nanog and SSEA-1 expression. Histochemical and immunofluorescent staining. Representative pictures.

4.8.2. Characterization of HO-1 WT and KO iPSC lines

Established cell lines displayed morphology characteristic for pluripotent cells and formed colonies when seeded on the iMEF (Fig. 4.57 A) or on the Geltrex membrane matrix (data not shown). We checked the expression of the pluripotency markers in the new iPSC lines and confirmed the expression of *Sall4, Nanog,* and *Rex-1* at mRNA level (Fig. 4.57 B). Both WT and HO-1 KO cells displayed alkaline phosphatase activity and retained Cdy1 dye. Moreover, they expressed Oct-4 and Nanog proteins, as well as SSEA-1 carbohydrate antigen (Fig. 4.57 B). We did not observe significant differences in the levels of pluripotency markers between cells of different HO-1 expression.

4.8.3. Spontaneous differentiation of the HO-1 WT and KO iPSC into three germ layers

We seeded cells for the formation of embryonic bodies (EB) and then allowed for their spontaneous differentiation by seeding cells on gelatin. Both WT and HO-1 KO cell lines were able to differentiate towards ectoderm (expression of heavy neurofilament filament NHF and nestin), mesoderm (expression of vimentin and α-smooth muscle actin, αSMA) and endoderm (expression of Gata4 and α-fetoprotein, AFP) lineages (Fig. 4.58).
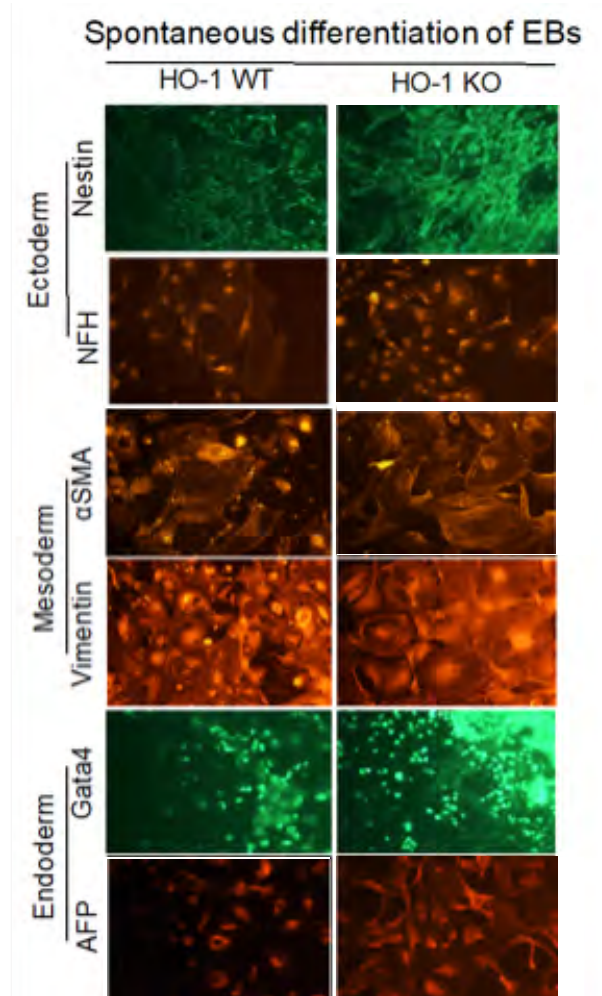
Figure 4.58. Spontaneous differentiation of iPSC towards three germ layers. Expression of proteins characteristic for ectoderm (NFH and nestin), mesoderm (vimentin and αSMA) and endoderm (AFP and Gata4). Immunofluorescent staining. Representative pictures.

4.8.4. Differentiation of WT and HO-1 KO iPSC into melanocytic lineage

We induced differentiation of WT and HO-1 KO iPS cells into melanocytic lineage using the protocol published by Yang and colleagues[236]. Briefly, after EB formation, cells were treated with retinoic acid and seeded on the fibronectin in the melanocyte differentiation medium (MDM), containing SCF (stem cell factor, kit-ligand), Wnt3, and endothelin-3 (Fig. 4.59 A). Cells were differentiated up to 40 days, but we saw the migration of cells from EB already on day 6 (Fig. 4.59 B). On day 15, cells of melanocytic morphology began to appear: they were small, star-shaped and some of them accumulated melanin (Fig. 4.59 B). Interestingly, we did not observe any impairment of melanin accumulation in the HO-1
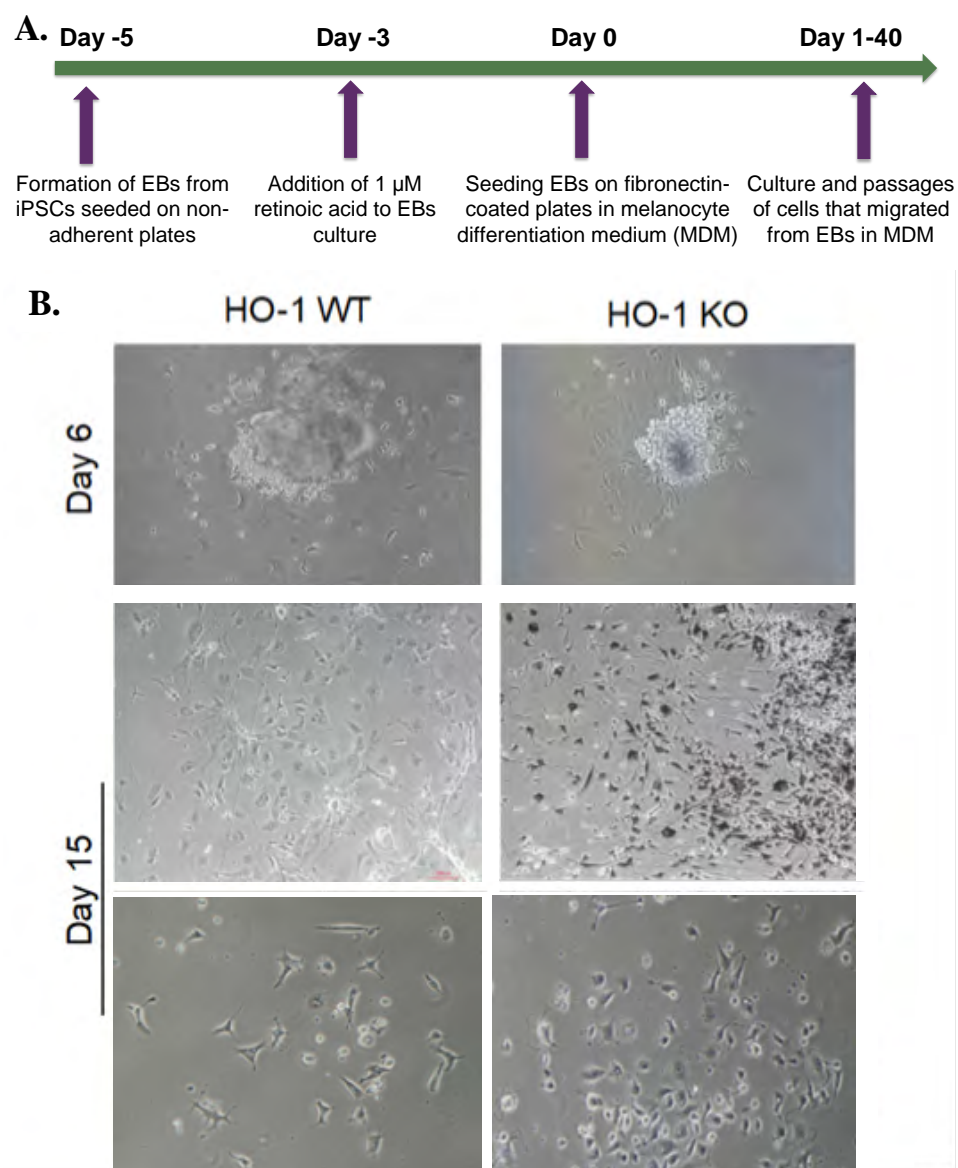
Figure 4.59. Differentiation of WT and HO-1 deficient (HO-1 KO) iPS cells into melanocytes. **A.** Timeline of the differentiation protocol. **B.** Appearance of cell cultures subjected to differentiation on day 6 and 15. Representative pictures. Experiments were performed with help of Grażyna Adamek.

deficient cells. On the contrary, HO-1 KO iPS cells seemed to accumulate pigment even more efficiently than their WT counterparts.

Induction of differentiation towards melanocytic lineage was confirmed by increased expression of *Mitf*, a master regulator of melanocyte development and function. Basal expression of *Mitf* in undifferentiated iPSC was very low, but was significantly upregulated already after 11 days of differentiation, and this increase was higher in HO-1 deficient cells (Fig. 4. 60 A). However, it should be emphasized that the level of Mitf expression in iPSC-derived cells is much lower than that characteristic for melanocytes. This is illustrated by a comparison with Melan-A cells (Fig. 4.60 A). Thus, we were able to induce melanocyte differentiation and obtain the pigmented, melanocyte-like cells, but they cannot be treated as full equivalent of mature melanocytes.

After differentiation, we analyzed the expression of several melanocytic markers in the WT and HO-1 KO cell lines. We found that expression of *Mitf*, although higher in the HO-1 KO cells at the beginning of differentiation, then evened out between the cell lines and was comparable, at least at the mRNA level, in the melanocytic cells of different HO-1 status (Fig. 4.60 B). We noticed however, that Mitf protein was differently localized in the WT and HO-1 KO cell lines. Namely, Mitf accumulated in the nucleus of WT cells, what was less clear in the HO-1 deficient cells (Fig. 4.60 B). One might suppose that intracellular localization can affect the activity of *Mitf* as a transcription factor. Indeed, when we checked the expression of *Mart-1*, the direct Mitf target, we observed a tendency of reduced level of *Mart-1* in the HO-1 KO cell lines (Fig. 4.60 D). We were also able to detect expression of tyrosinase, *Trp1* and *Trp2* in the differentiated cells. Comparison between WT cells and HO-1 KO cell lines showed, however, a very high variability, reflecting possibly the random efficacy of differentiation of a particular line, and not a direct effect of HO-1 on gene expression regulation (Fig. 4.60 D). Again, it should be stressed that expression of genes directly associated with melanogenesis (*Trp1*, *Trp2* and *Tyr*) was very low, at least three orders of magnitude lower than that characteristic for Melan-A cells. Generally, our results show that the presence of HO-1 is not essential for the induction of differentiation of iPSC towards melanocytes and for the formation of pigmented cells.
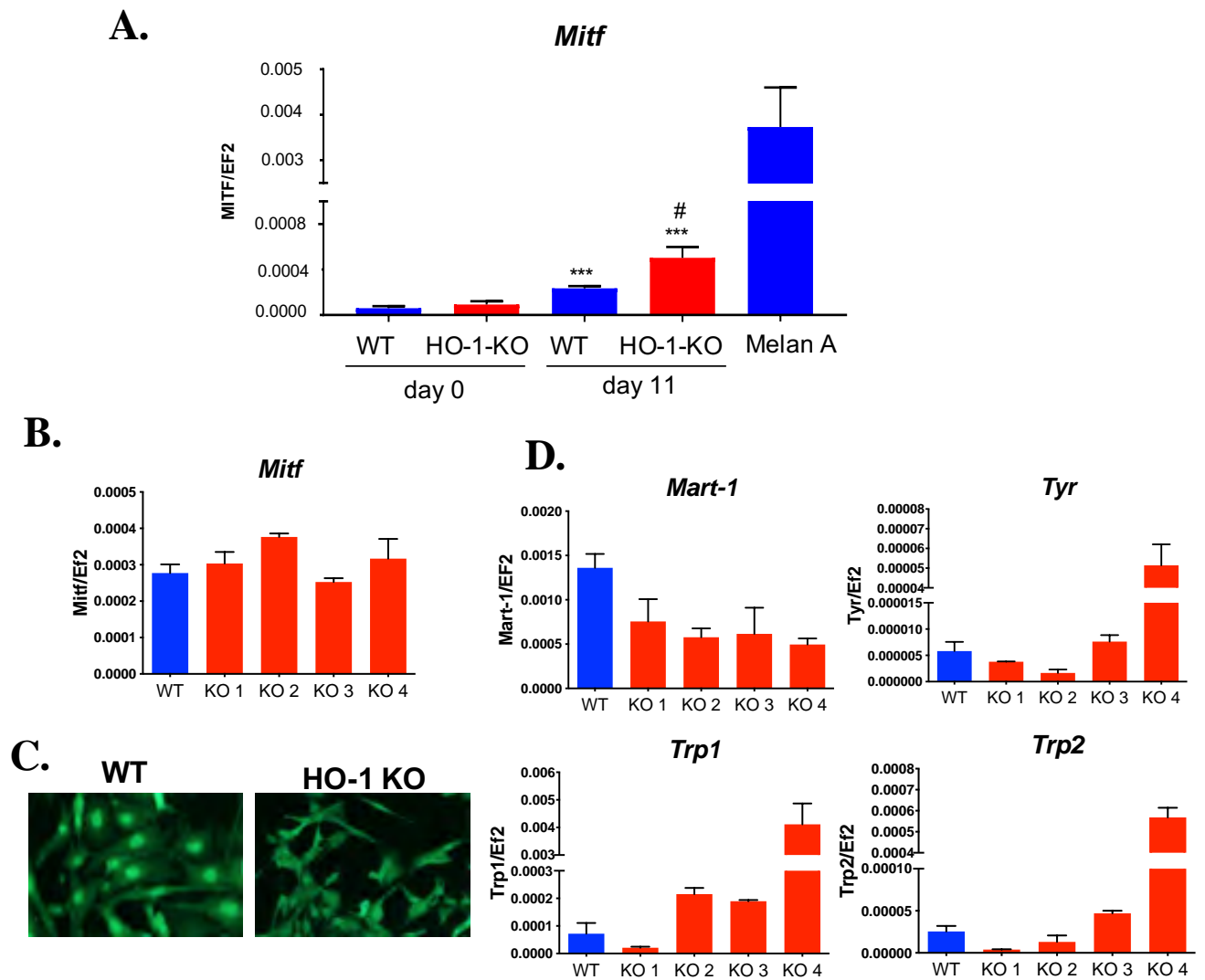
Figure 4.60. Expression of melanocyte markers in differentiated WT and HO-1 KO iPSC lines. **A.** Expression of *Mitf* mRNA before differentiation (day 0) and during differentiation (day 11), in comparison to Melan-A melanocytes. Quantitative RT-PCR; EF2 was used as a housekeeping gene; *** - p<0.001 versus day 0, # - p<0.05 versus WT. **B.** Expression of *Mitf* mRNA in the differentiated WT cells and four HO-1 KO cell lines. Quantitative RT-PCR; EF2 was used as a housekeeping gene. **C.** Localization of Mitf protein (green) in the differentiated WT and HO-1 KO cells. Immunofluorescent staining; representative pictures. **D**. Expression of *Mart-1*, *Trp1*, *Trp2* and *Tyr* mRNAs in the differentiated WT cells and four HO-1 KO cell lines. Quantitative RT-PCR; EF2 was used as a housekeeping gene. Experiments were performed with help of Grażyna Adamek and Agnieszka Seretny.

4.9. Effect of HO-1 silencing on murine melanocytes Melan-A

4.9.1. Establishment of Melan-A cell lines with stably silenced HO-1

Experiments performed in iPSC-derived cells of melanocyte lineage revealed that although the level of HO-1 may affect melanoma cell pigmentation, expression of HO-1 is not necessary for induction of melanocytic differentiation and formation of pigmented cells (Fig. 4.59, 4.60). However, the iPSC-derived cells are heterogenous and not fully differentiated. Therefore, in the last set of experiments we applied another model to check the importance of HO-1 in the biology of more mature melanocytes. For this purpose, we used Melan-A cell line, immortalized murine melanocytes syngeneic to C57BL/6 mice[262].

cell lines. A. shHO-1 Melan-A cell lines with phase contrast to visualize pigmented cells. Pictures taken in bright field without phase contrast to visualize pigmented cells representative gel. **B**. Picture of pellets of spun ctr, sc and two shHO-1 (A, D) Melan-A cell lines cultured in the RPMI medium for 48 h. **C.** Cells cultured in DMEM and RPMI media for 48-72 h. Pictures were taken in the bright field to visualize the pigmentation.

Using retroviral vectors we silenced HO-1 and generated four shHO-1 Melan-A cell lines and one scrambled control. We confirmed the decreased expression of HO-1 on the protein level (Fig. 4.61 A). We did not notice any macroscopic differences in the pigmentation of cell pellets after centrifugation (Fig. 4.61 B), despite that we have observed such differences in B16-F10 melanoma cell lines with different levels of HO-1 (Fig. 4.52 A).

When cultured in DMEM, Melan-A cells underwent further pigmentation (when compared to RPMI growth medium, Fig. 4.61 C). We did not observe any significant differences between the scrambled control and shRNA transduced cells in the induction of pigmentation visible under microscope (Fig. 4.61 C), and in the melanin content, evaluated using electron paramagnetic resonance (EPR; collaboration with dr. Michał Sarna, Fig. 4.62).
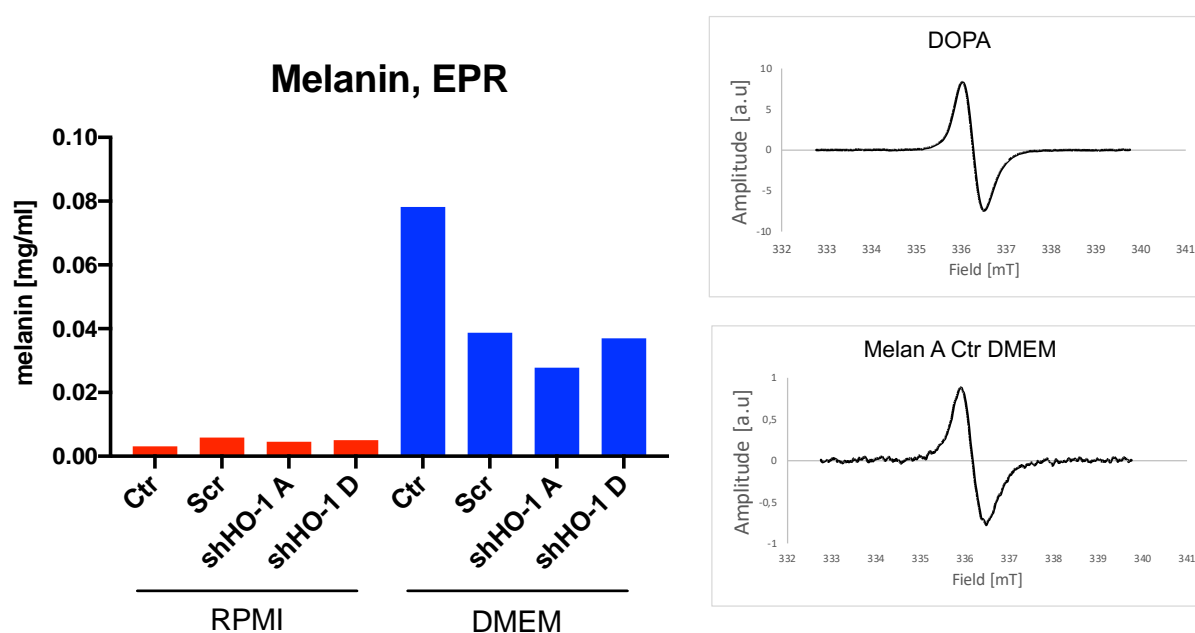
Figure 62. EPR measurement of melanin content in cells cultured in RPMI and DMEM. Data represented as mg/ml of melanin in the sample. Representative melanin spectra of DOPA control and Melan A cultured in DMEM. Data obtained in collaboration with Michał Sarna, PhD from the Department of Biophysics, Faculty of Biochemistry, Biophysics and Biotechnology at Jagiellonian University.

In accordance with microscopic and macroscopic observations of cell pigmentation, we did not see any influence of HO-1 silencing on the expression of genes involved in melanogenesis in Melan-A cells cultured in RPMI (Fig. 4.63 A) or DMEM (Fig. 4.63 B).
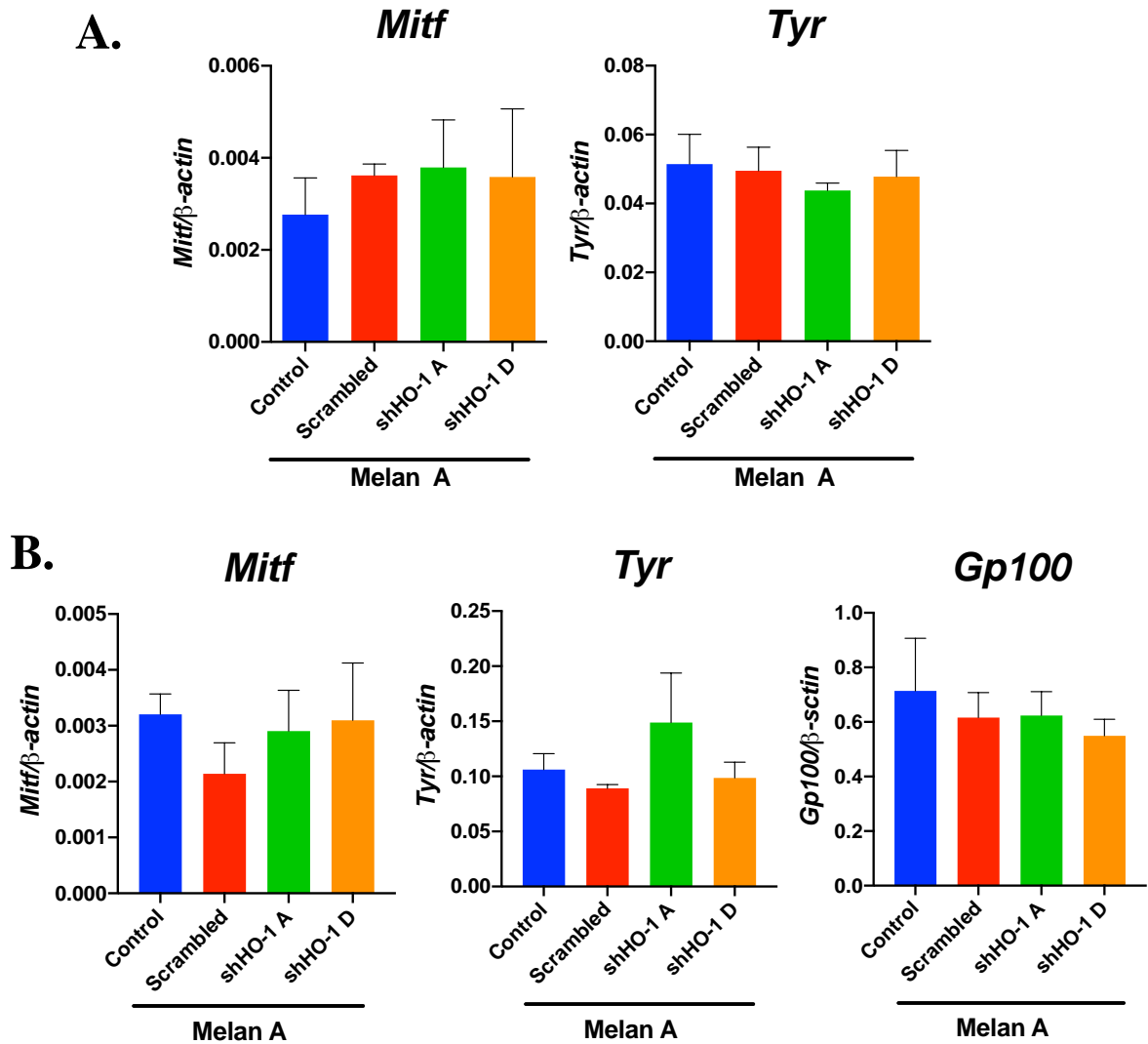
Figure 4.63. Expression of genes associated with melanocyte differentiation and melanogenesis (*Mitf*, *Tyr, Trp1* and *Gp100*) in untreated control (ctr), scrambled control (sc) and two HO-1 shRNA transduced (shHO-1 A, D) Melan-A cell lines, cultured in RPMI (**A**) or DMEM (**B**). Quantitative RT-PCR; β-actin was used as a housekeeping control; each bar represents mean + SEM.

It is worth noting that culture in DMEM led to the inhibition of proliferation of Melan-A cells (Fig. 4.64 B), which confirms the induction of pigmentation and differentiation. We did not observe, however, any effect of HO-1 silencing on the proliferation of Melan-A cells in RPMI and DMEM (Fig. 4.64 A, B) or on the viability of cells (data not shown). Overall, data obtained on Melan-A cell line showed that HO-1 does not regulate the melanogenesis in murine melanocytes.

A.

Proliferation, RPMI

Legend:
- Melan A control
- Melan A scrambled
- Melan A shHO-1 A
- Melan A shHO-1 D

B.

Proliferation, DMEM

Legend:
- Melan A control
- Melan A scrambled
- Melan A shHO-1 A
- Melan A shHO-1 D
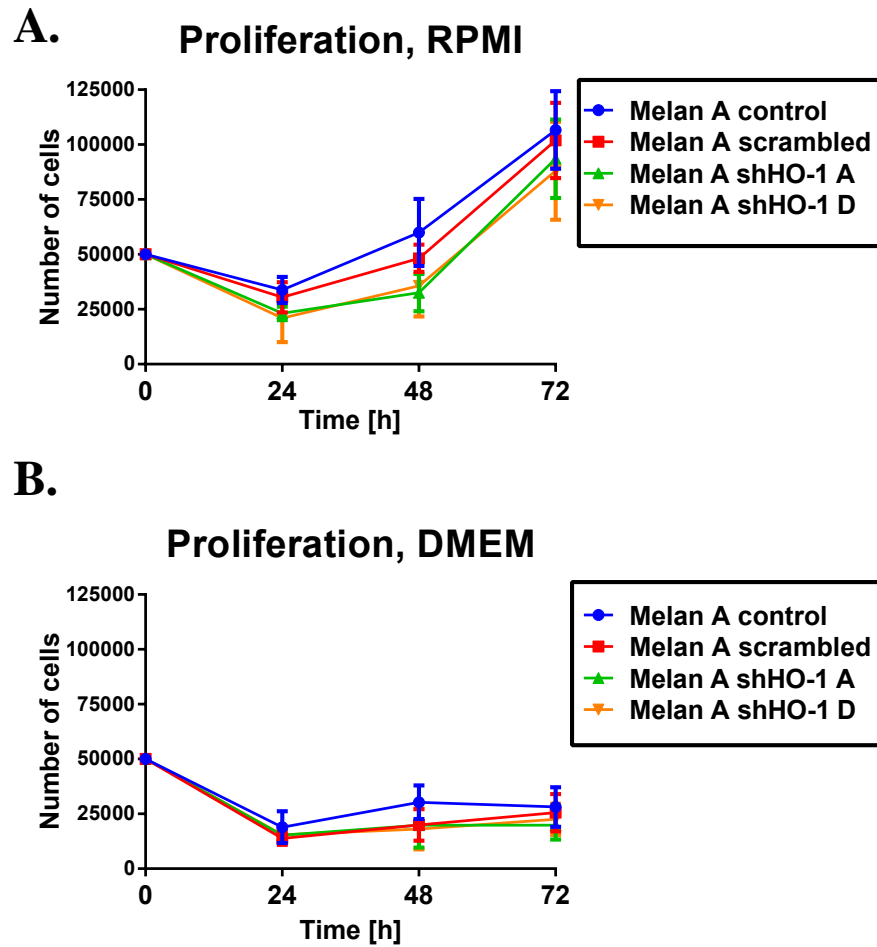
Figure 4.64. Proliferation of untreated control, scrambled control and two HO-1 shRNA transduced (shHO-1 A, D) Melan-A cell lines cultured in RPMI (**A**) or DMEM (**B**). Muse cell counter; each point represents mean ± SEM.

5. Discussion

5.1. B16-F10 cell line contains several MIC subpopulations

In this study, we used the B16-F10 murine melanoma cell line to examine the biology of different MIC subpopulations. Historically, the B16 cell line was isolated in 1954 from the lesion that spontaneously arose on the skin in the ear of C57BL/6J mice in the Jackson Laboratory[263]. The B16-F10 variant of this cell line was established in 1973 through intravenous (i.v) injection of B16 cells and subsequent isolation of lung metastases. The isolated cells were injected i.v. to another recipient and the whole process was repeated 5 times. In the end, the B16-F10 cell line was established, that was consistently able to metastasize to lungs after i.v. administration[264]. Since then, B16-F10 cell line was used in thousands of studies, helping to understand the formation of solid tumors and metastasis, it was used for screening of drugs, inventions of tumor-based vaccines and many more[265].

Recently, whole protein lysates isolated from B16-F10 cell lines were shown to be able to induce CSC-properties in normal NIH3T3 fibroblasts (e.g. induced expression of CSCs markers, alkaline phosphatase activity, colonies formation, anchorage-independent growth, tumorigenicity)[266]. This discovery indicates that the B16-F10 cell line can serve as an valuable model for studies on CSCs, as proteins isolated from these cells induce the de-differentiation of normal cells. Previously, our group used the B16-F10 cell line and discovered that HO-1 enhances aggressiveness of these cells, increases tumor angiogenesis and resistance toward oxidative stress[147]. In the present study, we decided to further explore the role of HO-1 in melanoma and we focused on the putative MIC subpopulations.

Using flow cytometry analyses we identified several subsets of cells expressing known CSC-associated markers. Cells were cultured in normoxia (21% O_2) and hypoxia (0.5% O_2), because we wanted to mimic physiological conditions for CSC that reside in hypoxic niches regulating their behavior[267]. Additionally, the oxygen concentration was shown to be an important factor in *in vitro* melanoma culture affecting the proliferation of cells, metabolism, or chemotherapy responsiveness[268]. Previously, Kuch and colleagues have checked several MIC markers in the B16-F10 cell line and found CD133+, ALDH^high, and CD44+ populations but no expression of CD20, CD24, and CD34[269]. Despite the fact that no expression of CD20 was reported[270], we were able to consistently identify small CD20+ subset in our experiments (Fig. 4.1 A, B, E). Moreover, we identified the CD24+ fraction (0.338% in normoxia) and our observation is consistent with the finding of Tang and colleagues, who also were able to identify small CD24+ subset (0.82%) in the B16-F10 melanoma cell line[270]. Interestingly, however, in

the study of Klimkiewicz et al. cells defined as CD24^{+} accounted for up to 98% of B16-F10 cells[271]. CD44 was also described to be highly expressed in the B16-F10 cell line[271], what was confirmed in our analyses (all cells were CD44^{+}, data not shown). Finally, the expression of CD133 in the B16-F10 seems to be consistent in several studies[265,269,271] including ours and accounts for a very small subpopulation (0.15% on average). However, in human patient-derived melanoma cell lines, CD133 is heterogeneously expressed, with the range from 0% to more than 60% of positive cells[272].

Identification of cells with a high activity of ALDH was more complicated. Initially, we identified quite large subpopulation of ALDH^{high} cells (16.8% in normoxia and 38.4% in hypoxia), similar to other reports (e.g., 12.3% described by Kuch et al.)[269]. But in many experiments, we observed a drastic decrease in the number of ALDH^{high} cells in the B16-F10 lines, and at some points of the study we were not able to detect them. It might be explained by the fact, that ALDH[high] subpopulation is highly sensitive to oxygen supply what is reflected by a significant increase in the percentage of this fraction after culture in hypoxia (Fig. 4.1 D). It was also observed by Klimkiewicz and colleagues, who found out that in normoxia the ALDH^{high} cells consisted of only around 0.2% fraction but hypoxia upregulated and stabilized this subset that reached up to 18% of cells[271]. Additionally, culture as spheroids increased the number of ALDH^{high} cells[269]. Thus, it seems that ALDH[high] subpopulation is very sensitive to oxygen availability and other changes in the cell culture conditions. In cells cultured according to our protocol, as a monolayer in regularly refreshed media, passaged before reaching confluency, the frequency of ALDH^{high} cells is probably decreased. Other MIC subsets were not so sensitive to oxygen concentration and we observed only a tendency towards an increasing number of MIC in hypoxia (Fig. 4.1 B, E).

Moreover, we identified melanoma subpopulation expressing stem cell antigen 1 (Sca-1). Sca-1 was previously described as a marker of CSC-like cells in murine mammary cancer[12], murine gastric cancer[13], and methylcholanthrene-induced sarcomas[14], but not in melanoma. Finally, we were able to identify the rarest MIC subsets, ABCB1 and ABCB5, that were previously described in the B16-F10 cell line[15–17]. However, we did not detect any cells with side population characteristic despite the fact that this subset of cells was previously identified in the B16-F10 cell line (data not shown)[18].

5.2. MIC[+] subsets have a similar differentiation status like MIC^{-} cells

Melanoma associated antigens (MAAs), also known as melanocyte differentiation antigens, consist of normal non-mutated proteins that are found exclusively in melanocytes and

melanomas[239]. MAAs are involved in melanogenesis, they are used for diagnosis and staging of melanoma, and can serve as targets for immunotherapies[239].

It was demonstrated that melanoma spheroids, enriched in CD20$^+$ cells, were able to differentiate and increase the expression of tyrosinase and MITF when cultured in melanocyte differentiation medium[58]. Another study showed that CD271$^+$ MIC isolated from melanoma patients completely or partially lack expression of TYR, MART-1 and melanoma-associated antigen C1 and C2 (MAGEC1/MAGEC2)[81]. Moreover, inhibition of MITF in murine and human melanoma, enhanced tumorigenic capacity and resulted in a more de-differentiated state of cells[273]. Altogether, these data suggest that MIC subsets might display an undifferentiated profile.

To check the differentiation status of MIC subsets in the B16-F10 cell line we analyzed the expression of *Tyr, Gp100,* and *Mart-1* in sorted subpopulations (Fig. 4.2 A-D), but the obtained results do not create a coherent picture. We found out that only CD133$^+$ cells decreased tyrosinase levels when compared to control CD133$^-$ cells. On the other hand, expression of tyrosinase was increased in ALDH^{high} fraction, and expression of *Gp100* was increased in CD24$^+$ cells. Other MIC$^+$ subsets did not differ from MIC$^-$ in the expression of MAAs.

5.3.   PKH26 retaining cells are a rare temporary subpopulation, independent of MIC markers

Quiescent phenotype is an important factor in melanoma resistance to treatments[274] and there is a growing body of evidence showing that slowly cycling cells are responsible for melanoma maintenance[92,94]. We decided to check the presence of slowly cycling subpopulations in the B16-F10 cell lines and then characterize them. Using labeling of cells with PKH26 dye we demonstrated that there is a small (around 0.1%) subpopulation of PKH26 retaining cells in murine melanoma (Fig. 4.3 A, B). This is consistent with other reports showing that slowly cycling cells represent a very small fraction in many types of cancers, like melanoma, colon cancer, breast cancer, glioblastoma or colorectal carcinoma[93,94,275,276].

Interestingly, in one study, the researchers used carboxyfluorescein succinimidyl ester (CFSE) dye and demonstrated that the slowly cycling CFSE^{high} fraction in the B16-F10 cell line was enriched for cells with low expression of *Mitf* and displayed high tumorigenic potential *in vivo*[273]. We checked the expression of *Mitf* in PKH26$^+$ and PKH26$^-$ cells and did not observe any differences between both subpopulations (Fig. 4.3 C). Accordingly, there were no differences in the tyrosinase mRNA levels, the main enzyme in melanin synthesis pathway, that is directly controlled by *Mitf* (Fig. 4.3 C). It should be remembered that we tested cells 10 days

after PKH26 staining, while CFSE^{+} cells were cultured only for 3 days[273]. However, our results indicate PKH26^{+} cells in B16-F10 melanoma have a similar differentiation status as their PKH26^{-} counterparts.

Slow cycling phenotype is regarded as a feature of CSC[91], so we analyzed the expression of CSC markers in PKH26^{+} cells. Our data revealed that PKH26^{+} fraction of B16-F10 line is enriched with ALDH^{high} and CD133^{+} cells (Fig. 4.3 D). Still, only a minority of PKH26^{+} cells expressed MIC markers, and we observed that with time the enrichment in ALDH^{high} cells was lost in parental cell lines formed from single PKH26^{+} cells (Fig. 4.24 B). Similarly, only a partial overlap of CSC markers and slow cycling phenotype was previously described in the pancreas adenocarcinoma[277]. Also, in human melanoma the label-retaining cells (LRC) did not differ in expression of CD271 and CD133 antigens from the non-LRC fraction, but were enriched in CD20^{+} cells[94]. Finally, it was shown that all slowly cycling melanoma cells, analyzed 3 days after labeling with CFSE, express MIC marker CD271, whereas their CFSE^{low} counterparts consisted of both CD271^{+} and CD271^{-} subpopulations[278]. Overall, our results support the opinion that slow cycling phenotype in melanoma is rather independent of the expression of known MIC markers.

Label-retaining cells in melanoma were shown to be arrested in G2/M phase[94] and the same was demonstrated in human colorectal cancer[275]. Additionally, slowly cycling cancer cells usually do not express Ki67 proliferation marker[92,93,269], what is characteristic for quiescent cells at G0 phase. We observed high variability in the proliferation rate between experiments, but without any significant differences between PKH26^{+} and PKH26^{-} fractions sorted from the same cell cultures (Fig. 4.3 E). This suggests that labeling with PKH26 dye identifies a temporary slow cycling state, not a separate, quiescent cell population. Label-retaining cells proliferated more slowly but with time they could re-start cycling. Such a temporary state of slow divisions in melanoma was previously described by Roesch and colleagues[17]. Moreover, melanoma cells were shown to rapidly exit G1 phase arrest in a more favorable environment, meaning that they are prone to rapid changes in cell cycle status[279].

Generally, we faced high variability of many parameters, including the percentage of MIC antigen expressions between experiments. This can reflect the high plasticity of melanoma cells and was observed before by other groups[98,102]. We believe that B16-F10 line can serve as a model for studies on MIC and MIC markers. However, one should not focus on the averaging of absolute numerical values from different experiments but rather directly compare MIC[+] and MIC[-] subsets from the cell cultures.

5.4. Expression of HO-1 has a greater effect on *in vitro* clonogenicity, melanosphere formation and *in vivo* tumorigenicity than expression of MIC markers

Increased expression of HO-1 augments the aggressiveness of CD24^{low} CD44^{high} CSC fraction in breast cancer[182]. The same study on CSCs in breast cancer showed the increased expression of HO-1 in mammospheres when compared to adherent culture[182]. Interestingly, our data revealed that expression of HO-1 is not altered in most of the MIC[+] subsets when compared to their MIC^{-} controls (Fig. 4.4). Culture of B16-F10 line in MIC medium induced non-adherent growth of cells what was associated with an increase in CD20^{+} fraction (Fig. 4.5). Similar enrichment with CD20^{+} cells was described by Fang and colleagues, who identified CD20 as a MIC marker in human melanospheres[58].

In our hands, B16-F10 cells formed melanospheres that resembled multicellular aggregates (Fig. 4.5 A). This phenomenon was previously described in some of the patient-derived melanoma cell lines cultured in serum-free media[272]. Although the high activity of ALDH was associated with enhanced melanosphere formation in human melanoma[280] we observed a tendency to decrease in ALDH[high] fraction in murine melanospheres. Inhibition of HO-1 with SnPP abolished non-adherent growth (Fig. 4.5 A) without changing HO-1 expression (data not shown), which highlights the important role of enzymatic activity HO-1 in melanosphere formation. Very recent data (published in June 2020) proved that HO-1 promotes the formation of melanospheres and highlighted the importance of HO-1 activity in this process[281], which is consistent with what we observed. Overall, our data indicate that it is rather a CD20^{+} fraction, not ALDH^{high} cells, that mediate sphere formation by B16-F10 cells in MIC medium. At the same time, HO-1 activity seems to facilitate formation of melanospheres.

Overexpression of HO-1 in human melanoma cells led to enhanced colony formation, and the opposite was observed when HO-1 was silenced[181]. The same relationships were described in cervical carcinoma[282], thyroid cancer[283], leiomyomatosis and renal cell carcinoma[284], or human pancreatic cancer cells[285]. Unexpectedly, we observed that overexpression of HO-1 in B16-F10 melanoma cells leads to decreased clonogenicity both in normoxia and hypoxia (Fig. 4.6, 4.7). Moreover, HO-1 clones had diminished survival in hypoxic culture (Fig. 4.7 B) and were significantly smaller and more pigmented than their WT counterparts (Fig. 4.8 A, C). We cultured cells in serum-free MIC media, as the presence of serum was shown to affect clonogenicity and tumorigenicity of melanoma cells[286,287]. Generally our data suggest that high level of HO-1 in single melanoma cells is not favorable for initiation of clonal proliferation and survival *in vitro*. To further investigate the effect of HO-1 on tumor

initiation capacity we performed *in vivo* serial transplantation of WT and HO-1 overexpressing cells into syngeneic C57BL/6J mice.

Our previous study showed that although overexpression of HO-1 in melanoma cells did not affect the size of growing tumors after subcutaneous transplantation to syngeneic mice, the density of melanoma cells within the tumors overexpressing HO-1 was higher than in the wild-type control[147]. Accordingly, in human melanoma, overexpression of HO-1 caused increased tumor growth[181]. However in both studies, the number of transplanted cells was high (100 000 and 10 000 000, respectively) so it was proliferation rate and survival of injected cells that were measured, not initiation of tumor growth. Here we wanted to check the influence of HO-1 on melanoma initiation.

According to CSC theory, injection of a very small number of CSCs, but not bulk cells, into mice should result in tumor formation[288]. In our experimental setting, injection of only 10 HO-1-overexpressing or WT B16-F10 melanoma cells resulted in the formation of tumors. HO-1 increased tumorigenicity in primary recipients, but significantly decreased initiation of tumors in secondary and tertiary recipients (Fig. 4.29).

Therefore, we propose two conclusions. First, B16-F10 cells are able to initiate tumor growth from a very limited number of cells when transplanted to syngeneic recipient, similarly to what was observed in human melanoma[95]. Human melanomas were highly tumorigenic even when single-cells were injected into NSG mice – this result put into question the existence of CSCs in melanoma[95]. Here, we showed that murine melanoma cells transplanted to immunocompetent, syngeneic mice also have a pronounced tumorigenic potential, what supports observations from human model.

Second, we showed that HO-1 decreases tumorigenicity in secondary and tertiary recipients, probably due to reduced self-renewal of melanoma cells. Early induction of HO-1 in Mdr2$^{-/-}$ mice (the model of chronic liver inflammation and inflammation-induced tumor development) delayed the initiation of liver tumors through amelioration of chronic inflammation[289]. Moreover, in chemically-induced squamous cell carcinoma, HO-1 KO mice developed lesions earlier than WT animals[290], suggesting that HO-1 is able to delay the initiation of tumor formation. Here we found that in B16-F10 melanoma, HO-1 increases the proliferation of MIC in primary recipients, measured as luminescence of tumor cells 7 days after the transplantation. However, HO-1 overexpression reduced induction of secondary and tertiary tumors, the activity depending of self-renewal of MIC. This reduced tumorigenesis was reflected by an increased survival rate of recipient mice (Fig. 4.31, 4.32). It is worth noting that improved survival was not associated with changes in metastatic potential, which was similar

in both groups (Fig. 4.33). Overall, HO-1 probably improves survival of transplanted cells but decreases initiation of tumor growth in the cell self-renewal dependent long term transplantation assay. This is consistent with diminished clonogenicity observed *in vitro*.

To assess the influence of HO-1 on MIC subsets we have chosen CD20, ALDH, and PKH26 retaining cells for further analysis. Although CD20 was shown to be associated with increased melanosphere formation[291], to our knowledge, the clonogenic capacity of CD20+ melanoma cells has not yet been characterized. We did not observe any significant differences in clonogenicity of CD20- and CD20+ cells both in normoxia and hypoxia (Fig. 4.9).

Knockdown of ALDH1A3 led to decreased clonogenicity in neuroblastoma[292] and non-small cell lung carcinoma[293], whereas ALDHhigh cells were associated with increased clonogenicity in Ewing's sarcoma[294]. Again, we did not observe any significant differences in clonogenic potential *in vitro* between ALDHlow and ALDHhigh subsets in WT control. Just like in unfractionated cells, overexpression of HO-1 decreased clonogenicity of melanoma, regardless of the ALDH status. Only in ALDHhigh cells cultured in normoxia, clonogenicity of HO-1 overexpressing cells was higher than in WT counterparts, but this may be an indirect effect of exceptionally low clonogenicity in the control group.

To sum up, we did not detect any significant influence of MIC expression on the clonogenicity of melanoma cells. Instead, we noticed a very heterogenic morphology of the B16-F10 clones that was previously demonstrated in human melanoma[98]. In MIC fractions, clones that overexpressed HO-1 in hypoxia were significantly smaller than those formed by WT cells (Fig. 4.10). Our results indicate that it is HO-1 overexpression that primarily affects clonogenicity and morphology of melanoma clones, not a MIC marker status. Only when we focused on PKH26 retaining cells, we found that PKH26+ subset formed fewer clones than PKH26- control, what was more pronounced in HO-1 overexpressing lines (Fig. 4.11 A).

Limiting dilution assay (LDA) is a gold standard for quantifying active cell fraction[242]. Its' use date back to the beginning of the XX century when it was used for quantification of bacteria[295]. Since then, LDA has been widely and successfully implemented in many research areas including immunology, stem cells, and CSC studies[242]. LDA enables quantification of CSC frequency after sorting or *in vivo* injections of putative CSC- and CSC+ fraction in different dilutions, followed by calculation of positive and negative events (e.g. clone formation vs. no clones, tumor formation vs. no tumor). Then, using the statistical end-point dilution assay (ELDA) tool, the exact active cell fraction is determined[242].

Using the ELDA approach, we calculated the fraction of clone initiating cells (CIC) in PKH26+ and PKH26- subsets *in vitro*. Consistently with results from the clonogenic assay,

ELDA revealed that PKH26^{+} subset has almost two times smaller fraction of clone initiating cells (1 in 8.4) than PKH26^{-} fraction (1 in 4.4; Fig. 4.13). The assessed frequency of CICs is in line with the results obtained in human melanoma, where the fraction of MIC in *in vivo* LDA was calculated as 1 in 4[95]. Interestingly, HO-1 increased the ability to initiate growth in PKH26^{+} cells that reached a similar level to that calculated for PKH26^{-} WT subset. It was visible both in primary and secondary clones (Fig. 4.13, 4.14), although one should be aware that only in secondary ELDA the goodness of fit test confirmed an actual difference in CIC fraction (Fig. 4.14). Once again, overexpression of HO-1 had an overriding effect. This might be partially explained by the observation that HO-1 overexpression upregulates *Dnmt1* and *Notch1* in PKH26^{+} and PKH26^{-} fractions, when compared to WT control (Fig. 4.18). The DNA methyltransferase DNMT1 is essential for CSC maintenance, for example in breast cancer[296,297]. In melanoma, DNMT1 is an important regulator of methylation pattern and some polymorphisms of the DNMT1 gene are associated with poor overall survival and recurrence-free survival of patients[298,299]. The second upregulated gene, Notch1, is involved in the self-renewal and differentiation of normal and cancer stem cells[300,301]. Inhibition of Notch signaling in melanoma cells reduces tumorigenicity[302]. Interestingly, HO-1 was shown to be a trigger of the Notch-1 signaling pathway in breast cancer stem cells[182].

Altogether, our data might suggest that upregulation of *Dnmt1* and *Notch1* by HO-1 mediates the increase in CIC fraction in PKH26^{+} subset. At the same time it does not further elevate the clonogenicity in PKH26^{-} cells, that were similar in HO-1 and WT cells. We do not expect, however, that changes in *Dnmt1* or *Notch1* expression levels are the primary cause of reduced clonogenicity in our PKH26^{+} WT cells, as their expression was comparable with that in PKH26^{-} WT cells. Generally, the stem cell-related gene expression profile between PKH26^{+} and PKH26^{-} cells was similar. We notice, however, one interesting exception. Namely, expression of *Nos2* is reduced in PKH26^{+} cells in B16-F10 WT line (not statistically significant, data not shown). This reduction is rescued by overexpression of HO-1. NOS2 promotes liver cancer stem cell development through ADAM17-dependent Notch signaling pathway[303]. Moreover, expression of NOS2 can be reduced in melanoma cells with cell cycle arrest caused by anti-mitogenic regulators, such as curcumin[304]. We believe that this pathway is worth investigating to validate experimentally the potential role of NOS2-dependent regulation in PKH26^{+} melanoma cells.

To investigate tumorigenicity of MIC subsets we performed *in vivo* serial transplantation assays. We found that PKH26^{+} cells were able to form tumors after transplantation of 10 cells, similarly as the bulk B16-F10 cells. It seems consistent with the observations from human

melanoma, where slowly cycling JARID1B^{+} cells and control JARID1B^{-} cells revealed a comparable tumorigenicity[17]. Interestingly, in B16-F10 line, the dye-retaining CFSE^{high} cells were shown to be tumorigenic, while CFSE^{low} cells failed to form tumors, even when 20 000 cells were transplanted[273]. In our experiments, after transplantation of only 10 PKH26^{-} cells, we also did not detect any primary tumors. Due to a small number of recipient animals we cannot exclude, however, a random variability, thus we cannot draw far-reaching conclusions. Finally, serial transplantation proved a self-renewal of PKH26^{+} and bulk cells (Fig. 4.39 B). Overexpression of HO-1 in the PKH26^{+} cells decreased tumorigenicity in secondary recipients, similarly to what was observed for unfractionated cells.

When human melanoma cells were labeled with PKH26 and one million cells were injected into SCID nude mice, the fluorescent signal was gradually lost in the primary tumors, but was still detectable in distant organs in forms of metastases[94]. The invasive phenotype of slowly cycling cells was also observed in the experiments showing that despite treatment-induced senescent phenotype, melanoma cells were able to invade and metastasize in a WNT5A dependent manner [305]. In our study, we did not observe significant differences in metastatic potential between PKH26^{+} subset and bulk cells. Not all mice developed metastases, but if metastases occurred, melanoma cells preferentially localized in intestines and livers (Fig. 4.40). Those are known sites for metastases in human melanoma[306].

5.5.   Progeny of MIC^{+} cells re-establish parent phenotypic heterogeneity

One of the characteristics of CSCs is the ability to give rise to more differentiated progeny what is reflected in the heterogeneity of cancers[307]. The true CSC[+] should be able to give rice to both CSC[-] and CSC[+] progeny, due to the self-renewal and differentiation abilities. At the same time, in the unidirectional model of CSC, CSC[-] fraction should not be able to give rise to CSC[+] population[308]. However, there is a growing body of evidence showing that plasticity of CSC progeny can lead to the formation of CSC[+] from non-CSC fraction[308].

We evidenced that progeny of PKH26^{+} cells is not enriched in PKH26^{+} fraction and heterogeneity of PKH26^{+} and PKH26^{-} cells is re-established after culture from single cells (Fig. 4.21 A). Apparently, PKH26^{-} cells were able to give rise to PKH26^{+} cells. This result is consistent with what was observed in human melanoma, where slowly cycling JARID1B^{+} cells were able to reconstitute parental heterogeneity giving rise to both JARID1B^{+} and JARID1B^{-} progeny[17]. Also, the CFSE[low] and CFSE[high] subpopulations in the B16-F10 cell line were dynamic and regained initial proportions after culture[273].

Examination of MIC progeny in our study revealed that they re-establish heterogeneity of parental cells in terms of CD20, CD24, and CD133 expression (Fig. 4.22). Interestingly, ALDH[high] derived cell lines showed a tendency to reduce ALDH[high] fraction when compared to the parental cell lines. It should be stressed once again, however, that we observed particular heterogeneity in melanoma ALDH activity. We did not find any influence of HO-1 overexpression on phenotypic heterogeneity of melanoma.

Our results are in line with the study showing that sorted and cultured CSC+ and CSC- cells (in different types of cancers) regained over time the proportions of CSC+ to CSC- cells, characteristic for the parental cell lines[99]. This study also pointed at an important issue that CSC- and CSC+ cells do not differ in terms of Ki67+ proliferating cells, suggesting that expression of CSC markers is not necessarily connected with a quiescent phenotype[99]. We also did not observe any differences in the cell cycle of MIC progeny, both in WT and HO-1 cell lines (Fig. 4.3 E, 4.21). *In vivo* studies in human melanoma proved that different subset of cells expressing CSC markers (e.g., CD271, ABCB5) were able to recapitulate the heterogeneity of parental tumors when injected into NSG mice[96]. Thus, the phenomenon of re-establishment of heterogeneity after purification of different subsets of melanoma cells is consistent in human and mouse cancer and seems to be irrespective of a marker used.

5.6.   Expression of CD20 and high ALDH activity do not mark cells with MIC properties in murine melanoma

Targeting CD20 with engineered cytotoxic lymphocytes (CTLs) causes the eradication of human melanoma biopsies transplanted to immunocompromised mice[309]. This was observed despite the fact that CD20 fraction was calculated to consist of only 2% of tumor cells, meaning that targeting of small subpopulations of cells can lead to elimination not only of CD20+ cells but also bulk tumor cells[309]. CD20 was also shown to be associated with resistance to targeted therapies, as melanoma cells resistant to dabrafenib (B-RAF inhibitor) had two-fold higher expression of CD20[310]. When CD20+ melanoma cells were targeted with salinomycin, the antibacterial drug that targets CSC in some cancers, scientists observed inhibition of melanoma growth *in vivo*[311]. Moreover, the administration of anti-CD20 antibody rituximab in late-stage melanoma patients caused long-lasting remission of injected melanoma lesion and increased overall survival[68,312]. These data indicate that CD20+ fraction plays an important role in human melanoma development.

In our experiments, we did not observe any differences in tumorigenic potential between CD20− and CD20+ fractions in murine melanoma (Fig. 4.36). Additionally, overexpression of

HO-1 did not affect tumorigenicity of CD20⁻ and CD20⁺ fractions. The only difference was that CD20⁺ HO-1 cells seemed to grow faster what was reflected in a higher luminescence of these cells at days 7 and 14 (Fig. 4.37 A). Additionally, HO-1 did not significantly affect the tumorigenicity or survival of mice despite the fact that HO-1 overexpression was associated with increased levels of many genes connected with CSC pathways (e.g., Hippo, Hedgehog, and Wnt pathways) in sorted cells *in vitro* (Fig. 4.16). The same analysis revealed no significant differences in expression of CSC genes between CD20⁺ and CD20⁻ fractions sorted from the WT cell line (Fig. 4.15). Moreover, when we attempted to investigate the differentiation capacities of CD20⁺ progeny we were unable to observe any differentiation potential toward adipogenic and osteogenic lineages in both CD20⁻ and CD20⁺ fractions (Fig. 4.28) despite the fact that such differentiation capacities have been previously described in human melanoma[58]. The only gene upregulated in CD20⁺ fraction after osteogenic differentiation was osteonectin, but alkaline phosphatase activity test did not confirm real differentiation (Fig. 4.28 B). Overall, our data suggest that expression of CD20 does not mark cells with MIC properties in murine melanoma both *in vitro* and *in vivo*.

Similarly, we found that high activity of ALDH does not mark MIC subsets in murine melanoma. Some previous reports showed that in human melanoma ALDH^high cells are highly tumorigenic when compared to control ALDH^low cells[246,313]. But one study of Prasmickaite and colleagues did not find enhanced tumorigenicity and CSC properties within ALDH^high fraction, similarly to our study[88]. What connects our experiments with that described by Prasmickaite, is the use of immortalized cell line to investigate CSCs, which can influence the tumorigenicity. In studies where ALDH^high fraction was described as a population with CSC properties the researchers used freshly obtained samples from melanoma patients[246,313].

Interestingly, one study on the B16-F10 murine melanoma identified ALDH^high fraction as less tumorigenic than ALDH^low cells[269]. This is consistent with our experiments, where only ALDH^low and not ALDH^high fraction, was able to initiate tumor growth after transplantation of 10 cells (Fig. 4.35), what might be related to the decreased expression of several CSC genes like *Lats1*, *Stat3*, or *Foxp1* in the ALDH^high cells (Fig. 4.19). These genes are associated with melanoma aggressiveness. For example, loss of Hippo pathway kinases, LATS1 and LATS2, increases tumor immunogenicity, leading to the destruction of melanoma cells[314]. In turn, knockdown of STAT3 in human and murine melanoma decreases stem-cell properties, including sphere formation, and decreases the number of side population cells[315]. Finally, increased expression of FOXP1 in melanoma is associated with lymph node metastases and shortened overall survival of patients[316]. However, the significance of these genes in the

potentially reduced tumorigenicity in ALDH^high B16-F10 cells requires experimental verification.

Additionally, tumors that grew after injection of WT and HO-1 unfractionated cells and after injection of sorted PKH26^- and PKH26^+ fractions, were not enriched in ALDH^high cells. We observed heterogenous ALDH activity, with no clear patterns between WT and HO-1 groups or between primary vs. secondary and tertiary recipients. This further implicates that ALDH^high cells in B16-F10 murine melanoma are not important for tumorigenicity.

5.7. Progeny of PKH26 retaining, not ALDH^high cells, display increased chemoresistance

The activity of ALDH was postulated as a promising target for anti-melanoma therapies. Treatment of melanoma cells with isoform-specific ALDH1 inhibitor or silencing of ALDH1A1 and ALDH1A3 genes lead to inhibition of tumor growth *in vivo*[317]. What is more, ALDH1 inhibitor was shown to additionally target slowly cycling melanoma cells, which further highlights the feasibility of ALDH inhibition as melanoma treatment[317].

In our experimental setting, we did not detect any enrichment in ALDH^high fraction in PKH26 retaining melanoma cells, which indicates that the outcomes of high activity of ALDH can be species-specific or cell line-specific. Moreover, we observed that the treatment of B16-F10 cells with N,N-diethylaminobenzaldehyde (DEAB) ALDH inhibitor does not affect the viability and proliferation of melanoma cells (data not shown). It is different from what was observed in human melanoma, where administration of multi-ALDH isoform inhibitors decreased growth of xenotransplanted melanomas through increased oxidative stress, lipid peroxidation, accumulation of toxic aldehydes, and apoptosis[318]. Moreover, targeted therapies (BRAF and MEK inhibitors) increase ALDH1 activity in melanoma cells[319]. This phenomenon was further used for the eradication of ALDH^high cells with nifuroxazide, that killed melanoma initiating cells and decreased tumor formation[319]. On the other hand, in murine melanoma, ALDH^high cells were shown to form a smaller number of spheroid clones than ALDH^low cells, although this effect was reversed in co-cultures with endothelial cells or fibroblasts[271]. Overall, it seems that ALDH^high cells can change their behavior depending on the microenvironmental context and that outcomes of ALDH inhibition in melanoma might be species-specific.

High activity of ALDH was shown to mediate chemoresistance in various cancers. In colorectal cancer, chemoresistant cells had increased ALDH activity, and silencing of ALDH1A3 sensitized them to many therapeutic agents[320]. In ovarian cancer, ALDH^high subpopulation was characterized by increased resistance to doxorubicin, and NRF2 was a

mediator of CSC-properties of ALDH^{high} cells[321]. Also melanoma cells with high ALDH activity displayed increased resistance to several chemotherapeutics, including doxorubicin[313]. In our hands, however, the progeny of ALDH^{high} cells responded identically to doxorubicin treatment as control cells (Fig. 4.27). This once again indicates that high ALDH activity is not an important factor in murine melanoma aggressiveness, contrary to what was observed in human melanoma.

As most chemotherapeutics kill rapidly proliferating cells, slow-cycling cells are regarded as a main population contributing to cancer chemoresistance. Chemoresistance of such cells was demonstrated *in vitro* and *in vivo* in human melanoma, glioblastoma, colorectal carcinoma, colon cancer or pancreas adenocarcinoma[93,275,277]. Treatment of melanoma with various drugs leads to increase in slow-cycling cells expressing JARID1B histone H3K4 demethylase, while inhibition of mitochondrial respiratory chain in such cells sensitizes them to anticancer agents[322].

To study chemoresistance in the progeny of PKH26^{-} and PKH26^{+} cells we treated the cells with doxorubicin and observed that progeny of PKH26^{+} were slightly more resistant to therapy than controls (Fig. 4.25). This result suggests that dye retaining cells may give rise in murine melanoma to drug-resistance and might contribute to the aggressiveness of melanoma.

5.8.   HO-1 overexpression affects melanoma vasculogenic mimicry

In the next step, we focused on the vasculogenic mimicry in the context of HO-1 activity. VM was first described in aggressive primary melanoma as a formation of non-endothelium-lined channels generated by tumor cells[323]. These channels are rich in laminin, collagen type IV, and glycosaminoglycans, and can be visualized using periodic acid-Schiff staining (PAS staining)[324]. The presence of PAS-positive networks in uveal melanoma is strongly correlated with a higher incidence of patient death[323]. Tumor cells that form the vasculogenic channels express, among others, laminin, VE-cadherin, and EphA2 [325].

In vitro experiments using matrigel-based tube formation assay facilitate studies on VM[252]. B16-F10 murine melanoma cells have been previously described to have VM-properties and were shown to be able to form VM structures in chick embryo chorioallantoic membrane (CAM)[326]. Moreover, B16-F10 line includes small subpopulation of cells positive for PECAM1 (CD31) that are involved in the VM[327].

One of the well-known markers of VM is VE-cadherin (CD144), characteristic also for endothelial cells. Its expression on the surface of tumor cells is essential for VM[328]. We found two small subsets of cells positive for VE-cadherin and Tie-2 within B16-F10 melanoma, and

revealed that B16-F10 cells are able to co-operate with endothelial cells in formation of tubes on Matrigel (Fig. 4.43). HO-1 seems to facilitate VM. When B16-F10 cells were seeded on Matrigel alone, HO-1 overexpressing cells started to form tubes earlier than control, WT cells (Fig. 4.45). This was not associated with increased expression of VE-cadherin or Tie-2. After a longer culture of cells on Matrigel, we observed interesting effect – HO-1 overexpressing cells formed more elongated structures that resembled the tubes formed by endothelial cells, while WT cells were more clustered (Fig. 4.46). This observation might indicate that HO-1 overexpressing cells form better quality structures than WT cells. However, only *in vivo* studies with high-resolution imaging of VM-structures would clarify this matter.

We believe that one of the mediators of HO-1 action on VM could be carbon monoxide (CO). To our knowledge, there are no data available that connect CO with VM, but CO is known signaling molecule, protective for endothelial cells, regulating angiogenesis, and exerting vasodilatory effects in blood vessels[329,330]. Deregulation of dimethylarginine dimethylaminohydrolase (DDAH) and increased production of nitric oxide (NO) lead to enhanced VM[331]. Interestingly, HO-1/CO was shown to prevent eNOS (endothelial NO synthase) downregulation under inflammatory conditions, meaning that CO can modulate NO levels[332]. This further points at CO as a potentially important molecule in VM. Interestingly, when we induced enzymatic activity of HO-1 using hemin, we also observed improved VM (Fig. 4.47). However, to finally conclude about the effect of CO, the HO-1 product, in melanoma VM, there is a need for further experiments using the treatment of cells with CORM (CO-releasing molecules).

There are other pathways that, we think, might play a role in the HO-1 mediation of VM. Melanoma cells that contribute to VM were described to express stem cell genes and stem-cell phenotype, associated with a high invasiveness[100]. Most of these features are connected with epithelial-to-mesenchymal transition (EMT) and CSCs. For example, ABCB5$^+$ MIC subsets express higher levels of genes involved in VM than their ABCB5$^-$ counterparts[71]. Blocking of VEGF-A signaling in melanoma cells triggers VE-cadherin dependent VM as an alternative vasculogenic strategy that increase MIC cells in perivascular niche[333]. Slug, through induction of EMT and stem-cell properties, is able to promote VM[334]. In our study, we observed that overexpression of HO-1 upregulated expression of Snail2/Slug (Fig. 4.17). Other CSC-associated genes that were described as regulators of VM and upregulated in our HO-1 cells are c-myc[335], Erbb2 (HER2)[336], Notch1[337], Integrin-ß1[338], and Jak2[339]. Altogether, we suppose that HO-1 might influence VM through up-regulation of CSC-associated pathways.

5.9. Lack of stromal HO-1 affects melanoma pigmentation

Tumor stroma is regarded as a key player in the regulation of the behavior of bulk tumor cells and CSCs[340,341]. It consists of extracellular niche, cancer associated fibroblasts (CAF), endothelial cells, adaptive and innate immune cells, and mesenchymal stromal cells (MSC)[340,342]. There are reports pointing at the stromal HO-1 as a regulator of melanoma growth. In malignant melanoma, HO-1 is strongly expressed by stromal and tumor-associated macrophages (TAMs)[343], and overexpression of HO-1 in tissues of C57BL/6J mice decreased lung metastases and leukocytes infiltration, while enhanced tumor angiogenesis[344]. Also our team found that HO-1$^{-/-}$ and HO-1$^{+/-}$ genotypes of mice act in favor of lung nodule formation by B16-F10 melanoma cells when compared to HO-1$^{+/+}$ animals (Was et al., under review). This latter observation indicates that not only overexpression but also lack of HO-1 in stroma can affect melanoma cells. Here, we investigated the role of HO-1 in stromal cells in the context of melanoma by performing a series of experiments using MSC isolated from HO-1$^{+/+}$ and HO-1$^{-/-}$ mice.

It was previously demonstrated that MSC co-cultured with melanoma cells are able to form capillary-like structures on Matrigel what suggests the involvement of MSC in melanoma VM[254]. To investigate the influence of HO-1 in MSC on melanoma VM we seeded B16-F10 cells on Matrigel in conditioned media from HO-1$^{+/+}$ and HO-1$^{-/-}$ cells. We did not observe any differences in melanoma tube formation on Matrigel between both conditions (Fig. 4.48). It is known that media conditioned by MSC are enriched in many growth factors and cytokines[345]. But studies from our lab, that focused on the comparison of HO-1$^{+/+}$ and HO-1$^{-/-}$ MSC, revealed that *Hmox-1* deficiency in MSC does not alter their growth factor secretory profile[191], which can explain the lack of effect on VM in the *in vitro* model. Moreover, when we co-cultured HO-1$^{-/-}$ and HO-1$^{+/+}$ MSC with B16-F10 cells under 2D conditions, we found no significant impact on melanoma proliferation rate (Fig. 4.49).

Interestingly, we noticed that lack of HO-1 in the MSC was associated with decreased pigmentation in the co-cultured melanoma cells. First, we saw this in 2D co-cultures (Fig. 4.49 D) and were wondering if this is a direct or indirect interaction between MSC and B16-F10 cells that affect melanoma pigmentation. Our 3D fibrin bead assay revealed, somewhat unexpectedly, that the indirect effect of HO-1 expression in MSC, mediated by some soluble factors, is sufficient to affect melanoma cell pigmentation (Fig. 4.50, 4.51).

It has previously been demonstrated that MSC can regulate the differentiation status of melanoma. Culture of B16-F10 cells in conditioned media from human umbilical cord–blood

derived MSC inhibited melanin synthesis in melanoma cells by downregulation of TRP-1 and tyrosinase[346]. Moreover, treatment of melanocytes with IL-6, IL-1α, and tumor necrosis factor α (TNF-α) was shown to mediate paracrine inhibition of melanogenesis[347]. Our data showed that HO-1^{-/-} MSC secrete the same levels of IL-6 as HO-1^{+/+} cells and MSC of both genotypes do not secrete IL-1α or TNF-α[191]. Thus, these are not the mediators of de-pigmentation in our model. Another important factor secreted by MSC that affects melanogenesis is transforming growth factor β1 (TGF-β1). TGF-β1 secreted by the adipose tissue MSC decreases the levels of tyrosinase and TRP-1 in B16-F10 melanoma cells[347]. However, when we checked the secretion of TGF-β1 by HO-1^{-/-} and HO-1^{+/+} MSC, once again, we did not observe any significant differences between genotypes (data not shown).

5.10. Lack of HO-1 in melanoma cells impairs the pigmentation

Although we failed to clarify the mechanisms underlying the effect of HO-1 deficiency in stromal cells on melanoma cells, our data highlighted a role of HO-1 on melanoma pigmentation. At the beginning, we hypothesized that HO-1 might modulate differentiation and thereby melanogenesis in melanoma cells. Therefore, we performed a series of experiments using B16-F10 cells with overexpressed and silenced HO-1. We choose the silencing of HO-1 with shRNA as the best strategy, because chemical protoporphyrin inhibitors (such as ZnPP), might influence melanogenesis independently of HO-1 activity, due to the presence of heavy metals that can affect the activity of melanogenesis enzymes[224]. The effect of HO-1 on melanoma pigmentation was apparent even macroscopically – HO-1 overexpressing cells formed darker pellets than cells with silenced HO-1 (Fig. 4.52 A). It was consistent with our result with MSC co-culture, where lack of HO-1 in MSC was associated with depigmentation of melanoma. The differences in B16-F10 cell pigmentation were not associated with altered expression of several melanogenesis genes (*Tyr*, *Mitf*, *Gp100,* and *Trp1*) but were caused by differences in tyrosinase activity (Fig. 4.52, 4.53). It is consistent with the fact that posttranslational regulation of tyrosinase, not necessarily its expression levels, plays a critical role in melanogenesis regulation[348,349]. The activity of tyrosinase is 10 times higher in melanocytes isolated from dark skin when compared to light skin, and it is not associated with increased levels of tyrosinase[350]. This further highlights the essential role of tyrosinase activity in melanocyte pigmentation and is consistent with our findings.

Decreased pigmentation and activity of tyrosinase in shHO-1 cells might be connected to oxidative stress. It is known that melanogenesis can be a source of oxidative stress through the production of ROS[351]. Previously we described that overexpression of HO-1 in melanoma

cells protects them against H_2O_2-induced oxidative stress[147]. Additionally, we observed that shHO-1 cells respond to oxidative stress with increased ROS production when compared to HO-1-overexpressing or control WT cells (data not shown). Oxidative stress decreases the activity of tyrosinase and causes downregulation of melanogenesis enzymes through MITF-dependent manner[352]. Altogether, we suspect that decreased pigmentation of shHO-1 cells might be connected to the aberrant response of these cells to oxidative stress.

The second important relationship that we observed was the altered mitochondrial respiration in the HO-1 silenced melanoma cells. It resulted in decreased production of ATP in shHO-1 B16-F10 cells, to the level characteristic for Melan-A melanocytes (Fig. 4.55). Recently, it was demonstrated that UV exposure of keratinocytes induces the release of extracellular ATP, and that such ATP promotes melanin production in melanocytes through induction of P2X7/CREB/MITF axis[353]. It is also worth noting that cyclic AMP (cAMP) and protein kinase A (PKA) signaling pathways are involved in the regulation of melanogenesis[354]. Conversion of ATP to cAMP is catalyzed by adenylyl cyclase, which is followed by the activation of PKA by cAMP, and then phosphorylation of CREB and CREB-binding protein (CBP). Interaction between CREB and CBP leads to the upregulation of MITF, which further induces expression of melanogenesis enzymes and enhances pigmentation[354]. Altogether, these data suggest that the pool of cellular ATP is able to indirectly affect melanogenesis. It is possible that the decreased levels of ATP in HO-1 silenced melanoma cells can contribute to the altered pigmentation, although the mechanisms would rather be independent of regulation of MITF transcriptional activity. One could also hypothesize the involvement of extracellular ATP, possibly released from MSC, in this process. However, further studies are needed to verify such suppositions.

Induction of melanogenesis by culturing the cells in DMEM led to the robust pigmentation in the HO-1 overexpressing but not in the HO-1 silenced B16-F10 melanoma (Fig. 4.54). Interestingly, cells with silenced HO-1 excreted more melanin to the media and were less granulated. Similar phenomenon was described in melanocytes carrying the *underwhite* mutation, the model for oculocutaneous albinism (OCA) type 4, the hypopigmentary disorder that affects the pigmentation of the skin, hair, and eyes[355]. In culture, OCA4 melanocytes constantly secrete dark vesicles to the media that contain melanogenic enzymes, including tyrosinase. As a result, maturation of melanocytes is disturbed, what leads to hypopigmentation[355]. Thus, it seemed possible that HO-1 deficiency impairs the maturation or trafficking of melanosomes. To investigate this possibility we used iPSC generated from

HO-1^{+/+} and HO-1^{-/-} mice and differentiated them towards melanocytes to check if HO-1 is needed for proper differentiation.

5.11. HO-1 is dispensable to melanocyte differentiation

Generation of the induced pluripotent stem cells is a technique described in 2006 by Kazutoshi Takahashi and Shinya Yamanaka[356]. The discovery revolutionized the field of regenerative medicine and in 2012 Shinya Yamanaka, jointly with John Gurdon, won a Nobel Prize in Physiology or Medicine "for the discovery that mature cells can be reprogrammed to become pluripotent"[357].

The iPSC generation is based on the de-differentiation of somatic cells into pluripotent stem cells through transduction of cells with pluripotency genes: c-myc, Sox2, Klf4, and Oct-4[356]. Induced pluripotent stem cells differentiate into cells from three germ layers and are the invaluable source of cells for further mechanistic studies. Differentiation of pluripotent cells into melanocytes was first performed using human embryonic stem cells (hESC) that were treated with Wnt3a, endothelin-3, and SCF[358]. Later, a similar protocol was applied to induce melanocytic differentiation of human and murine iPSC[236,359].

We used iPSC derived from tail-tips fibroblasts of HO-1^{-/-} and HO-1^{+/+} mice for differentiation towards melanocytes. Culture of cells according to the differentiation protocol resulted in enhanced pigmentation, especially in the HO-1 KO cells (Fig. 4.59). We obtained one WT cell line and four KO cell lines. When we analyzed the expression of melanocytic markers, we saw high heterogeneity between iPSC lines of the same genotype (Fig. 4.60), that made impossible to perform reliable quantitative analyzes. It highlights the importance of using more than one iPSC cell line in differentiation experiments, not only just technical replicates of one clone. The heterogeneity of iPSC is associated with several aspects. One of them is the fact that cell lines are derived from single cells/colonies and pre-existing somatic mutations might cause genetic heterogeneity between cell lines[360]. The heterogeneity might be connected to *de-novo* mutations during cell reprogramming and cell to cell variation in the same cell line[360]. Also, the level of differentiation reached in particular cell cultures can be different. Thus, there is a need to use many cell lines to capture actual differences between studied groups.

One conclusion that we can definitely draw from the differentiation experiments was that HO-1 is dispensable for lineage commitment and at least first stages of melanocyte differentiation. It is a very interesting observation, not consistent with what we observed in B16-F10 murine melanoma, where cells with silenced HO-1 had altered pigmentation. But it was consistent with what we observed after the silencing of HO-1 in Melan-A murine

melanocytes. Melan-A with silenced HO-1 did not change their behavior when compared to control cells. They had the same pigmentation capacities as control counterparts (Fig. 4.61 and 4.63) which suggests, once again, that HO-1 expression is not necessary for physiological pigmentation. However, our results indicate that HO-1 may exert different effects in pathological conditions (melanoma) and in physiological settings (melanocytes and iPSC differentiated towards melanocytes). Probably, the activity of HO-1 in physiological conditions is involved in the protection of cells against oxidative stress and is not necessarily connected with a direct regulation of pigmentation. It is in agreement with several other studies where HO-1 was shown to protect melanocytes against UV and H_2O_2-induced oxidative stress[224,361]. In melanoma, the effects of HO-1 seem to be associated with susceptibility of cells to oxidative stress but also with changes in energy metabolism.

6. Conclusions

We characterized phenotypically and functionally defined MICs and investigated the role of HO-1 in their biology. We also examined a potential influence of HO-1 in differentiation and melanogenesis of melanoma cells and melanocytes. Our studies revealed that:

1. B16-F10 murine melanoma cell line contains cells expressing MIC surface markers (CD20, CD133, CD24, ABCB1, ABCB5, Sca-1) and cells with functional CSC features (high activity of ALDH and PKH26 label retention). Together with observation that B16-F10 cells initiate tumor growth from a limited number of cells in syngeneic recipients, our results indicate that this cell line can be a good supporting model to study MIC biology.

2. Although HO-1 expression in not significantly changed in MIC subsets, its activity is important for non-adherent growth of melanoma cells, a characteristic of CSC.

3. HO-1 has a greater impact on melanoma cell clonogenicity than MIC markers expression and a high level of HO-1 in single melanoma cells is unfavorable for initiation of clonal proliferation *in vitro*.

4. *In vivo* HO-1 overexpression decreases tumorigenicity in secondary and tertiary recipients in serial transplantation assay, probably due to reduced self-renewal of melanoma cells. This conclusion is also consistent with *in vitro* studies.

5. Expression of MIC markers does not select CSC-like cells in murine melanoma. MIC$^-$ and MIC$^+$ subsets display similar clonogenicity *in vitro* and tumorigenicity *in vivo* and progeny of both MIC$^-$ and MIC$^+$ cells regain heterogeneity of the bulk subpopulation.

6. Lack of HO-1 affects pigmentation of B16-F10 melanoma cells through decreased tyrosinase activity, independently of the expression of melanogenesis genes. At the same time HO-1 is dispensable for differentiation and pigmentation of melanocytes.

Altogether, our data points at the dual role of HO-1 in melanoma. As previous study of our group showed that overexpression of HO-1 increased aggressiveness of bulk B16-F10 cells in growing tumors[147], here we found that HO-1 might decrease a risk of melanoma initiation. We demonstrated that overexpression of HO-1 during clonal growth induction *in vitro* and *in vivo*

can play an anti-tumorigenic role. Our results draw a broader picture of melanoma therapy and suggest that pharmacological inhibitors of HO-1 in melanoma treatment might have a different effect on tumor growth than on tumor initiation.

7. Literature

1. Davis LE, Shalin SC, Tackett AJ. Current state of melanoma diagnosis and treatment. *Cancer Biol Ther*. 2019;20(11):1366-1379. doi:10.1080/15384047.2019.1640032
2. Garbe C, Amaral T, Peris K, et al. European consensus-based interdisciplinary guideline for melanoma. Part 1: Diagnostics – Update 2019. *Eur J Cancer*. 2020;126:141-158. doi:10.1016/j.ejca.2019.11.014
3. Mcclain SE, Mayo KB, Shada AL, Smolkin ME, Patterson JW, Slingluff CL. Amelanotic Melanomas Presenting as Red Skin Lesions: A Diagnostic Challenge with Potentially Lethal Consequences. *Int J Dermatol*. 2015;51(4):420-426. doi:10.1111/j.1365-4632.2011.05066.x.Amelanotic
4. Schadendorf D, Fisher DE, Garbe C, et al. Melanoma. *Nat Rev Dis Prim*. 2015;1(April):1-20. doi:10.1038/nrdp.2015.3
5. Matthews NH, Li W-Q, Qureshi AA, Weinstock MA, Cho E. *Epidemiology of Melanoma. In: Ward WH, Farma JM, Editors. Cutaneous Melanoma: Etiology and Therapy [Internet].*; 2017. doi:10.1038/nrendo.2010.189.Glycogen
6. Leonardi GC, Falzone L, Salemi R, et al. Cutaneous melanoma: From pathogenesis to therapy (Review). *Int J Oncol*. 2018;52(4):1071-1080. doi:10.3892/ijo.2018.4287
7. Lawrence MS, Stojanov P, Polak P, et al. Mutational heterogeneity in cancer and the search for new cancer-associated genes. *Nature*. 2013;499(7457):214-218. doi:10.1038/nature12213
8. Hodis E, Watson IR, Kryukov G V, et al. A Landscape of Driver Mutations in Melanoma. *Cell*. 2012;150(2):251-263. doi:10.1016/j.cell.2012.06.024.A
9. Amaral T, Sinnberg T, Meier F, et al. The mitogen-activated protein kinase pathway in melanoma part I – Activation and primary resistance mechanisms to BRAF inhibition. *Eur J Cancer*. 2017;73:85-92. doi:10.1016/j.ejca.2016.12.010
10. Rissmann R, Hessel MHM, Cohen AF. Vemurafenib/dabrafenib and trametinib. *Br J Clin Pharmacol*. 2015;80(4):765-767. doi:10.1111/bcp.12651
11. Uribe P, Wistuba II, González S. BRAF Mutation: A Frequent Event in Benign, Atypical, and Malignant Melanocytic Lesions of the Skin. *Am J Dermatopathol*. 2003;25(5):365-370.
12. Jakob JA, Bassett RL, Ng CS, et al. NRAS mutation status is an independent prognostic factor in metastatic melanoma. *Cancer*. 2012;118(16):4014-4023. doi:10.1002/cncr.26724
13. Kiuru M, Bausam KJ. The NF1 gene in tumor syndromes and melanoma. *Lab Investig*. 2016;97(2):146-157. doi:10.1016/j.physbeh.2017.03.040
14. Beadling C, Jacobson-Dunlop E, Hodi FS, et al. KIT gene mutations and copy number in melanoma subtypes. *Clin Cancer Res*. 2008;14(21):6821-6828. doi:10.1158/1078-0432.CCR-08-0575
15. Wu H, Goel V, Haluska FG. PTEN signaling pathways in melanoma. *Oncogene*. 2003;22(20):3113-3122. doi:10.1038/sj.onc.1206451
16. Davies MA. The Role of the PI3K-AKT Pathway in Melanoma. *Cancer J*. 2012;18(2):142-147.
17. Guarneri C, Bevelacqua V, Polesel J, et al. NF-κB inhibition is associated with OPN/MMP-9 downregulation in cutaneous melanoma. *Oncol Rep*. 2017;37(2):737-746. doi:10.3892/or.2017.5362
18. Sinnberg T, Levesque MP, Krochmann J, et al. Wnt-signaling enhances neural crest migration of melanoma cells and induces an invasive phenotype. *Mol Cancer*. 2018;17(1):1-19. doi:10.1186/s12943-018-0773-5
19. Hartman ML, Sztiller-Sikorska M, Czyz M. Whole-exome sequencing reveals novel genetic variants associated with diverse phenotypes of melanoma cells. *Mol Carcinog*. 2019;58(4):588-602. doi:doi:10.1002/mc.22953
20. Breslow A. Thickness, cross-sectional areas and depth of invasion in the prognosis of cutaneous melanoma. *Ann Surg*. 1970;172(5):902-908. doi:10.1097/00000658-197011000-00017
21. Howlader N, Noone A, Krapcho M, et al. *SEER Cancer Statistics Review, 1975-2016*.
22. Lee C, Collichio F, Ollila D, Moschos S. Historical review of melanoma treatment and outcomes. *Clin Dermatol*. 2013;31(2):141-147. doi:10.1016/j.clindermatol.2012.08.015
23. Eggermont AMM, Kirkwood JM. Re-evaluating the role of dacarbazine in metastatic melanoma: What have we learned in 30 years? *Eur J Cancer*. 2004;40(12):1825-1836. doi:10.1016/j.ejca.2004.04.030
24. Lugowska I, Teterycz P, Rutkowski P. Immunotherapy of Melanoma. *Contemp Oncol*. 2018;22(1A):61-

67. doi:10.1016/j.hoc.2006.02.005

25. Davies H, Bignell GR, Cox C, et al. Mutations of the BRAF gene in human cancer. *Nature*. 2002;417(6892):949-954. doi:10.1038/nature00766

26. Chapman PB, Hauschild A, Robert C, et al. Improved survival with vemurafenib in melanoma with BRAF V600E mutation. *N Engl J Med*. 2011;364(26):2507-2516. doi:10.1056/NEJMoa1103782

27. McArthur GA, Chapman PB, Robert C, et al. Safety and efficacy of vemurafenib in BRAF(V600E) and BRAF(V600K) mutation-positive melanoma (BRIM-3): extended follow-up of a phase 3, randomised, open-label study. *Lancet Oncol*. 2014;15(3):323-332. doi:10.1016/S1470-2045(14)70012-9

28. Kozar I, Margue C, Rothengatter S, Haan C, Kreis S. Many ways to resistance: How melanoma cells evade targeted therapies. *Biochim Biophys Acta - Rev Cancer*. 2019;1871(2):313-322. doi:10.1016/j.bbcan.2019.02.002

29. Callahan MK, Flaherty CR, Postow MA. Checkpoint Blockade for the Treatment of Advanced Melanoma. In: *Cancer Treatment and Research. Melanoma*. ; 2016:231-250.

30. Rowshanravan B, Halliday N, Sansom DM. CTLA-4: a moving target in immunotherapy. *Blood*. 2018;131(1):58-67. doi:10.1182/blood-2017-06-741033

31. Okazaki T, Honjo T. PD-1 and PD-1 ligands: From discovery to clinical application. *Int Immunol*. 2007;19(7):813-824. doi:10.1093/intimm/dxm057

32. Phan GQ, Rosenberg SA. Adoptive cell transfer for patients with metastatic melanoma: The potential and promise of cancer immunotherapy. *Cancer Control*. 2013;20(4):289-297. doi:10.1177/107327481302000406

33. Andor N, Graham TA, Jansen M, et al. Pan-cancer analysis of the extent and consequences of intra-tumor heterogeneity. *Nat Med*. 2016;22(1):105-113. doi:10.1038/nm.3984

34. Grzywa TM, Paskal W, Włodarski PK. Intratumor and Intertumor Heterogeneity in Melanoma. *Transl Oncol*. 2017;10(6):956-975. doi:10.1016/j.tranon.2017.09.007

35. Sensi M, Nicolini G, Petti C, et al. Mutually exclusive NRASQ61R and BRAFV600E mutations at the single-cell level in the same human melanoma. *Oncogene*. 2006;25(24):3357-3364. doi:10.1038/sj.onc.1209379

36. Lin J, Goto Y, Murata H, et al. Polyclonality of BRAF mutations in primary melanoma and the selection of mutant alleles during progression. *Br J Cancer*. 2011;104(3):464-468. doi:10.1038/sj.bjc.6606072

37. Colombino M, Capone M, Lissia A, et al. BRAF/NRAS Mutation Frequencies Among Primary Tumors and Metastases in Patients With Melanoma. *J Clin Oncol*. 2012;30(20):2522-2529. doi:10.1200/JCO.2011.41.2452

38. Yancovitz M, Litterman A, Yoon J, et al. Intra- and Inter-Tumor Heterogeneity of BRAFV600EMutations in Primary and Metastatic Melanoma. *PLoS One*. 2012;7(1):e29336. https://doi.org/10.1371/journal.pone.0029336.

39. Shannan B, Perego M, Somasundaram R, Herlyn M. Heterogeneity in Melanoma. In: *Cancer Treatment and Research. Melanoma*. ; 2016:1-16.

40. Arozarena I, Wellbrock C. Phenotype plasticity as enabler of melanoma progression and therapy resistance. *Nat Rev Cancer*. 2019;19(7):377-391. doi:10.1038/s41568-019-0154-4

41. Tirosh I, Izar B, Prakadan SM, et al. Dissecting the multicellular ecosystem of metastatic melanoma by single-cell RNA-seq. *Science (80-)*. 2016;352(6282):189-196. doi:10.1126/science.aad0501

42. Croteau W, Jenkins MH, Ye S, Mullins DW, Brinckerhoff CE. Differential mechanisms of tumor progression in clones from a single heterogeneous human melanoma. *J Cell Physiol*. 2013;228(4):773-780. doi:10.1002/jcp.24225

43. Seftor EA, Seftor REB, Weldon D, et al. Melanoma tumor cell heterogeneity: a molecular approach to study subpopulations expressing the embryonic morphogen nodal. *Semin Oncol*. 2014;41(2):259-266. doi:10.1053/j.seminoncol.2014.02.001

44. Cintra Lopes Carapeto F, Neves Comodo A, Germano A, et al. Marker Protein Expression Combined With Expression Heterogeneity is a Powerful Indicator of Malignancy in Acral Lentiginous Melanomas. *Am J Dermatopathol*. 2017;39(2):114-120. doi:10.1097/DAD.0000000000000635

45. Mirkina I, Hadzijusufovic E, Krepler C, et al. Phenotyping of Human Melanoma Cells Reveals a Unique Composition of Receptor Targets and a Subpopulation Co-Expressing ErbB4, EPO-R and NGF-R. *PLoS One*. 2014;9(1):e84417. https://doi.org/10.1371/journal.pone.0084417.

46. Botti G, Fratangelo F, Cerrone M, et al. COX-2 expression positively correlates with PD-L1 expression in human melanoma cells. *J Transl Med*. 2017;15(1):46. doi:10.1186/s12967-017-1150-7

47. Lenggenhager D, Curioni-Fontecedro A, Storz M, et al. An aggressive hypoxia related subpopulation of melanoma cells is TRP-2 negative. *Transl Oncol*. 2014;7(2):206-212. doi:10.1016/j.tranon.2014.02.018

48. Afify SM, Seno M. Conversion of stem cells to cancer stem cells: Undercurrent of cancer initiation. *Cancers (Basel)*. 2019;11(3):1-19. doi:10.3390/cancers11030345

49. Tirino V, Desiderio V, Paino F, et al. Cancer stem cells in solid tumors: An overview and new

approaches for their isolation and characterization. *FASEB J*. 2013;27(1):13-24. doi:10.1096/fj.12-218222

50.   Clarke MF, Dick JE, Dirks PB, et al. Cancer stem cells - perspectives on current status and future directions: AACR Workshop on cancer stem cells. *Cancer Res*. 2006;66(19):9339-9344. doi:10.1158/0008-5472.CAN-06-3126

51.   Schatton T, Frank MH. The in vitro spheroid melanoma cell culture assay: Cues on tumor initiation. *J Invest Dermatol*. 2010;130(7):1769-1771. doi:10.1038/jid.2010.135

52.   Clarke MF, Fuller M. Stem Cells and Cancer: Two Faces of Eve. *Cell*. 2006;124(6):1111-1115. doi:10.1016/j.cell.2006.03.011

53.   Friedmann-Morvinski D, Verma IM. Dedifferentiation and reprogramming: Origins of cancer stem cells. *EMBO Rep*. 2014;15(3):244-253. doi:10.1002/embr.201338254

54.   Mani SA, Guo W, Liao M-J, et al. The epithelial-mesenchymal transition generates cells with properties of stem cells. *Cell*. 2008;133(4):704-715. doi:10.1016/j.cell.2008.03.027

55.   Daley GQ. Common themes of dedifferentiation in somatic cell reprogramming and cancer. *Cold Spring Harb Symp Quant Biol*. 2008;73:171-174. doi:10.1101/sqb.2008.73.041

56.   Lapidot T, Sirard C, Vormoor J, et al. A cell initiating human acute myeloid leukaemia after transplantation into SCID mice. *Nature*. 1994;367:645-648. https://doi.org/10.1038/367645a0.

57.   Al-Hajj M, Wicha MS, Benito-Hernandez A, Morrison SJ, Clarke MF. Prospective identification of tumorigenic breast cancer cells. *Proc Natl Acad Sci U S A*. 2003;100(7):3983-3988. doi:10.1073/pnas.0530291100

58.   Fang D, Nguyen TK, Leishear K, et al. A tumorigenic subpopulation with stem cell properties in melanomas. *Cancer Res*. 2005;65(20):9328-9337. doi:10.1158/0008-5472.CAN-05-1343

59.   Singh SK, Clarke ID, Terasaki M, et al. Identification of a Cancer Stem Cell in Human Brain Tumors. *Cancer Res*. 2003;63(18):5821-5828. http://cancerres.aacrjournals.org/content/63/18/5821.abstract.

60.   Takaishi S, Okumura T, Tu S, et al. Identification of gastric cancer stem cells using the cell surface marker CD44. *Stem Cells*. 2009;27(5):1006-1020. doi:10.1002/stem.30

61.   Collins AT, Berry PA, Hyde C, Stower MJ, Maitland NJ. Prospective identification of tumorigenic prostate cancer stem cells. *Cancer Res*. 2005;65(23):10946-10951. doi:10.1158/0008-5472.CAN-05-2018

62.   Eramo A, Lotti F, Sette G, et al. Identification and expansion of the tumorigenic lung cancer stem cell population. *Cell Death Differ*. 2008;15(3):504-514. doi:10.1038/sj.cdd.4402283

63.   Tirino V, Desiderio V, Paino F, et al. Human primary bone sarcomas contain CD133+ cancer stem cells displaying high tumorigenicity in vivo. *FASEB*. 2011;25(6):2022-2030. doi:10.1096/fj.10-179036

64.   Bapat SA, Mali AM, Koppikar CB, Kurrey NK. Stem and progenitor-like cells contribute to the aggressive behavior of human epithelial ovarian cancer. *Cancer Res*. 2005;65(8):3025-3029. doi:10.1158/0008-5472.CAN-04-3931

65.   Rappa G, Fodstad O, Lorico A. The stem cell-associated antigen CD133 (Prominin-1) is a molecular therapeutic target for metastatic melanoma. *Stem Cells*. 2008;26(12):3008-3017. doi:10.1634/stemcells.2008-0601

66.   Clark DW, Palle K. Aldehyde dehydrogenases in cancer stem cells: Potential as therapeutic targets. *Ann Transl Med*. 2016;4(24):1-8. doi:10.21037/atm.2016.11.82

67.   Greve B, Kelsch R, Spaniol K, Eich HT, Götte M. Flow cytometry in cancer stem cell analysis and separation. *Cytom Part A*. 2012;81 A(4):284-293. doi:10.1002/cyto.a.22022

68.   Schlaak M, Schmidt P, Bangard C, Kurschat P, Mauch C, Abken H. Regression of metastatic melanoma by targeting cancer stem cells. *Oncotarget*. 2012;3(1):22-30. doi:10.18632/oncotarget.437

69.   Wagner SN, Somasundaram R, Pinc A, et al. CD20-immunotargeting of malignant melanoma. *J Clin Oncol*. 2010;28(15_suppl):8565. doi:10.1200/jco.2010.28.15_suppl.8565

70.   Frank NY, Margaryan A, Huang Y, et al. ABCB5-Mediated Doxorubicin Transport and Chemoresistance in Human Malignant Melanoma. *Cancer Res*. 2005;65(10):4320-4333. papers://5aa36326-f23d-4d75-b12e-bf93c65dd1bd/Paper/p934.

71.   Schatton T, Murphy GF, Frank NY, et al. Identification of cells initiating human melanomas. *Nature*. 2008;451(7176):345-349. doi:10.1038/nature06489

72.   Wilson BJ, Saab KR, Ma J, et al. ABCB5 maintains melanoma-initiating cells through a proinflammatory cytokine signaling circuit. *Cancer Res*. 2014;74(15):4196-4207. doi:10.1158/0008-5472.CAN-14-0582

73.   Wu C, Alman BA. Side population cells in human cancers. *Cancer Lett*. 2008;268(1):1-9. doi:10.1016/j.canlet.2008.03.048

74.   Wouters J, Stas M, Gremeaux L, et al. The human melanoma side population displays molecular and functional characteristics of enriched chemoresistance and tumorigenesis. *PLoS One*. 2013;8(10):e76550-e76550. doi:10.1371/journal.pone.0076550

75. Luo Y, Ellis LZ, Dallaglio K, et al. Side population cells from human melanoma tumors reveal diverse mechanisms for chemoresistance. *J Invest Dermatol*. 2012;132(10):2440-2450. doi:10.1038/jid.2012.161

76. Si X, Gao Z, Xu F, Zheng Y. SOX2 upregulates side population cells and enhances their chemoresistant ability by transactivating ABCC1 expression contributing to intrinsic resistance to paclitaxel in melanoma. *Mol Carcinog*. 2020;59(3):257-264. doi:10.1002/mc.23148

77. Monzani E, Facchetti F, Galmozzi E, et al. Melanoma contains CD133 and ABCG2 positive cells with enhanced tumourigenic potential. *Eur J Cancer*. 2007;43(5):935-946. doi:10.1016/j.ejca.2007.01.017

78. Rappa G, Fodstad O, Lorico A. The stem cell-associated antigen CD133 (Prominin-1) is a molecular therapeutic target for metastatic melanoma. *Stem Cells*. 2008;26(12):3008-3017. doi:10.1634/stemcells.2008-0601

79. Grasso C, Anaka M, Hofmann O, et al. Iterative sorting reveals CD133+ and CD133- melanoma cells as phenotypically distinct populations. *BMC Cancer*. 2016;16(1):726. doi:10.1186/s12885-016-2759-2

80. Madjd Z, Erfani E, Gheytanchi E, Moradi-Lakeh M, Shariftabrizi A, Asadi-Lari M. Expression of CD133 cancer stem cell marker in melanoma: a systematic review and meta-analysis. *Int J Biol Markers*. 2016;31(2):e118-25. doi:10.5301/jbm.5000209

81. Boiko AD, Razorenova OV, van de Rijn M, et al. Human melanoma-initiating cells express neural crest nerve growth factor receptor CD271. *Nature*. 2010;466(7302):133-137. doi:10.1038/nature09161

82. Civenni G, Walter A, Kobert N, et al. Human CD271-positive melanoma stem cells associated with metastasis establish tumor heterogeneity and long-term growth. *Cancer Res*. 2011;71(8):3098-3109. doi:10.1158/0008-5472.CAN-10-3997

83. Restivo G, Diener J, Cheng PF, et al. The low affinity neurotrophin receptor CD271 regulates phenotype switching in melanoma . *Nat Commun*. 2017;8(1):1988. doi:10.1038/s41467-017-01573-6

84. Radke J, Roßner F, Redmer T. CD271 determines migratory properties of melanoma cells. *Sci Rep*. 2017;7(1):9834. doi:10.1038/s41598-017-10129-z

85. Boyle SE, Fedele CG, Corbin V, et al. CD271 Expression on Patient Melanoma Cells Is Unstable and Unlinked to Tumorigenicity. *Cancer Res*. 2016;76(13):3965-3977. doi:10.1158/0008-5472.CAN-15-2377

86. Tomita H, Tanaka K, Tanaka T, Hara A. Aldehyde dehydrogenase 1A1 in stem cells and cancer. *Oncotarget*. 2016;7(10):11018-11032. doi:10.18632/oncotarget.6920

87. Luo Y, Dallaglio K, Chen Y, et al. ALDH1A isozymes are markers of human melanoma stem cells and potential therapeutic targets. *Stem Cells*. 2012;30(10):2100-2113. doi:10.1002/stem.1193

88. Prasmickaite L, Engesaeter BØ, Skrbo N, et al. Aldehyde dehydrogenase (ALDH) activity does not select for cells with enhanced aggressive properties in malignant melanoma. *PLoS One*. 2010;5(5):e10731. doi:10.1371/journal.pone.0010731

89. Taylor LA, Abraham RM, Tahirovic E, et al. High ALDH1 expression correlates with better prognosis in tumorigenic malignant melanoma. *Mod Pathol*. 2017;30(5):634-639. doi:10.1038/modpathol.2016.226

90. Nguyen N, Luo Y, Fujita M. Aldehyde dehydrogenase isozymes: Markers of cancer stem cells in human melanoma. *Expert Rev Dermatol*. 2013;8(2):111-113. doi:10.1586/edm.13.2

91. Moore N, Lyle S. Quiescent, slow-cycling stem cell populations in cancer: A review of the evidence and discussion of significance. *J Oncol*. 2011;2011(396076). doi:10.1155/2011/396076

92. Roesch A, Fukunaga-Kalabis M, Schmidt EC, et al. A temporarily distinct subpopulation of slow-cycling melanoma cells is required for continuous tumor growth. *Cell*. 2010;141(4):583-594. doi:10.1016/j.cell.2010.04.020

93. Puig I, Tenbaum SP, Chicote I, et al. TET2 controls chemoresistant slow-cycling cancer cell survival and tumor recurrence. *J Cinical Investig*. 2018;128(9):3887-3905. https://www.jci.org/articles/view/96393.

94. Perego M, Maurer M, Wang JX, et al. A slow-cycling subpopulation of melanoma cells with highly invasive properties. *Oncogene*. 2018;37(3):302-312. doi:10.1038/onc.2017.341

95. Quintana E, Shackleton M, Sabel MS, Fullen DR, Johnson TM, Morrison SJ. Efficient tumour formation by single human melanoma cells. *Nature*. 2008;456(7222):593-598. doi:10.1038/nature07567

96. Quintana E, Shackleton M, Foster HR, et al. Phenotypic heterogeneity among tumorigenic melanoma cells from patients that is reversible and not hierarchically organized. *Cancer Cell*. 2010;18(5):510-523. doi:10.1016/j.ccr.2010.10.012

97. Gupta PB, Chaffer CL, Weinberg RA. Cancer stem cells: Mirage or reality? *Nat Med*. 2009;15(9):1010-1012. doi:10.1038/nm0909-1010

98. Prasmickaite L, Skrbo N, Høifødt HK, et al. Human malignant melanoma harbours a large fraction of highly clonogenic cells that do not express markers associated with cancer stem cells. *Pigment Cell Melanoma Res*. 2010;23(3):449-451. doi:10.1111/j.1755-148X.2010.00690.x

99. Huang S-D, Yuan Y, Tang H, et al. Tumor cells positive and negative for the common cancer stem cell markers are capable of initiating tumor growth and generating both progenies. *PLoS One*. 2013;8(1):e54579. doi:10.1371/journal.pone.0054579

100. Girouard SD, Murphy GF. Melanoma stem cells: Not rare, but well done. *Lab Investig*. 2011;91(5):647-664. doi:10.1038/labinvest.2011.50

101. Kelly PN, Dakic A, Adams JM, Nutt SL, Strasser A. Tumor growth need not be driven by rare cancer stem cells. *Science (80-)*. 2007;317(5836):337. doi:10.1126/science.1142596

102. Held MA, Curley DP, Dankort D, McMahon M, Muthusamy V, Bosenberg MW. Characterization of melanoma cells capable of propagating tumors from a single cell. *Cancer Res*. 2010;70(1):388-397. doi:10.1158/0008-5472.CAN-09-2153

103. Shackleton M, Quintana E. Progress in understanding melanoma propagation. *Mol Oncol*. 2010;4(5):451-457. doi:10.1016/j.molonc.2010.06.006

104. Was H, Dulak J, Jozkowicz A. Heme oxygenase-1 in tumor biology and therapy. *Curr Drug Targets*. 2010;11(12):1551-1570. http://www.ncbi.nlm.nih.gov/pubmed/20704546.

105. Keyse SM, Tyrrell RM. Heme oxygenase is the major 32-kDa stress protein induced in human skin fibroblasts by UVA radiation, hydrogen peroxide, and sodium arsenite. *Proc Natl Acad Sci U S A*. 1989;86(1):99-103. doi:10.1073/pnas.86.1.99

106. Maines MD, Trakshel GM, Kutty RK. Characterization of two constitutive forms of rat liver microsomal heme oxygenase. Only one molecular species of the enzyme is inducible. *J Biol Chem*. 1986;261(1):411-419.

107. Alam J, Shibahara S, Smith A. Transcriptional activation of the heme oxygenase gene by heme and cadmium in mouse hepatoma cells. *J Biol Chem*. 1989;264(11):6371-6375.

108. Lin C-Y, Hsiao W-C, Huang C-J, Kao C-F, Hsu G-SW. Heme oxygenase-1 induction by the ROS-JNK pathway plays a role in aluminum-induced anemia. *J Inorg Biochem*. 2013;128:221-228. doi:10.1016/j.jinorgbio.2013.07.026

109. Prestera T, Talalay P, Alam J, Ahn YI, Lee PJ, Choi AM. Parallel induction of heme oxygenase-1 and chemoprotective phase 2 enzymes by electrophiles and antioxidants: regulation by upstream antioxidant-responsive elements (ARE). *Mol Med*. 1995;1(7):827-837. https://pubmed.ncbi.nlm.nih.gov/8612205.

110. Kuesap J, Na-Bangchang K. Possible role of heme oxygenase-1 and prostaglandins in the pathogenesis of cerebral malaria: heme oxygenase-1 induction by prostaglandin D(2) and metabolite by a human astrocyte cell line. *Korean J Parasitol*. 2010;48(1):15-21. doi:10.3347/kjp.2010.48.1.15

111. Motterlini R, Foresti R, Bassi R, Calabrese V, Clark JE, Green CJ. Endothelial heme oxygenase-1 induction by hypoxia. Modulation by inducible nitric-oxide synthase and S-nitrosothiols. *J Biol Chem*. 2000;275(18):13613-13620. doi:10.1074/jbc.275.18.13613

112. Terry CM, Clikeman JA, Hoidal JR, Callahan KS. TNF-alpha and IL-1alpha induce heme oxygenase-1 via protein kinase C, Ca2+, and phospholipase A2 in endothelial cells. *Am J Physiol*. 1999;276(5):H1493-501. doi:10.1152/ajpheart.1999.276.5.H1493

113. André M, Felley-Bosco E. Heme oxygenase-1 induction by endogenous nitric oxide: influence of intracellular glutathione. *FEBS Lett*. 2003;546(2-3):223-227. doi:10.1016/s0014-5793(03)00576-3

114. Rushworth SA, Chen X-L, Mackman N, Ogborne RM, O'Connell MA. Lipopolysaccharide-induced heme oxygenase-1 expression in human monocytic cells is mediated via Nrf2 and protein kinase C. *J Immunol*. 2005;175(7):4408-4415. doi:10.4049/jimmunol.175.7.4408

115. Lin Q, Weis S, Yang G, et al. Heme oxygenase-1 protein localizes to the nucleus and activates transcription factors important in oxidative stress. *J Biol Chem*. 2007;282(28):20621-20633. doi:10.1074/jbc.M607954200

116. Biswas C, Shah N, Muthu M, et al. Nuclear heme oxygenase-1 (HO-1) modulates subcellular distribution and activation of Nrf2, impacting metabolic and anti-oxidant defenses. *J Biol Chem*. 2014;289(39):26882-26894. doi:10.1074/jbc.M114.567685

117. Bansal S, Biswas G, Avadhani NG. Mitochondria-targeted heme oxygenase-1 induces oxidative stress and mitochondrial dysfunction in macrophages, kidney fibroblasts and in chronic alcohol hepatotoxicity. *Redox Biol*. 2014;2:273-283. doi:10.1016/j.redox.2013.07.004

118. Kim HP, Wang X, Galbiati F, Ryter SW, Choi AMK. Caveolae compartmentalization of heme oxygenase-1 in endothelial cells. *FASEB J*. 2004;18(10):1080-1089. doi:10.1096/fj.03-1391com

119. Nitti M, Piras S, Marinari UM, Moretta L, Pronzato MA, Furfaro AL. HO-1 induction in cancer progression: A matter of cell adaptation. *Antioxidants*. 2017;6(2):1-20. doi:10.3390/antiox6020029

120. Makino R, Obata Y, Tsubaki M, et al. Mechanistic Insights into the Activation of Soluble Guanylate Cyclase by Carbon Monoxide: A Multistep Mechanism Proposed for the BAY 41-2272 Induced Formation of 5-Coordinate CO–Heme. *Biochemistry*. 2018;57(10):1620-1631. doi:10.1021/acs.biochem.7b01240

121. Otterbein LE, Bach FH, Alam J, et al. Carbon monoxide has anti-inflammatory effects involving the mitogen-activated protein kinase pathway. *Nat Med*. 2000;6(4):422-428. doi:10.1038/74680

122. Zuckerbraun BS, Chin BY, Bilban M, et al. Carbon monoxide signals via inhibition of cytochrome c oxidase and generation of mitochondrial reactive oxygen species. *FASEB J*. 2007;21(4):1099-1106.

doi:10.1096/fj.06-6644com

123. MacGarvey NC, Suliman HB, Bartz RR, et al. Activation of mitochondrial biogenesis by heme oxygenase-1-mediated NF-E2-related factor-2 induction rescues mice from lethal Staphylococcus aureus sepsis. *Am J Respir Crit Care Med.* 2012;185(8):851-861. doi:10.1164/rccm.201106-1152OC

124. Piantadosi CA, Carraway MS, Babiker A, Suliman HB. Heme oxygenase-1 regulates cardiac mitochondrial biogenesis via Nrf2-mediated transcriptional control of nuclear respiratory factor-1. *Circ Res.* 2008;103(11):1232-1240. doi:10.1161/01.RES.0000338597.71702.ad

125. Vogel ME, Zucker SD. Bilirubin acts as an endogenous regulator of inflammation by disrupting adhesion molecule-mediated leukocyte migration. *Inflamm cell Signal.* 2016;3(1):e1178. doi:10.14800/ics.1178

126. Song S, Wang S, Ma J, et al. Biliverdin reductase/bilirubin mediates the anti-apoptotic effect of hypoxia in pulmonary arterial smooth muscle cells through ERK1/2 pathway. *Exp Cell Res.* 2013;319(13):1973-1987. doi:10.1016/j.yexcr.2013.05.015

127. Stocker R, Yamamoto Y, McDonagh AF, Glazer AN, Ames BN. Bilirubin is an antioxidant of possible physiological importance. *Science.* 1987;235(4792):1043-1046. doi:10.1126/science.3029864

128. Dudnik LB, Khrapova NG. Characterization of bilirubin inhibitory properties in free radical oxidation reactions. *Membr Cell Biol.* 1998;12(2):233-240.

129. Goodman AI, Choudhury M, da Silva JL, Schwartzman ML, Abraham NG. Overexpression of the heme oxygenase gene in renal cell carcinoma. *Proc Soc Exp Biol Med.* 1997;214(1):54-61. doi:10.3181/00379727-214-44069

130. Maines MD, Abrahamsson PA. Expression of heme oxygenase-1 (HSP32) in human prostate: normal, hyperplastic, and tumor tissue distribution. *Urology.* 1996;47(5):727-733. doi:10.1016/s0090-4295(96)00010-6

131. Miyake M, Ishii M, Kawashima K, et al. siRNA-mediated knockdown of the heme synthesis and degradation pathways: modulation of treatment effect of 5-aminolevulinic acid-based photodynamic therapy in urothelial cancer cell lines. *Photochem Photobiol.* 2009;85(4):1020-1027. doi:10.1111/j.1751-1097.2009.00543.x

132. Chau LY. Heme oxygenase-1: Emerging target of cancer therapy. *J Biomed Sci.* 2015;22(1):1-7. doi:10.1186/s12929-015-0128-0

133. Marinissen MJ, Tanos T, Bolós M, de Sagarra MR, Coso OA, Cuadrado A. Inhibition of heme oxygenase-1 interferes with the transforming activity of the Kaposi sarcoma herpesvirus-encoded G protein-coupled receptor. *J Biol Chem.* 2006;281(16):11332-11346. doi:10.1074/jbc.M512199200

134. Mayerhofer M, Florian S, Krauth M-T, et al. Identification of heme oxygenase-1 as a novel BCR/ABL-dependent survival factor in chronic myeloid leukemia. *Cancer Res.* 2004;64(9):3148-3154. doi:10.1158/0008-5472.can-03-1200

135. Ciesla M, Marona P, Kozakowska M, et al. Heme Oxygenase-1 Controls an HDAC4-miR-206 Pathway of Oxidative Stress in Rhabdomyosarcoma. *Cancer Reasearch.* 2016;206(15):5707-5719. doi:10.1158/0008-5472.CAN-15-1883

136. Podkalicka P, Mucha O, Józkowicz A, Dulak J, Łoboda A. Heme oxygenase inhibition in cancers: Possible tools and targets. *Wspolczesna Onkol.* 2017;2(1A):23-32. doi:10.5114/wo.2018.73879

137. Tsai J-R, Wang H-M, Liu P-L, et al. High expression of heme oxygenase-1 is associated with tumor invasiveness and poor clinical outcome in non-small cell lung cancer patients. *Cell Oncol (Dordr).* 2012;35(6):461-471. doi:10.1007/s13402-012-0105-5

138. Furfaro AL, Macay JRZ, Marengo B, et al. Resistance of neuroblastoma GI-ME-N cell line to glutathione depletion involves Nrf2 and heme oxygenase-1. *Free Radic Biol Med.* 2012;52(2):488-496. doi:10.1016/j.freeradbiomed.2011.11.007

139. Tan Q, Wang H, Hu Y, et al. Src/STAT3-dependent heme oxygenase-1 induction mediates chemoresistance of breast cancer cells to doxorubicin by promoting autophagy. *Cancer Sci.* 2015;106(8):1023-1032. doi:10.1111/cas.12712

140. Lv X, Song D, Niu Y, Wang B. Inhibition of heme oxygenase-1 enhances the chemosensitivity of laryngeal squamous cell cancer Hep-2 cells to cisplatin. *Apoptosis.* 2016;21(4):489-501. doi:10.1007/s10495-016-1216-7

141. Jeon W-K, Hong H-Y, Seo W-C, et al. Smad7 sensitizes A549 lung cancer cells to cisplatin-induced apoptosis through heme oxygenase-1 inhibition. *Biochem Biophys Res Commun.* 2012;420(2):288-292. doi:10.1016/j.bbrc.2012.02.151

142. Miyake M, Fujimoto K, Anai S, et al. Inhibition of heme oxygenase-1 enhances the cytotoxic effect of gemcitabine in urothelial cancer cells. *Anticancer Res.* 2010;30(6):2145-2152.

143. Liu Y-S, Li H-S, Qi D-F, et al. Zinc protoporphyrin IX enhances chemotherapeutic response of hepatoma cells to cisplatin. *World J Gastroenterol.* 2014;20(26):8572-8582. doi:10.3748/wjg.v20.i26.8572

144. Zhang W, Qiao T, Zha L. Inhibition of heme oxygenase-1 enhances the radiosensitivity in human nonsmall cell lung cancer a549 cells. *Cancer Biother Radiopharm*. 2011;26(5):639-645. doi:10.1089/cbr.2010.0939

145. Frank J, Lornejad-Schäfer MR, Schöffl H, Flaccus A, Lambert C, Biesalski HK. Inhibition of heme oxygenase-1 increases responsiveness of melanoma cells to ALA-based photodynamic therapy. *Int J Oncol*. 2007;31(6):1539-1545.

146. Berberat PO, Dambrauskas Z, Gulbinas A, et al. Inhibition of heme oxygenase-1 increases responsiveness of pancreatic cancer cells to anticancer treatment. *Clin Cancer Res*. 2005;11(10):3790-3798. doi:10.1158/1078-0432.CCR-04-2159

147. Was H, Cichon T, Smolarczyk R, et al. Overexpression of heme oxygenase-1 in murine melanoma: Increased proliferation and viability of tumor cells, decreased survival of mice. *Am J Pathol*. 2006;169(6):2181-2198. doi:10.2353/ajpath.2006.051365

148. Hsu F-F, Yeh C-T, Sun Y-J, et al. Signal peptide peptidase-mediated nuclear localization of heme oxygenase-1 promotes cancer cell proliferation and invasion independent of its enzymatic activity. *Oncogene*. 2015;34(18):2360-2370. doi:10.1038/onc.2014.166

149. Sacca P, Meiss R, Casas G, et al. Nuclear translocation of haeme oxygenase-1 is associated to prostate cancer. *Br J Cancer*. 2007;97(12):1683-1689. doi:10.1038/sj.bjc.6604081

150. Gandini NA, Fermento ME, Salomón DG, et al. Nuclear localization of heme oxygenase-1 is associated with tumor progression of head and neck squamous cell carcinomas. *Exp Mol Pathol*. 2012;93(2):237-245. doi:10.1016/j.yexmp.2012.05.001

151. Zou C, Zou C, Cheng W, et al. Heme oxygenase-1 retards hepatocellular carcinoma progression through the microRNA pathway. *Oncol Rep*. 2016;36(5):2715-2722. doi:10.3892/or.2016.5056

152. Tertil M, Golda S, Skrzypek K, et al. Nrf2-heme oxygenase-1 axis in mucoepidermoid carcinoma of the lung: Antitumoral effects associated with down-regulation of matrix metalloproteinases. *Free Radic Biol Med*. 2015;89:147-157. doi:10.1016/j.freeradbiomed.2015.08.004

153. Skrzypek K, Tertil M, Golda S, et al. Interplay between heme oxygenase-1 and miR-378 affects non-small cell lung carcinoma growth, vascularization, and metastasis. *Antioxid Redox Signal*. 2013;19(7):644-660. doi:10.1089/ars.2013.5184

154. Kozakowska M, Ciesla M, Stefanska A, et al. Heme oxygenase-1 inhibits myoblast differentiation by targeting myomirs. *Antioxid Redox Signal*. 2012;16(2):113-127. doi:10.1089/ars.2011.3964

155. Loboda A, Jazwa A, Grochot-przeczek A, et al. Heme Oxygenase-1 and the Vascular Bed : From Molecular Mechanisms to Therapeutic Opportunities. *Antioxid Redox Signal*. 2008;10(10):1767-1812. doi:10.1089/ars.2008.2043

156. Deshane J, Chen S, Caballero S, et al. Stromal cell-derived factor 1 promotes angiogenesis via a heme oxygenase 1-dependent mechanism. *J Exp Med*. 2007;204(3):605-618. doi:10.1084/jem.20061609

157. Sunamura M, Duda DG, Ghattas MH, et al. Heme oxygenase-1 accelerates tumor angiogenesis of human pancreatic cancer. *Angiogenesis*. 2003;6(1):15-24. doi:10.1023/a:1025803600840

158. Cheng C-C, Guan S-S, Yang H-J, et al. Blocking heme oxygenase-1 by zinc protoporphyrin reduces tumor hypoxia-mediated VEGF release and inhibits tumor angiogenesis as a potential therapeutic agent against colorectal cancer. *J Biomed Sci*. 2016;23:18. doi:10.1186/s12929-016-0219-6

159. Shang F, Hui L, An X, Zhang X, Guo S, Kui Z. ZnPPIX inhibits peritoneal metastasis of gastric cancer via its antiangiogenic activity. *Biomed Pharmacother*. 2015;71:240-246. doi:10.1016/j.biopha.2015.03.005

160. Hirai K, Sasahira T, Ohmori H, Fujii K, Kuniyasu H. Inhibition of heme oxygenase-1 by zinc protoporphyrin IX reduces tumor growth of LL/2 lung cancer in C57BL mice. *Int J cancer*. 2007;120(3):500-505. doi:10.1002/ijc.22287

161. Miyake M, Fujimoto K, Anai S, et al. Heme oxygenase-1 promotes angiogenesis in urothelial carcinoma of the urinary bladder. *Oncol Rep*. 2011;25(3):653-660. doi:10.3892/or.2010.1125

162. Ferrando M, Gueron G, Elguero B, et al. Heme oxygenase 1 (HO-1) challenges the angiogenic switch in prostate cancer. *Angiogenesis*. 2011;14(4):467-479. doi:10.1007/s10456-011-9230-4

163. Seo GS, Jiang W-Y, Chi JH, et al. Heme oxygenase-1 promotes tumor progression and metastasis of colorectal carcinoma cells by inhibiting antitumor immunity. *Oncotarget*. 2015;6(23):19792-19806. doi:10.18632/oncotarget.4075

164. Di Biase S, Lee C, Brandhorst S, et al. Fasting-Mimicking Diet Reduces HO-1 to Promote T Cell-Mediated Tumor Cytotoxicity. *Cancer Cell*. 2016;30(1):136-146. doi:10.1016/j.ccell.2016.06.005

165. Fest S, Soldati R, Christiansen NM, et al. Targeting of heme oxygenase-1 as a novel immune regulator of neuroblastoma. *Int J Cancer*. 2016;138(8):2030-2042. doi:10.1002/ijc.29933

166. Dey M, Chang AL, Wainwright DA, et al. Heme oxygenase-1 protects regulatory T cells from hypoxia-induced cellular stress in an experimental mouse brain tumor model. *J Neuroimmunol*. 2014;266(1-2):33-42. doi:10.1016/j.jneuroim.2013.10.012

167. Choi B-M, Pae H-O, Jeong Y-R, Kim Y-M, Chung H-T. Critical role of heme oxygenase-1 in Foxp3-mediated immune suppression. *Biochem Biophys Res Commun*. 2005;327(4):1066-1071. doi:10.1016/j.bbrc.2004.12.106

168. Wegiel B, Hedblom A, Li M, et al. Heme oxygenase-1 derived carbon monoxide permits maturation of myeloid cells. *Cell Death Dis*. 2014;5(3):e1139. doi:10.1038/cddis.2014.97

169. Wegiel B, Gallo D, Csizmadia E, et al. Carbon Monoxide Expedites Metabolic Exhaustion to Inhibit Tumor Growth. *Cancer Res*. 2013;73(23):7009 LP - 7021. doi:10.1158/0008-5472.CAN-13-1075

170. Pae H-O, Oh G-S, Choi B-M, et al. Carbon monoxide produced by heme oxygenase-1 suppresses T cell proliferation via inhibition of IL-2 production. *J Immunol*. 2004;172(8):4744-4751. doi:10.4049/jimmunol.172.8.4744

171. Arnold JN, Magiera L, Kraman M, Fearon DT. Tumoral Immune Suppression by Macrophages Expressing Fibroblast Activation Protein-α and Heme Oxygenase-1. *Cancer Immunol Res*. 2014;2(2):121 LP - 126. doi:10.1158/2326-6066.CIR-13-0150

172. Taha H, Skrzypek K, Guevara I, et al. Role of heme oxygenase-1 in human endothelial cells: lesson from the promoter allelic variants. *Arterioscler Thromb Vasc Biol*. 2010;30(8):1634-1641. doi:10.1161/ATVBAHA.110.207316

173. Okamoto I, Kr J, Endler G, et al. A microsatellite polymorphism in the heme oxygenase-1 gene promoter is associated with risk for melanoma. *Int J Cancer*. 2006;6(119):1312-1315. doi:10.1002/ijc.21937

174. Barbagallo I, Parenti R, Zappalà A, et al. Combined inhibition of Hsp90 and heme oxygenase-1 induces apoptosis and endoplasmic reticulum stress in melanoma. *Acta Histochem*. 2015;117(8):705-711. doi:10.1016/j.acthis.2015.09.005

175. Tampa M, Sarbu MI, Matei C, et al. Photodynamic therapy: A hot topic in dermato-oncology (Review). *Oncol Lett*. 2019;17(5):4085-4093. doi:10.3892/ol.2019.9939

176. Nowis D, Legat M, Grzela T, et al. Heme oxygenase-1 protects tumor cells against photodynamic therapy-mediated cytotoxicity. *Oncogene*. 2006;25(24):3365-3374. doi:10.1038/sj.onc.1209378

177. Ivanov VN, Hei TK. Regulation of apoptosis in human melanoma and neuroblastoma cells by statins , sodium arsenite and TRAIL : a role of combined treatment versus monotherapy. *Apoptosis*. 2011;16:1268-1284. doi:10.1007/s10495-011-0649-2

178. Ivanov VN, Hei TK. Arsenite sensitizes human melanomas to apoptosis via tumor necrosis factor alpha-mediated pathway. *J Biol Chem*. 2004;279(21):22747-22758. doi:10.1074/jbc.M314131200

179. Furfaro AL, Ottonello S, Loi G, et al. HO-1 downregulation favors BRAFV600 melanoma cell death induced by Vemurafenib/PLX4032 and increases NK recognition. *Int J Cancer*. 2020;146(7):1950-1962. doi:10.1002/ijc.32611

180. Wang T-Y, Liu C-L, Chen M-J, Lee J-J, Pun PC, Cheng S-P. Expression of haem oxygenase-1 correlates with tumour aggressiveness and BRAF V600E expression in thyroid cancer. *Histopathology*. 2015;66(3):447-456. doi:10.1111/his.12562

181. Liu L, Wu Y, Bian C, et al. Heme oxygenase 1 facilitates cell proliferation via the B-Raf-ERK signaling pathway in melanoma. *Cell Commun Signal*. 2019;17(3):1-12.

182. Kim DH, Yoon HJ, Cha YN, Surh YJ. Role of heme oxygenase-1 and its reaction product, carbon monoxide, in manifestation of breast cancer stem cell-like properties: Notch-1 as a putative target. *Free Radic Res*. 2018;52(11-12):1336-1347. doi:10.1080/10715762.2018.1473571

183. Herrmann H, Kneidinger M, Cerny-Reiterer S, et al. The Hsp32 Inhibitors SMA-ZnPP and PEG-ZnPP Exert Major Growth-Inhibitory Effects on D34+/CD38+ and CD34+/CD38- AML Progenitor Cells. *Curr Cancer Drug Targets*. 2012;12(1):51-63. doi:10.2174/156800912798888992

184. Wang W, Tabu K, Hagiya Y, et al. Enhancement of 5-aminolevulinic acid-based fluorescence detection of side population-defined glioma stem cells by iron chelation. *Sci Rep*. 2017;7(January):1-12. doi:10.1038/srep42070

185. Ding S, Li C, Cheng N, Cui X, Xu X, Zhou G. Redox regulation in cancer stem cells. *Oxid Med Cell Longev*. 2015;(750798):1-11.

186. Ogasawara MA, Zhang H. Redox regulation and Its emerging roles in stem cells and stem-like cancer cells. *Antioxidants Redox Signal*. 2009;11(5):1107-1122. doi:10.1089/ars.2008.2308

187. Kozakowska M, Szade K, Dulak J, Jozkowicz A. Role of heme oxygenase-1 in postnatal differentiation of stem cells: A possible cross-talk with MicroRNAs. *Antioxidants Redox Signal*. 2014;20(11):1827-1850. doi:10.1089/ars.2013.5341

188. Fraser ST, Midwinter RG, Coupland LA, et al. Heme oxygenase-1 deficiency alters erythroblastic island formation, steady-state erythropoiesis and red blood cell lifespan in mice. *Haematologica*. 2015;100(5):601-610. doi:10.3324/haematol.2014.116368

189. Watanabe-Matsui M, Muto A, Matsui T, et al. Heme regulates B-cell differentiation, antibody class switch, and heme oxygenase-1 expression in B cells as a ligand of Bach2. *Blood*. 2011;117(20):5438-5448. doi:10.1182/blood-2010-07-296483

190. Szade K, Zukowska M, Szade A, et al. Heme oxygenase-1 deficiency triggers exhaustion of hematopoietic stem cells. *EMBO Rep*. 2020;21(2):e47895. doi:10.15252/embr.201947895

191. Nowak WN, Taha H, Kachamakova-Trojanowska N, et al. Murine Bone Marrow Mesenchymal Stromal Cells Respond Efficiently to Oxidative Stress Despite the Low Level of Heme Oxygenases 1 and 2. *Antioxid Redox Signal*. 2018;29(2):111-127. doi:10.1089/ars.2017.7097

192. Liu N, Wang H, Han G, Cheng J, Hu W, Zhang J. Enhanced proliferation and differentiation of ho-1 gene-modified bone marrow-derived mesenchymal stem cells in the acute injured kidney. *Int J Mol Med*. 2018;42(2):946-956. doi:10.3892/ijmm.2018.3670

193. Barbagallo I, Vanella A, Peterson SJ, et al. Overexpression of heme oxygenase-1 increases human osteoblast stem cell differentiation. *J Bone Miner Metab*. 2010;28(3):276-288. doi:10.1007/s00774-009-0134-y

194. Stepniewski J, Pacholczak T, Skrzypczyk A, et al. Heme oxygenase-1 affects generation and spontaneous cardiac differentiation of induced pluripotent stem cells. *IUBMB Life*. 2018;70(2):129-142. doi:10.1002/iub.1711

195. Yamaguchi Y, Brenner M, Hearing VJ. The regulation of skin pigmentation. *J Biol Chem*. 2007;282(38):27557-27561. doi:10.1074/jbc.R700026200

196. D'Mello SAN, Finlay GJ, Baguley BC, Askarian-Amiri ME. Signaling pathways in melanogenesis. *Int J Mol Sci*. 2016;17(7):1-18. doi:10.3390/ijms17071144

197. Sitaram A, Marks MS. Mechanisms of protein delivery to melanosomes in pigment cells. *Physiol*. 2012;27(2):85-99. doi:10.1152/physiol.00043.2011

198. dos Santos Videra IF, Moura DFL, Magina S. Mechanisms regulating melanogenesis. *An Bras Dermatol*. 2013;88(1):76-83. doi:10.1007/978-3-642-45407-3_24

199. Millington GWM. Proopiomelanocortin (POMC): the cutaneous roles of its melanocortin products and receptors. *Clin Exp Dermatol*. 2006;31(3):407-412. doi:10.1111/j.1365-2230.2006.02128.x

200. Widlund HR, Fisher DE. Microphthalamia-associated transcription factor: A critical regulator of pigment cell development and survival. *Oncogene*. 2003;22(20):3035-3041. doi:10.1038/sj.onc.1206443

201. Hartman ML, Czyz M. MITF in melanoma : mechanisms behind its expression and activity. *Cell Mol Life Sci*. 2015;72:1249-1260. doi:10.1007/s00018-014-1791-0

202. Garraway LA, Widlund HR, Rubin MA, et al. Integrative genomic analyses identify MITF as a lineage survival oncogene amplified in malignant melanoma. *Nature*. 2005;436(7047):117-122. doi:10.1038/nature03664

203. Du J, Widlund HR, Horstmann MA, et al. Critical role of CDK2 for melanoma growth linked to its melanocyte-specific transcriptional regulation by MITF. *Cancer Cell*. 2004;6(6):565-576. doi:10.1016/j.ccr.2004.10.014

204. Carreira S, Goodall J, Aksan I, et al. Mitf cooperates with Rb1 and activates p21Cip1 expression to regulate cell cycle progression. *Nature*. 2005;433(7027):764-769. doi:10.1038/nature03269

205. McGill GG, Horstmann M, Widlund HR, et al. Bcl2 regulation by the melanocyte master regulator Mitf modulates lineage survival and melanoma cell viability. *Cell*. 2002;109(6):707-718. doi:10.1016/s0092-8674(02)00762-6

206. Buscà R, Berra E, Gaggioli C, et al. Hypoxia-inducible factor 1{alpha} is a new target of microphthalmia-associated transcription factor (MITF) in melanoma cells. *J Cell Biol*. 2005;170(1):49-59. doi:10.1083/jcb.200501067

207. McGill GG, Haq R, Nishimura EK, Fisher DE. c-Met expression is regulated by Mitf in the melanocyte lineage. *J Biol Chem*. 2006;281(15):10365-10373. doi:10.1074/jbc.M513094200

208. Kuzel P, Chien A. *The Role of Cellular Differentiation and Cell Fate in Malignant Melanoma. From: Research on Melanoma - A Glimpse into Current Directions and Future Trends*. IntechOpen; 2011. doi:DOI: 10.5772/20002

209. Brożyna AA, Jóźwicki W, Carlson JA, Slominski AT. Melanogenesis affects overall and disease-free survival in patients with stage III and IV melanoma. *Hum Pathol*. 2013;44(10):2071-2074. doi:https://doi.org/10.1016/j.humpath.2013.02.022

210. Brożyna AA, Jóźwicki W, Roszkowski K, Filipiak J, Slominski AT. Melanin content in melanoma metastases affects the outcome of radiotherapy. *Oncotarget*. 2016;7(14):17844-17853. doi:10.18632/oncotarget.7528

211. Takeuchi H, Kuo C, Morton DL, Wang HJ, Hoon DSB. Expression of Differentiation Melanoma-associated Antigen Genes Is Associated with Favorable Disease Outcome in Advanced-Stage Melanomas. *Cancer Res*. 2003;63(2):441-448. doi:10.1158/0008-5472.can-03-2440

212. Slingluff CLJ, Colella TA, Thompson L, et al. Melanomas with concordant loss of multiple melanocytic differentiation proteins: immune escape that may be overcome by targeting unique or undefined antigens. *Cancer Immunol Immunother*. 2000;48(12):661-672. doi:10.1007/s002620050015

213. Hoek KS, Schlegel NC, Brafford P, et al. Metastatic potential of melanomas defined by specific gene

expression profiles with no BRAF signature. *Pigment Cell Res*. 2006;19(4):290-302. doi:10.1111/j.1600-0749.2006.00322.x

214. Bittner M, Meltzer P, Chen Y, et al. Molecular classification of cutaneous malignant melanoma by gene expression profiling. *Nature*. 2000;406(6795):536-540. doi:10.1038/35020115

215. Ennen M, Keime C, Gambi G, et al. MITF-high and MITF-low cells and a novel subpopulation expressing genes of both cell states contribute to intra- and intertumoral heterogeneity of primary melanoma. *Clin Cancer Res*. 2017;23(22):7097-7107. doi:10.1158/1078-0432.CCR-17-0010

216. Bennett DC. Differentiation in mouse melanoma cells: Initial reversibility and an on-off stochastic model. *Cell*. 1983;34(2):445-453. doi:10.1016/0092-8674(83)90378-1

217. Pinner S, Jordan P, Sharrock K, et al. Intravital imaging reveals transient changes in pigment production and Brn2 expression during metastatic melanoma dissemination. *Cancer Res*. 2009;69(20):7969-7977. doi:10.1158/0008-5472.CAN-09-0781

218. Sáez-Ayala M, Montenegro MF, Sánchez-del-Campo L, et al. Directed Phenotype Switching as an Effective Antimelanoma Strategy. *Cancer Cell*. 2013;24(1):105-119. doi:10.1016/j.ccr.2013.05.009

219. Elassiuty YE, Klarquist J, Speiser J, et al. Heme oxygenase-1 expression protects melanocytes from stress-induced cell death: Implications for vitiligo. *Exp Dermatol*. 2011;20(6):496-501. doi:10.1111/j.1600-0625.2010.01232.x

220. Marrot L, Belai J, Jones C, Perez P, Meunier J, Recherche LO. Molecular Responses to Stress Induced in Normal Human Caucasian Melanocytes in Culture by Exposure to Simulated Solar UV. *Photochem Photobiol*. 2005;81:367-375.

221. Jian Z, Li K, Liu L, et al. Heme oxygenase-1 protects human melanocytes from H2O2-induced oxidative stress via the Nrf2-ARE pathway. *J Invest Dermatol*. 2011;131(7):1420-1427. doi:10.1038/jid.2011.56

222. Lim H, Jin S, Yun SJ. Modulation of Melanogenesis by Heme Oxygenase-1 via p53 in Normal Human Melanocytes. *Chonnam Med J*. 2016;52:45-52.

223. Kim JY, Lee H, Lee EJ, et al. Keap1 knockdown in melanocytes induces cell proliferation and survival via HO-1-associated β-catenin signaling. *J Dermatol Sci*. 2017;88(1):85-95. doi:10.1016/j.jdermsci.2017.05.007

224. Suzuki M, Otsuki A, Keleku-Lukwete N, Yamamoto M. Overview of redox regulation by Keap1–Nrf2 system in toxicology and cancer. *Curr Opin Toxicol*. 2016;1:29-36. doi:https://doi.org/10.1016/j.cotox.2016.10.001

225. Mou K, Pan W, Han D, et al. Glycyrrhizin protects human melanocytes from H2O2-induced oxidative damage via the Nrf2-dependent induction of HO-1. *Int J Mol Med*. 2019;44(1):253-261. doi:10.3892/ijmm.2019.4200

226. Hu Y, Huang J, Li Y, et al. Cistanche deserticola polysaccharide induces melanogenesis in melanocytes and reduces oxidative stress via activating NRF2/HO-1 pathway. *J Cell Mol Med*. 2020;24(January):4023-4035. doi:10.1111/jcmm.15038

227. Suo D, Zeng S, Zhang J, Meng L, Weng L. PM2.5 induces apoptosis, oxidative stress injury and melanin metabolic disorder in human melanocytes. *Exp Ther Med*. 2020;19:3227-3238. doi:10.3892/etm.2020.8590

228. Stecca B, Santini R, Pandolfi S, Penachioni J. Culture and isolation of melanoma-initiating cells. *Curr Protoc Stem Cell Biol*. 2013;24:3.6.1-3.6.12. doi:10.1002/9780470151808.sc0306s24

229. Szade K, Zukowska M, Szade A, et al. Spheroid-plug model as a tool to study tumor development, angiogenesis, and heterogeneity in vivo. *Tumor Biol*. 2016;37(2):2481-2496. doi:10.1007/s13277-015-4065-z

230. Foresti R, Clark JE, Green CJ, Motterlini R. Thiol Compounds Interact with Nitric Oxide in Regulating Heme Oxygenase-1 Induction in Endothelial Cells. *J Biol Chem*. 1997;272(29):18411-18417.

231. Mucha O, Podkalicka P, Czarnek M, et al. Pharmacological versus genetic inhibition of heme oxygenase-1 - The comparison of metalloporphyrins, shRNA and CRISPR/Cas9 system. *Acta Biochim Pol*. 2018;65(2):277-286. doi:10.18388/abp.2017_2542

232. Zhu H, Guo ZK, Jiang XX, et al. A protocol for isolation and culture of mesenchymal stem cells from mouse compact bone. *Nat Protoc*. 2010;5(3):550-560. doi:10.1038/nprot.2009.238

233. Sommer CA, Stadtfeld M, Murphy GJ, Hochedlinger K, Kotton DN, Mostoslavsky G. Induced Pluripotent Stem Cell Generation Using a Single Lentiviral Stem Cell Cassette. *Stem Cells*. 2009;27(3):543-549. doi:10.1634/stemcells.2008-1075

234. Stepniewski J, Ogrocki D, Szopa M, et al. Induced pluripotent stem cells as a model for diabetes investigation. *Sci Rep*. 2015;5(8597):1-14. doi:10.1038/srep08597

235. Kang NY, Yun SW, Ha HH, Park SJ, Chang YT. Embryonic and induced pluripotent stem cell staining and sorting with the live-cell fluorescence imaging probe CDy1. *Nat Protoc*. 2011;6(7):1044-1052. doi:10.1038/nprot.2011.350

236. Yang R, Jiang M, Kumar SM, et al. Generation of Melanocytes from Induced Pluripotent Stem Cells. *J*

Invest Dermatol. 2011;131(12):2458-2466. doi:10.1038/jid.2011.242

237. Refaeli Y, Bhoumik A, Roop DR, Ronai Z a. Melanoma-initiating cells: a compass needed. *EMBO Rep*. 2009;10(9):965-972. doi:10.1038/embor.2009.184

238. Widmer DS, Hoek KS, Cheng PF, et al. Hypoxia Contributes to Melanoma Heterogeneity by Triggering HIF1α-Dependent Phenotype Switching. *J Invest Dermatol*. 2013;133(10):2436-2443. doi:https://doi.org/10.1038/jid.2013.115

239. Pitcovski J, Shahar E, Aizenshtein E, Gorodetsky R. Melanoma antigens and related immunological markers. *Crit Rev Oncol Hematol*. 2017;115:36-49. doi:10.1016/j.critrevonc.2017.05.001

240. Franco SS, Szczesna K, Iliou MS, et al. In vitro models of cancer stem cells and clinical applications. *BMC Cancer*. 2016;16(Suppl 2). doi:10.1186/s12885-016-2774-3

241. Reya T, Morrison SJ, Clarke MF, Weissman IL. Stem cells, cancer, and cancer stem cells. *Nature*. 2001;414(6859):105-111. doi:10.1038/35102167

242. Hu Y, Smyth GK. ELDA: Extreme limiting dilution analysis for comparing depleted and enriched populations in stem cell and other assays. *J Immunol Methods*. 2009;347(1-2):70-78. doi:10.1016/j.jim.2009.06.008

243. Girotti MR, Fernández M, López JA, et al. SPARC promotes cathepsin B-mediated melanoma invasiveness through a collagen i/α2B1 integrin axis. *J Invest Dermatol*. 2011;131(12):2438-2447. doi:10.1038/jid.2011.239

244. Botti G, Scognamiglio G, Marra L, et al. SPARC/osteonectin is involved in metastatic process to the lung during melanoma progression. *Virchows Arch*. 2014;465(3):331-338. doi:10.1007/s00428-014-1616-4

245. Alison MR, Lim SML, Nicholson LJ. Cancer stem cells: problems for therapy? *J Pathol*. 2011;223(2):148-162. doi:10.1002/path.2793

246. Boonyaratanakornkit JB, Yue L, Strachan LR, et al. Selection of Tumorigenic Melanoma Cells Using ALDH. *J Invest Dermatol*. 2010;130(12):2799-2808. doi:10.1038/jid.2010.237.Selection

247. Yue L, Huang ZM, Fong S, et al. Targeting ALDH1 to decrease tumorigenicity, growth and metastasis of human melanoma. *Melanoma Res*. 2015;25(2):138-148. doi:10.1097/CMR.0000000000000144

248. Ge H, Luo H. Overview of advances in vasculogenic mimicry-a potential target for tumor therapy. *Cancer Manag Res*. 2018;10:2429-2437. doi:10.2147/CMAR.S164675

249. Frank NY, Schatton T, Kim S, et al. VEGFR-1 expressed by malignant melanoma-initiating cells is required for tumor growth. *Cancer Res*. 2011;71(4):1474-1485. doi:10.1158/0008-5472.CAN-10-1660

250. Hendrix MJC, Seftor EA, Meltzer PS, et al. Expression and functional significance of VE-cadherin in aggressive human melanoma cells: Role in vasculogenic mimicry. *Proc Natl Acad Sci U S A*. 2001;98(14):8018-8023. doi:10.1073/pnas.131209798

251. Shirakawa K, Kobayashi H, Heike Y, et al. Hemodynamics in vasculogenic mimicry and angiogenesis of inflammatory breast cancer xenograft. *Cancer Res*. 2002;62(2):560-566.

252. Francescone RA, Faibish M, Shao R. A matrigel-based tube formation assay to assess the vasculogenic activity of tumor cells. *J Vis Exp*. 2011;(55):2-5. doi:10.3791/3040

253. Kamdje AHN, Kamga PT, Simo RT, et al. Mesenchymal stromal cells' role in tumor microenvironment: involvement of signalling pathways. *Cancer Biol Med*. 2017;14(2):129-141. doi:10.20892/j.issn.2095-3941.2016.0033

254. Vartanian A, Karshieva S, Dombrovsky V, Belyavsky A. Melanoma educates mesenchymal stromal cells towards vasculogenic mimicry. *Oncol Lett*. 2016;11(6):4264-4268. doi:10.3892/ol.2016.4523

255. Nakatsu MN, Davis J, Hughes CCW. Optimized fibrin gel bead assay for the study of angiogenesis. *J Vis Exp*. 2007;(3):2-3. doi:10.3791/186

256. Kim DS, Park SH, Park KC. Transforming growth factor-β1 decreases melanin synthesis via delayed extracellular signal-regulated kinase activation. *Int J Biochem Cell Biol*. 2004;36(8):1482-1491. doi:10.1016/j.biocel.2003.10.023

257. Chang TS. An updated review of tyrosinase inhibitors. *Int J Mol Sci*. 2009;10(6):2440-2475. doi:10.3390/ijms10062440

258. Prezioso JA, Wang N, Duty L, Bloomer WD, Gorelik E. Enhancement of pulmonary metastasis formation and gamma-glutamyltranspeptidase activity in B16 melanoma induced by differentiation in vitro. *Clin Exp Metastasis*. 1993;11(3):263-274. doi:10.1007/bf00121169

259. Meira WV, Heinrich TA, Cadena SMSC, Martinez GR. Melanogenesis inhibits respiration in B16-F10 melanoma cells whereas enhances mitochondrial cell content. *Exp Cell Res*. 2017;350(1):62-72. doi:https://doi.org/10.1016/j.yexcr.2016.11.006

260. Kalainayakan SP, FitzGerald KE, Konduri PC, Vidal C, Zhang L. Essential roles of mitochondrial and heme function in lung cancer bioenergetics and tumorigenesis. *Cell Biosci*. 2018;8(1):56. doi:10.1186/s13578-018-0257-8

261. Almeida AS, Figueiredo-Pereira C, Vieira HLA. Carbon monoxide and mitochondria-modulation of cell

metabolism, redox response and cell death. *Front Physiol*. 2015;6:33. doi:10.3389/fphys.2015.00033

262. Bennett DC, Cooper PJ, Hart IR. A line of non-tumorigenic mouse melanocytes, syngeneic with the B16 melanoma and requiring a tumour promoter for growth. *Int J Cancer*. 1987;39(3):414-418. doi:10.1002/ijc.2910390324

263. Alvarez E. B16 Murine Melanoma. In: *Tumor Models in Cancer Research*. ; 2002:73-89. doi:10.1007/978-1-59259-100-8

264. Fidler IJ. Selection of Successive Tumour Lines for Metastasis. *Nat New Biol*. 1973;242(118):148-149. doi:10.1038/newbio242148a0

265. Zhao F, He X, Sun J, et al. Cancer stem cell vaccine expressing ESAT-6-gpi and IL-21 inhibits melanoma growth and metastases. *Am J Transl Res*. 2015;7(10):1870-1882.

266. Park SY, Lee DG, Jo A, et al. Extracellular Microenvironmental Change by B16F10 Melanoma-derived Proteins Induces Cancer Stem-like Cell Properties from NIH3T3 Cells. *Sci Rep*. 2019;9(1):1-10. doi:10.1038/s41598-019-53326-8

267. Najafi M, Farhood B, Mortezaee K, Kharazinejad E, Majidpoor J, Ahadi R. Hypoxia in solid tumors: a key promoter of cancer stem cell (CSC) resistance. *J Cancer Res Clin Oncol*. 2020;146(1):19-31. doi:10.1007/s00432-019-03080-1

268. Osrodek M, Hartman ML, Czyz M. Physiologically relevant oxygen concentration (6% o2) as an important component of the microenvironment impacting melanoma phenotype and melanoma response to targeted therapeutics in vitro. *Int J Mol Sci*. 2019;20(17). doi:10.3390/ijms20174203

269. Kuch V, Schreiber C, Thiele W, Umansky V, Sleeman JP. Tumor-initiating properties of breast cancer and melanoma cells in vivo are not invariably reflected by spheroid formation in vitro, but can be increased by long-term culturing as adherent monolayers. *Int J Cancer*. 2013;132(3):94-105. doi:10.1002/ijc.27785

270. Tang M-R, Guo J, Wang D, Xu N. Identification of CD24 as a marker for tumorigenesis of melanoma. *Onco Targets Ther*. 2018;11:3401-3406.

271. Klimkiewicz K, Weglarczyk K, Collet G, et al. A 3D model of tumour angiogenic microenvironment to monitor hypoxia effects on cell interactions and cancer stem cell selection. *Cancer Lett*. 2017;396:10-20. doi:10.1016/j.canlet.2017.03.006

272. Sztiller-Sikorska M, Hartman ML, Talar B, Jakubowska J, Zalesna I, Czyz M. Phenotypic diversity of patient-derived melanoma populations in stem cell medium. *Lab Investig*. 2015;95(6):672-683. doi:10.1038/labinvest.2015.48

273. Cheli Y, Guiliano S, Botton T, et al. Mitf is the key molecular switch between mouse or human melanoma initiating cells and their differentiated progeny. *Oncogene*. 2011;30(20):2307-2318. doi:10.1038/onc.2010.598

274. Ahn A, Chatterjee A, Eccles MR. The Slow Cycling Phenotype: A Growing Problem for Treatment Resistance in Melanoma. *Mol Cancer Ther*. 2017;16(6):1002-1009. doi:10.1158/1535-7163.MCT-16-0535

275. Moore N, Houghton J, Lyle S. Slow-Cycling Therapy-Resistant Cancer Cells. *Stem Cells Dev*. 2012;21(10):1822-1830. doi:10.1089/scd.2011.0477

276. Richichi C, Brescia P, Alberizzi, V, Fornasari L, Pelicci G. Marker-independent Method for Isolating Slow-Dividing Cancer Stem Cells in Human Glioblastoma. *Neoplasia*. 2013;15(7):840-847. doi:10.1593/neo.13662

277. Dembinski JL, Krauss S. Characterization and functional analysis of a slow cycling stem cell-like subpopulation in pancreas adenocarcinoma. *Clin Exp Metastasis*. 2009;26(7):611-623. doi:10.1007/s10585-009-9260-0

278. Cheli Y, Bonnazi VF, Jacquel A, et al. CD271 is an imperfect marker for melanoma initiating cells. *Oncotarget*. 2014;5(14):5272-5283. doi:10.18632/oncotarget.1967

279. Haass NK, Beaumont KA, Hill DS, et al. Real-time cell cycle imaging during melanoma growth, invasion, and drug response. *Pigment Cell Melanoma Res*. 2014;27(5):764-776. doi:10.1111/pcmr.12274

280. Santini R, Vinci MC, Pandolfi S, et al. HEDGEHOG-GLI signaling drives self-renewal and tumorigenicity of human melanoma-initiating cells. *Stem Cells*. 2012;30(9):1808-1818. doi:10.1002/stem.1160

281. Jasmer KJ, Hou J, Mannino P, Cheng J, Hannink M. Heme Oxygenase Promotes B-Raf-dependent Melanosphere Formation. *Pigment Cell Melanoma Res*. 2020;n/a(n/a). doi:10.1111/pcmr.12905

282. Shin CH, Ryu S, Kim HH. hnRNPK-regulated PTOV1-AS1 modulates heme oxygenase-1 expression via miR-1207-5p. *BMB Rep*. 2017;50(4):220-225. doi:10.5483/bmbrep.2017.50.4.024

283. Yang P-S, Hsu Y-C, Lee J-J, Chen M-J, Huang S-Y, Cheng S-P. Heme Oxygenase-1 Inhibitors Induce Cell Cycle Arrest and Suppress Tumor Growth in Thyroid Cancer Cells. *Int J Mol Sci*. 2018;19(9):2502. doi:10.3390/ijms19092502

284. Podkalicka P, Mucha O, Kruczek S, et al. Synthetically Lethal Interactions of Heme Oxygenase-1 and

Fumarate Hydratase Genes. *Biomolecules*. 2020;10(1). doi:10.3390/biom10010143

285. Mucha O, Podkalicka P, Mikulski M, et al. Development and characterization of a new inhibitor of heme oxygenase activity for cancer treatment. *Arch Biochem Biophys*. 2019;671:130-142. doi:10.1016/j.abb.2019.07.002

286. Sztiller-Sikorska M, Koprowska K, Jakubowska J, et al. Sphere formation and self-renewal capacity of melanoma cells is affected by the microenvironment. *Melanoma Res*. 2012;22(3):215-224. doi:10.1097/CMR.0b013e3283531317

287. Perego M, Tortoreto M, Tragni G, et al. Heterogeneous phenotype of human melanoma cells with in vitro and in vivo features of tumor-initiating cells. *J Invest Dermatol*. 2010;130(7):1877-1886. doi:10.1038/jid.2010.69

288. Abbaszadegan MR, Bagheri V, Razavi MS, Momtazi AA, Sahebkar A, Gholamin M. Isolation, identification, and characterization of cancer stem cells: A review. *J Cell Physiol*. 2017;232(8):2008-2018. doi:10.1002/jcp.25759

289. Barikbin R, Berkhout L, Bolik J, et al. Early heme oxygenase 1 induction delays tumour initiation and enhances DNA damage repair in liver macrophages of Mdr2−/− mice. *Sci Rep*. 2018;8(1):16238. doi:10.1038/s41598-018-33233-0

290. Was H, Sokolowska M, Sierpniowska A, et al. Effects of heme oxygenase-1 on induction and development of chemically induced squamous cell carcinoma in mice. *Free Radic Biol Med*. 2011;51(9):1717-1726. doi:10.1016/j.freeradbiomed.2011.07.025

291. Chen X, Zhang Z, Yang S, Chen H, Wang D, Li J. All-trans retinoic acid-encapsulated, CD20 antibody-conjugated poly(lactic-co-glycolic acid) nanoparticles effectively target and eliminate melanoma-initiating cells in vitro. *Onco Targets Ther*. 2018;11:6177-6187. doi:10.2147/OTT.S169957

292. Flahaut M, Jauquier N, Chevalier N, et al. Aldehyde dehydrogenase activity plays a Key role in the aggressive phenotype of neuroblastoma. *BMC Cancer*. 2016;16(1):781. doi:10.1186/s12885-016-2820-1

293. Shao C, Sullivan JP, Girard L, et al. Essential role of aldehyde dehydrogenase 1A3 for the maintenance of non-small cell lung cancer stem cells is associated with the STAT3 pathway. *Clin Cancer Res*. 2014;20(15):4154-4166. doi:10.1158/1078-0432.CCR-13-3292

294. Awad O, Yustein JT, Shah P, et al. High ALDH Activity Identifies Chemotherapy-Resistant Ewing's Sarcoma Stem Cells That Retain Sensitivity to EWS-FLI1 Inhibition. *PLoS One*. 2010;5(11):e13943. https://doi.org/10.1371/journal.pone.0013943.

295. Phelps EB. A Method of Calculating the Numbers of B. Coli from the Results of Dilution Tests. *Am J Public Hygiene*. 1908;18(2):141-145.

296. Pathania R, Ramachandran S, Elangovan S, et al. DNMT1 is essential for mammary and cancer stem cell maintenance and tumorigenesis. *Nat Commun*. 2015;6:6910. doi:10.1038/ncomms7910

297. Choi DS, Blanco E, Kim Y-S, et al. Chloroquine eliminates cancer stem cells through deregulation of Jak2 and DNMT1. *Stem Cells*. 2014;32(9):2309-2323. doi:10.1002/stem.1746

298. Maric H, Supic G, Kandolf-Sekulovic L, et al. DNMT1 and DNMT3B genetic polymorphisms affect the clinical course and outcome of melanoma patients. *Melanoma Res*. 2019;29(6):596-602. doi:10.1097/CMR.0000000000000612

299. Micevic G, Theodosakis N, Bosenberg M. Aberrant DNA methylation in melanoma: biomarker and therapeutic opportunities. *Clin Epigenetics*. 2017;9(1):34. doi:10.1186/s13148-017-0332-8

300. Venkatesh V, Nataraj R, Thangaraj GS, et al. Targeting Notch signalling pathway of cancer stem cells. *Stem cell Investig*. 2018;5:5. doi:10.21037/sci.2018.02.02

301. Müller CSL. Notch Signaling and Malignant Melanoma. In: Reichrath J, Reichrath S, eds. *Notch Signaling in Embryology and Cancer*. New York, NY: Springer US; 2012:258-264. doi:10.1007/978-1-4614-0899-4_19

302. Huynh C, Poliseno L, Segura MF, et al. The novel gamma secretase inhibitor RO4929097 reduces the tumor initiating potential of melanoma. *PLoS One*. 2011;6(9):e25264. doi:10.1371/journal.pone.0025264

303. Wang R, Li Y, Tsung A, et al. iNOS promotes CD24(+)CD133(+) liver cancer stem cell phenotype through a TACE/ADAM17-dependent Notch signaling pathway. *Proc Natl Acad Sci U S A*. 2018;115(43):E10127-E10136. doi:10.1073/pnas.1722100115

304. Zheng M, Ekmekcioglu S, Walch ET, Tang C-H, Grimm EA. Inhibition of nuclear factor-kappaB and nitric oxide by curcumin induces G2/M cell cycle arrest and apoptosis in human melanoma cells. *Melanoma Res*. 2004;14(3):165-171. doi:10.1097/01.cmr.0000129374.76399.19

305. Webster MR, Xu M, Kinzler KA, et al. Wnt5A promotes an adaptive, senescent-like stress response, while continuing to drive invasion in melanoma cells. *Pigment Cell Melanoma Res*. 2015;28(2):184-195. doi:10.1111/pcmr.12330

306. Zbytek B, Carlson JA, Granese J, Ross J, Mihm Jr MC, Slominski A. Current concepts of metastasis in melanoma. *Expert Rev Dermatol*. 2008;3(5):569-585. doi:10.1586/17469872.3.5.569

307. Clarke MF, Dick JE, Dirks PB, et al. Cancer stem cells--perspectives on current status and future directions: AACR Workshop on cancer stem cells. *Cancer Res*. 2006;66(19):9339-9344. doi:10.1158/0008-5472.CAN-06-3126

308. Nguyen N, Couts KL, Luo Y, Fujita M. Understanding melanoma stem cells. *Melanoma Manag*. 2015;2(2):179-188. doi:10.2217/mmt.15.4

309. Schmidt P, Kopecky C, Hombach A, Zigrino P, Mauch C, Abken H. Eradication of melanomas by targeted elimination of a minor subset of tumor cells. *PNAS*. 2011;108(6):2474-2479. doi:10.1073/pnas.1009069108/-/DCSupplemental.www.pnas.org/cgi/doi/10.1073/pnas.1009069108

310. Cordaro FG, De Presbiteris AL, Camerlingo R, et al. Phenotype characterization of human melanoma cells resistant to dabrafenib. *Oncol Rep*. 2017;38(5):2741-2751. doi:10.3892/or.2017.5963

311. Zeng Y, Yu Z, He Y, et al. Salinomycin-loaded lipid-polymer nanoparticles with anti-CD20 aptamers selectively suppress human CD20+ melanoma stem cells. *Acta Pharmacol Sin*. 2018;39(2):261-274. doi:10.1038/aps.2017.166

312. Pinc A, Somasundaram R, Wagner C, et al. Targeting CD20 in melanoma patients at high risk of disease recurrence. *Mol Ther*. 2012;20(5):1056-1062. doi:10.1038/mt.2012.27

313. Luo Y, Dallaglio K, Chen Y, et al. ALDH1A isozymes are markers of human melanoma stem cells and potential therapeutic targets. *Stem Cells*. 2012;30:2100-2113. doi:10.1002/stem.1193

314. Moroishi T, Hayashi T, Pan W-W, et al. The Hippo Pathway Kinases LATS1/2 Suppress Cancer Immunity. *Cell*. 2016;167(6):1525-1539.e17. doi:10.1016/j.cell.2016.11.005

315. Kulesza DW, Przanowski P, Kaminska B. Knockdown of STAT3 targets a subpopulation of invasive melanoma stem-like cells. *Cell Biol Int*. 2019;43(6):613-622. doi:10.1002/cbin.11134

316. Donizy P, Pagacz K, Marczuk J, et al. Upregulation of FOXP1 is a new independent unfavorable prognosticator and a specific predictor of lymphatic dissemination in cutaneous melanoma patients. *Onco Targets Ther*. 2018;11:1413-1422. doi:10.2147/OTT.S151286

317. Pérez-Alea M, Mcgrail K, Sánchez-Redondo S, et al. ALDH1A3 is epigenetically regulated during melanocyte transformation and is a target for melanoma treatment. *Oncogene*. 2017;36(41):5695-5708. doi:10.1038/onc.2017.160

318. Dinavahi SS, Gowda R, Gowda K, et al. Development of a novel multi-isoform ALDH inhibitor effective as an anti-melanoma agent. *Mol Cancer Ther*. January 2019:molcanther.0360.2019. doi:10.1158/1535-7163.MCT-19-0360

319. Sarvi S, Crispin R, Lu Y, et al. ALDH1 Bio-activates Nifuroxazide to Eradicate ALDHHigh Melanoma-Initiating Cells. *Cell Chem Biol*. 2018;25(12):1456-1469.e6. doi:https://doi.org/10.1016/j.chembiol.2018.09.005

320. Durinikova E, Kozovska Z, Poturnajova M, et al. ALDH1A3 upregulation and spontaneous metastasis formation is associated with acquired chemoresistance in colorectal cancer cells. *BMC Cancer*. 2018;18(1):848. doi:10.1186/s12885-018-4758-y

321. Kim D, Choi B, Ryoo I, Kwak M-K. High NRF2 level mediates cancer stem cell-like properties of aldehyde dehydrogenase (ALDH)-high ovarian cancer cells: inhibitory role of all-trans retinoic acid in ALDH/NRF2 signaling. *Cell Death Dis*. 2018;9(9):896. doi:10.1038/s41419-018-0903-4

322. Roesch A, Vultur A, Bogeski I, et al. Overcoming intrinsic multidrug resistance in melanoma by blocking the mitochondrial respiratory chain of slow-cycling JARID1Bhigh cells. *Cancer Cell*. 2013;23(6):811-825. doi:10.1016/j.ccr.2013.05.003

323. Maniotis AJ, Folberg R, Hess A, et al. Vascular Channel Formation by Human Melanoma Cells in Vivo and in Vitro: Vasculogenic Mimicry. *Am J Pathol*. 1999;155(3):739-752. doi:10.1016/S0002-9440(10)65173-5

324. Folberg R, Maniotis AJ. Vasculogenic mimicry. *Apmis*. 2004;112(7-8):508-525. doi:10.1111/j.1600-0463.2004.apm11207-0810.x

325. Paulis YWJ, Soetekouw PMMB, Verheul HMW, Tjan-Heijnen VCG, Griffioen AW. Signalling pathways in vasculogenic mimicry. *Biochim Biophys Acta - Rev Cancer*. 2010;1806(1):18-28. doi:10.1016/j.bbcan.2010.01.001

326. Ribatti D, Nico B, Cimpean AM, et al. B16-F10 melanoma cells contribute to the new formation of blood vessels in the chick embryo chorioallantoic membrane through vasculogenic mimicry. *Clin Exp Med*. 2013;13(2):143-147. doi:10.1007/s10238-012-0183-8

327. Dunleavey JM, Xiao L, Thompson J, et al. Vascular channels formed by subpopulations of PECAM1+ melanoma cells. *Nat Commun*. 2014;5:5200. doi:10.1038/ncomms6200

328. Sun B, Zhang D, Zhao N, Zhao X. Epithelial-to-endothelial transition and cancer stem cells: Two cornerstones of vasculogenic mimicry in malignant tumors. *Oncotarget*. 2017;8(18):30502-30510. doi:10.18632/oncotarget.8461

329. Brouard S, Otterbein LE, Anrather J, et al. Carbon Monoxide Generated by Heme Oxygenase 1 Suppresses Endothelial Cell Apoptosis. *J Exp Med*. 2000;192(7):1015-1026.

doi:10.1084/jem.192.7.1015

330. Motterlini R, Foresti R. Biological signaling by carbon monoxide and carbon monoxide-releasing molecules. *Am J Physiol Physiol*. 2017;312(3):C302-C313. doi:10.1152/ajpcell.00360.2016

331. Hulin J-A, Gubareva EA, Jarzebska N, Rodionov RN, Mangoni AA, Tommasi S. Inhibition of Dimethylarginine Dimethylaminohydrolase (DDAH) Enzymes as an Emerging Therapeutic Strategy to Target Angiogenesis and Vasculogenic Mimicry in Cancer. *Front Oncol*. 2020;9:1455. doi:10.3389/fonc.2019.01455

332. Choi S, Kim J, Kim J-H, et al. Carbon monoxide prevents TNF-α-induced eNOS downregulation by inhibiting NF-κB-responsive miR-155-5p biogenesis. *Exp Mol Med*. 2017;49(11):e403-e403. doi:10.1038/emm.2017.193

333. Schnegg CI, Yang MH, Ghosh SK, Hsu MY. Induction of vasculogenic mimicry overrides VEGF-A silencing and enriches stem-like cancer cells in melanoma. *Cancer Res*. 2015;75(8):1682-1690. doi:10.1158/0008-5472.CAN-14-1855

334. Liu Q, Qiao L, Liang N, et al. The relationship between vasculogenic mimicry and epithelial-mesenchymal transitions. *J Cell Mol Med*. 2016;20(9):1761-1769. doi:10.1111/jcmm.12851

335. Lin X, Sun R, Zhao X, et al. C-myc overexpression drives melanoma metastasis by promoting vasculogenic mimicry via c-myc/snail/Bax signaling. *J Mol Med (Berl)*. 2017;95(1):53-67. doi:10.1007/s00109-016-1452-x

336. Liu T, Sun B, Zhao X, et al. HER2/neu expression correlates with vasculogenic mimicry in invasive breast carcinoma. *J Cell Mol Med*. 2013;17(1):116-122. doi:10.1111/j.1582-4934.2012.01653.x

337. Zhu M-S, Xu L-B, Zeng H, Shi X-D, Wu W-R, Liu C. Association of Notch1 with vasculogenic mimicry in human hepatocellular carcinoma cell lines. *Int J Clin Exp Pathol*. 2014;7(9):5782-5791. https://pubmed.ncbi.nlm.nih.gov/25337219.

338. Kawahara R, Niwa Y, Simizu S. Integrin β1 is an essential factor in vasculogenic mimicry of human cancer cells. *Cancer Sci*. 2018;109(8):2490-2496. doi:10.1111/cas.13693

339. Hu A, Huang J-J, Jin X-J, et al. Curcumin suppresses invasiveness and vasculogenic mimicry of squamous cell carcinoma of the larynx through the inhibition of JAK-2/STAT-3 signaling pathway. *Am J Cancer Res*. 2015;5(1):278-288.

340. Werb Z, Lu P. The Role of Stroma in Tumor Development. *Cancer J*. 2015;21(4):250-253. doi:10.1097/PPO.0000000000000127

341. Plaks V, Kong N, Werb Z. The cancer stem cell niche: how essential is the niche in regulating stemness of tumor cells? *Cell Stem Cell*. 2015;16(3):225-238. doi:10.1016/j.stem.2015.02.015

342. Valenzuela Alvarez M, Gutierrez LM, Correa A, Lazarowski A, Bolontrade MF. Metastatic Niches and the Modulatory Contribution of Mesenchymal Stem Cells and Its Exosomes. *Int J Mol Sci*. 2019;20(8):1946. doi:10.3390/ijms20081946

343. Torisu-itakura H, Furue M, Kuwano M, Ono M. Co-expression of Thymidine Phosphorylase and Heme Oxygenase-1 in Macrophages in Human Malignant Vertical Growth Melanomas. *Japanese J Cancer Res*. 2000;91(September):906-910.

344. Liu Q, Wang B, Yin Y, et al. Overexpression of HO-1/HO-1G143H in C57/B6J mice affect melanoma B16F10 lung metastases rather than change the survival rate of mice-bearing tumours. *Exp Biol Med*. 2013;238:696-704. doi:10.1177/1535370213490628

345. Joseph A, Baiju I, Bhat IA, et al. Mesenchymal stem cell-conditioned media: A novel alternative of stem cell therapy for quality wound healing. *J Cell Physiol*. 2020;235(7-8):5555-5569. doi:10.1002/jcp.29486

346. Hwang S-H, Son E-S, Park Y-J, Lee C-S, Chun HJ. Effect of cultured medium of human umbilical cord blood-derived mesenchymal stem cells on melanogenic enzyme activity in mouse B16 melanoma cells. *Tissue Eng Regen Med*. 2014;11(5):414-422. doi:10.1007/s13770-014-4042-4

347. Swope VB, Zalfa A-M, Lina KM, Nordlum JJ. Interleukins 1alpha and 6 and Tumor Necrosis Factor-alpha Are Paracrine Inhibitors of Human Melanocyte Proliferation and Melanogenesis. *J Invest Dermatol*. 1991;96:180-185.

348. Slominski A, Tobin DJ, Shibahara S, Wortsman J. Melanin Pigmentation in Mammalian Skin and Its Hormonal Regulation. *Physiol Rev*. 2004;84(4):1155-1228. doi:10.1152/physrev.00044.2003

349. Kameyama K, Jiménez M, Muller J, Ishida Y, Hearing VJ. Regulation of mammalian melanogenesis by tyrosinase inhibition. *Differentiation*. 1989;42(1):28-36. doi:https://doi.org/10.1111/j.1432-0436.1989.tb00604.x

350. Iozumi K, Hoganson GE, Pennella R, Everett MA, Fuller BB. Role of Tyrosinase as the Determinant of Pigmentation in Cultured Human Melanocytes. *J Invest Dermatol*. 1993;100(6):806-811. doi:https://doi.org/10.1111/1523-1747.ep12476630

351. Smit NPM, van Nieuwpoort FA, Marrot L, et al. Increased melanogenesis is a risk factor for oxidative DNA damage--study on cultured melanocytes and atypical nevus cells. *Photochem Photobiol*. 2008;84(3):550-555. doi:10.1111/j.1751-1097.2007.00242.x

352. Jiménez-Cervantes C, Martínez-Esparza M, Pérez C, Daum N, Solano F, García-Borrón JC. Inhibition of melanogenesis in response to oxidative stress: transient downregulation of melanocyte differentiation markers and possible involvement of microphthalmia transcription factor. *J Cell Sci*. 2001;114(Pt 12):2335-2344.

353. Lee EJ, Kim JY, Ahn Y, et al. Critical Role of ATP-P2X7 Axis in UV-Induced Melanogenesis. *J Invest Dermatol*. 2019;139(7):1554-1563.e6. doi:10.1016/j.jid.2019.02.031

354. Lee A-Y, Noh M. The regulation of epidermal melanogenesis via cAMP and/or PKC signaling pathways: insights for the development of hypopigmenting agents. *Arch Pharm Res*. 2013;36(7):792-801. doi:10.1007/s12272-013-0130-6

355. Costin G-E, Valencia JC, Vieira WD, Lamoreux ML, Hearing VJ. Tyrosinase processing and intracellular trafficking is disrupted in mouse primary melanocytes carrying the underwhite (uw) mutation. A model for oculocutaneous albinism (OCA) type 4. *J Cell Sci*. 2003;116(15):3203 LP - 3212. doi:10.1242/jcs.00598

356. Takahashi K, Yamanaka S. Induction of Pluripotent Stem Cells from Mouse Embryonic and Adult Fibroblast Cultures by Defined Factors. *Cell*. 2006;126(4):663-676. doi:10.1016/j.cell.2006.07.024

357. Press release. NobelPrize.org. Nobel Media AB 2020. Mon. 8 Jun 2020. <https://www.nobelprize.org/prizes/medicine/2012/press-release/>.

358. Fang D, Leishear K, Nguyen TK, et al. Defining the Conditions for the Generation of Melanocytes from Human Embryonic Stem Cells. *Stem Cells*. 2006;24:1668-1677. doi:10.1634/stemcells.2005-0414

359. Ohta S, Imaizumi Y, Okada Y, et al. Generation of human melanocytes from induced pluripotent stem cells. *PLoS One*. 2011;6(1):e16182. doi:10.1371/journal.pone.0016182

360. Hayashi Y, Ohnuma K, Furue MK. Pluripotent Stem Cell Heterogeneity. In: Birbrair A, ed. *Stem Cells Heterogeneity - Novel Concepts*. Cham: Springer International Publishing; 2019:71-94. doi:10.1007/978-3-030-11096-3_6

361. Jian Z, Li K, Liu L, et al. Heme Oxygenase-1 Protects Human Melanocytes from H 2 O 2 -Induced Oxidative Stress via the Nrf2-ARE Pathway. *J Invest Dermatol*. 2011;131(7):1420-1427. doi:10.1038/jid.2011.56